Titre: Title:	Analysis and Optimization of Power Distribution Networks with High Penetration of Grid-Edge Technologies Under Uncertainty
Auteur: Author:	Feng Li
Date:	2024
Type:	Mémoire ou thèse / Dissertation or Thesis
Référence: Citation:	Li, F. (2024). Analysis and Optimization of Power Distribution Networks with High Penetration of Grid-Edge Technologies Under Uncertainty [Thèse de doctorat, Polytechnique Montréal]. PolyPublie. https://publications.polymtl.ca/62500/

URL de PolyPublie: PolyPublie URL:	https://publications.polymtl.ca/62500/
Directeurs de recherche: Advisors:	Antoine Lesage-Landry, & Ilhan Kocar
Programme: Program:	Génie électrique

POLYTECHNIQUE MONTRÉAL
affiliée à l'Université de Montréal

Analysis and Optimization of Power Distribution Networks with High Penetration of Grid-Edge Technologies Under Uncertainty

FENG LI
Département de génie éléctrique

Thèse présentée en vue de l'obtention du diplôme de *Philosophiæ Doctor*
Génie éléctrique

Décembre 2024

POLYTECHNIQUE MONTRÉAL
affiliée à l'Université de Montréal

Cette thèse intitulée :

Analysis and Optimization of Power Distribution Networks with High Penetration of Grid-Edge Technologies Under Uncertainty

présentée par **Feng LI**
en vue de l'obtention du diplôme de *Philosophiæ Doctor*
a été dûment acceptée par le jury d'examen constitué de :

Hanane DAGDOUGUI, présidente
Antoine LESAGE-LANDRY, membre et directeur de recherche
İlhan KOCAR, membre et codirecteur de recherche
Mohsen GHAFOURI, membre
Claudio A. CAÑIZARES, membre externe

DEDICATION

To my family, and to Jacob, Jeremie, and Joyce
Never too late to pursue your dreams . . .

ACKNOWLEDGEMENTS

I am sincerely grateful to my supervisor Professor Antoine Lesage-Landry and my co-supervisor Professor Ilhan Kocar at Polytechnique Montréal for their continuous guidance and supervision throughout the research work. In particular, I would like to thank Professor Lesage-Landry for encouraging and empowering me to explore multiple ideas in this research. With his expertise in optimization and learning theories, he provided me valuable advice in finding solutions to technical difficulties. I wish to thank Professor Kocar for his valuable guidance to strengthen the technical aspects of the work with his extensive knowledge in power systems. I am very honoured of having the opportunity to work with both of them, and this work would not be the way it is now without the help they offered.

I thank Professor Hanane Dagougui, Professor Mohsen Ghafouri, and Professor Claudio A. Cañizares for having accepted to be members of my committee and for their time to read this dissertation.

To all my colleagues and people I met at Laboratoire d'Optimisation des Réseaux Électriques Renouvelables (LORER), Groupe d'Études et de Recherche en Analyse des Décisions (GERAD) and Mila – Quebec Artificial Intelligence Institute, thank you all for the discussions and support.

I also want to express my gratitude for the support from Eaton Corporation. My special thanks to Patrick Jacques, Manager of the Power System Engineering team at Eaton's CYME International, for offering me the flexibility and accommodation in fulfilling my work at CYME. I also want to thank Francis Therrien, Lead Engineer at CYME, for offering his help and advice.

Last but not least, I would like to thank my family for their support and patience along the journey. This work is my gift to them.

RÉSUMÉ

Les diverses technologies en périphérie du réseau (TPR), telles que les véhicules électriques (VÉ), les systèmes photovoltaïques (PV), les programmes de gestion de la demande de puissance (GDP), etc., sont installées sur les sites des clients (périphérie du réseau) et connectées aux réseaux électriques de distribution. Avec la transition énergétique en cours, le nombre de TPR augmente rapidement. Il est essentiel pour les fournisseurs d'électricité d'évaluer leur influence sur le réseau de distribution afin de maintenir la fiabilité du système et la qualité de l'alimentation, et d'éviter les interruptions de service. Étant donné que la demande d'électricité des clients due à l'utilisation de TPR se produit derrière le compteur et est aléatoire en termes de comportements d'utilisation, il est difficile de modéliser ces technologies sur les réseaux et d'évaluer leurs impacts, en particulier à des taux de pénétration élevés. Un outil d'analyse est donc nécessaire pour évaluer les impacts des TPR sur les réseaux électriques tout en tenant compte des incertitudes associées à l'utilisation de ces technologies. Cette thèse vise également à relever des défis posés par la pénétration croissante de ces technologies. Des plans d'atténuation pour minimiser des conditions anormales du réseau causées par l'utilisation de ces TPR sont proposés afin de maintenir un fonctionnement sécuritaire et optimal du système.

Nous introduisons une méthode d'estimation rapide (MER) pour analyser les impacts stochastiques des TPR sur le réseau de distribution. Cette méthode utilise l'équation de Fokker-Planck pour modéliser les fonctions de densité de probabilité des états du réseau, tels que les niveaux de charge des équipements et les niveaux de tension, sous divers taux de pénétration des TPR. Pour améliorer l'exactitude de la MER, une étape de calibration optionnelle est proposée. Afin d'appliquer la MER aux études d'impact des VÉ, les profils de recharge des propriétaires de VÉ en termes de distributions de probabilité sont requis comme intrants. En l'absence de telles informations, nous proposons une méthode pour détecter les événements de recharge des VÉ à partir des données de compteurs intelligents, qui sont plus accessibles aux fournisseurs d'électricité. Cette méthode permet de déduire les habitudes de recharge des clients et construit des distributions de probabilité des profils de recharge, qui sont ensuite utilisées dans la MER pour les analyses d'impact des VÉ.

Lors de l'utilisation de MER pour analyser les impacts des véhicules électriques sur le réseau de distribution, il est possible que des équipements du réseau soient surchargés à des taux de pénétration élevés. Des stratégies d'atténuation doivent être conçues pour faire face à ces problèmes de surcharge potentiels. Elles permettent d'éviter une défaillance prématurée de

l'équipement qui peut entraîner des événements beaucoup plus graves et même des pannes sur le réseau de distribution. Dans la thèse, nous décrivons une méthodologie pour leur atténuation. Notre stratégie implique de déplacer les probabilités de recharge des VÉ des clients durant des heures de pointe aux heures de faible consommation grâce à des programmes incitatifs. Un problème d'optimisation à deux niveaux est formulé pour concevoir la stratégie d'atténuation, qui est ensuite reformulée en un programme convexe pour une solution efficace. La MER est également appliquée pour déterminer la stratégie optimale.

Les impacts des PV sur le réseau de distribution peuvent également être étudiés à l'aide de MER. Pour un réseau avec une forte intégration des PV, des problèmes de surtension peuvent survenir, notamment pendant les périodes de pointe de production solaire. Pour résoudre ces problèmes potentiels de surtension, une stratégie d'optimisation volt-var (VVO) est développée pour réguler les niveaux de tension sur le réseau de distribution. Cette stratégie inclut des réglages optimaux pour les dispositifs de régulation de tension conventionnels et les onduleurs intelligents, en tenant compte des incertitudes de la demande et de la génération PV. Le problème de VVO est d'abord formulé comme un programme stochastique et est résolu en utilisant une approche d'optimisation stochastique par boîte noire basée sur des scénarios.

Les méthodologies et les stratégies proposées dans cette thèse sont validées par des études de cas approfondies sur le grand réseau de test IEEE-8500, démontrant leur applicabilité pratique et leurs avantages pour les systèmes de distribution d'électricité modernes.

ABSTRACT

As grid-edge technologies (GETs), such as electric vehicles (EVs) and photovoltaic systems (PVs) are becoming popular on power distribution networks, their impacts need to be studied. This dissertation aims to address the challenges posed by the increasing penetration of these technologies, and mitigation plans to abnormal network conditions caused by the use of these GETs are proposed to maintain safe and optimal operation of the system.

We introduce a rapid estimation method (REM) to perform stochastic impact analyses of GETs on distribution networks. This method leverages the Fokker-Planck equation to model the probability density functions (PDFs) of network states, such as equipment loading levels and voltage levels, under various penetration rates of GETs. An optional calibration step is proposed to enhance the accuracy of the REM. To apply the REM for EV impact studies, EV owners charging habits in terms of probabilities are needed as input data. In absence of such information, we propose a non-intrusive and training-free method to detect EV charging events from smart meter data, which are more accessible to utilities. This method infers customers' charging habits and constructs probability distributions of charging profiles, which are then used in the REM for EV impact analyses.

When using the REM to analyze impacts of EVs to the distribution network, it is possible that network equipment may be overloaded at high EV penetration rates. Mitigation strategies should be prepared to address such potential overloading issues to avoid premature failure of the equipment which can lead to much more serious events and even faults on the distribution network. We describe a methodology to design an incentive-based mitigation strategy. This strategy involves shifting customers' EV charging probabilities from peak to off-peak hours through incentive programs. A bi-level optimization problem is formulated to design the mitigation strategy, which is then reformulated into a convex program for efficient solution. The REM is also applied to search for the optimal strategy.

Impacts of PVs to the distribution network can also be studied using the REM. For PV-rich networks, over-voltage issues can be created especially during peak solar generation periods. To address such issues, we develop a volt-var optimization (VVO) strategy to regulate voltage levels on the distribution network. This strategy includes optimal settings for conventional voltage-regulating devices and smart inverters, considering uncertainties in demand and PV generation. The VVO problem first formulated as a stochastic program, and is solved using a scenario-based stochastic blackbox optimization approach.

The methodologies and strategies proposed in this dissertation are validated through exten-

sive case studies on the large-scale IEEE-8500 test feeder, showcasing their practical applicability and benefits for modern power distribution systems.

TABLE OF CONTENTS

LIST OF TABLES

LIST OF FIGURES

LIST OF SYMBOLS AND ABBREVIATIONS

Abbreviations

AMI	Advanced metering infrastructure
ANN	Artificial neural network
BBO	Blackbox optimization
BTM	Behind-the-meter
CNN	Convolution neural network
DFT	Discrete Fourier transform
DR	Demand response
DER	Distributed energy resource
DQN	Deep Q-network
DRL	Deep reinforcement learning
EV	Electric vehicle
FPE	Fokker-Planck equation
FVM	Finite volumn method
GET	Grid-edge technology
HMM	Hidden Markov models
HVAC	Heating, ventilation and air conditioning
ICA	Independent component analysis
MADS	Mesh Adaptive Direct Search
MANA	Modified augmented nodal analysis
MANA-NR	Modified augmented nodal analysis using Newton-Raphson
MC	Monte Carlo
MICQP	Mixed-integer convex quadratic program
MINLP	Mixed-integer nonlinear program
NILM	Non-intrusive load monitoring
NR	Newton-Raphson
OLTC	On-load tap changer
ORPD	Optimal reactive power dispatch
OPF	Optimal power flow
PCE	Polynomial chaos expansion
PDF	Probability density function
PV	Photovoltaic system
REM	Rapid estimation method

RL	Reinforcement learning
SDR	Semidefinite relaxation
SOCR	Second-order cone relaxation
SVM	Support vector machine
TAM	Thermal-aging model
TCL	Thermostatically controlled loads
TOU	Time-of-use
ts-REM	Time-series rapid estimation method
VNS	Variable neighbourhood search
VVO	Volt-var optimization

Notations

$\mathcal{L}_k$	Set of load offset profiles for GET k
L_k	Number of profiles in $\mathcal{L}_k$
$\mathcal{T}$	Time horizon of a profile in $\mathcal{L}_k$
$\mathcal{T}^{\mathrm{P}}$	Peak period during time horizon $\mathcal{T}$
$\mathcal{T}^{\mathrm{OP}}$	Off-peak period during time horizon $\mathcal{T}$
$\mathcal{T}^{\mathrm{MP}}$	Mid-peak period during time horizon $\mathcal{T}$
$\mathbb{N}_0$	Set of natural numbers including 0, i.e., $\mathbb{N}_0 = \{0, 1, \cdots\}$
$\Pr^i[\mathcal{L}_k]$	Probabilities of customer i to adopt profiles in $\mathcal{L}_k$ of GET k
$\Pr^{i,\mathrm{P}}[\mathcal{L}_k]$	Extracted probabilities (non-normalized) from $\Pr^i[\mathcal{L}_k]$ on profiles active during $\mathcal{T}^{\mathrm{P}}$
$\Pr^{i,\mathrm{OP}}[\mathcal{L}_k]$	Extracted probabilities (non-normalized) from $\Pr^i[\mathcal{L}_k]$ on profiles active during $\mathcal{T}^{\mathrm{OP}}$ but not during $\mathcal{T}^{\mathrm{P}}$
$\Pr^{i,\mathrm{MP}}[\mathcal{L}_k]$	Extracted probabilities (non-normalized) from $\Pr^i[\mathcal{L}_k]$ on profiles active during $\mathcal{T}^{\mathrm{MP}}$ but not during $\mathcal{T}^{\mathrm{OP}} \cup \mathcal{T}^{\mathrm{OP}}$
$\Pr^i_{\mathrm{num},k}(n)$	Probability of customer i having $n \in \mathbb{N}_0$ GET k devices
$\mathcal{N}$	A generic distribution network
$\mathcal{B}$	The set of buses on network $\mathcal{N}$
ϕ	Network phase $\phi \in \{a, b, c\}$
p_k	Penetration rate of GET k on network $\mathcal{N}$
n_k	Number of GET k devices on the network to reach its penetration p_k
N_{m}	Number of customers/meters on network $\mathcal{N}$
$m(x, p)$	PDF of network state x at GET penetration rate p
$u(x, p)$	Drift velocity of x with respect to p
$d(x, p)$	Diffusion velocity of x with respect to p
$\mathrm{sgn}(k)$	sign function where $\mathrm{sgn}(k) = 1$ if GET k consumes active power and $\mathrm{sgn}(k) = -1$ otherwise
$g^{\phi}_{e,k}(p)$	Change of loading level on phase ϕ with respect to p when GET k devices are installed
$\Pr^{\phi}_{e,k}$	Probability that GET k devices are installed to sections downstream of equipment e on phase ϕ
$\mathbb{E}[S^{\phi}_{e,k}]$	Expected apparent power (in kVA) of one GET k device installed downstream of e on phase ϕ
$\mathbb{E}[S_{e,k}]$	Total expected apparent power (in kVA) of one GET k device installed downstream of e on all connected phases
S^{ϕ}_e	Rated power (in kVA) of e on phase ϕ

$\Delta v_{o,k}^{\phi}(p)$	Change to voltage of node o on phase ϕ at penetration p for GET k
$\Pr_{o,k}^{\phi}$	Probability that GET k devices are installed to node o on phase ϕ
$\mathbb{E}[S_{o,k}^{\phi}]$	Expected apparent power of a GET k device connected to o on phase ϕ
λ_p	Factor of customers' participation into the mitigation strategy for EV charging on the network, $\lambda_p \in [0, 1]$
$\Sigma^{i,\mathrm{P}}$	Total probability of customer i charging during $\mathcal{T}^{\mathrm{P}}$
$\Delta_{\mathrm{prob}}^{i}$	Reduction of probability of customer i charging during $\mathcal{T}^{\mathrm{P}}$ when participating into the mitigation strategy, $\Delta_{\mathrm{prob}}^{i} \in [0, \Sigma^{i,\mathrm{P}}]$
$\mathbf{P}$	Real power measured in kW by the smart meters for N_{m} customers on the distribution network $\mathcal{N}$ and for N_{D} days, i.e., $\mathbf{P} = [\mathrm{P}_i]_{i=1}^{N_{\mathrm{m}}} \in \mathbb{R}^{N_{\mathrm{m}} \times N_{\mathrm{D}} T}$
$\mathbf{P}^{\mathrm{EV}}$	Power demand to charge EVs for all customers during N_{D} days
$\mathbf{D}$	Demand profiles (complex power) of the N_{m} loads
$\mathbf{G}$	Generation profiles (complex power) of the N_{der} DERs modelled on the network
$\mathbf{\Gamma}_{\mathrm{cb}}$	Set of On/Off states of capacitor banks on the network
$\mathbf{V}_{\mathrm{D,vr}}$	Set of desired voltage levels for all voltage regulators on the network
$\mathbf{V}_{\mathrm{D,xfo}}$	Set of desired voltage levels for transformers with OLTCs
$\mathbf{C}_{\mathrm{der}}$	Set of volt-var curve settings for DERs on the network

LIST OF APPENDICES

CHAPTER 1 INTRODUCTION

1.1 Motivation

Grid-edge technologies (GET), e.g., plug-in electric vehicles (EV), rooftop photovoltaic systems (PV), demand response (DR) programs, etc., are being installed at customers' sites and connected to the power distribution networks. With the energy transition happening, the number of these grid-edge technologies is rapidly growing, and it becomes critical to assess their influence on the distribution network in order to maintain system reliability and power quality, and to avoid service interruptions. However, due to the limited observability and randomness with the customers' consumption and/or generation behaviours, it is difficult to assess their impacts especially at high penetration rates. Taking EVs as an example of a GET, charging of EVs may introduce undesired impacts to power networks such as overloading of key equipment, severe voltage variations, phase unbalancing, harmonic distortions, etc., just to name a few [1, 2]. Analyses of these impacts depend on various factors such as charging locations of EVs, charging time and duration, charging power, and battery capacities, which are uncertain and non-observable to utilities as EV chargers are usually installed behind-the-meter (BTM). Given the challenges to model the EV consumption behaviours, it is necessary to perform a stochastic analysis to evaluate the network states, i.e., equipment loading levels, voltage levels, etc., with different penetration levels of EVs installed. Such an analysis framework should also be extended to include other grid-edge technologies than EVs, as well as to study the combined impacts when multiple technologies are installed to the same power network.

Analysis results of the GETs' impacts on the distribution networks may reveal abnormal conditions such as equipment overloading, under/over-voltages, excessive network losses, etc., when high penetration of grid-edge technologies are installed on the networks. Mitigation plans and network optimization must be considered for the operation and the planning of power networks to maintain quality of service. While upgrades to the network infrastructure such as expansion of equipment capacity, installation of voltage regulators and reactive power support devices may provide immediate relief to abnormal network conditions, they require high levels of capital expenditure. Alternatively, reconfiguration of the network can be performed such as in [3, 4] where the optimal power flow (OPF) framework is adopted. To mitigate overloading issues for networks with high penetration of GETs like EVs, load shaping techniques have been proposed to reduce their impacts to the networks. For example, time-of-use (TOU) rates can be designed to reduce EV charging demand at peak hours, and

an EV charging schedule can be correspondingly developed in response to published TOU rates to minimize users' charging costs [5,6]. Coordinated EV charging is another technique aiming for an optimal charging schedule of EVs connected to the network [7,8]. Similarly, for networks with high penetration of PVs, the risk of over-voltage can be mitigated by using an energy storage devices (such as a battery) as proposed in [9,10]. Dedicated demand response programs integrating network constraints are also ongoing efforts to ensure safer distribution network operations [11]. For networks with voltage regulating devices like voltage regulators, volt-var optimization (VVO) technique can also be adopted to improve the voltage profiles on the network [12]. GETs like PVs can also be included in VVO to control the amount of reactive power absorbed or injected if they have such capability.

1.2 Research Objectives

This dissertation aims to address the following needs in planning, operations, and optimization of today's power distribution networks with increasing penetration of GETs:

- How to rapidly assess impacts of single or multiple types of distributed GETs on the distribution networks for a range of penetration levels by considering the randomness associated with the location and the usage of these GETs?
- What is a cost-effective way to reduce the likelihood of key network equipment being overloaded under the impacts of GETs (e.g., EVs) without spending significant capital expenditure to upgrade the network infrastructure?
- Can a voltage regulating strategy be designed to optimize voltage levels of the distribution network and to minimize the energy losses when fluctuations in demand and GET generation (e.g., PVs) are taken account for?

To develop solutions and methodologies in answering these research questions, the following information are assumed generally available:

A1. Base load profiles for customer demand (e.g., household consumption) and generation for existing distributed energy resources (DERs) on the network. These data are usually from meter measurement or forecasted by the utilities.

A2. Probability data related to adoption of GETs (e.g., how likely a customer owns an EV) and their usage patterns (e.g., how many times a customer charges the EV from 8 pm to midnight during the past year). The assumption is mild as the information can be extracted from A1. if it is not readily available. The

methodology is presented in Chapter 3.

A3. Network models containing network topology and devices/equipment on the network. Device parameters such as impedance and nominal ratings are also available.

A4. Analysis parameters such as the desired ranges of simulation time and penetration levels. Key network locations/sections that utilities want to monitor should also be specified.

1.3 Contributions

The contributions aligning with the research objectives are described below, and their relations are depicted in Figure 1.1. We want to highlight that the contributions target at addressing difficulties that utility planners may encounter during their planning journeys for the distribution networks with GETs. As GETs can have different impacts to the networks according to their types, each methodology focuses on one GET type (i.e., whether EVs or PVs but not both), except the stochastic impact analysis method which is applicable to multiple GET types.

1.3.1 Rapid estimation method for stochastic impact analyses of GETs

The first and the main contribution of the research is to formulate an analytical and rapid approach to perform a stochastic analysis on the impact of GETs to power distribution networks. Uncertainties associated with locations of GETs as well as their power consumption/generation profiles are considered. We propose a method to provide a rapid evaluation of the network states at a wide range of penetration levels and to indicate likely locations of the network where abnormal conditions, e.g., equipment overloading and under/over-voltages, may occur at any given penetration level. From another perspective, results from the proposed approach can also indicate the maximum penetration level possible that can be hosted by the network at which the network can securely operate before network expansion and/or mitigation action is required.

1.3.1.1 Related work to stochastic analyses

In the literature, deterministic methods have been proposed to study the impacts of EVs [13–16] and PVs [17–19], and their combined impacts [20] to the power distribution networks. These methods normally evaluate network states by generating typical or worst-case scenarios from the parameters with uncertainties, e.g., power flow analysis is usually used to study

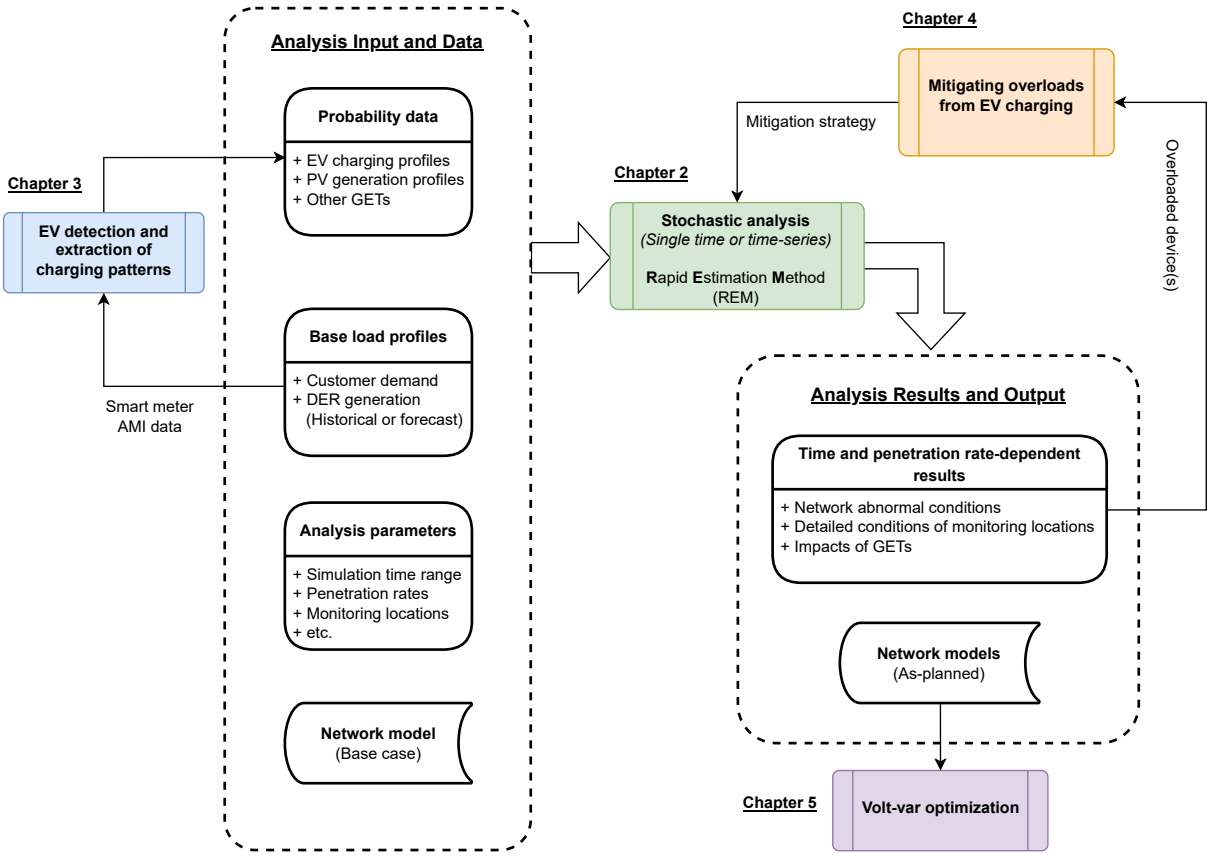

Figure 1.1 Mapping of research contributions

the impacts in each scenario. While these deterministic simulation models are easier to implement, uncertainty is often ignored when looking at selected scenarios. Analysis results may be consequently inaccurate and cannot provide meaningful insights for power system plannings. It is important to model the uncertainty in the input variables such as the locations and the charging/generation profiles of EVs/PVs, etc., and use stochastic approaches to compute the network states and their associated probability density functions (PDFs).

Such stochastic approaches can be categorized into numerical, analytical, and approximation approaches. Due to the simplicity in the implementation, several Monte Carlo simulation-based studies have been performed in the context of GET integration. Monte Carlo simulations can provide accurate results to complicated and/or non-linear systems with many random variables involved. For example, in [21], impacts of voltage drops and loading conditions of lines due to EV charging are studied, and in [22], network losses, voltage variations and transformer loadings are studied at various penetration levels of EVs. In [23, 24], the harmonic impacts due to EV charging are analyzed, where not only locations of EVs and

charging patterns are randomized, but also the operating states of the residential household loads. Finally, impacts of multiple technologies including EVs and PVs to the distribution network in terms of abnormal voltages and transformer loading levels are studied in [25].

While the Monte Carlo simulation approach is a straightforward numerical method for the stochastic analysis and can provide accurate results if all uncertain variables are covered, it has a very slow rate of convergence. The construction of a large number of samples is time-consuming, and performing a power flow analysis to each sample is computationally expensive. Multiple techniques can be applied to improve the efficiency of Monte Carlo simulations, such as variance reduction techniques [26], quasi-static Monte Carlo [27], combination with learning methods [28], bootstrapping techniques [29], etc. While the convergence rate may be accelerated by using these techniques, the results obtained correspond to a single GET penetration. For multiple penetration levels, samples still need to be generated for each penetration. Analytical approaches are, therefore, an alternative to derive PDFs of output variables from PDFs of input variables, such as in probabilistic power flow analysis. For example, the PDF of an output random variable can be computed from the convolution of input random variables which are independent. However, the convolution operation requires extensive computation, even with the discrete Fourier transform (DFT) applied to reduce the computational burden [30]. Approximation methods for probabilistic power flow analysis are developed to improve the computational efficiency [31–37]. In [31], PDFs of power flows in transmission lines are approximated in terms of *cumulants*, which are an alternative set of quantitative measures to *moments* related to the shape of PDFs with the computational time significantly reduced. Another approximation method is the point estimation method which approximates the PDF of an output variable from its first and second moments as in [32]. In recent years, polynomial chaos expansion (PCE)-based methods have shown promising results in quantifying uncertainties in power systems; however, limitations still exist which make them less applicable to the stochastic analysis of large-scale distribution systems. For example, it suffers from the "curse of dimensionality" [33] when the number of random input variables is large. Hence, the computation for the polynomial coefficients of the surrogate model is challenging even if the expansion degree is limited to 2 [34]. Also, separate approaches are required to accompany the PCE method such as using the Copula theory in [35, 36] when random variables are correlated and certain constraints are to be considered, and using the Stieltjes procedure to construct the orthogonal basis for PCE such as in [37] when random variables have arbitrary probability distributions. Although such advancements have been made to characterize uncertainties in power systems, a common drawback of the analytical and approximated methods in the literature is that the models are developed for a fixed penetration rate. To consider multiple penetration rates of GETs,

models will have to be recomputed, which is inefficient.

1.3.1.2 Proposed methodology in the first contribution

We focus on EV and PV as GET types and suppose that a set of nominal charging and generation profiles of EVs and PVs are given. Such sets of profiles reflect diversified charging behaviours and charger types for EVs and different PV generation outputs related to weather types. Probabilities of customers' adoption for EVs and PVs as well as their preference of profiles are also given, which can often be obtained from statistical surveys or socio-economic analysis [38–40]. Alternatively, these probabilities can also be inferred from customers' meter data, which is the focus of the next contribution. Based on these data, one can characterize the impacts of EVs/PVs on the distribution network either by Monte Carlo simulations or by a numerical/analytical method based on probabilistic analysis, viz., an "estimation" method. The latter, being the focus of the research, is an analytical approach which can provide quick assessment of the network states at any penetration level of EVs and PVs without performing repetitive power flow analysis to the network. Such an estimation method models the network states of interests (equipment loading level and node/bus voltage) by probability density functions. Drifting velocities of the network states, being the changes to the network states under the influence of EVs/PVs, can be analytically computed, in terms of an expected "density" of EVs/PVs at each customer's site and an expected "load offset" value for an EV/PV device. Such an expected "density" of EVs/PVs and "load offset" value can be computed based on customers' preference of adoption for EVs and PVs and their preference of usage profiles of EVs/PVs, respectively. The Fokker-Planck equation is then adopted and numerically solved to describe the evolution of the network state PDFs as the penetration level of EVs/PVs is increasing. At any penetration level, probabilities of equipment overloading and node/bus voltage exceeding specific limits can then be calculated, which indicates susceptible equipment or network sections to EVs/PVs.

1.3.2 Method to infer EV charging patterns from meter data

To apply the stochastic analysis method developed in the first contribution described in Section 1.3.1 to study impacts of EV charging specifically, probability data characterizing customers' EV charging profiles are required. While such probabilities can be constructed based on historical EV charging events, utilities do not have direct access to the charging events as EV chargers are often installed behind-the-meter. Thus, the second contribution is to propose a method to detect BTM EV charging events from the data measured by advanced metering infrastructure (AMI), which are readily available to the utilities. PDFs

are also empirically constructed to characterize customers' EV charging behaviours, which are used as input data to the stochastic analysis method.

It is remarked that to study impacts of PVs, a similar method is also required if probability data associated with PV generation profiles are not directly available. However, it is out of the scope of this dissertation and not considered in the research work.

1.3.2.1 Related work to EV detection

In the literature, there exist mainly two groups of methods to detect EV charging events from the smart meter data: supervised learning-based and training-free methods. Supervised machine learning methods, e.g., convolutional neural networks and recurrent neural networks, have been trained to detect EV charging events with the best average accuracy of 71% [41–44]. These methods primarily focus on identifying time periods associated with EV charging activities. Supervised classification methods, e.g., random forest algorithm, k-nearest neighbour, and classification trees, are also deployed for qualitative purposes, such as distinguishing EV owners from other consumers [45, 46]. The downside of these methods is that labelled data, i.e., training samples, are required but they may not be readily available, and the performance of these methods is highly dependent on and sensitive to the quality and quantity of data available for training.

In addition to supervised learning-based methods, training-free methods have also been utilized in EV detection. These approaches take advantage of contextual information (e.g., standardized power level of EV chargers), and for this reason, they are widely applicable to customers' data on different distribution networks and/or regions. Models based on cross-correlation and pattern recognition are proposed in [43,47]. These models use sliding windows and pattern search techniques to identify EV's charging events. For improved accuracy, filtering techniques are proposed in [48, 49] to specifically remove data segments that do not meet typical values of power levels and of duration of an EV charging event. Signal decomposition is also utilized and takes advantage of trends in measured meter data to target EV signatures [50]. These methods are easily interpretable, but are limited by the assumptions made about EV charging behaviours. More refined models further leverage statistical and probabilistic methods. For example, [51, 52] use independent component analysis (ICA) to detect EV charging events. Probabilistic models such as hidden Markov models (HMM) allow to account for the uncertainty around EV charging profiles in terms of the start time, the initial state-of-charge, duration, or the power level. In [53, 54], the authors used HMM to separate individual appliances from an aggregate load without requiring complete knowledge of the types of appliances in the households. Even though no training is required, hyperparameter

tuning is still necessary for optimal performance.

Disaggregating EV charging consumption from the aggregated consumption falls into the broader technique of non-intrusive load monitoring (NILM), where energy consumption of multiple household appliances are detected. Similarly, NILM methods can be categorized into learning-based and pattern matching methods. Readers are referred to [55] for a detailed review on methods of NILM.

1.3.2.2 Proposed methodology in the second contribution

We aim to develop a non-intrusive and training free method to detect BTM EV charging events from smart meter data. To do so, we leverage the contextual information of EV charging and we formulate a mixed-integer convex quadratic program (MICQP) to detect EV charging events from customers' daily meter data. We do not require any labelled training data or hyperparameter tuning procedures, and the MICQP can be efficiently solved with an off-the-shelf solver. By collecting information about the start time, the charging duration, and the power level of each detected charging event, we infer customers' charging patterns in terms of probabilities of charging profiles through a data-driven approach using one year's meter data.

1.3.3 Mitigation strategy to remove equipment overloads due to EV charging

From the stochastic analysis of EV impact studies on distribution networks, key network equipment may be identified as being overloaded especially at high penetration of EVs. To avoid premature failure of these equipment and to maintain their usable lifetime, utilities must develop strategies to mitigate the overloads. Hence, the third contribution of the research is to develop a methodology to design plans to mitigate overloads to equipment due to EV charging.

1.3.3.1 Related work to mitigate equipment overloading

Conventional approaches to mitigate equipment overloading issues include expanding equipment capacity [56], installing distributed generation [57], or deploying voltage control and reactive power equipment [58]. These solutions come with substantial capital costs as well as rigorous planning activities. Alternatively, optimal charging schedule for EVs connected to the network can be derived through coordination to minimize network losses [7, 8], reduce the peak demand [59, 60], limit transformers' loading [61, 62], and respect feeder capacity constraints [63]. Decentralized algorithms based on game theory are also proposed to achieve

valley-filling [64, 65]. In these strategies, an ε-Nash equilibrium based on a given price signal is searched as a fixed-point solution to the game model. However, how incentive plans or the price signal are designed to attract customers to participate in coordinated charging is not discussed in these works. On the other hand, demand response programs with incentive plans, either incentive-based [66] or price-based [5, 6], are designed to address the challenges posed by EV charging by shifting EV charging loads to periods when the grids are lightly loaded. For example, in [66] an incentive-based DR program is proposed to minimize impacts of controllable loads to distribution networks. A constrained optimization problem is formulated to allocate a demand limit for each customer during a time period, and customers can select charging hours for their EVs as long as the demand limit is respected at all times. Effectiveness of the DR program is shown at different EV penetration levels; however, the relationship between the incentive and the demand limit is not clear. In [5], load patterns are studied when a DR strategy is implemented to non-critical loads (including EV charging) with time-of-use (TOU) rates. In [6], to reduce EV charging demand during peak hours, a schedule is developed in response to the TOU rates to minimize users' charging costs. In both works, TOU rates are assumed to be pre-defined but not optimized for variations of load demands which includes EVs. In other words, uncertainties in EV charging are not considered.

A common shortcoming of all the aforementioned works is that the proposed strategies are not demonstrated on large-scale networks for effectiveness while considering uncertainties in EV charging. This could be due to the heavy computation burden when assessing the network conditions under the strategies for a large number of EVs and accounting for charging behaviour uncertainties. Further, communication systems for prices or control signals are necessary to implement DR programs, which may lead to cybersecurity concerns [67].

1.3.3.2 Proposed methodology in the third contribution

We propose a framework to develop new mitigation strategies to temporally shift EV charging from periods where network equipment may be overloaded to alternative time periods when the network is lightly loaded. Incentives in the form of rewards or time-of-use tariff are offered to EV owners to participate. We first formulate a bi-level optimization problem to restore overloaded equipment's lifetime as close as possible to the nominal value and to minimize utilities' costs by determining optimal incentive levels. To solve it in a more computationally efficient way, we then reformulate it into a convex optimization problem which is shown to be a convex restriction to the bi-level problem under some conditions. To search for an optimal incentive level for the mitigation strategy, the convex problem is embedded into a

search algorithm, and the rapid method developed in the first contribution of Section 1.3.1 is used to estimate impacts of EV charging on equipment's loading level under each potential strategy searched.

1.3.4 Volt-var optimization method considering DER settings

As the penetration rate of DERs is increasing, it is becoming more important to manage and optimize voltage levels on the distribution network. Volt-var optimization (VVO) is a critical technique in modern power distribution systems to achieve this, and at the same time network losses are minimized. In the last contribution of the research, we consider PVs as the GET type and propose VVO strategies to regulate voltage levels on the network. We propose an optimal reactive power dispatch (ORPD) stochastic program for VVO of power distribution networks, while uncertainties in demand and PV generation are considered. The formulation should consider not only control settings for voltage regulators, capacitor banks, and on-load tap changers which are conventional devices for VVO, but also the capability of inverter-based DERs to absorb and inject reactive power to regulate the voltage levels. Here, we mainly optimize the settings of the volt-var droop curves of the DERs for reactive power dispatch, which can be seen as decentralized control policy of voltage vs. reactive power.

1.3.4.1 Related work to VVO

Optimizing the amount of reactive power that DERs should inject/absorb is known as an optimal reactive power dispatch problem, where optimal settings for legacy devices in VVO are also determined. It can be considered as a sub-problem of the optimal power flow (OPF) problem and is often formulated in the framework thereof. Given that ORPD contains both continuous and discrete control variables, e.g., the tap positions, connection states of capacitor banks, etc., a mixed-integer nonlinear programming (MINLP) problem needs to be solved [12, 68–77]. Various techniques have been proposed to solve the nonlinear and non-convex ORPD. In [12, 68], the nonlinear power flow equations are linearized and mixed-integer linear programs are solved to optimize settings for capacitors, voltage regulators, and OLTCs. Linear power flow equations are used in [69] to optimize the volt-var droop curve settings of PVs. Convex relaxation techniques have also been applied to convexify ORPD which can lead to global optimal solutions. The two main convex relaxation methods are the semidefinite relaxation (SDR) [70, 71] and the second-order cone relaxation (SOCR) [72]. While computationally efficient, these relaxations may provide infeasible solutions with respect to the initial problem. Among all these works, only [72] considers the integration and reactive power control of DERs/PVs; however, controls of legacy devices of VVO are excluded

even though they exist on the test networks the authors utilized. To consider uncertainties in loads and power generation from DERs, approaches such as stochastic programming [73, 74] and robust optimization [75–77] are incorporated into the ORPD problems. A two-stage VVO is formulated in [73] where settings for capacitor banks and OLTCs are optimized in the first stage, and variations in loads and DER generations are included in the second stage. Scenarios are constructed based on the probability distributions of the uncertainties and the problem is then converted to a deterministic mixed-integer program. In [75–77], multi-stage optimization models are proposed and solved for the worst case rather than considering only the expected values of the random variables. Hence, the VVO solutions are robust to uncertainties in minimizing the losses while maintaining the voltage levels in the desired range. A distributed algorithm is used in [77] to efficiently solve the robust optimization model. The OPF or ORPD-based models formulated for VVO in the literature above are in essence mixed-integer programs. Linearization or relaxations are necessary to efficiently solve them; however, exactness or feasibility of the solutions cannot be guaranteed, especially for non-radial networks [78]. The scalability of these approaches is also a concern for an entire distribution network containing thousands of nodes and maybe millions of constraints in the optimization models [79]. Both limitations raise important practical implementation questions for these methods.

Alternatively, data-driven [80, 81] and machine learning approaches [82–85] are increasingly used for VVO. Based on the historical data measured on the network, statistical techniques, e.g., regression models, are used in [80, 81] to develop control strategies for VVO. When information of optimal control settings (i.e., data labels) are available in addition to historical measurement data, models can be trained to predict near-optimal VVO solutions using supervised learning methods like a support vector machine (SVM) [82] and deep learning methods approaches, e.g., artificial neural network (ANN) [83] and convolution neural network (CNN) [84,85]. While these data-driven and learning-based approaches may be computationally faster than ORPD-based methods as physical network models nor power balance equations are necessary, they do rely on high-quality data, i.e., the prediction accuracy may be degraded by measurement noise or missing data. Further, labelled data with optimal control settings to train learning models may be difficult to collect in practice and may still need to be generated by solving the ORPD models. Significant progresses have been made in reinforcement learning (RL), especially deep reinforcement learning (DRL) techniques, making them applicable for VVO. Conventional voltage-regulating devices and DERs are considered as agents, and the impacts of their settings (i.e., actions) to the distribution network (i.e., the environment) are observed to learn optimal control strategies dynamically adapting to fluctuating demand and DER generation. The distribution network is often considered as a

blackbox, and is either simulated by power flow analyses/solvers (offline training) [86–89], is represented by a surrogate model through a data-driven process [90], or uses real-time data measured on the network (online training) [91]. It is worth noting that among the mentioned RL literature, only [86] considers controls of legacy VVO devices and reactive power of DERs for voltage support, while others focus either on tap changers or DERs but not both. They also suffer from noises in observations, and methods such as in [92] are necessary to improve robustness and to prevent distorted actions of agents. In addition, training steps ranging from a few thousand up to 20,000 are necessary before convergence is reached, and similar to ORPD-based approaches, none of the RL approaches demonstrates the performance on a large-scale distribution network.

1.3.4.2 Proposed methodology in the fourth contribution

An ORPD problem generally include power flow equations in the formulation which makes it nonlinear and nonconvex. It is also an NP-hard problem which is difficult to solve [93]. Our contribution is to propose to move the power flow equations out of the optimization problem, and use a power flow solver as a blackbox to solve the problem by blackbox optimization (BBO) [94]. The VVO strategy obtained minimizes the expected losses on the network while maintaining all voltage levels within a desired range using a scenario-based BBO reformulation of the problem. The derived solution sustains various demand and DER generation scenarios such that device settings do not need to be constantly changed, making the solution practical for utilities to implement on their networks.

1.4 Structure of the dissertation

In the first chapter so far, we have introduced the motivations and the objectives of the dissertation. The four contributions as well as literature review of related work are also presented. Each contribution is discussed in details in one of the following chapters. To be specific, in Chapter 2, we present the development of a rapid estimation method to analyze the impacts of GETs on the distribution networks at a range of penetration rates. In Chapter 3, we discuss how EV charging patterns can be inferred from the smart meter data using a mixed-integer convex program, and the results serve as input data to the stochastic impact analyses of EVs when such data are not readily available to utilities. In Chapter 4, we formulate an optimization problem to mitigate equipment overloading issues due to EV charging, and we discuss how to efficiently solve it and the mitigation strategy can be designed based on the solution. In Chapter 5, we focus on PVs as the GET type and propose VVO strategies to regulate voltage levels on the network when variations in demand and PV

generation exist. In Chapters 2, 4, and 5, we use the IEEE-8500 node test feeder which is a large-scale and unbalanced distribution network to demonstrate our methodologies. Finally, we conclude in Chapter 6 by summarizing the research work and discussing potential future work and extensions to the contributions achieved in this dissertation.

1.5 Publications and presentations related to the dissertation

This dissertation has lead to the publication of two journal papers and one conference paper, and upcoming submission of two journal papers.

Accepted journal papers

J1. **Feng Li**, Élodie Campeau, Ilhan Kocar, and Antoine Lesage-Landry. Inferring electric vehicle charging patterns from smart meter data for impact studies. *Electric Power Systems Research*, 235 (2024): 110789.

J2. **Feng Li**, Ilhan Kocar, and Antoine Lesage-Landry. A Rapid Method for Impact Analysis of Grid-edge Technologies on Power Distribution Networks, *IEEE Transactions on Power Systems*. vol. 39, no. 1, pp. 1530-1542, Jan. 2024.

Journal papers under review or to be submitted

J3. **Feng Li**, Ilhan Kocar, and Antoine Lesage-Landry. Volt-var Optimization and Optimal Settings for Smart Inverters Using Blackbox Optimization, *IEEE Transactions on Smart Grid*. 2024. (Under review)

J4. **Feng Li**, Ilhan Kocar, and Antoine Lesage-Landry. Convex Reformulation of Bi-Level Optimization for Mitigating Electric Vehicle Charging Overloads in Distribution Systems, *IEEE Transactions on Industrial Informatics*. 2024. (To be submitted)

Conference papers

C1. **Feng Li**, Ilhan Kocar, and Antoine Lesage-Landry. Mitigation of Equipment Overloads due to Electric Vehicles Considering Customer Incentives. *2023 IEEE Power & Energy Society General Meeting (PESGM)*, July 2023.

Talks and presentations

T1. Inferring Electric Vehicle Charging Patterns from Smart Meter Data for Impact Studies. *23rd Power Systems Computation Conference (PSCC 2024)*, Paris, France, 2024.

T2. Mixed-Integer Convex Optimization to Infer Electric Vehicle Charging Patterns for Impact Studies. *Optimization Days (JOPT 2024)*, Montreal, Canada, 2024.

T3. Mitigating Power Network Equipment Overloads due to Electric Vehicle Charging Using Customer Incentives. *Optimization Days (JOPT 2023)*, Montreal, Canada, 2023.

CHAPTER 2 A RAPID METHOD FOR IMPACT ANALYSIS OF GRID-EDGE TECHNOLOGIES ON POWER DISTRIBUTION NETWORKS

2.1 Introduction

Grid-edge technologies (GETs), e.g., plug-in electric vehicles (EVs), rooftop photovoltaic systems (PVs), demand response (DR) programs, etc., are being installed at customers' sites (edges of the grid) from which they are connected to the power distribution networks. With the on-going energy transition, the number of GETs is rapidly growing. It becomes critical to assess their influence on the distribution network in order to maintain system reliability and power quality, and to avoid service interruptions. As changes to customers' power demands (*load offset*) due to the use of GETs are behind-the-meter and are stochastic in terms of customers' usage behaviours, it is difficult to evaluate their impacts especially at high penetration rates. For example, EV charging may introduce undesired impacts to power networks such as the overloading of key equipment, severe voltage variations, phase unbalancing, harmonic distortions, etc. [1, 2]. Various uncertain factors such as charging locations of EVs, charging time and duration, charging power, and battery capacities, must be properly modelled to perform an impact analysis to evaluate the network states with different penetration levels of EVs installed. The analysis should be extended to other GETs than EVs, and combined impacts should be studied when multiple types of GETs are installed to the same power network.

In this chapter, our objective is to develop a model which can characterize the evolution of network state PDFs in terms of the uncertainties of GETs while the penetration rate is taken as a parameter. Such a model can be derived from the Fokker-Planck Equation (FPE). In [95], an advection equation which is a simplified FPE is used to describe the evolution of temperature PDFs for a group of thermostatically controlled loads (TCLs). In [96], the FPE is modelled and is solved to describe the probability of power network stability over time under perturbations. We propose a rapid estimation method (denoted as REM hereinafter) based on FPE to perform a stochastic analysis on the impact of EVs and PVs to power distribution networks. The REM approach provides a rapid assessment of the network states at a wide range of penetration levels. It also indicates concentrated areas where GETs are installed on the network, and network sections susceptible to abnormal conditions, e.g., equipment overloading and under/over-voltages, at any given penetration level. Results from the REM can also identify the maximum penetration level possible that can be hosted by each network section for the network to operate securely. Conversely, the REM approach

permits to determine the penetration level at which network expansion and/or mitigation actions are required.

The rest of the chapter is organized as follows: in Section 2.2 the REM approach to perform a stochastic impact analysis based on FPE is presented. The solution to the FPE model characterizes the evolution of equipment loading levels and voltage levels on the network with the GET penetration rate. In Section 2.3, a numerical method to solve the FPE model is briefly introduced, where details of the numerical method can be found in Appendix A. To improve the accuracy of the solution, a calibration method is also proposed in this section. Section 2.4 demonstrates the performance of the REM by evaluating the impacts of EVs on the modified IEEE-8500 test feeder. Finally the conclusion is made in Section 2.5 along with some future work directions pointed out.

2.2 Stochastic impact analysis model

In this section, the REM model for the stochastic impact analysis of EVs/PVs is proposed.

2.2.1 Assumptions

In line with the general assumptions of this dissertation outlined in Section 1.2, we assume that the following information is provided. This information can often be obtained from statistical surveys or socio-economic analysis [38–40].

- Quantity probability $\Pr^{i}_{\mathrm{num},k}(n) \in [0,1]$ which specifies the probabilities of any customer $i \in \{1, 2, \cdots, N_{\mathrm{m}}\}$ of customers having $n \in \mathbb{N}_0 = \{0, 1, \cdots\}$ GET k devices where N_{m} is the total number of customers and $k \in \{\mathrm{EV}, \mathrm{PV}\}$.
- A set of load offset profiles $\mathcal{L}_k$ for GET k containing L_k profiles, i.e., $\mathcal{L}_k = \{l^j_k(t)\}_{j=1,2,\cdots,L_k}$, where $l^j_k(t)$ is an EV charging or a PV generation profile for time $t \in \mathcal{T} = \{1, 2, \cdots, T\}$, and L_k is the total number of profiles. The diversity of $\mathcal{L}_k$ characterizes different usage patterns of EVs and PVs.
- Probabilities $\Pr^{i}[\mathcal{L}_k] \in [0,1]^{L_k}$ attached to customer i to adopt a load offset profile j in $\mathcal{L}_k$.

Based on the given data, the REM approach is formulated in the next section which provides PDFs of network states (equipment loading level and node/bus voltage level) at any penetration level of EVs and PVs without performing repetitive power flow analysis to the network.

In some work such as [97], the penetration rate is defined as the ratio of the number of GET devices in service to the total number of GET devices on the network. This definition is not applicable to our analysis because we do not know the total number of GET devices on the network. However, we do know the total number of customers/meters on the network. Hence in this chapter and the rest of the dissertation, the penetration rate is defined as the ratio of the number of GET devices to the total number of customers/meters on the distribution network.

Definition 2.1 (Penetration rate)**.** *The penetration rate p_k for GET k is defined as*

$$p_k \triangleq \frac{T_k}{N_m} = \frac{n_k + n_k^0}{N_m}, \tag{2.1}$$

where N_m is the total number of customers/meters on the network, T_k is the number of GET k devices, n_k^0 is the number of GET k devices already existing on the network, and n_k is the number of devices that are required to add in order to reach p_k. The initial penetration rate of GET k of the network is therefore $p_k^0 = \frac{n_k^0}{N_m}$.

Note that the definition is somewhat similar to that adopted in [98], but we extend it to consider the case in which some GET k devices may already exist on the network (i.e., $p_k^0 > 0$). When simultaneous impacts of multiple GET types are studied, a separate penetration rate should be defined for each GET type. By this definition, p_k can exceed 100%, which indicates that *on average* each customer has more than one device of GET type k. While other forms of penetration rate are available, e.g., percentage of technology power over the total power that can be hosted by the network as in [99], our definition is more practical to utilities. The number of total customers on the network is not only known information to the utilities, but also the value stays relatively stable with time even in the long term, making it easier for utilities to set the penetration rate as an analysis parameter.

For simplicity, when referring to one GET type, the subscript k in the penetration rate is dropped from hereinafter, unless stated otherwise.

2.2.2 Stochastic model

Let $x \in \mathbb{R}$ denote a network state of interests, whether the loading level of a network equipment or the voltage level of a network node/bus. The following general model is proposed here to describe the network state when GET k devices are installed to the network with respect to p:

$$\mathrm{d}x = u(x,p)\mathrm{d}p + \sigma(x,p)\mathrm{d}W_p, \tag{2.2}$$

where W_p is a Wiener process indexed by p. The term $u(x,p)$ is the drift velocity of the network state under the influence of EVs/PVs, and $\sigma(x,p) > 0$ denotes the magnitude of the additive disturbances.

Due to the presence of the Wiener process, the trajectory $x(p)$ does not have an analytical form, but given an initial network state $x(p^0)$, one can generate a single trajectory by the numerical integration of (2.2) [100]. To study the stochastic behaviour, one can further generate a large set of trajectories and construct a histogram of x at each p to approximate the PDF of x at p, denoted as $m(x,p)$. This approach is similar to Monte Carlo which is computationally heavy. Therefore, we derive a method that can directly describe the propagation of $m(x,p)$ with the penetration rate. To obtain such a method, the Fokker-Planck equation [101] can be used:

$$\frac{\partial m(x,p)}{\partial p} + \frac{\partial}{\partial x}\Big\{m(x,p)u(x,p)\Big\} = \frac{\partial^2}{\partial x^2}\Big\{m(x,p)d(x,p)\Big\}, \tag{2.3}$$

subject to $m_0 = m(x,p^0)$. Here, $d(x,p) = \sigma(x,p)^2/2$ is the diffusion velocity. It can be generally assumed that the magnitude of additive disturbances to the network states due to GETs is much smaller than the magnitude of the drift velocity, i.e., $\sigma(x,p) \ll |u(x,p)|$. Hence, we assume that the diffusion velocity is a small constant, i.e., $d(x,p) \triangleq d, \forall x,p$. We can then rewrite (2.3) as

$$\frac{\partial m(x,p)}{\partial p} + \frac{\partial}{\partial x}\{m(x,p)u(x,p)\} = d\frac{\partial^2 m(x,p)}{\partial x^2}. \tag{2.4}$$

To solve (2.4) for the propagation of $m(x,p)$, the drift term $u(x,p)$ must first be computed. The term depends on what network state x is describing, either the loading level of a device/equipment or the voltage level of a bus/node. In the following sections, we describe how $u(x,p)$ can be computed based on the stochastic data of customer's quantity probability $\Pr^i_{\text{num},k}[\mathbb{N}_0]$, load offset profiles $\mathcal{L}_k$, and customer's adoption probability $\Pr[\mathcal{L}_k]^i$.

2.2.3 Drift velocity of loading level

Let $m(x,p)$ refer to the PDF of equipment loading level x at penetration rate p. For equipment on distribution networks, the loading level is computed by-phase, hence we denote $x = z^\phi_{e,k}(p)$ as the loading level of equipment e on phase $\phi \in \{a,b,c\}$ when devices of GET k are to be added to the network. The drift velocity, therefore, is the derivative of $z^\phi_{e,k}(p)$ with respect to p. Let $z^\phi_e(p^0)$ be the initial loading level of e without installing additional GET k devices other than those already existing on the network (which represent the penetration

rate p^0). The value of $z_e^\phi(p^0)$ can be obtained from the power flow solution of the network. For a given technology k, let $g_{e,k}^\phi(p)$ denote the change of loading level on phase ϕ with respect to p. We can express $z_{e,k}^\phi(p)$ as devices of GET k are installed in the network by the following equation.

$$z_{e,k}^\phi(p) = z_e^\phi(p^0) + g_{e,k}^\phi(p). \tag{2.5}$$

The term $g_{e,k}^\phi(p)$ can be expressed as:

$$g_{e,k}^\phi(p) = \operatorname{sgn}(k)\frac{n_k(p)\Pr_{e,k}^\phi(p)\mathbb{E}[S_{e,k}^\phi] + \mathbb{E}[\Delta S_{e,\text{loss}}^\phi(p)]}{S_e^\phi}. \tag{2.6}$$

Here, $\operatorname{sgn}(k)$ is a sign function where $\operatorname{sgn}(k) = 1$ if GET k consumes active power and $\operatorname{sgn}(k) = -1$ otherwise, $n_k(p) = N_\text{m}p - n_k^0$ by (2.1), $\Pr_{e,k}^\phi(p)$ is the probability that GET k devices are installed to sections downstream of e on the desired phase ϕ, $\mathbb{E}[S_{e,k}^\phi] \in \mathbb{R}$ is the expected apparent load offset (in kVA) of one GET k device installed downstream of e and on phase ϕ, $\mathbb{E}[\Delta S_{e,\text{loss}}^\phi(p)] \in \mathbb{R}$ is the expected change of network losses (in kVA) of all sections downstream of e on ϕ from adding GET k devices, and $S_e^\phi \in \mathbb{R}$ is the rated power (in kVA) of e on ϕ which is assumed given. For certain equipment whose S_e^ϕ is expressed in amperes (e.g., overhead lines or switches), their S_e^ϕ can be converted into kVA by multiplying the nominal voltage. The first term in (2.6)'s numerator can be interpreted as the expected apparent power contributed by GET k devices. We simplify (2.6) by assuming $\mathbb{E}[\Delta S_{e,\text{loss}}^\phi(p)] \ll n_k(p)\Pr_{e,k}^\phi(p)\mathbb{E}[S_{e,k}^\phi]$. To see this, let $\mathbb{E}[I_{e,k}^\phi] \in \mathbb{R}$ and $\mathbb{E}[I_{l,k}^\phi] \in \mathbb{R}$ be the expected currents *contributed by* GET k flowing through e and through each section l downstream of e on ϕ, respectively, $\mathbb{E}[V_{e,k}^\phi] \in \mathbb{R}$ be the expected voltage of e on ϕ, and $\mathbb{E}[\delta V_{l,k}^\phi] \in \mathbb{R}$ be the expected voltage drop on section l. Hence, we have

$$n_k(p)\Pr_{e,k}^\phi(p)\mathbb{E}[S_{e,k}^\phi] = \mathbb{E}[V_{e,k}^\phi]\mathbb{E}[I_{e,k}^\phi], \tag{2.7}$$

and

$$\begin{aligned}\mathbb{E}[\Delta S_{e,\text{loss}}^\phi(p)] &= \textstyle\sum_l \mathbb{E}[I_{l,k}^\phi]\mathbb{E}[\delta V_{l,k}^\phi] \\ &\le \textstyle\sum_l \mathbb{E}[I_{l,k}^\phi]\overline{\delta V} \\ &= \overline{\delta V}\textstyle\sum_l \mathbb{E}[I_{l,k}^\phi],\end{aligned} \tag{2.8}$$

where $\overline{\delta V}$ is an upper bound of the voltage drops for all sections. Given that in general $\overline{\delta V} \ll \mathbb{E}[V_{e,k}^\phi]$ and $\sum_l \mathbb{E}[I_{l,k}^\phi] \approx \mathbb{E}[I_{e,k}^\phi]$ if phase angles of currents are similar, we can establish

$\mathbb{E}[\Delta S^{\phi}_{e,\text{loss}}(p)] \ll n_k(p)\Pr^{\phi}_{e,k}(p)\mathbb{E}[S^{\phi}_{e,k}]$ by (2.7) and (2.8). Hence $g^{\phi}_{e,k}$ can be approximated by,

$$g^{\phi}_{e,k}(p) \approx \text{sgn}(k)\frac{n_k(p)\Pr^{\phi}_{e,k}(p)\mathbb{E}[S^{\phi}_{e,k}]}{S^{\phi}_{e}}. \tag{2.9}$$

By (2.5), we have $\frac{\mathrm{d}}{\mathrm{d}p}\left(z^{\phi}_{e,k}(p)\right) = \frac{\mathrm{d}}{\mathrm{d}p}\left(g^{\phi}_{e,k}(p)\right)$. To obtain an analytical form of $\frac{\mathrm{d}}{\mathrm{d}p}\left(g^{\phi}_{e,k}(p)\right)$, $\Pr^{\phi}_{e,k}(p)$ and $\mathbb{E}[S^{\phi}_{e,k}]$ need to be computed.

2.2.3.1 Computation of $\Pr^{\phi}_{e,k}(p)$

To derive an analytical form for $\Pr^{\phi}_{e,k}(p)$, we first denote $\mathcal{K}$ as the set of all customers, and let $\mathcal{K}^{\phi}_{e} = \{i \in \mathcal{K} \mid i \text{ is downstream of } e \text{ and on phase } \phi\}$ be the set of customers who are downstream of equipment e on phase ϕ. Suppose for now that n^i_k, the number of GET k devices allocated to customer i at any p, is proportional to their expected number of GET devices, which is $\mathbb{E}[n^i_k] = \sum_{n=0,1,\ldots} n\Pr^{i}_{\text{num},k}(n)$. We have,

$$n^i_k(p) = \begin{cases} n_k(p)\dfrac{\mathbb{E}[n^i_k]}{\sum_{i\in\mathcal{K}}\mathbb{E}[n^i_k]}, & \text{if } p < \overline{p}^i_k, \\ \overline{n}^i_k, & \text{if } p \geq \overline{p}^i_k. \end{cases} \tag{2.10}$$

Here, $\overline{n}^i_k = \text{argmax}_n\{\Pr^{i}_{\text{num},k}(n) > 0\}$ is the maximum number of devices that i is allowed to add, and $\overline{p}^i_k$ is the penetration rate at which $\overline{n}^i_k$ devices would have been added to i. Given that such $\overline{p}^i_k$ may differ from one customer to another, for a given p, some customer, say i, may already have hit the upper bound ($p > \overline{p}^i_k$) while another customer j still has room to add more devices ($p \leq \overline{p}^j_k$). In such a case, the total number of devices actually added to the network (denoted as $\tilde{n}_k$) will be less than the desired n_k.

Let $\Delta n_k(p) = n_k(p) - \tilde{n}_k(p)$ be the gap between the desired n_k and the actual $\tilde{n}_k$ at p, and $\mathcal{K}_{>p,k} = \{i \in \mathcal{K} | p < \overline{p}^i_k\}$ be the set of customers who still have room to add more devices. Then for each $i \in \mathcal{K}_{>p,k}$, we can compute the available room to add more GET k devices, which is $\Delta^i_k = \overline{n}^i_k - n^i_k > 0$. To bridge the gap of Δn_k, each customer in $\mathcal{K}_{>p,k}$ should receive some additional number of devices to n^i_k in (2.10). Such an additional number $n^{i,+}_k$ for $i \in \mathcal{K}_{>p,k}$ is computed by,

$$n^{i,+}_k(p) = \Delta n_k(p)\frac{\Delta^i_k}{\sum_{i\in\mathcal{K}_{>p,k}}\Delta^i_k}.$$

The computed $n^{i,+}_k$ for a customer i never exceeds their available room Δ^i_k because $\Delta n_k \leq \sum_{i\in\mathcal{K}_{>p,k}}\Delta^i_k$. Note that for $i \notin \mathcal{K}_{>p,k}$, $n^{i,+}_k = 0$.

Hence, the number of devices added to customer i can be modified from (2.10) by the following equation,

$$n_k^i(p) = \begin{cases} n_k^{i,\text{old}}(p) + n_k^{i,+}(p), & \text{if } p < \overline{p}_k^i, \\ \overline{n}_k^i, & \text{otherwise,} \end{cases} \tag{2.11}$$

where $n_k^{i,\text{old}}(\text{p})$ is computed by (2.10).

The probability $\Pr_{e,k}^{\phi}(p)$ can then be expressed as the ratio of the total numbers of devices that can be installed to all customers in $\mathcal{K}_e^{\phi}$ over those in $\mathcal{K}$:

$$\Pr_{e,k}^{\phi}(p) = \frac{\sum_{i \in \mathcal{K}_e^{\phi}} n_k^i(p)}{\sum_{i \in \mathcal{K}} n_k^i(p)}. \tag{2.12}$$

2.2.3.2 Calculation of $\mathbb{E}[S_{e,k}^{\phi}]$

Recall that $\mathbb{E}[S_{e,k}^{\phi}]$ is the expected load offset of one GET k device for all customers in $\mathcal{K}_e^{\phi}$. Let $s_k^i(t) \in \mathbb{C}$ be the complex load offset value at time t for 1 GET k device added to i. Based on $\mathcal{L}_k$ and $\Pr[\mathcal{L}_k]^i$, one can compute the expected value of $s_k^i(t)$.

$$\mathbb{E}[s_k^i(t)] = \sum_j l_k^j(t) \Pr(\mathcal{L}_k^i(j)). \tag{2.13}$$

To calculate $\mathbb{E}[S_{e,k}^{\phi}]$, one can sum up $\mathbb{E}[s_k^i(t)]$ for all customers in $\mathcal{K}_e^{\phi}$ and then divided by the number of customers in $\mathcal{K}_e^{\phi}$. Specifically,

$$\mathbb{E}[S_{e,k}^{\phi}] = \frac{1}{|\mathcal{K}_e^{\phi}|} \left| \sum_{i \in \mathcal{K}_e^{\phi}} \mathbb{E}[s_k^i(t)] \right|, \tag{2.14}$$

where $|\mathcal{K}_e^{\phi}|$ is the cardinality of $\mathcal{K}_e^{\phi}$. Note that in (2.14), the magnitude is taken to the summation because $\mathbb{E}[s_k^i(t)]$ may be a complex value.

2.2.4 Calculation of drift velocity of $g_{e,k}^{\phi}(p)$

In the last part, we need to compute $\frac{\mathrm{d}}{\mathrm{d}p}\left(z_e^{\phi}(p)\right)$ which is the drift velocity of $z_e^{\phi}(p)$ with respect to p. By (2.5), $\frac{\mathrm{d}}{\mathrm{d}p}\left(z_e^{\phi}(p)\right) = \frac{\mathrm{d}}{\mathrm{d}p}\left(g_{e,k}^{\phi}(p)\right)$. In the following, we discuss how $\frac{\mathrm{d}}{\mathrm{d}p}\left(g_{e,k}^{\phi}(p)\right)$ can be

computed by taking derivative of (2.6) with respect to p. We have,

$$\begin{aligned}
\frac{\mathrm{d}}{\mathrm{d}p}\left(g_{e,k}^{\phi}(p)\right) &= \frac{\mathrm{d}}{\mathrm{d}p}\left(\frac{n_k(p)\Pr_{e,k}^{\phi}(p)\mathbb{E}[S_k^{\phi}]}{S_e^{\phi}}\right) \\
&= \frac{\mathbb{E}[S_k^{\phi}]}{S_e^{\phi}}\frac{\mathrm{d}}{\mathrm{d}p}\left(n_k(p)\Pr_{e,k}^{\phi}(p)\right) \\
&= \frac{\mathbb{E}[S_k^{\phi}]}{S_e^{\phi}}\left(\frac{\mathrm{d}}{\mathrm{d}p}n_k(p)\Pr_{e,k}^{\phi}(p) + n_k(p)\frac{\mathrm{d}}{\mathrm{d}p}\Pr_{e,k}^{\phi}(p)\right) \\
&= \frac{\mathbb{E}[S_k^{\phi}]}{S_e^{\phi}}\left(N_{\mathrm{m}}\Pr_{e,k}^{\phi}(p) + n_k(p)\frac{\mathrm{d}}{\mathrm{d}p}\Pr_{e,k}^{\phi}(p)\right).
\end{aligned} \tag{2.15}$$

Before computing $\frac{\mathrm{d}}{\mathrm{d}p}\Pr_{e,k}^{\phi}(p)$, we expand the expression in (2.12).

$$\begin{aligned}
\Pr_{e,k}^{\phi}(p) &= \frac{\sum_{i\in\mathcal{K}_e^{\phi}} n_k^i}{\sum_{i\in\mathcal{K}} n_k^i} \\
&= \frac{\sum_{i\in\mathcal{K}_e^{\phi}\cap\mathcal{K}_{>p,k}} n_k^i + \sum_{i\in\mathcal{K}_e^{\phi}\cap(\mathcal{K}_{>p,k})^C} n_k^i}{\sum_{i\in\mathcal{K}_{>p,k}} n_k^i + \sum_{i\in(\mathcal{K}_{>p,k})^C} n_k^i} \\
&= \frac{\sum_{i\in\mathcal{K}_e^{\phi}\cap\mathcal{K}_{>p,k}} n_k^i + \sum_{i\in\mathcal{K}_e^{\phi}\cap(\mathcal{K}_{>p,k})^C} \overline{n}_k^i}{\sum_{i\in\mathcal{K}_{>p,k}} n_k^i + \sum_{i\in(\mathcal{K}_{>p,k})^C} \overline{n}_k^i}.
\end{aligned} \tag{2.16}$$

In (2.16), $(\mathcal{K}_{>p,k})^C$ denotes the complement of $\mathcal{K}_{>p,k}$ which is the set of customers who have reached $\overline{n}_k^i$, the maximum number of GET k devices. Letting a denote the numerator of (2.12), and b the denominator of (2.12), we have

$$\begin{aligned}
a &:= \sum_{i\in\mathcal{K}_e^{\phi}} n_k^i, \\
b &:= \sum_{i\in\mathcal{K}} n_k^i, \text{where both } a \text{ and } b \text{ are functions of } p.
\end{aligned} \tag{2.17}$$

Taking the derivative of (2.16) with respect to p, we have

$$\begin{aligned}
\frac{\mathrm{d}}{\mathrm{d}p}\left(\Pr_{e,k}^{\phi}(p)\right) &= \frac{\mathrm{d}}{\mathrm{d}p}(ab^{-1}) \\
&= b^{-1}\frac{\mathrm{d}a}{\mathrm{d}p} + a\frac{\mathrm{d}}{\mathrm{d}p}\left(b^{-1}\right) \\
&= b^{-1}\frac{\mathrm{d}}{\mathrm{d}p}\left(\sum_{i\in\mathcal{K}_e^{\phi}\cap\mathcal{K}_{>p,k}} n_k^i\right) - ab^{-2}\frac{\mathrm{d}}{\mathrm{d}p}\left(\sum_{i\in\mathcal{K}_{>p,k}} n_k^i\right) \\
&= b^{-1}\sum_{i\in\mathcal{K}_e^{\phi}\cap\mathcal{K}_{>p,k}} \frac{\mathrm{d}}{\mathrm{d}p}\left(n_k^i\right) - ab^{-2}\sum_{i\in\mathcal{K}_{>p,k}} \frac{\mathrm{d}}{\mathrm{d}p}\left(n_k^i\right).
\end{aligned} \tag{2.18}$$

To evaluate the term $\frac{\mathrm{d}}{\mathrm{d}p}\left(n_k^i\right)$ in (2.18) for each individual customer i in $\mathcal{K}_{>p,k}$, we take the derivative of (2.11) with respect to p. Note that the derivative is non-zero only in the first case of (2.11).

$$\begin{aligned}
\frac{\mathrm{d}}{\mathrm{d}p}\left(n_k^i\right) &= \frac{\mathrm{d}}{\mathrm{d}p}\left(n_k^{i,\mathrm{old}} + n_k^{i,+}\right) \\
&= \frac{\mathrm{d}}{\mathrm{d}p}\left(\left(pN_{\mathrm{m}} - n_k^0\right)\frac{\mathbb{E}[n_k^i]}{\sum_{i\in\mathcal{K}}\mathbb{E}[n_k^i]}\right) + \frac{\mathrm{d}}{\mathrm{d}p}\left(n_k^{i,+}\right) \\
&= N_{\mathrm{m}}\frac{\mathbb{E}[n_k^i]}{\sum_{i\in\mathcal{K}}\mathbb{E}[n_k^i]} + \frac{\mathrm{d}}{\mathrm{d}p}\left(\left(n_k - \tilde{n}_k\right)\frac{\Delta_k^i}{\sum_{i\in\mathcal{K}_{>p,k}}\Delta_k^i}\right) \\
&= N_{\mathrm{m}}\frac{\mathbb{E}[n_k^i]}{\sum_{i\in\mathcal{K}}\mathbb{E}[n_k^i]} + \frac{\mathrm{d}}{\mathrm{d}p}\left(n_k - \tilde{n}_k\right)\left(\frac{\Delta_k^i}{\sum_{i\in\mathcal{K}_{>p,k}}\Delta_k^i}\right) \\
&\qquad + \left(n_k - \tilde{n}_k\right)\frac{\mathrm{d}}{\mathrm{d}p}\left(\frac{\Delta_k^i}{\sum_{i\in\mathcal{K}_{>p,k}}\Delta_k^i}\right).
\end{aligned} \tag{2.19}$$

We now evaluate the two derivative terms in (2.19),

$$\begin{aligned}
\frac{\mathrm{d}}{\mathrm{d}p}\left(n_k-\tilde{n}_k\right) &= \frac{\mathrm{d}}{\mathrm{d}p}\left(n_k\right)-\frac{\mathrm{d}}{\mathrm{d}p}\left(\tilde{n}_k\right)\\
&= \frac{\mathrm{d}}{\mathrm{d}p}\left(pN_{\mathrm{m}}-n_k^0\right)-\frac{\mathrm{d}}{\mathrm{d}p}\left(\sum_{i\in\mathcal{K}} n_k^{i,\mathrm{old}}\right)\\
&= N_{\mathrm{m}}-\sum_{i\in\mathcal{K}}\frac{\mathrm{d}}{\mathrm{d}p}\left(n_k^{i,\mathrm{old}}\right)\\
&= N_{\mathrm{m}}-\sum_{i\in\mathcal{K}_{>p,k}}\frac{\mathrm{d}}{\mathrm{d}p}\left(n_k^{i,\mathrm{old}}\right)-\sum_{i\in(\mathcal{K}_{>p,k})^C}\frac{\mathrm{d}}{\mathrm{d}p}\left(n_k^{i,\mathrm{old}}\right)\\
&= N_{\mathrm{m}}-\sum_{i\in\mathcal{K}_{>p,k}}\frac{\mathrm{d}}{\mathrm{d}p}\left(n_k^{i,\mathrm{old}}\right)-\sum_{i\in(\mathcal{K}_{>p,k})^C}\frac{\mathrm{d}}{\mathrm{d}p}\left(\overline{n}_k^{i}\right)\\
&= N_{\mathrm{m}}-\sum_{i\in\mathcal{K}_{>p,k}}\frac{\mathrm{d}}{\mathrm{d}p}\left(n_k^{i,\mathrm{old}}\right)\\
&= N_{\mathrm{m}}-\frac{N_{\mathrm{m}}}{\sum_{i\in\mathcal{K}}\mathbb{E}[n_k^i]}\sum_{i\in\mathcal{K}_{>p,k}}\mathbb{E}[n_k^i],
\end{aligned} \tag{2.20}$$

and,

$$\begin{aligned}
\frac{\mathrm{d}}{\mathrm{d}p}\left(\frac{\Delta_k^i}{\sum_{i\in\mathcal{K}_{>p,k}}\Delta_k^i}\right) &= \frac{\frac{\mathrm{d}}{\mathrm{d}p}\left(\Delta_k^i\right)}{\sum_{i\in\mathcal{K}_{>p,k}}\Delta_k^i}-\frac{\Delta_k^i}{\left(\sum_{i\in\mathcal{K}_{>p,k}}\Delta_k^i\right)^2}\frac{\mathrm{d}}{\mathrm{d}p}\left(\sum_{i\in\mathcal{K}_{>p,k}}\Delta_k^i\right)\\
&= \frac{\frac{\mathrm{d}}{\mathrm{d}p}\left(\Delta_k^i\right)}{\sum_{i\in\mathcal{K}_{>p,k}}\Delta_k^i}-\frac{\Delta_k^i}{\left(\sum_{i\in\mathcal{K}_{>p,k}}\Delta_k^i\right)^2}\sum_{i\in\mathcal{K}_{>p,k}}\frac{\mathrm{d}}{\mathrm{d}p}\left(\Delta_k^i\right),
\end{aligned} \tag{2.21}$$

where,

$$\begin{aligned}
\frac{\mathrm{d}}{\mathrm{d}p}\left(\Delta_k^i\right) &= \frac{\mathrm{d}}{\mathrm{d}p}\left(\overline{n}_k^i-n_k^{i,\mathrm{old}}\right)\\
&= -\frac{\mathrm{d}}{\mathrm{d}p}\left(n_k^{i,\mathrm{old}}\right)\\
&= -N_{\mathrm{m}}\frac{\mathbb{E}[n_k^i]}{\sum_{i\in\mathcal{K}}\mathbb{E}[n_k^i]}
\end{aligned} \tag{2.22}$$

Hence by (2.19)−(2.22), we can compute $\frac{\mathrm{d}}{\mathrm{d}p}\left(n_k^i\right)$ for $i\in\mathcal{K}_{>p,k}$. By (2.18), we can compute $\frac{\mathrm{d}}{\mathrm{d}p}\left(\mathrm{Pr}_{e,k}^{\phi}(p)\right)$, and finally by (2.15) we can compute $\frac{\mathrm{d}}{\mathrm{d}p}\left(g_e^{\phi}(p)\right)$ which is the drift velocity u of the probability distribution of loading level x. The above derivations also establish that u depends only on the penetration rate p and not on x.

2.2.5 Drift velocity of voltage level

As GET devices are added to the distribution network, voltage levels will be affected. For example, undervoltage conditions are likely to happen to areas with a high penetration rate of EVs, whereas overvoltage conditions may occur where high penetration levels of distributed energy resources (e.g., PVs) are installed on the network. In this section, the computation of the drift velocity $u(x, p)$ is outlined, where $m(x, p)$ is the PDF of voltage level x at various penetration rate p. Unless specified otherwise, all complex variables in this section refer to per-unit values.

We first consider a simple case where *one* GET k device is installed to a customer. We can then compute the current injected by such GET k device, Δi, by the following equation, from which the change of voltage of this customer can be approximated,

$$\Delta i = \frac{\Delta v}{z_{\text{th}}} \approx \left(\frac{\Delta S}{v}\right)^*, \tag{2.23}$$

where $v \in \mathbb{C}$ is the customer's voltage before installing the GET device, $z_{\text{th}} \in \mathbb{C}$ is the equivalent network impedance at the customer's location, $\Delta S \in \mathbb{C}$ is the complex power of the GET device, and $\Delta v \in \mathbb{C}$ is the change of voltage after installing the GET device. The $*$ operator denotes the complex conjugate.

It should be noted that Δv in (2.23) is an approximated value for the following two reasons:

1. The equivalent impedance z_{th} is assumed to be computed from a linearized network. In reality, the distribution network is not fully linear (due to load/generation models, tap changers, and voltage-controlled devices, etc.).

2. Even if the network is fully linear, the current injected by the GET device is non-linear because it depends on the voltage $(v+\Delta v)$ after the GET device is connected. However, on (2.23)'s right-hand side, the voltage v before adding GET devices is used, thus any voltage difference is neglected.

Model (2.23) can be extended to simultaneously installing multiple GET devices to multiple customers in a matrix form,

$$\begin{aligned} \Delta \mathbf{v}(p) &= \mathbf{Z}\Delta \mathbf{i}(p) \\ &= \left[\Delta v_{o,k}^{\phi}(p), o = 1, 2, \cdots, N, \phi = a, b, c\right]^\top, \end{aligned} \tag{2.24}$$

where $\Delta \mathbf{v} \in \mathbb{C}^{3N}$ is the voltage change of all N nodes of the network, and $\Delta \mathbf{i} \in \mathbb{C}^{3N}$ is the vector of currents injected to each node due to the GET devices installed. It is assumed that

each node is three-phase, and for a non-connected phase, the voltage and current injection are zero. The matrix $\mathbf{Z} \in \mathbb{C}^{3N\times 3N}$ is the sensitivity impedance of voltage with respect to current injection, which can be computed from the modified augmented nodal analysis (MANA) formulation [102, 103].

2.2.6 Computation of Z

For a given network $\mathcal{N}$, let $\mathbf{A} \in \mathbb{C}^{(3N+M)\times(3N+M)}$ be the full MANA matrix formulated for the network, where $N = |\mathcal{N}|$ is the number of network nodes, and M is the number of "augmented" nodes. We partition $\mathbf{A}$ into the a 2×2 form, i.e., $\mathbf{A} = \begin{bmatrix} \mathbf{A}_{11} & \mathbf{A}_{12} \\ \mathbf{A}_{21} & \mathbf{A}_{22} \end{bmatrix}$ where $\mathbf{A}_{11} \in \mathbb{C}^{3N\times 3N}$, $\mathbf{A}_{12} \in \mathbb{C}^{3N\times M}$, $\mathbf{A}_{21} \in \mathbb{C}^{M\times 3N}$, and $\mathbf{A}_{22} \in \mathbb{C}^{M\times M}$.

In the MANA formulation we have,

$$\begin{aligned} \mathbf{A}\mathbf{x} &= \mathbf{b}, \\ \begin{bmatrix} \mathbf{A}_{11} & \mathbf{A}_{12} \\ \mathbf{A}_{21} & \mathbf{A}_{22} \end{bmatrix} \begin{bmatrix} \mathbf{v}_1 \\ \mathbf{x}_2 \end{bmatrix} &= \begin{bmatrix} \mathbf{i}_1 \\ \mathbf{b}_2 \end{bmatrix}, \end{aligned} \tag{2.25}$$

where $\mathbf{x} = \left[\mathbf{v}_1^\top, \mathbf{x}_2^\top\right]^\top$ and $\mathbf{b} = \left[\mathbf{i}_1^\top, \mathbf{b}_2^\top\right]^\top$. Here, $\mathbf{v}_1 \in \mathbb{C}^{3N}$ comprises nodal three-phase voltages of the network, $\mathbf{x}_2 \in \mathbb{C}^M$ represents source currents, dependent currents, switch currents, etc., $\mathbf{i}_1 \in \mathbb{C}^{3N}$ is the current injection vector, and $\mathbf{b}_2 \in \mathbb{C}^M$ contains voltage source values and zero elements. As GET devices are added to the network, variations are introduced to $\mathbf{x}$ and $\mathbf{b}$, and (2.25) can be written in terms of such variations:

$$\begin{bmatrix} \mathbf{A_{11}} & \mathbf{A_{12}} \\ \mathbf{A_{21}} & \mathbf{A_{22}} \end{bmatrix} \begin{bmatrix} \Delta\mathbf{v_1} \\ \Delta\mathbf{x_2} \end{bmatrix} = \begin{bmatrix} \Delta\mathbf{i_1} \\ \Delta\mathbf{b_2} \end{bmatrix}. \tag{2.26}$$

Note that here, $\Delta\mathbf{v_1}$ and $\Delta\mathbf{i_1}$ are identical to $\Delta\mathbf{v}$ and $\Delta\mathbf{i}$ in (2.24), respectively, and a subscript is added for clarity. If we assume that source voltage values remain constant before and after adding GET devices, we have $\Delta\mathbf{b_2} = \mathbf{0}$. From (2.26), we then have the following two equations,

$$\mathbf{A}_{11}\Delta\mathbf{v}_1 + \mathbf{A}_{12}\Delta\mathbf{x}_2 = \Delta\mathbf{i}_1 \tag{2.27}$$

$$\mathbf{A}_{21}\Delta\mathbf{v}_1 + \mathbf{A}_{22}\Delta\mathbf{x}_2 = \mathbf{0}. \tag{2.28}$$

Solving for $\Delta\mathbf{x}_2$ in (2.28) and inserting it into (2.27) yields,

$$\left(\mathbf{A}_{11} - \mathbf{A}_{12}\mathbf{A}_{22}^{-1}\mathbf{A}_{21}\right)\Delta\mathbf{v}_1 = \Delta\mathbf{i}_1. \tag{2.29}$$

Comparing (2.29) to (2.24), we have,

$$\mathbf{Z} = \left(\mathbf{A}_{11} - \mathbf{A}_{12}\mathbf{A}_{22}^{-1}\mathbf{A}_{21}\right)^{-1}. \tag{2.30}$$

2.2.7 Calculation of $\Delta\mathbf{i}(p)$

When multiple GET devices are connected to a node o, the current injected to o on phase ϕ, which is a single element of $\Delta\mathbf{i}$, can be computed using:

$$\Delta i_{o,k}^{\phi}(p) \approx n_k(p)\,\mathrm{Pr}_{o,k}^{\phi}(p)\left(\frac{\mathbb{E}[S_{o,k}^{\phi}]}{v_o^{\phi}(p^0)}\right)^*, \tag{2.31}$$

where $\mathrm{Pr}_{o,k}^{\phi}(p)$ is the probability of a GET k device directly installed to o on phase ϕ, $\mathbb{E}[S_{o,k}^{\phi}]$ is the expected load offset of a GET k device directly connected to o on ϕ, and $v_o^{\phi}(p^0)$ is the initial phase voltage of node o on phase ϕ which can be obtained from a power flow analysis.

To derive the analytical forms of $\mathrm{Pr}_{o,k}^{\phi}(p)$ and $\mathbb{E}[S_{o,k}^{\phi}]$, let $\mathcal{K}_o^{\phi}$ be the set of customers who are directly connected to node o and on phase ϕ. Then $\mathrm{Pr}_{o,k}^{\phi}(p)$ can be computed in a similar way as in (2.12), such that,

$$\mathrm{Pr}_{o,k}^{\phi}(p) = \frac{\sum_{i\in\mathcal{K}_o^{\phi}} n_k^i(p)}{\sum_{i\in\mathcal{K}} n_k^i(p)},$$

where $n_k^i(p)$ is given by (2.11). Recall that $\mathcal{K}$ is the set of all customers on the network. The expected load offset $\mathbb{E}[S_{o,k}^{\phi}]$ can be obtained from (2.14) where $\mathcal{K}_e^{\phi}$ is replaced by $\mathcal{K}_o^{\phi}$.

Having computed the current injection to each node on each phase from (2.31), we can construct the column vector $\Delta\mathbf{i}(p)$ by,

$$\Delta\mathbf{i}(p) = \left[\Delta i_{o,k}^{\phi}(p), o = 1, 2, \cdots, N, \phi = a, b, c\right]^{\top}.$$

Using the resulting $\Delta\mathbf{i}(p)$ in (2.24), we can obtain the column vector $\Delta\mathbf{v}(p)$ which has the voltage changes to all nodes on all phases. The voltage of node o on phase ϕ can be written as,

$$v_{o,k}^{\phi}(p) \triangleq v_o^{\phi}(p^0) + \Delta v_{o,k}^{\phi}(p).$$

As x refers to the voltage level and $v_{o,k}^{\phi}(p)$ is the per-unit voltage in phasor, we let $x = |v_{o,k}^{\phi}(p)|$, and the drift velocity of x can be analytically computed by taking the derivative of $|v_{o,k}^{\phi}(p)|$

with respect to p. To derive the analytical expression for the derivative for node o on ϕ, we first denote $\mathbf{z}_o^\phi \in \mathbb{C}^{1\times 3N}$ as corresponding row in $\mathbf{Z}$, hence,

$$\begin{aligned} v_{o,k}^\phi(p) &= v_o^\phi(p^0) + \Delta v_{o,k}^\phi(p) \\ &= v_o^\phi(p^0) + \mathbf{z}_o^\phi \Delta\mathbf{i}(p). \end{aligned}$$

We then write the explicit vector form of $\mathbf{z}_o^\phi$ and $\Delta\mathbf{i}(p)$, respectively, where

$$\begin{aligned} \mathbf{z}_o^\phi &= [z_1, z_2, \cdots, z_n, \cdots, z_{3N}] \\ \Delta\mathbf{i}(p) &= [\Delta i_1, \Delta i_2, \cdots, \Delta i_n, \cdots, \Delta i_{3N}]^\top, \end{aligned}$$

where n is a generic index of a node on a specific phase. It is remarked that the dependency of p in each Δi_n and the subscript k are omitted for simplicity of notation. The magnitude of $v_{o,k}^\phi(p)$ can be expressed by the following:

$$\begin{aligned} \left|v_{o,k}^\phi(p)\right| &= \left|v_o^\phi(p^0) + \mathbf{z}_o^\phi \Delta\mathbf{i}(p)\right| \\ &= \left|v_o^\phi(p^0) + \sum_{n=1}^{3N} z_n \Delta i_n\right| \\ &= \left|v_{o,\mathrm{R}}^\phi(p^0) + jv_{o,\mathrm{I}}^\phi(p^0) + \sum_{n=1}^{3N} \Delta v_{n,\mathrm{R}} + j\Delta v_{n,\mathrm{I}}\right| \\ &= \left|\left(v_{o,\mathrm{R}}^\phi(p^0) + \sum_{n=1}^{3N} \Delta v_{n,\mathrm{R}}\right) + j\left(v_{o,\mathrm{I}}^\phi(p^0) + \sum_{n=1}^{3N} \Delta v_{n,\mathrm{I}}\right)\right| \\ &= \left(\left(v_{o,\mathrm{R}}^\phi(p^0) + \sum_{n=1}^{3N} \Delta v_{n,\mathrm{R}}\right)^2 + \left(v_{o,\mathrm{I}}^\phi(p^0) + \sum_{n=1}^{3N} \Delta v_{n,\mathrm{I}}\right)^2\right)^{\frac{1}{2}}. \end{aligned} \tag{2.32}$$

In (2.32), we write $v_o^\phi(p^0)$ and $z_n\Delta i_n$ in rectangular forms, i.e., $v_o^\phi(p^0) = v_{o,\mathrm{R}}^\phi(p^0) + jv_{o,\mathrm{I}}^\phi(p^0)$ and $z_n\Delta i_n = \Delta v_{n,\mathrm{R}} + j\Delta v_{n,\mathrm{I}}$. To determine the expressions for p-dependent terms $\Delta v_{n,\mathrm{R}}$ and $\Delta v_{n,\mathrm{I}}$, we also write z_n and Δi_n in rectangular forms where $z_n = z_{n,\mathrm{R}} + jz_{n,\mathrm{I}}$ and $\Delta i_n = \Delta i_{n,\mathrm{R}} + j\Delta i_{n,\mathrm{I}}$, respectively. We then obtain:

$$\begin{aligned} z_n\Delta i_n &= \Delta v_{n,\mathrm{R}} + j\Delta v_{n,\mathrm{I}} \\ &= (z_{n,\mathrm{R}} + jz_{n,\mathrm{I}})(\Delta i_{n,\mathrm{R}} + j\Delta i_{n,\mathrm{I}}) \\ &= (z_{n,\mathrm{R}}\Delta i_{n,\mathrm{R}} - z_{n,\mathrm{I}}\Delta i_{n,\mathrm{I}}) + j\left(z_{n,\mathrm{R}}\Delta i_{n,\mathrm{I}} + z_{n,\mathrm{I}}\Delta i_{n,\mathrm{R}}\right). \end{aligned}$$

Hence,

$$\begin{aligned}\Delta v_{n,\mathrm{R}} &= z_{n,\mathrm{R}}\Delta i_{n,\mathrm{R}} - z_{n,\mathrm{I}}\Delta i_{n,\mathrm{I}} \\ \Delta v_{n,\mathrm{I}} &= z_{n,\mathrm{R}}\Delta i_{n,\mathrm{I}} + z_{n,\mathrm{I}}\Delta i_{n,\mathrm{R}}.\end{aligned} \tag{2.33}$$

Through (2.31) we can calculate Δi_n and find analytical expressions for $\Delta i_{n,\mathrm{R}}$ and $\Delta i_{n,\mathrm{I}}$, where

$$\begin{aligned}\Delta i_n(p) &= n_k(p)\,\mathrm{Pr}_n(p)\left(\frac{\mathbb{E}[S_n]}{v_n(p^0)}\right)^* \\ &= n_k(p)\,\mathrm{Pr}_n(p)\left(\Re\left(\frac{\mathbb{E}[S_n]}{v_n(p^0)}\right) - j\Im\left(\frac{\mathbb{E}[S_n]}{v_n(p^0)}\right)\right) \\ &= \Delta i_{n,\mathrm{R}} + j\Delta i_{n,\mathrm{I}}.\end{aligned}$$

Recall that $\mathbb{E}[S_n]$ is the expected load offset installed to n and $v_n(p^0)$ is its nodal voltage determined from a power flow analysis at p^0. Therefore,

$$\Delta i_{n,\mathrm{R}} = n_k(p)\,\mathrm{Pr}_n(p)\Re\left(\frac{\mathbb{E}[S_n]}{v_n(p^0)}\right) \tag{2.34}$$

$$\Delta i_{n,\mathrm{I}} = -n_k(p)\,\mathrm{Pr}_n(p)\Im\left(\frac{\mathbb{E}[S_n]}{v_n(p^0)}\right). \tag{2.35}$$

By denoting $A = \left(v^{\phi}_{o,\mathrm{R}}(p^0) + \sum_{n=1}^{3N}\Delta v_{n,\mathrm{R}}\right)^2 + \left(v^{\phi}_{o,\mathrm{I}}(p^0) + \sum_{n=1}^{3N}\Delta v_{n,\mathrm{I}}\right)^2$, (2.32) can be expressed as $\left|v^{\phi}_{o,k}(p)\right| = \sqrt{A}$. The drift velocity is then the derivative of $\left|v^{\phi}_{o,k}(p)\right|$ with respect to p, leading to,

$$\begin{aligned}\frac{\mathrm{d}}{\mathrm{d}p}\left|v^{\phi}_{o,k}(p)\right| &= \frac{1}{2}A^{-\frac{1}{2}}\frac{\mathrm{d}}{\mathrm{d}p}A \\ &= \frac{1}{2}A^{-\frac{1}{2}}\frac{\mathrm{d}}{\mathrm{d}p}\left(\left(v^{\phi}_{o,\mathrm{R}}(p^0) + \sum_{n=1}^{3N}\Delta v_{n,\mathrm{R}}\right)^2 + \left(v^{\phi}_{o,\mathrm{I}}(p^0) + \sum_{n=1}^{3N}\Delta v_{n,\mathrm{I}}\right)^2\right) \\ &= \frac{1}{2}A^{-\frac{1}{2}}\left(2\left(v^{\phi}_{o,\mathrm{R}}(p^0) + \sum_{n=1}^{3N}\Delta v_{n,\mathrm{R}}\right)\frac{\mathrm{d}}{\mathrm{d}p}\left(v^{\phi}_{o,\mathrm{R}}(p^0) + \sum_{n=1}^{3N}\Delta v_{n,\mathrm{R}}\right)\right. \\ &\qquad\left. + 2\left(v^{\phi}_{o,\mathrm{I}}(p^0) + \sum_{n=1}^{3N}\Delta v_{n,\mathrm{I}}\right)\frac{\mathrm{d}}{\mathrm{d}p}\left(v^{\phi}_{o,\mathrm{I}}(p^0) + \sum_{n=1}^{3N}\Delta v_{n,\mathrm{I}}\right)\right) \\ &= A^{-\frac{1}{2}}\left(\left(v^{\phi}_{o,\mathrm{R}}(p^0) + \sum_{n=1}^{3N}\Delta v_{n,\mathrm{R}}\right)\sum_{n=1}^{3N}\frac{\mathrm{d}}{\mathrm{d}p}\Delta v_{n,\mathrm{R}}\right.\end{aligned}$$

$$
\begin{aligned}
&\quad + \left(v_{o,\mathrm{I}}^{\phi}(p^0) + \sum_{n=1}^{3N} \Delta v_{n,\mathrm{I}} \right) \sum_{n=1}^{3N} \frac{\mathrm{d}}{\mathrm{d}p} \Delta v_{n,\mathrm{I}} \Bigg) \\
&= A^{-\frac{1}{2}} \Bigg(\left(v_{o,\mathrm{R}}^{\phi}(p^0) + \sum_{n=1}^{3N} \Delta v_{n,\mathrm{R}} \right) \sum_{n=1}^{3N} \frac{\mathrm{d}}{\mathrm{d}p} \left(z_{n,\mathrm{R}} \Delta i_{n,\mathrm{R}} - z_{n,\mathrm{I}} \Delta i_{n,\mathrm{I}} \right) \\
&\qquad + \left(v_{o,\mathrm{I}}^{\phi}(p^0) + \sum_{n=1}^{3N} \Delta v_{n,\mathrm{I}} \right) \sum_{n=1}^{3N} \frac{\mathrm{d}}{\mathrm{d}p} \left(z_{n,\mathrm{R}} \Delta i_{n,\mathrm{I}} + z_{n,\mathrm{I}} \Delta i_{n,\mathrm{R}} \right) \Bigg) \\
&= A^{-\frac{1}{2}} \Bigg(\left(v_{o,\mathrm{R}}^{\phi}(p^0) + \sum_{n=1}^{3N} \Delta v_{n,\mathrm{R}} \right) \sum_{n=1}^{3N} \left(z_{n,\mathrm{R}} \frac{\mathrm{d}}{\mathrm{d}p} \Delta i_{n,\mathrm{R}} - z_{n,\mathrm{I}} \frac{\mathrm{d}}{\mathrm{d}p} \Delta i_{n,\mathrm{I}} \right) \\
&\qquad + \left(v_{o,\mathrm{I}}^{\phi}(p^0) + \sum_{n=1}^{3N} \Delta v_{n,\mathrm{I}} \right) \sum_{n=1}^{3N} \left(z_{n,\mathrm{R}} \frac{\mathrm{d}}{\mathrm{d}p} \Delta i_{n,\mathrm{I}} + z_{n,\mathrm{I}} \frac{\mathrm{d}}{\mathrm{d}p} \Delta i_{n,\mathrm{R}} \right) \Bigg). \qquad (2.36)
\end{aligned}
$$

Now we derive the expressions for $\frac{\mathrm{d}}{\mathrm{d}p}\Delta i_{n,\mathrm{R}}$ and $\frac{\mathrm{d}}{\mathrm{d}p}\Delta i_{n,\mathrm{I}}$. By taking the derivatives of (2.34) and (2.35), respectively, we get:

$$
\begin{aligned}
\frac{\mathrm{d}}{\mathrm{d}p}\Delta i_{n,\mathrm{R}} &= \frac{\mathrm{d}}{\mathrm{d}p} \left(n_k(p) \Pr_n(p) \Re \left(\frac{\mathbb{E}[S_n]}{v_n(p^0)} \right) \right) \\
&= \Re \left(\frac{\mathbb{E}[S_n]}{v_n(p^0)} \right) \left(\frac{\mathrm{d}}{\mathrm{d}p} n_k(p) \Pr_n(p) + n_k(p) \frac{\mathrm{d}}{\mathrm{d}p} \Pr_n(p) \right) \\
&= \Re \left(\frac{\mathbb{E}[S_n]}{v_n(p^0)} \right) \left(\frac{\mathrm{d}}{\mathrm{d}p} \left(pN_{\mathrm{m}} - n_k^0 \right) \Pr_n(p) + \left(pN_{\mathrm{m}} - n_k^0 \right) \frac{\mathrm{d}}{\mathrm{d}p} \Pr_n(p) \right) \\
&= \Re \left(\frac{\mathbb{E}[S_n]}{v_n(p^0)} \right) \left(N_{\mathrm{m}} \Pr_n(p) + \left(pN_{\mathrm{m}} - n_k^0 \right) \frac{\mathrm{d}}{\mathrm{d}p} \Pr_n(p) \right), \qquad (2.37)
\end{aligned}
$$

and,

$$
\begin{aligned}
\frac{\mathrm{d}}{\mathrm{d}p}\Delta i_{n,\mathrm{I}} &= -\frac{\mathrm{d}}{\mathrm{d}p} \left(n_k(p) \Pr_n(p) \Im \left(\frac{\mathbb{E}[S_n]}{v_n(p^0)} \right) \right) \\
&= -\Im \left(\frac{\mathbb{E}[S_n]}{v_n(p^0)} \right) \left(\frac{\mathrm{d}}{\mathrm{d}p} n_k(p) \Pr_n(p) + n_k(p) \frac{\mathrm{d}}{\mathrm{d}p} \Pr_n(p) \right) \\
&= -\Im \left(\frac{\mathbb{E}[S_n]}{v_n(p^0)} \right) \left(\frac{\mathrm{d}}{\mathrm{d}p} \left(pN_{\mathrm{m}} - n_k^0 \right) \Pr_n(p) + \left(pN_{\mathrm{m}} - n_k^0 \right) \frac{\mathrm{d}}{\mathrm{d}p} \Pr_n(p) \right) \\
&= -\Im \left(\frac{\mathbb{E}[S_n]}{v_n(p^0)} \right) \left(N_{\mathrm{m}} \Pr_n(p) + \left(pN_{\mathrm{m}} - n_k^0 \right) \frac{\mathrm{d}}{\mathrm{d}p} \Pr_n(p) \right). \qquad (2.38)
\end{aligned}
$$

The only undetermined term in (2.37) and (2.38) is $\frac{\mathrm{d}}{\mathrm{d}p} \Pr_n(p)$, which is computed similarly to $\frac{\mathrm{d}}{\mathrm{d}p} \Pr_{e,k}^{\phi}(p)$ in (2.18). Recall that $\mathcal{K}$ is the set of all N_{m} customers on the network, and let $\mathcal{K}_n$ denote the set of customers who are directed connected to node n. By denoting the

following:

$$\begin{aligned} c &:= \sum_{i \in \mathcal{K}_n} n_k^i, \\ d &:= \sum_{i \in \mathcal{K}} n_k^i, \end{aligned} \tag{2.39}$$

we can express $\Pr_n(p)$ by:

$$\Pr_n(p) = cd^{-1}. \tag{2.40}$$

We then take the derivative of (2.40) with respect to p, and we have:

$$\begin{aligned} \frac{\mathrm{d}}{\mathrm{d}p}\left(\Pr_n(p)\right) &= \frac{\mathrm{d}}{\mathrm{d}p}(cd^{-1}) \\ &= d^{-1}\frac{\mathrm{d}c}{\mathrm{d}p} + c\frac{\mathrm{d}}{\mathrm{d}p}\left(d^{-1}\right) \\ &= d^{-1}\frac{\mathrm{d}}{\mathrm{d}p}\left(\sum_{i \in \mathcal{K}_n \cap \mathcal{K}_{>p,k}} n_k^i\right) - cd^{-2}\frac{\mathrm{d}}{\mathrm{d}p}\left(\sum_{i \in \mathcal{K}_{>p,k}} n_k^i\right) \\ &= d^{-1}\sum_{i \in \mathcal{K}_n \cap \mathcal{K}_{>p,k}} \frac{\mathrm{d}}{\mathrm{d}p}\left(n_k^i\right) - cd^{-2}\sum_{i \in \mathcal{K}_{>p,k}} \frac{\mathrm{d}}{\mathrm{d}p}\left(n_k^i\right), \end{aligned} \tag{2.41}$$

where the term $\frac{\mathrm{d}}{\mathrm{d}p}\left(n_k^i\right)$ can be computed by following (2.19)−(2.22).

By now, all terms in (2.36) are derived in analytical forms, and the drift velocity of a node o on phase ϕ can be evaluated.

2.3 Numerical solution

In this section, we first introduce a numerical method to solve the FPE. To improve the accuracy of the obtained numerical solution, an optional calibration step is also utilized.

2.3.1 Numerical solution to the FPE

Let the solution to the FPE be $M = \{m(x,p)\}_{p \in \mathcal{P}}$ which is a sequence of PDFs for each p in a discretized set of penetration rates $\mathcal{P} = \{p^0, p^0 + \Delta p, p_0 + 2\Delta p, \cdots, p^{\max}\}$ with a step size Δp. The conservation law is to be satisfied such that the cumulative probability of each PDF must sum up to 1. For advection-diffusion partial differential equations such as the Fokker-Planck equation under the conservation law, finite-volume method (FVM) [104, 105] is a suitable class of numerical methods to solve them. Using an implicit scheme, we can

write the following generalized equation:

$$m(x,p) = f\left(m(x,p+\Delta p), u(x,p+\Delta p)\right), \tag{2.42}$$

where the mapping $f : \mathbb{R}^{n_x} \mapsto \mathbb{R}^{n_x}$ depends on the selected discretization scheme and n_x is the number of discretized points of x. For some schemes such as backwards Euler or Crank–Nicolson, the mapping f is linear such that it can be represented by a matrix $\mathbf{S}_u \in \mathbb{R}^{n_x \times n_x}$ which depends on $u(x, p+\Delta p)$. Hence, (2.42) can be written as:

$$m(x,p) = \mathbf{S}_u m(x,p+\Delta p).$$

By taking the inverse of $\mathbf{S}_u$, we can compute $m(x,p+\Delta p)$ given $m(x,p)$ by the following equation:

$$m(x,p+\Delta p) = \mathbf{S}_u^{-1} m(x,p).$$

The detailed form of the $\mathbf{S}_u$ matrix is presented in Appendix A, and the readers can refer to [104, 105] for more details. It is remarked that $\mathbf{S}_u$ is tridiagonal, where its diagonal elements are always non-zero, and lower/upper-diagonal elements on each row are also non-zero and differ from any diagonal element. Hence, for any given row of $\mathbf{S}_u$, it must be linearly independent of any other row. Therefore, $\mathbf{S}_u$ has always full rank and is non-singular. Consequently, the implicit scheme is numerically stable and unconditional on the discretization step size of x or Δp.

2.3.2 Calibration of $m(x,p)$

Due to the approximations made in (2.9) and (2.31), the drift velocity term $u(x,p)$ computed in Section 2.2.3 for equipment loading levels and in Section 2.2.5 for voltage levels may become less accurate when (i) the penetration rate is high enough such that magnitudes of voltage drop/rise caused by GET devices are non-negligible, and (ii) transformers with load-tap changers, voltage regulators and volt-var devices are active on the network causing non-linearity to voltages and network loadings. Under these situations, the obtained sequence of $m(x,p)$ by numerically solving the FPE may not accurately reflect the evolution of network states as a function of the penetration rate. To improve the accuracy, a calibration process is proposed.

Based on (2.11) and (2.13), we can compute the expected number of GET k devices $n_k^i(p)$ that should be added to customer i at penetration p and the expected offset of one GET k device $\mathbb{E}[s_k^i(t)]$ at the time of analysis t. We can then compute an aggregated offset value

of $n_k^i(p)\mathbb{E}[s_k^i(t)]$ which is to be added to each customer i in the network model. A power flow analysis will be performed to the modified network to extract the "true" mean network state $\tilde{x}(p)$. In the ideal case, such $\tilde{x}(p)$ should be identical to the mean value $\mathbb{E}[x(p)]$ which is computed from $\mathbb{E}[x(p)] = \int_{-\infty}^{+\infty} xm(x,p)\mathrm{d}x$. If $\mathbb{E}[x(p)] \neq \tilde{x}(p)$, then $m(x,p)$ should be calibrated to $m(x+\Delta x, p)$ where $\Delta x(p) \triangleq \tilde{x}(p) - \mathbb{E}[x(p)]$ is the shift value at p.

To maintain the computation efficiency, the power flow analysis of the network with aggregated offset values added to customers is not done for all $p \in \mathcal{P}$. Rather, the power flow is only performed at a few selected penetration rates, and the calibration is interpolated for all penetration rates. The process is as follow. Suppose that $\mathcal{P}_{\mathrm{pf}}$ is the set of selected penetration rates for power flow analyses, then we construct $\mathcal{D} = \{\Delta x(p) = \tilde{x}(p) - \mathbb{E}[x(p)]\}_{p\in\mathcal{P}_{\mathrm{pf}}}$ which are differences between the mean $\mathbb{E}[x(p)]$ from the REM and the power flow mean values $\tilde{x}(p)$ at these penetration rates. Then for any $p \in \mathcal{P}$, we compute $\Delta x(p)$ by,

$$\Delta x(p) = \frac{p - p_-}{p_+ - p_-}\left[\Delta x(p_+) - \Delta x(p_-)\right] + \Delta x(p_-),$$

where $p_- \triangleq \max\{\mathcal{P}_{\mathrm{pf}} \cap [p^0, p]\}$ is the greatest element in $\mathcal{P}_{\mathrm{pf}}$ that is less than or equal to p, $p_+ \triangleq \min\{\mathcal{P}_{\mathrm{pf}} \cap [p, p^{\max}]\}$ is the least element in $\mathcal{P}_{\mathrm{pf}}$ that is greater than or equal to p, and $\Delta x(p_-), \Delta x(p_+) \in \mathcal{D}$. The calibrated PDF $m(\tilde{x}, p) = m(x + \Delta x(p), p)$ is reported as the REM results. The number of power flow analyses required by the calibration process is independent of the number of network sections for analysis but only corresponds to the number of penetration rates included in $\mathcal{P}_{\mathrm{pf}}$, which is a much smaller set than $\mathcal{P}$. Thus, the calibration process adds negligible computation efforts to the REM.

It is remarked that this calibration step is optional. It does not produce any PDF, but rather it "shifts" the mean values of the PDFs computed numerically from the FPE. For large-scale distribution networks such as the IEEE-8500 test feeder used in the next section, voltage control (e.g., regulators) and VAR control (e.g., switchable shunt capacitors) devices are usually installed. Without the calibration step, the PDFs obtained by solving the FPE while neglecting impacts of these volt-var devices may result in observable errors even at low penetration rates, and become much less accurate as the penetration rate increases. On the other hand, the calibration step can be skipped without impacts on the accuracy for small networks or networks without volt-var control devices.

We would also like to point out that it may not be possible to perform the calibration step at high penetration rate. This is mainly because when trying to do a power flow analysis to the network with high penetration of GETs modelled, the power flow may not converge, hence we cannot obtain a value for $\tilde{x}(p)$. In this case, the accuracy of the numerical solution

of $m(x,p)$ may be reduced at high penetration.

2.3.3 Combined impact of multiple GETs

In the sections above, we present the methodology to study the impact of one GET type (EV or PV) installed to the network at various penetration rates. Throughout this section, the subscript k in the notation is conserved for clarity. Recall that $M_k = \{m(x,p_k)\}_{p_k \in \mathcal{P}_k}$ is the sequence of PDFs computed and calibrated from the REM for each $p_k \in \mathcal{P}_k$ when only GET type k exists on the network. In the following, we explain how the model can be extended to the analysis of networks where multiple GET types exist.

We start with the case in which two GET types k_1 and k_2 are installed to the network. We first compute $M_{k_1|k_2} = \{m(x,p_{k_1})|p_{k_2}\}_{p_{k_1} \in \mathcal{P}_{k_1}}$ when the penetration rate of GET type k_2 is fixed at p_{k_2} as a parameter. To do so, the numerical FVM in Section 2.3.1 is first used to solve for $m(x,p_{k_1})|p_{k_2}$ from the FPE under the drift velocity of $u(x,p_{k_1})|p_{k_2}$. By assuming the impacts of GET types k_1 and k_2 are independent, we have $u(x,p_{k_1})|p_{k_2} = u(x,p_{k_1}) + u(x,p_{k_2})$ by superposition. For example, if the two GET types considered are EVs and PVs, then $u(x,p_{k_1})$ and $u(x,p_{k_2})$ would drift the PDFs with the penetration rate towards opposite directions, and the *net* drifting velocity characterized by $u(x,p_{k_1})|p_{k_2}$ is used to compute the PDF of the network state under the impacts of both technologies. If necessary, the method in Section 2.3.2 is then applied to calibrate the resulting $m(x,p_{k_1})|p_{k_2}$. We repeat this process to construct $M_{k_1,k_2} = \{M_{k_1|k_2}\}_{p_{k_2} \in \mathcal{P}_{k_2}}$ which is a sequence of $M_{k_1|k_2}$ for each $p_{k_2} \in \mathcal{P}_{k_2}$. Each element of M_{k_1,k_2} represents the network state PDF under the combined impacts of GET types k_1 and k_2 with penetrations p_{k_1} and p_{k_2}, respectively.

For combined impacts of more than two GET types, the same process is adopted to compute $M_{k_1,k_2,\cdots}$, where sequences of PDFs are solved and calibrated by varying the penetration rate of one GET type at a time.

2.4 Test results

In this section, results from the stochastic impact analysis are illustrated on a test feeder.

2.4.1 Test setup

The IEEE-8500 test feeder [106] is selected to demonstrate REM's ability to conduct a rapid stochastic impact analysis. The following modifications to the network are made:

- The network contains 1177 spot loads and a total of 4205 customers, where some spot

loads contain more than 1 customer (the original IEEE-8500 network assumes each spot load models 1 customer).

- The substation transformer is changed to Wye-wye configuration such that its loading on each phase can be more easily seen.

To assess impacts of EVs and PVs on the network, we assume that the following information are given.

- 4 levels of EV charging power are considered (1.8kW, 3.6kW, 6.6kW, 7.2kW). Charging may start at any hour during the day and can last 2, 4, or 8 hours. Hence the set $\mathcal{L}_{\text{EV}}$ contains 288 charging profiles, where each profile $l^j_{\text{EV}}(t)$ is time-series data over a 24-hour period.

- 4 levels of PV nominal generation capacity are considered (1.6kW, 2.4kW, 3.6kW, 4kW). We consider 8 solar radiance profiles under different weather types [107], hence we have a total of 32 PV generation profiles in $\mathcal{L}_{\text{PV}}$.

- Each customer is assumed to have at most 1 EV.[1] Quantity probability $\Pr^i_{\text{num,EV}}(1)$ for customer $i = 1, 2, \ldots, 4205$ is randomly generated from the uniform distribution $\mathcal{U}[0, 1]$, and $\Pr^i_{\text{num,EV}}(0) = 1 - \Pr^i_{\text{num,EV}}(1)$. The probability $\Pr(\mathcal{L}^i_{\text{EV}}(j))$ for adopting charging profile $j \in [1, 288]$ is also randomly generated from $\mathcal{U}[0, 1]$, and $\Pr[\mathcal{L}^i_{\text{EV}}]$ is normalized such that $\sum_j \Pr(\mathcal{L}^i_{\text{EV}}(j)) = 1$.

- Each customer is assumed to have at most 1 PV.[1] Quantity probability $\Pr^i_{\text{num,PV}}(1)$ for customer $i = 1, 2, \ldots, 4205$ is randomly generated from $\mathcal{U}[0, 1]$, and $\Pr^i_{\text{num,PV}}(0) = 1 - \Pr^i_{\text{num,PV}}(1)$. To consider the correlation between the weather and the generation profiles, we first randomly generate the probabilities of the 8 solar radiance profiles from $\mathcal{U}[0, 1]$, denoted as $\Pr_{\text{solar}}$. Then for each customer i we generate the probabilities of PV generation capacity from $\mathcal{U}[0, 1]$, denoted as $\Pr^i_{\text{PVgen}}$. Then, we let $\Pr[\mathcal{L}^i_{\text{PV}}] = \Pr_{\text{solar}} \times \Pr^i_{\text{PVgen}}$. Finally, $\Pr[\mathcal{L}^i_{\text{PV}}]$ is normalized such that $\sum_j \Pr(\mathcal{L}^i_{\text{PV}}(j)) = 1$.

The information assumed above can be obtained from socio-economic or statistical studies. Taking EV as an example, in [38, 40] the adoption rate of electric vehicles in terms of different demographic and socio-economic characteristics (such as education levels, age group, household income, etc.) are studied. The results can be used to quantify the customer's quantity probabilities. Probability distributions of EV charging start time, state-of-charge

[1] The REM approach is not restricted to this assumption. Rather, this assumption is made to reduce the amount of the probability data required and, hence, simplifies the simulation.

(SOC), and EV travel information (mileage and duration per trip) are collected in [21, 22], and can be used to generate EV charging profiles along with the adoption probability. In the next chapter, we will also discuss an approach to infer the profile and adoption probability information from customers' meter data. Although there may exist much more possible profiles from the statistical studies, here we use a smaller set of representative EV charging and PV generation profiles (288 and 32, respectively) for illustration purpose. As increasing the number of profiles only affects the calculations of the expected value in (2.13) and (2.14), it has negligible impacts on the efficiency of the REM. Thus, the number of profiles is not limited in the REM approach, nor does it affect its efficiency.

The modified network is modelled in the CYME software which is also used to perform power flow analysis. The numerical solution and the calibration process of the REM analysis are implemented in `Python`.

2.4.2 Result validation

For validation of accuracy, a Monte Carlo simulation-based approach is also developed, where samples are constructed by randomly sampling from the same data set as given above. Although such a Monte Carlo simulation-based approach is slow in convergence rate and requires extensive computation for power flow analysis, the obtained results can be considered accurate once convergence is reached. Stochastic analysis results based on power flow solutions, i.e., the empirical distributions of loading levels of equipment and voltage levels of network sections, serve as benchmarks for the REM and is used to evaluate its performance.

2.4.3 Test results – EV

The analysis time is set to 8:00PM when peak load usually occurs, and 2000 samples are constructed for Monte Carlo simulations.

2.4.3.1 Loading level at selected penetration levels

Figure 2.1 illustrates the loading levels of the substation transformer when EVs are installed to the modified IEEE-8500 network at 3 penetration rates (10%, 30%, 50%). Because the power flow solution to a Monte Carlo sample is likely to diverge if the penetration rate is too high, completing the Monte Carlo simulations of 2000 samples with feasible power flow solutions takes too long. For this reason, the maximum penetration rate of 50% is chosen for Monte Carlo simulations. However, no limitation to the maximum penetration rate exists for our REM approach (i.e., see Section 2.4.3.3 and Figure 2.3 below). Results from the

REM with and without calibrations at these penetration rates are compared with empirical distributions from Monte Carlo simulations. It should be noted that the y-axis represents the probability density and the total area under each curve sums up to 1.

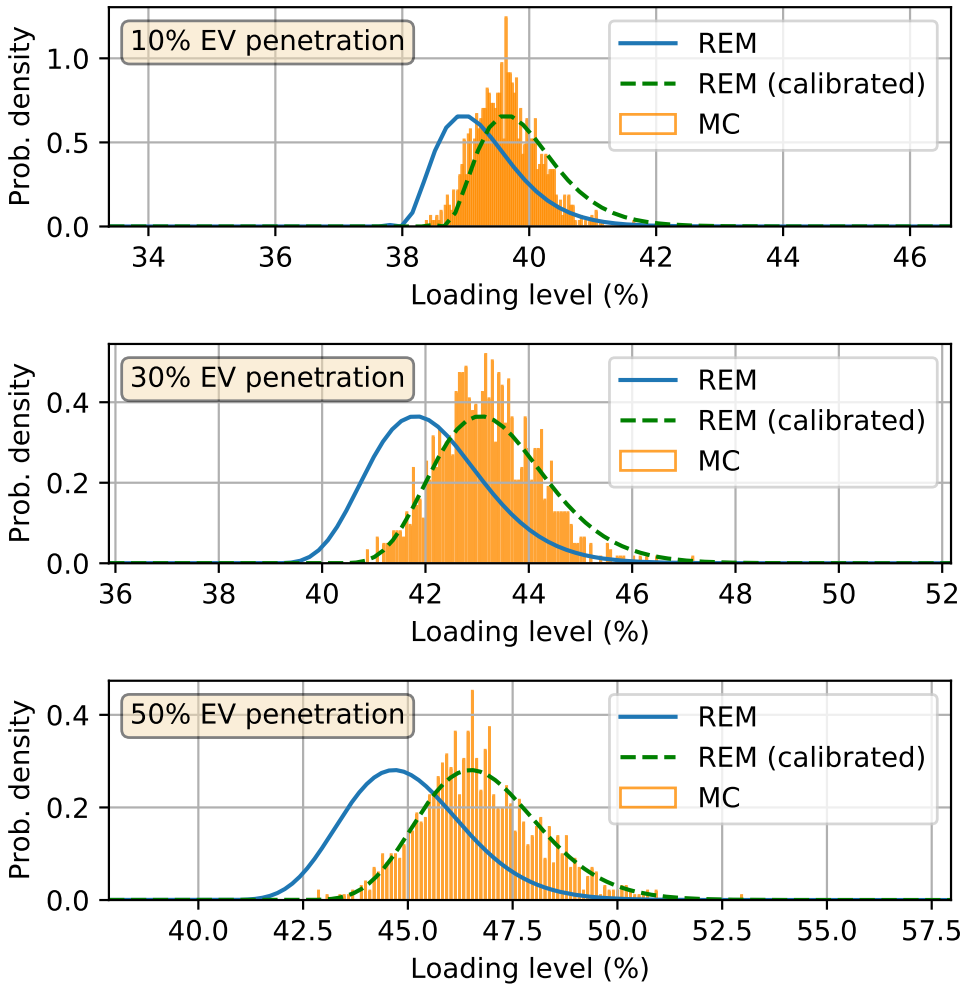

Figure 2.1 Comparison of probabilities of the substation transformer loading levels at various EV penetration rates, REM results (blue) vs. calibrated REM results (green dashed) vs. Monte Carlo (orange)

2.4.3.2 Voltage level at selected penetration levels

Figure 2.2 illustrates the probability distributions of the voltage level (in percentage) of a section called "M1125994". This section is 4.8 km from the substation and 1.2 km from a downstream voltage regulator. Due to its long distance from the substation, this section is expected to suffer from undervoltage when EV penetration is high. While, the substation voltage is regulated at 1.05 p.u., Figure 2.2 confirms that this section has a small probability

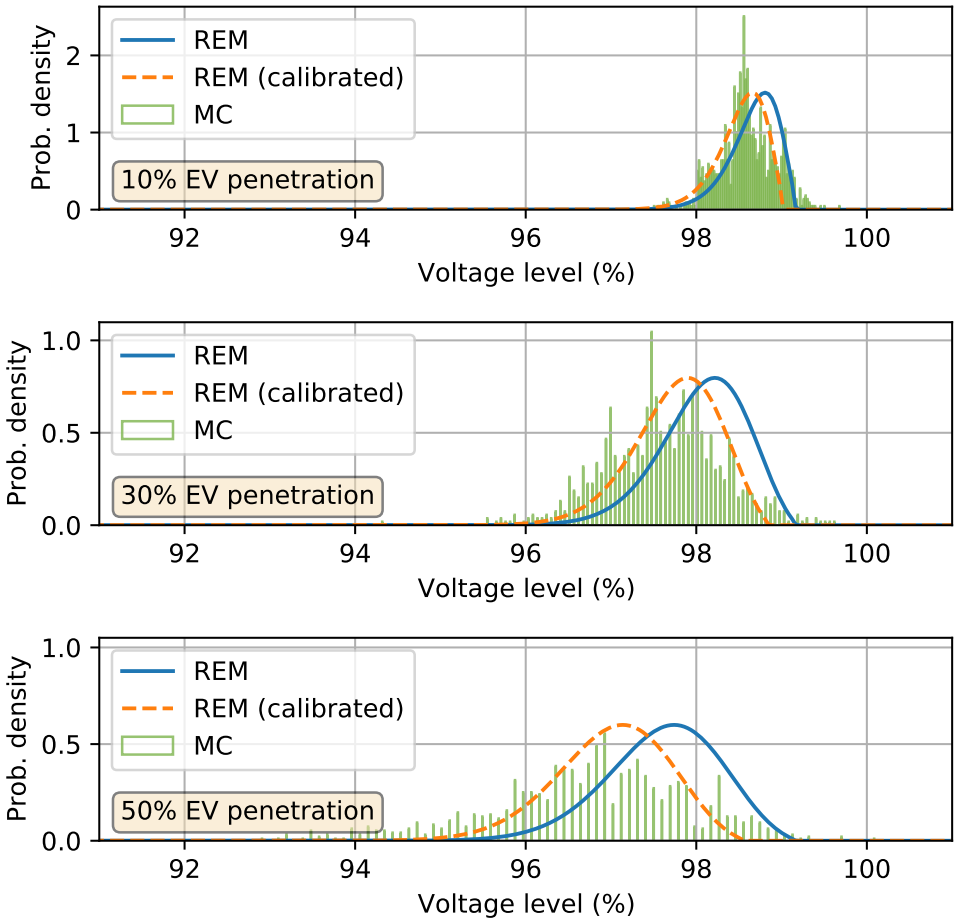

Figure 2.2 Comparison of probabilities of voltage levels the M1125994 section at various EV penetration rates, REM results (blue) vs. calibrated REM results (orange dashed) vs. Monte Carlo (green)

of having undervoltage issues at 50% EV penetration if the lower voltage limit is set at 0.95 p.u.

2.4.3.3 Network state estimation across a wide range of penetration rates

The REM provides a rapid estimation of network states (minimum, average, maximum levels) across a wide range of penetration rates, based on the computed PDFs. It also enables fast assessment for probabilities of abnormal conditions on the network (overloading, under/over-voltages) as the penetration rate increases. For example, Figure 2.3 shows the average, minimum, and maximum loading levels as well as overloading probabilities of a main line section near the substation of the IEEE-8500 network up to 100% EV penetration rate. Here, we take the mean value of the calibrated PDF at each p as the average loading level, and

minimum and maximum loading levels are ± 2× standard deviation from the mean value, respectively. This type of results can provide insightful information on what penetration level can be supported by the network before severe abnormalities occur.

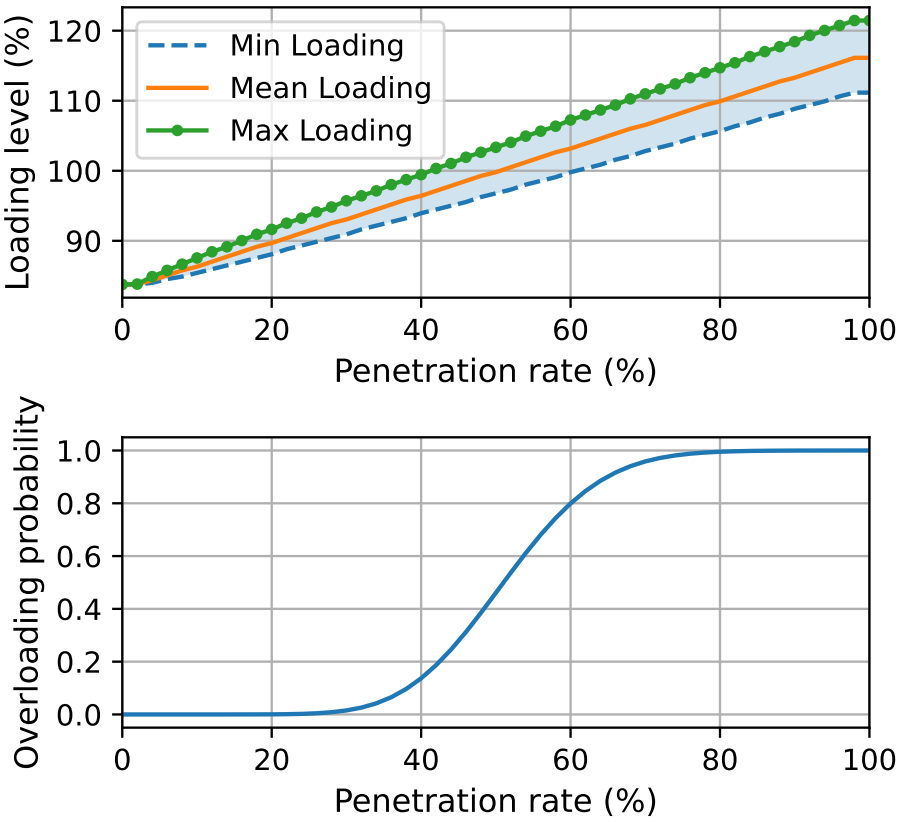

Figure 2.3 Loading levels (top) and overloading probabilities (bottom) of a line section vs. penetration rates of EVs added to the IEEE-8500 network

2.4.3.4 Network locations susceptible to abnormal conditions

In the last experiment related to EVs, we select a total of 183 network sections on which the initial equipment loading level is greater than 50% or the initial voltage level is less than 0.965 p.u. before any EV is installed to the network. These sections are likely to have equipment overloading or undervoltage issues as EVs are installed to the network. The impact analysis is performed to these sections to estimate network states and probabilities of abnormal conditions at different EV penetration rates. Figure 2.4 visualizes the locations of the network sections with the calculated probabilities of abnormal conditions at 50% EV penetration rate. Here, we create *Overloading probability* and *Undervoltage probability* keywords in CYME to highlight the locations according to the computed overloading and undervoltage

probabilities, respectively. Almost all selected network equipment have some probability of overloading. The line sections near the substation have an overloading probability close to 50%, which is consistent with the results of Figure 2.3. There are also multiple distribution transformers on the network which can have up to 20% probabilities of being overloaded at 50% EV penetration. As the EV penetration increases, all the identified locations will have even higher probabilities of overloads. The undervoltage issue is less severe on the network mainly due to the presence of voltage regulators (indicated by the green droplets). Only some sections that are far from the substation and upstream of a voltage regulator show some probability of undervoltage, and this is where the section M1125994 is located.

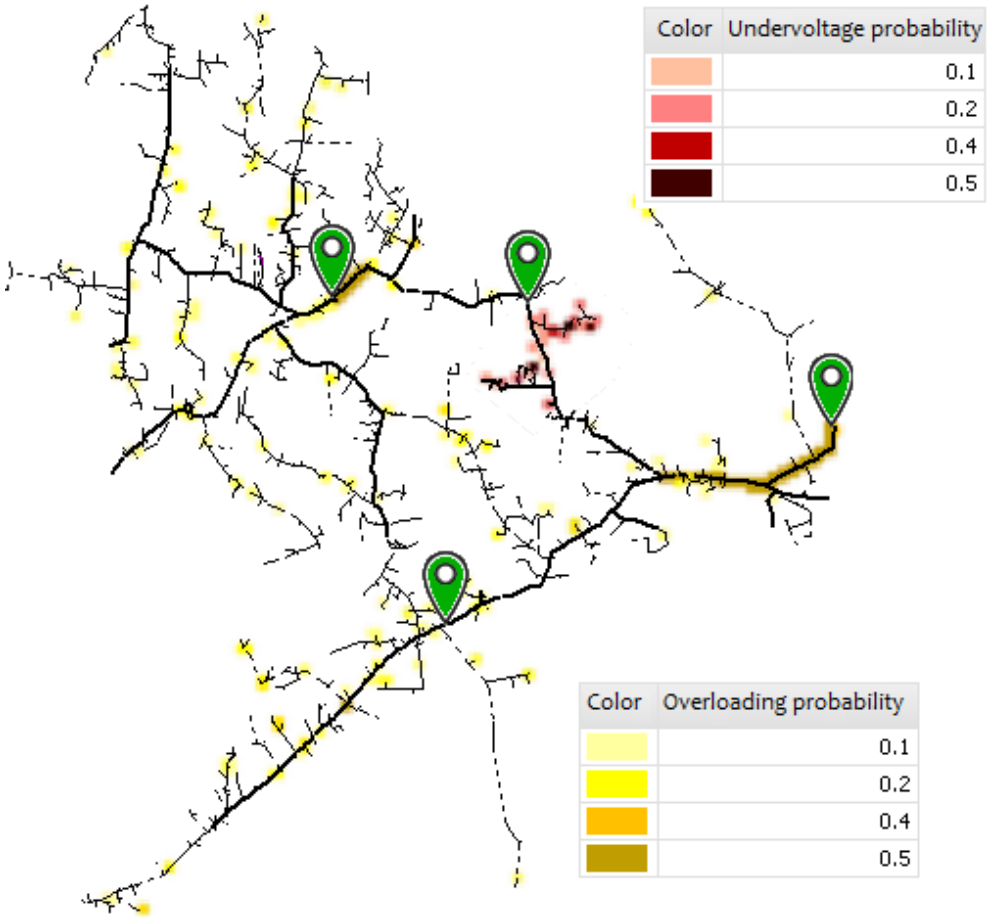

Figure 2.4 IEEE-8500 network sections susceptible to equipment overloading and undervoltage issues at 50% EV penetration rate

2.4.4 Test results – PV

The analysis time is set to 11:00AM when the solar irradiance starts to reach its peak. While customers can have diversified EV charging profiles, the PV generation profiles are correlated with the weather type, thus the analysis should be performed conditional on each weather type. Then weighted average results based on probabilities of all weather types are computed. Here, we present only the results when considering PV generation profiles during sunny days to avoid running Monte Carlo simulations for other weather types. In Monte Carlo simulations, 2000 samples are constructed.

2.4.4.1 Loading level at selected penetration levels

Figure 2.5 illustrates the loading levels of the substation transformer when PV are installed to the network at 3 penetration rates (10%, 30%, 50%). Similar to the EV case, 50% penetration is selected for comparison purpose. Results from the REM with and without calibrations are compared with empirical distributions from Monte Carlo simulations.

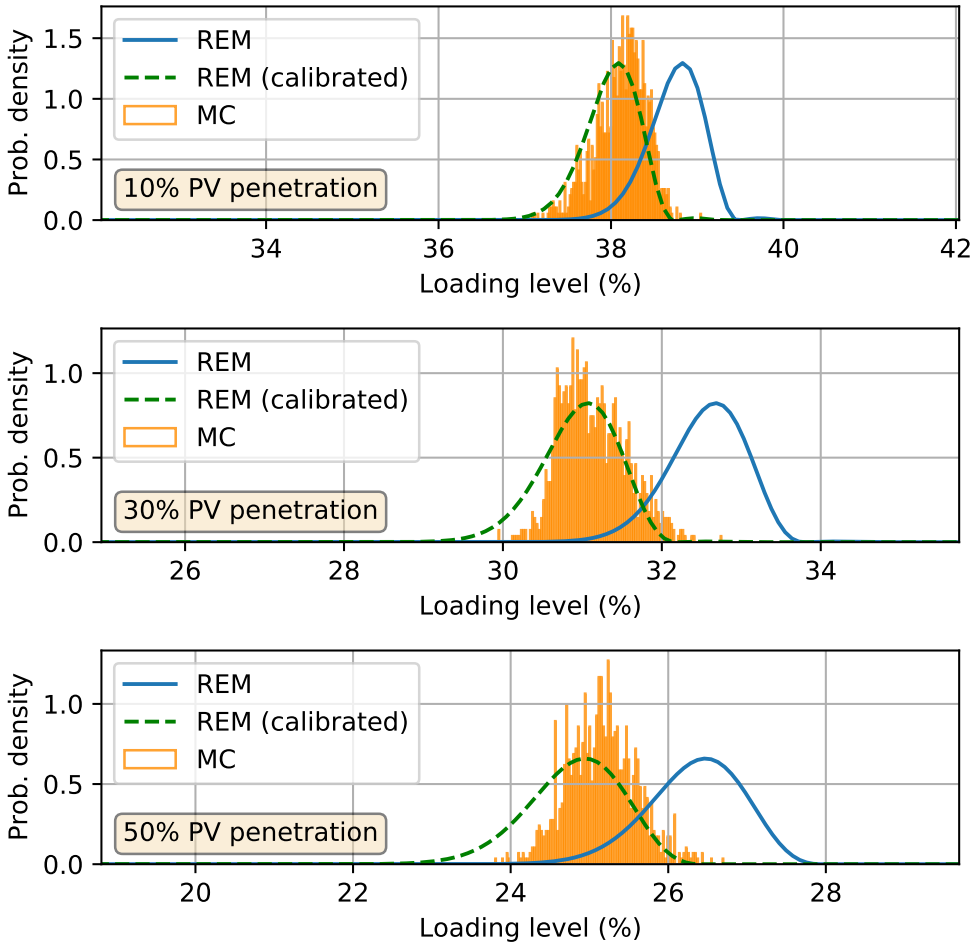

Figure 2.5 Comparison of probabilities of the substation transformer loading levels at various PV penetration rates, REM results (blue) vs. calibrated REM results (green dashed) vs. Monte Carlo (orange)

2.4.4.2 Voltage level at selected penetration levels

Figure 2.6 illustrates the probability distributions of the voltage level (in percentage) of the M1125994 section when PVs are installed. Although no overvoltage (by taking 1.05 p.u. as the upper voltage limit) occurs to this section due to its distance from the substation, it is observed that REM well captures the trend of increasing voltage levels with the PV penetration. Therefore, overvoltage would possibly occur as the penetration continues to increase, and calibrated results from the REM approach would accurately indicate the probabilities.

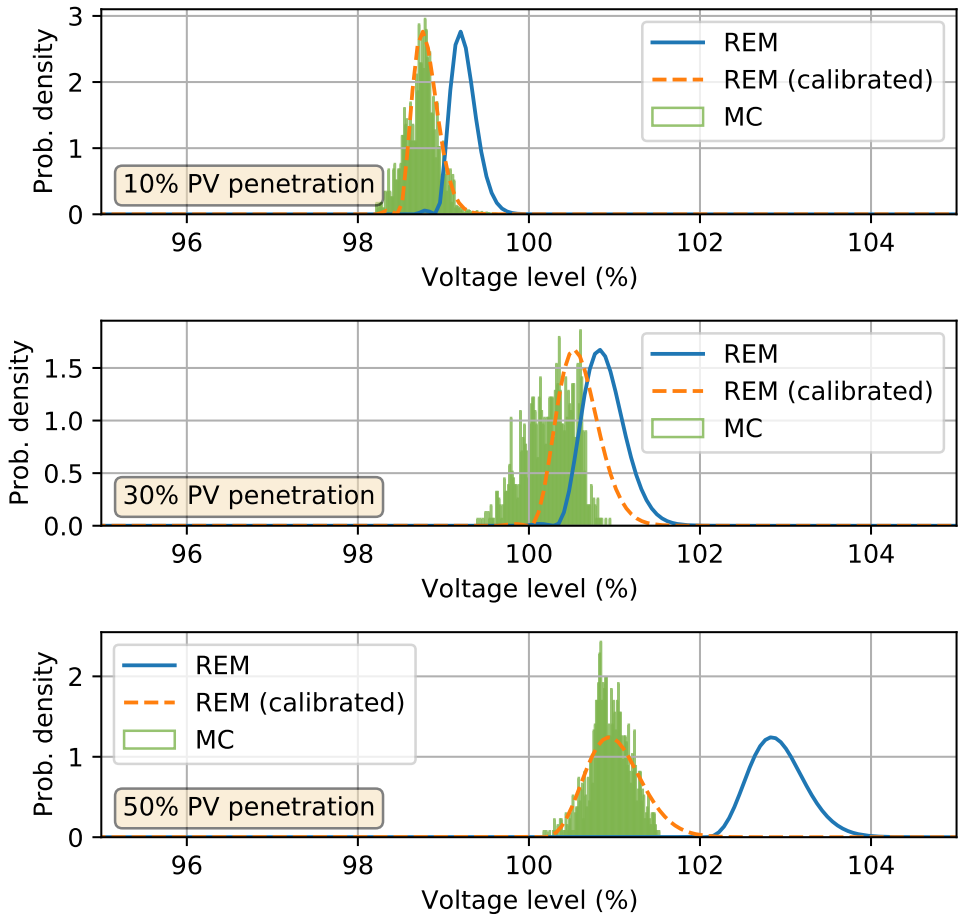

Figure 2.6 Comparison of probabilities of voltage levels of the M1125994 section at various PV penetration rates, REM results (blue) vs. calibrated REM results (orange dashed) vs. Monte Carlo (green)

2.4.4.3 Network locations susceptible to overvoltage

In this experiment, we select a total of 114 locations whose voltage level is greater than 1.04 p.u. before any PV is installed to the network. When setting the upper voltage limit to 1.05 p.u., more than half of these locations have overvoltage probabilities at 50% PV penetration. The calibrated probability values from REM are used to create the *Overvoltage probability* keyword in CYME to highlight network sections in Figure 2.7. It is observed that sections near the substation have close to 100% probability of overvoltage, while some sections immediately downstream of voltage regulators also have overvoltage issues with different probabilities.

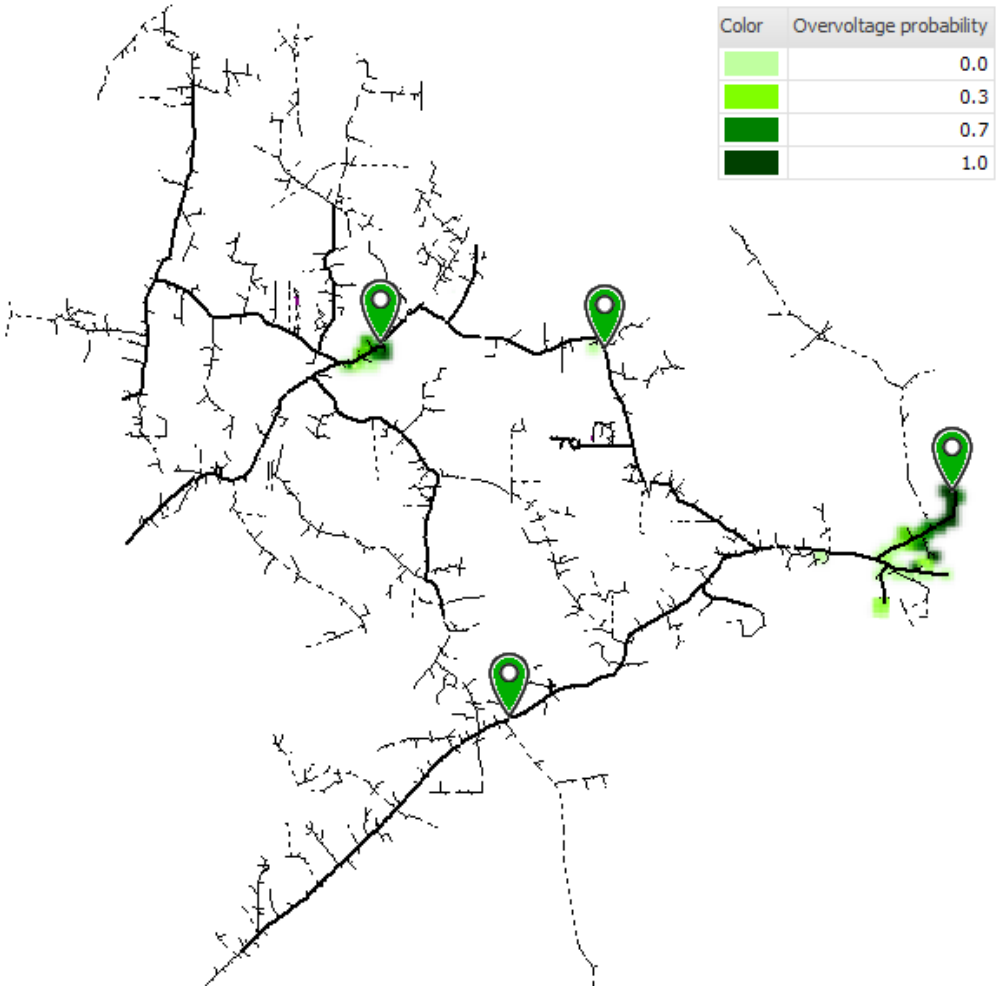

Figure 2.7 IEEE-8500 network sections susceptible to overvoltage issues at 50% PV penetration rate

2.4.5 Discussion of results

We discuss the results presented in the previous sections on impacts of EVs and PVs to the network.

2.4.5.1 Impacts of EV

As the EV penetration level increases, more power demand is expected on the network due to EV charging. This will increase the loading level of the substation transformer, and more voltage drops will be incurred on each network section. These can be confirmed from observations of Figures 2.1 and 2.2: empirical distributions of the substation transformer loading levels constructed from Monte Carlo simulations shift towards the heavier loading side, and

distributions of the voltage level shift towards the lower voltage side. The same dynamics are also observable from the PDFs computed and calibrated from the REM approach. In addition, as the level of uncertainties increases with the penetration rate, so does the *dispersion* of the distributions which is well captured by both Monte Carlo and our method.

Tables 2.1 and 2.2 provide quantitative comparisons of the mean and standard deviation values for the substation transformer loading levels using the two methods at various EV penerations. Here, the standard deviation is the square root of the variance. For the Monte Carlo method, the variance is empirically computed from the result set of all Monte Carlo samples constructed. For the REM, let $m(x, p)$ and $m(\tilde{x}, p)$ be the non-calibrated and calibrated PDFs, respectively. Hence, we have $\sigma^2 = \int_{-\infty}^{\infty}(x - \mathbb{E}[x])^2 m(x, p)\mathrm{d}x$ and $\tilde{\sigma}^2 = \int_{-\infty}^{\infty}(\tilde{x} - \mathbb{E}[\tilde{x}])^2 m(\tilde{x}, p)\mathrm{d}\tilde{x}$ for the variance of $m(x, p)$ and $m(\tilde{x}, p)$, respectively. From the calibration process, we have $\tilde{x} = x + \Delta x$, hence $\sigma^2 = \tilde{\sigma}^2$ and the standard deviation values with and without calibration are identical. For this reason, only one cell is used for the standard deviation (Std) of REM PDFs at each penetration rate in Tables 2.2, 2.4, 2.6, and 2.8. From Table 2.1, the calibration step significantly reduces the errors of the mean values, i.e., from 4.32% to less than 0.5% at 50% penetration rate. From Table 2.2, the Std errors are negligible, and the increasing values reflect higher levels of uncertainties with the penetrations.

Tables 2.3 and 2.4 list the mean and standard deviation values of voltage levels of the section M1125994 at various EV penetrations. The mean values from both methods are almost identical without the calibration step, and the calibration step further reduces the errors. The standard deviation values are also observed to increase with the penetration rates, which captures the higher levels of uncertainties.

Table 2.1 Mean values of substation transformer loading levels at various EV penetration rates

Substation transformer loading levels (Mean)					
Penetration	Monte Carlo (p.u.)	Non-calibrated (p.u.) and *relative error*		Calibrated (p.u.) and *relative error*	
10%	0.396	0.389	*−1.97%*	0.397	*0.08%*
30%	0.432	0.419	*−3.06%*	0.432	*−0.08%*
50%	0.467	0.447	*−4.32%*	0.465	*−0.45%*

Table 2.2 Standard deviations of substation transformer loading levels at various EV penetration rates

Substation transformer loading levels (Std)			
Penetration	Monte Carlo (p.u.)	Calibrated/non-calibrated (p.u.) and *error* (p.u.)	
10%	1.31×10^{-2}	1.06×10^{-2}	-2.5×10^{-3}
30%	1.80×10^{-2}	1.42×10^{-2}	-3.8×10^{-3}
50%	2.13×10^{-2}	2.13×10^{-2}	2.5×10^{-5}

Table 2.3 Mean values of voltage levels on the M1125994 section at various EV penetration rates

Voltage levels (Mean)					
Penetration	Monte Carlo (p.u.)	Non-calibrated (p.u.) and *relative error*		Calibrated (p.u.) and *relative error*	
10%	0.9860	0.9881	*0.21%*	0.9866	*0.06%*
30%	0.9764	0.9821	*0.59%*	0.9790	*0.26%*
50%	0.9679	0.9774	*0.98%*	0.9714	*0.35%*

Table 2.4 Standard deviations of voltage levels on the M1125994 section at various EV penetration rates

Voltage levels (Std)			
Penetration	Monte Carlo (p.u.)	Calibrated/non-calibrated (p.u.) and *error* (p.u.)	
10%	3.26×10^{-3}	2.76×10^{-3}	-4.96×10^{-4}
30%	6.76×10^{-3}	5.92×10^{-3}	-8.32×10^{-4}
50%	1.18×10^{-2}	8.69×10^{-3}	-3.11×10^{-3}

2.4.5.2 Impacts of PV

It is generally expected that PVs have opposite impacts on the network to those by EVs, such that network equipment's loadings should decrease, and voltage rise usually happens on network sections as PV penetration increases. From Figures 2.5 and 2.6, it is observed that empirical distributions of the substation transformer loading levels shift towards the lighter loading side, while distributions of the voltage levels of the M1125994 section shift towards

the higher voltage side. The PDFs computed and calibrated from our REM approach show similar dynamics.

Tables 2.5 and 2.6 provide quantitative comparisons of the mean and standard deviation values using the two methods. As in the EV case, the calibration step reduces errors of the mean values, and errors of the standard deviation values are negligible.

Table 2.5 Mean values of substation transformer loading levels at various PV penetration rates

Substation transformer loading levels (Mean)					
Penetration	Monte Carlo (p.u.)	Non-calibrated (p.u.) and *relative error*		Calibrated (p.u.) and *relative error*	
10%	0.381	0.388	*1.85%*	0.381	*−0.10%*
30%	0.311	0.327	*4.94%*	0.306	*−1.82%*
50%	0.252	0.265	*5.13%*	0.248	*−1.35%*

Table 2.6 Standard deviations of substation transformer loading levels at various PV penetration rates

Substation transformer loading levels (Std)			
Penetration	Monte Carlo (p.u.)	Calibrated/non-calibrated (p.u.) and *error* (p.u.)	
10%	5.82×10^{-3}	5.19×10^{-3}	-6.33×10^{-4}
30%	8.31×10^{-3}	8.65×10^{-3}	3.48×10^{-4}
50%	8.70×10^{-3}	1.04×10^{-2}	1.68×10^{-3}

Tables 2.7 and 2.8 list the mean and standard deviation values of voltage levels on the M1125994 section at various PV penetrations. The mean values from Monte Carlo and the REM have a relative difference of 1.85% in the worst case without the calibration step, and the calibration step further reduces the relative errors to below 0.35%.

Table 2.7 Mean values of voltage levels on the M1125994 section at various PV penetration rates

Voltage levels (Mean)					
Penetration	Monte Carlo (p.u.)	Non-calibrated (p.u.) and *relative error*		Calibrated (p.u.) and *relative error*	
10%	0.9881	0.9920	*0.40%*	0.9876	*−0.05%*
30%	1.0026	1.0083	*0.57%*	1.0060	*0.34%*
50%	1.0096	1.0282	*1.85%*	1.0092	*−0.03%*

Table 2.8 Standard deviations of voltage levels on the M1125994 section at various PV penetration rates

Voltage levels (Std)			
Penetration	Monte Carlo (p.u.)	Calibrated/non-calibrated (p.u.) and *error* (p.u.)	
10%	1.85×10^{-3}	1.21×10^{-3}	6.39×10^{-4}
30%	2.87×10^{-3}	1.81×10^{-3}	-1.06×10^{-3}
50%	2.32×10^{-2}	2.41×10^{-3}	9.49×10^{-5}

2.4.5.3 Quantile-Quantile plots

Besides comparing the mean and standard deviation values, we use Quantile-Quantile (Q-Q) plots to compare the calibrated PDFs from the REM against the empirical distributions from Monte Carlo simulations in Figure 2.8. Given that the latter are considered as the benchmark, we use them on the x-axis as the *theoretical* distribution and quantiles of the calibrated PDFs are plotted on the y-axis [108]. It is observed that in most plots the points in the center region mainly lie on a 45° straight line, indicating that the mean values of the calibrated PDFs from the REM well match those from Monte Carlo simulations. Some skewness and deviations from the straight line at both ends can also be observed. This could be due to the use of a constant diffusion velocity value in the FPE, which results in errors at the tail regions of the PDFs. Diffusion velocity's dependency on the penetration rate and on the network model can be studied in future work.

2.4.5.4 Computation speed

All the experiments are performed on a workstation equipped with Intel Core i7-11800H @ 2.30GHz CPU and 16GB RAM. Table 2.9 lists the computation time for experiments in Section 2.4.3 when EVs are installed to the network. In Table 2.9, the time spent on numerically solving the FPE is reported in the "Non-calibrated" column. As the FPE is solved for *one location at a time*, the time is expected to increase linearly with the number of locations to be simulated. However, for the time in the "Calibration" column, because network states of *all locations* can be obtained from a single power flow, the time may only be slightly increased for data processing as the number of locations for simulation increases. The total time spent on each experiment using the REM is the sum of times in these two columns.

For the Monte Carlo simulation approach, because the results are based on power flow solutions of all the samples constructed, the time shown in Table 2.9 is similar for all experiments,

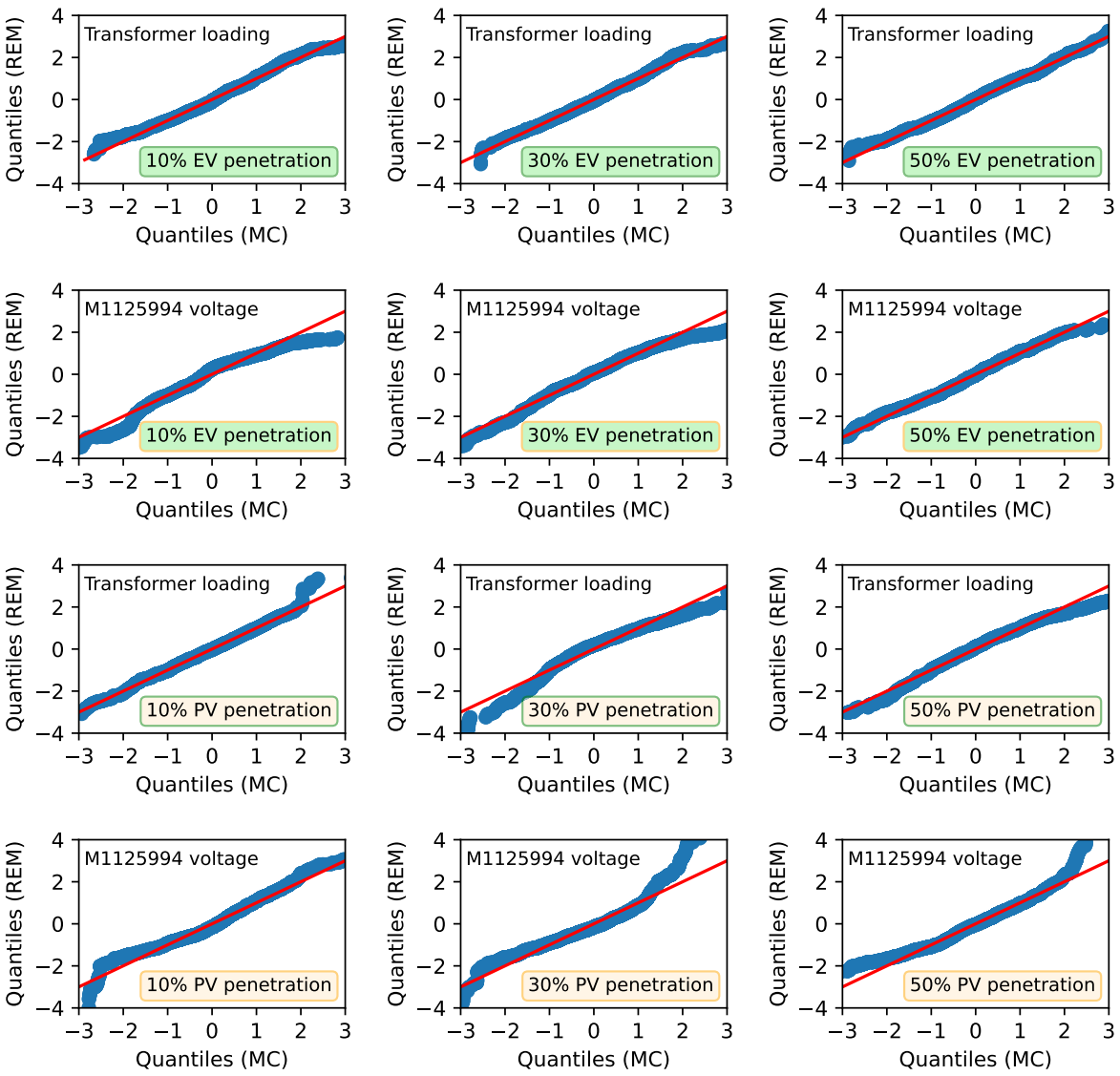

Figure 2.8 Q-Q plots to compare quantiles of distributions from Monte Carlo simulations and calibrated PDFs obtained from the REM

independent of the number of network sections included for stochastic impact analysis. It is also remarked that we use the Naive Monte Carlo approach such that no parallelization is utilized to directly compare with REM. For the REM approach, it is significantly faster to conduct an impact analysis to a single network section (within a few minutes including the calibration). However, in the last experiment, as 183 network sections are to be included for analysis, the time to obtain non-calibrated PDFs increases to 5.69 hours which is 190× that required for a single network section. On the other hand, as the time on calibrations does not depend linearly on the number of sections for analysis, it takes only 0.29 hour in the

last experiment which is increased by only 10× on more data processing. Finally, although not shown in the table, the analysis time also depends linearly on the maximum penetration level for both approaches.

Table 2.9 Comparison of computation speed

Experiments	Time (hr)		
	Monte Carlo	Non-calibrated	Calibration
Substation transformer loading levels	20.84	0.03	0.03
Section M1125994 voltage levels	21.79	0.03	0.03
Line loading levels across a wide range of penetration rates	-	0.06	0.03
Identifying locations with potential abnormal conditions	21.90	5.69	0.29

2.5 Conclusion and future work

In this chapter, we present a rapid estimation approach to perform a stochastic analysis on the impact of EVs and PVs to power distribution networks. A calibration step is also proposed to improve the accuracy of the REM. Quantitative assessments on a large-scale realistic distribution network indicate that results from the REM well follow those from Monte Carlo simulations with minimal errors, hence Monte Carlo simulations can be avoided for such a stochastic analysis and the computation efficiency can be greatly improved. After using REM to screen out locations where abnormal conditions may occur due to GET impacts, additional detailed analyses using power flow can be carried out if more accurate results are necessary.

As outlined in the Assumptions section, we rely on the information of load offset profiles of GETs as well as customers' adoption probabilities of different profiles. Although there exist statistical studies to obtain such information, they are not necessarily applicable to all utilities which may lead to inaccurate results when using REM. However, most utilities do have access to customers' consumption data measured by smart meters, and information can be inferred and be used as input data to REM. In Chapter 3, we introduce a method to extract EV charging profiles and probabilities from smart meter data and use the information in REM to study EV impacts.

The impacts of EVs and PVs to the distribution network are evaluated at their respective "peak" time. We can extend the approach to time-series analyses to study the impacts of GETs during a time period. The approach can also be extended to analyze the impacts of GETs with control schemes, which modify the set of offset profiles and shift customers' adoption probabilities. The effectiveness and resulting impacts to the networks can be rapidly

evaluated by the REM. In Chapter 4, we extend REM to study impacts of EV charging to the distribution network on a typical day, and discuss how it can be used to evaluate the effectiveness of strategies to mitigate overloads due to EV charging through design of optimal incentive plans.

Last but not least, we propose a sketch on how the method can be applied to study simultaneous impacts of multiple GET types, and the performance can be verified through more case studies on a distribution network. As penetration levels of GETs are expected to increase over the next few years, REM offers an analysis framework dedicated to these technologies which allows utilities to properly plan and optimize their networks.

CHAPTER 3 INFERRING ELECTRIC VEHICLE CHARGING PATTERNS FROM SMART METER DATA FOR IMPACT STUDIES

3.1 Introduction

With the increasing penetration levels of EVs on the power distribution networks, utility planners need to evaluate the impacts of EV charging on their networks to maintain system reliability and power quality. Due to the randomness associated with the usage of EVs, stochastic methods are usually adopted to analyze the impact by characterizing EV owners' charging habits in terms of probabilities of charging profiles. In the previous chapter, we presented a stochastic method based on given probabilities of EV charging. While such probabilities can be constructed based on historical EV charging events, as EV chargers are often installed behind-the-meter (BTM), the charging events are using invisible to utilities. It is hence challenging to directly observe customers' charging behaviours to infer the probability distributions.

In this chapter, we propose a method to detect customers' charging events from the smart meter data, which are readily available to the utilities. For each charging event detected, the start time, the duration, and the power level of the charger is extracted. We then infer customers' charging patterns in terms of probability distributions based on the extracted information out of all charging events detected. To detect the EV charging events from smart meter data, we formulate a mixed-integer convex program, which can be solved in a computationally efficient way using an off-the-shelf solver. Our method leverages the contextual information of EV charging, and does not rely on any supervised or unsupervised learning models hence no labelled training samples or hyperparameter tuning are necessary, making it readily implementable for utilities. Through a data-driven approach, we construct the charging patterns of all customers in terms of probability distributions from the detection results. Using the inferred charging patterns and probability information, impacts of these customers' EV charging behaviours to the power distribution network can then be analyzed using the REM developed in Chapter 2.

The rest of the chapter is organized as follows: in Section 3.2, we state the main assumptions about the contextual information of EV charging. We then formulate a mixed-integer convex quadratic program to detect a customer's EV charging events during a day. In Section 3.3, we present our methodology to infer EV charging patterns for a set of customers on the distribution network, based on the detected EV charging events. The charging patterns are represented by distributions of charging start time, duration, and power levels. We present

a case study to illustrate the EV charging patterns extracted by our proposed approach. We then showcase in Section 3.4 the quality and accuracy of the inferred patterns by using them in a stochastic analysis of EV impacts to a test distribution network based on the REM. Finally, we conclude in Section 3.5 and point out some future work directions.

3.2 Detection of EV charging events

Let $\mathbf{P} = [\mathrm{P}_i]_{i=1}^{N_\mathrm{m}} \in \mathbb{R}^{N_\mathrm{m} \times N_\mathrm{D} T}$ be the real power data measured in kW by the smart meters for a set of N_m customers on the distribution network $\mathcal{N}$ and for N_D days, where T is the time horizon or the number of data samples during a day. Here, we assume that $\mathrm{P}_i \in \mathbb{R}^{N_\mathrm{D} T}$ is measured at a 15-minute interval, hence $T = 96$. Let $\mathbf{P}^\mathrm{EV}, \mathbf{P}^\mathrm{BL} \in \mathbb{R}^{N_\mathrm{m} \times N_\mathrm{D} T}$ refer to, respectively, the power demands to charge customers' EVs and those of the baseload, i.e., all other appliances and devices in the households. Hence, we write $\mathbf{P} = \mathbf{P}^\mathrm{EV} + \mathbf{P}^\mathrm{BL}$. Our goal is to disaggregate $\mathbf{P}^\mathrm{EV}$ from $\mathbf{P}$ through a detection procedure for EV charging events.

3.2.1 Contextual information

In this section, we state several assumptions based on characteristics of EV charging events and results of statistical studies. Here, we limit our scope to the residential customers, as they account for up to 80% of charging events with diversified and stochastic charging patterns [109]. Therefore, in the proposed formulation, we assume that the smart meter data correspond to an individual customer, and not to aggregated consumption of multiple customers.

- The charging power levels depend on the vehicle models and the type of chargers. For residential customers, Level 1 or Level 2 chargers are usually used. As the time required for a full-charge by Level 2 chargers is shorter and the associated costs to install them keep decreasing over time, they are becoming more popular among residential customers [110]. Further, as the maximum power of Level 1 chargers does not exceed 2 kW, they do not cause much stress to the distribution system and utilities are less concerned with their impacts. Hence, we focus on Level 2 chargers, and the set of possible charging power levels depending on vehicle models is assumed to be $\mathcal{P} = \{3.6, 6.6, 7.2, 9.6, 11.5, 15\}$, in kW.
- Based on a statistical study on Pecan Street data [111], the duration of charging events is usually more than 30 minutes, and the number of charging events during a day is usually less than 3 [50]. In another statistical study on HVAC systems, the average

duty cycle of an HVAC system is about 30 minutes [112]. In order to differentiate EV charging events from HVAC duty cycles, we ignore charging events that last less than 1 hour.

- We assume that the profile of a charging event follows a rectangular waveform, i.e., the power consumption is constant during the entire charging period [113], and is voltage independent. The variations in power consumption are ignored when the charging starts and completes, as well as due to voltage fluctuations during charging. As shown later in the case study section, the assumption is valid, e.g., when comparing the waveform of the detected EV charging event with the true waveform, the difference is negligible.
- According to a survey on multi-vehicle households [114], 90% of EV owners have more than 1 vehicle but only 1% of them own another EV. Hence, we assume that only 1 EV is charged each day, even for households with multiple EVs. Thus, all charging events in a day should have the same power level.

We remark that in some cases where utilities only have data of lower temporal resolution, e.g., hourly measurements, our EV detection approach can still be applied but reduced accuracy may be expected as illustrated in the case study section.

3.2.2 Mixed-integer convex quadratic program

Let $\mathrm{P}_{i,d} \in \mathbb{R}^T$ be customer i's power demand during day d, and $\mathrm{P}^{\mathrm{EV}}_{i,d}, \mathrm{P}^{\mathrm{BL}}_{i,d} \in \mathbb{R}^T$ be the demand for EV charging and baseload, respectively. The mixed-integer convex quadratic program (MICQP) to determine $\mathrm{P}^{\mathrm{EV}}_{i,d}$ is formulated as:

$$\min_{\mathrm{P}^{\mathrm{EV}}_{i,d},\mathbf{x},\mathbf{y},\mathbf{z},\boldsymbol{\delta}} \quad \mathrm{Var}(\mathrm{P}^{\mathrm{BL}}_{i,d}) = \frac{1}{T}\sum_{t=1}^{T}\left(\mathrm{P}^{\mathrm{BL}}_{i,d}(t) - \overline{\mathrm{P}^{\mathrm{BL}}_{i,d}}\right)^2 \tag{3.1}$$

$$\text{subject to} \quad \overline{\mathrm{P}^{\mathrm{BL}}_{i,d}} = \frac{1}{T}\textstyle\sum_{t=1}^{T}\mathrm{P}^{\mathrm{BL}}_{i,d}(t), \tag{3.2}$$

$$\mathrm{P}_{i,d} = \mathrm{P}^{\mathrm{EV}}_{i,d} + \mathrm{P}^{\mathrm{BL}}_{i,d}, \tag{3.3}$$

$$\mathbf{x}, \mathbf{y}, \mathbf{z} \in \{0,1\}^T, \tag{3.4}$$

$$\boldsymbol{\delta} \in \{0,1\}^{|\mathcal{P}|\times T}, \tag{3.5}$$

$$\boldsymbol{\delta}^h \in \mathbb{R}^{|\mathcal{P}|}, \tag{3.6}$$

$$\mathbf{1}_T^\top \mathbf{y} \leq 2, \tag{3.7}$$

$$\textstyle\sum_{n=0}^{\min\{T-t,3\}} \mathbf{y}(t+n) + \mathbf{z}(t+n) \leq 1, \forall t, \tag{3.8}$$

$$\boldsymbol{\delta}^\top \mathbf{1}_{|\mathcal{P}|} \leq \mathbf{x}, \tag{3.9}$$

$$\boldsymbol{\delta}^\top(\mathcal{P} - \varepsilon \mathbf{1}_{|\mathcal{P}|}) \leq \mathrm{P}_{i,d}^{\mathrm{EV}} \leq \boldsymbol{\delta}^\top(\mathcal{P} + \varepsilon \mathbf{1}_{|\mathcal{P}|}), \tag{3.10}$$

$$\boldsymbol{\delta}^h = \frac{1}{T}\boldsymbol{\delta}\mathbf{1}_T, \tag{3.11}$$

$$\boldsymbol{\delta}(p,t) \leq 1 - \textstyle\sum_{n=1}^{|\mathcal{P}|-p} \boldsymbol{\delta}^h(p+n),\ \forall p,t, \tag{3.12}$$

$$\mathrm{P}_{i,d}^{\mathrm{EV}}(t) - \mathrm{P}_{i,d}^{\mathrm{EV}}(t-1) \leq \mathbf{y}(t)M,\ \forall t, \tag{3.13}$$

$$\mathrm{P}_{i,d}^{\mathrm{EV}}(t-1) - \mathrm{P}_{i,d}^{\mathrm{EV}}(t) \leq \mathbf{z}(t)M,\ \forall t, \tag{3.14}$$

$$\mathrm{P}_{i,d}^{\mathrm{EV}}(t) \leq \mathbf{x}(t)M,\ \forall t, \tag{3.15}$$

$$\mathrm{P}_{i,d}^{\mathrm{EV}}(t), \mathrm{P}_{i,d}^{\mathrm{BL}}(t) \geq 0,\ \forall t, \tag{3.16}$$

$$\mathbf{x}(t) - \mathbf{x}(t-1) = \mathbf{y}(t) - \mathbf{z}(t),\ \forall t. \tag{3.17}$$

The objective (3.1) is to minimize the variance of the baseload $\mathrm{P}_{i,d}^{\mathrm{BL}}$ after $\mathrm{P}_{i,d}^{\mathrm{EV}}$ is subtracted from $\mathrm{P}_{i,d}$, where $\overline{\mathrm{P}_{i,d}^{\mathrm{BL}}}$ is the mean value of the resulting baseload as computed in (3.2). The binary variables $\mathbf{x}, \mathbf{y}, \mathbf{z} \in \{0,1\}^T$ indicate, respectively, whether an EV is being charged ($\mathbf{x}(t) = 1$), the start time ($\mathbf{y}(t) = 1$), and the end time ($\mathbf{z}(t) = 1$) of a charging event for each time step t during the horizon T. As we assume that EVs are not charged more than twice during a day, we limit the detection of charging events to 2 by (3.7), i.e., $\mathbf{y}(t) = 1$ at no more than 2 time steps, and $\mathbf{1}_T$ is the column vector of ones of dimension T. As we do not consider charging events that last less than 1 hour, we use (3.8) to enforce that we cannot have an active $\mathbf{y}$ and an active $\mathbf{z}$ during any time window of 4 time steps. With (3.9) and (3.10), the power level at each time step t takes a single value from $\mathcal{P}$ (within some tolerance $\varepsilon > 0$), and the activated power level is indicated by the binary variable $\boldsymbol{\delta} \in \{0,1\}^{|\mathcal{P}| \times T}$. Here, $|\mathcal{P}|$ is the cardinality of $\mathcal{P}$, and $\mathbf{1}_{|\mathcal{P}|}$ is the column vector of ones of dimension $|\mathcal{P}|$. It is possible that different power levels may occur during a charging event, i.e., step changes, hence we need to ensure that the same power level is adopted during all charging events of the day. An intermediate variable $\boldsymbol{\delta}^h \in \mathbb{R}^{|\mathcal{P}|}$ is defined in (3.11) to calculate the fraction of power levels activated during the day. By (3.12), we force that the higher power level with a corresponding non-zero $\boldsymbol{\delta}^h$ value is always used during this day. By (3.13)$-$(3.17), the profile of a charging event must follow a rectangular waveform at the activated power level, where M is a large constant, i.e., $M \gg \max(\mathcal{P})$. Finally, the resulting $\mathrm{P}_{i,d}^{\mathrm{EV}}$ and $\mathrm{P}_{i,d}^{\mathrm{BL}}(t)$ should be non-negative at all times.

Note that for the simplicity in notation, the subscripts i and d on all binary and intermediate variables, namely, $\mathbf{x}, \mathbf{y}, \mathbf{z}$, $\boldsymbol{\delta}$, and $\boldsymbol{\delta}^h$, are omitted in the formulation of the MICQP.

3.3 Customers' EV charging patterns

Let T^{s} and T^{d} be random variables on sample space $\mathcal{T}$ and P^{c} be a random variable on sample space $\mathcal{P}$, which represent, respectively, the start time, the duration, and the charger power level of EV charging events for all customers on the network $\mathcal{N}$. Here, $\mathcal{T} = [0, \Delta t, 2\Delta t, \cdots, (T-1)\Delta t]$ is the discretized time horizon with a time step $\Delta t = 15$ minutes. The charging patterns can be characterized through the inferred probability mass functions (PMFs) of these random variables, namely, $\hat{f}_{T^{\mathrm{s}}}(t)$, $\hat{f}_{T^{\mathrm{d}}}(t)$, and $\hat{f}_{P^{\mathrm{c}}}(p)$.

Let $t^{\mathrm{d}}_{i,d}, t^{\mathrm{s}}_{i,d}, t^{\mathrm{e}}_{i,d}$, and $P^{\mathrm{c}}_{i,d}$ be, respectively, the duration, the start time, the end time, and the power level of the EV charging events detected for customer i on day d by solving the MICQP proposed in the previous section. From the solution obtained, we compute $t^{\mathrm{s}}_{i,d} = \{t \in \mathcal{T} \mid \mathbf{y}(t) = 1\}$, $t^{\mathrm{e}}_{i,s} = \{t \in \mathcal{T} \mid \mathbf{z}(t) = 1\}$, $t^{\mathrm{d}}_{i,d} = t^{\mathrm{e}}_{i,s} - t^{\mathrm{s}}_{i,s}$, and $P^{\mathrm{c}}_{i,d} = \{\max_t(\mathrm{P}^{\mathrm{EV}}_{i,d})\}$. We note that as we detect up to two charging events in each day, two values may be collected in each of sets. By repeatedly solving the MICQP for all customers and for all days, i.e., to extract all charging events in $\mathbf{P}$, we obtain the following multisets of detected results:

$$
\begin{aligned}
\mathcal{T}^{\mathrm{s}} &= \{t^{\mathrm{s}}_{i,d},\ d = 1, 2, \cdots, N_{\mathrm{D}},\ i = 1, 2, \cdots, N_{\mathrm{m}}\} \\
\mathcal{T}^{\mathrm{d}} &= \{t^{\mathrm{d}}_{i,d},\ d = 1, 2, \cdots, N_{\mathrm{D}},\ i = 1, 2, \cdots, N_{\mathrm{m}}\} \\
\mathcal{P}^{\mathrm{c}} &= \{P^{\mathrm{c}}_{i,d},\ d = 1, 2, \cdots, N_{\mathrm{D}},\ i = 1, 2, \cdots, N_{\mathrm{m}}\},
\end{aligned}
$$

We remark that $\mathcal{T}^{\mathrm{s}}, \mathcal{T}^{\mathrm{d}}$, and $\mathcal{P}^{\mathrm{c}}$ contain the same number of elements. The probability mass functions (PMFs) for the random variables $T^{\mathrm{s}}, T^{\mathrm{d}}$, and P^{c} are then approximated by the empirical distributions:

$$
\begin{aligned}
\hat{f}_{T^{\mathrm{s}}}(t) &= \frac{1}{|\mathcal{T}^{\mathrm{s}}|} \sum_{t^{\mathrm{s}} \in \mathcal{T}^{\mathrm{s}}} \mathbb{1}_{\{t^{\mathrm{s}}\}}(t),\ t \in \mathcal{T} \\
\hat{f}_{T^{\mathrm{d}}}(t) &= \frac{1}{|\mathcal{T}^{\mathrm{d}}|} \sum_{t^{\mathrm{d}} \in \mathcal{T}^{\mathrm{d}}} \mathbb{1}_{\{t^{\mathrm{d}}\}}(t),\ t \in \mathcal{T} \\
\hat{f}_{P^{\mathrm{c}}}(p) &= \frac{1}{|\mathcal{P}^{\mathrm{c}}|} \sum_{p^{\mathrm{c}} \in \mathcal{P}^{\mathrm{c}}} \mathbb{1}_{\{p^{\mathrm{c}}\}}(p),\ p \in \mathcal{P},
\end{aligned}
\tag{3.18}
$$

where $\mathbb{1}$ is an indicator function, i.e., $\mathbb{1}_{\{p^{\mathrm{c}}\}}(p) = 1$ if $p^{\mathrm{c}} = p$ and $\mathbb{1}_{\{p^{\mathrm{c}}\}}(p) = 0$ otherwise.

Based on $\mathcal{T}^{\mathrm{s}}$ and $\mathcal{T}^{\mathrm{d}}$, we then construct a set of all possible charging profiles in per-unit (p.u.) values:

$$
\mathcal{L}^{\mathrm{p.u.}}_{\mathrm{EV}} = \{l_{t^{\mathrm{s}}, t^{\mathrm{d}}}(t) \mid t^{\mathrm{s}} \in \underline{\mathcal{T}}^{\mathrm{s}}, t^{\mathrm{d}} \in \underline{\mathcal{T}}^{\mathrm{d}}\}, \tag{3.19}
$$

where $\underline{\mathcal{T}}^{\mathrm{s}}$ and $\underline{\mathcal{T}}^{\mathrm{d}}$ are the support of $\mathcal{T}^{\mathrm{s}}$ and $\mathcal{T}^{\mathrm{d}}$, respectively, and

$$l_{t^{\mathrm{s}},t^{\mathrm{d}}}(t) = \begin{cases} 1, & \text{if } t^{\mathrm{s}} \leq t < t^{\mathrm{s}} + t^{\mathrm{d}}, \\ 0, & \text{otherwise.} \end{cases} \tag{3.20}$$

A profile $l_{t^{\mathrm{s}},t^{\mathrm{d}}}(t)$ reconstructs the per-unit rectangular waveform of a charging event that has been detected from customers' smart meter data. To conduct an impact analysis of EV charging, we also need to calculate the probability that each $l_{t^{\mathrm{s}},t^{\mathrm{d}}}(t)$ is adopted, which is given by:

$$\begin{aligned} \Pr(l_{t^{\mathrm{s}},t^{\mathrm{d}}}) &= \Pr(T^{\mathrm{s}} = t^{\mathrm{s}}, T^{\mathrm{d}} = t^{\mathrm{d}}) \\ &= \Pr(T^{\mathrm{s}} = t^{\mathrm{s}} \mid T^{\mathrm{d}} = t^{\mathrm{d}}) \hat{f}_{T^{\mathrm{d}}}(t^{\mathrm{d}}), \end{aligned} \tag{3.21}$$

where $\Pr(T^{\mathrm{s}} = t^{\mathrm{s}} \mid T^{\mathrm{d}} = t^{\mathrm{d}})$ is approximated by $\frac{m}{n}$, where n is the total number of detected charging events lasting for t^{d} and m is the number of charging events starting at t^{s} out of the n events. We remark that as $t^{\mathrm{d}} \in \underline{\mathcal{T}}^{\mathrm{d}}$, we have $n \geq 1$.

3.4 Case study

We use the Pecan Street data [111] to evaluate the performance of our method to extract customers' EV charging habits. The dataset contains smart meter data measured for 76 customers with EVs for the full year of 2021. Daily power demand of EV charging is also recorded for each customer, which serves as the "ground truth" to verify the accuracy of the detection results using our approach.

3.4.1 Distributions of charging patterns

The first step is to detect daily charging events of each customer from the smart meter data by solving the MICQP in Section 3.2.2. We remark that some customers have photovoltaic (PV) systems, so the measured consumption has already been reduced by the PV generation. In order to avoid under-estimation and to compare the detected events with the ground truth, the smart meter data for these customers are pre-processed by adding back the consumption that has been offest by the PV generation. Figures 3.1 and 3.2 show examples of the charging events detected during a day of selected customers. Two experiments are performed: (1) using smart meter data measured at a 15-minute interval and (2) using hourly measurements.

We observe in Figure 3.1 that EV charging events are accurately detected from the meter data measured at every 15 minutes in terms of start time, duration, and the power level. We

demonstrate that our method can accurately detect the EV charging events in the following cases: multiple events occur during the day (e.g., Load 1517 and Load 2018), periods with constant higher power consumption are not identified as EV charging (e.g., Load 2470), and the pause between two charging events is correctly recognized (e.g., Load 2018). We also test our approach on the same customers/days but using hourly meter measurements, and the results are shown in Figure 3.2.

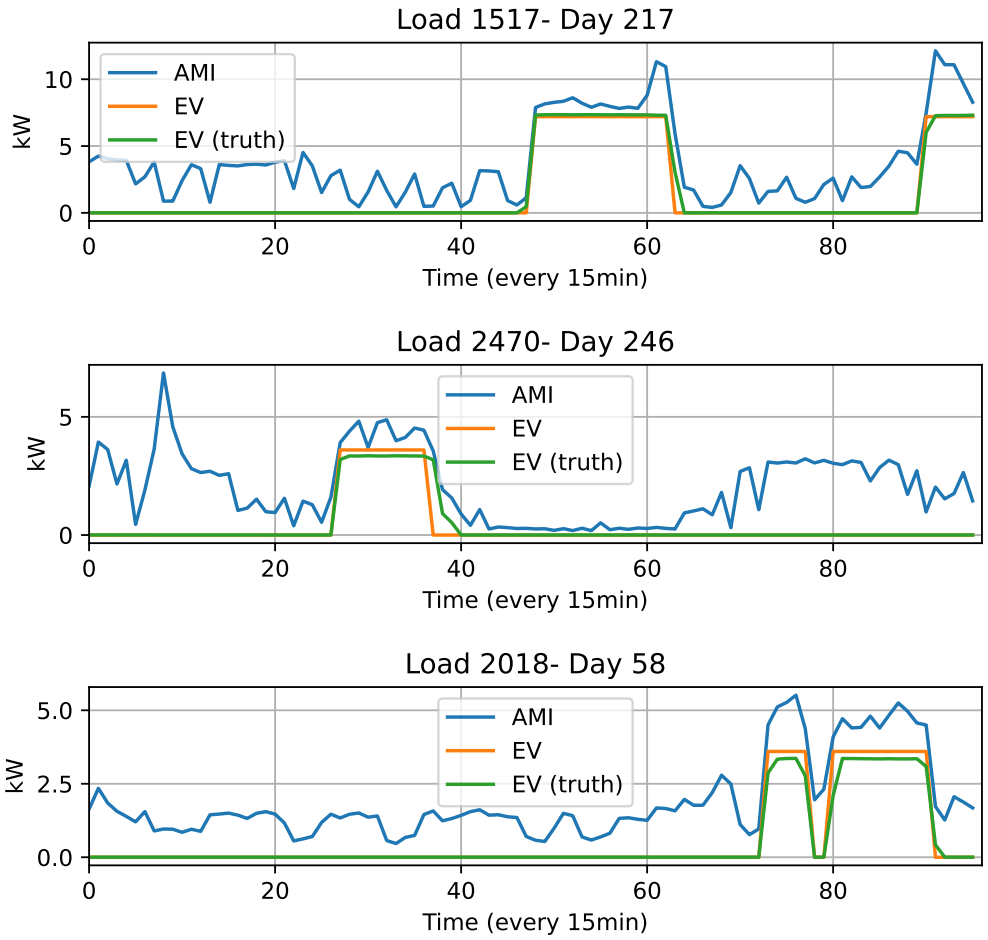

Figure 3.1 Examples of EV charging events detected from smart meter data measured throughout a day at every 15 minutes

We observe that while EV charging events can still be detected, the level of accuracy is reduced mainly due to the lack of data. For example, the power level is determined to be 3.6kW for Load 1517 because the baseload consumption during the day would become negative if the power level were set at 7.2kW. For Load 2470, a peak demand at 2AM is mistakenly identified as a charging event for 1 hour. Lastly, the brief pause between the two

charging events for Load 2018 is not picked up, hence the extracted information on start time and duration of the charging event is not exact.

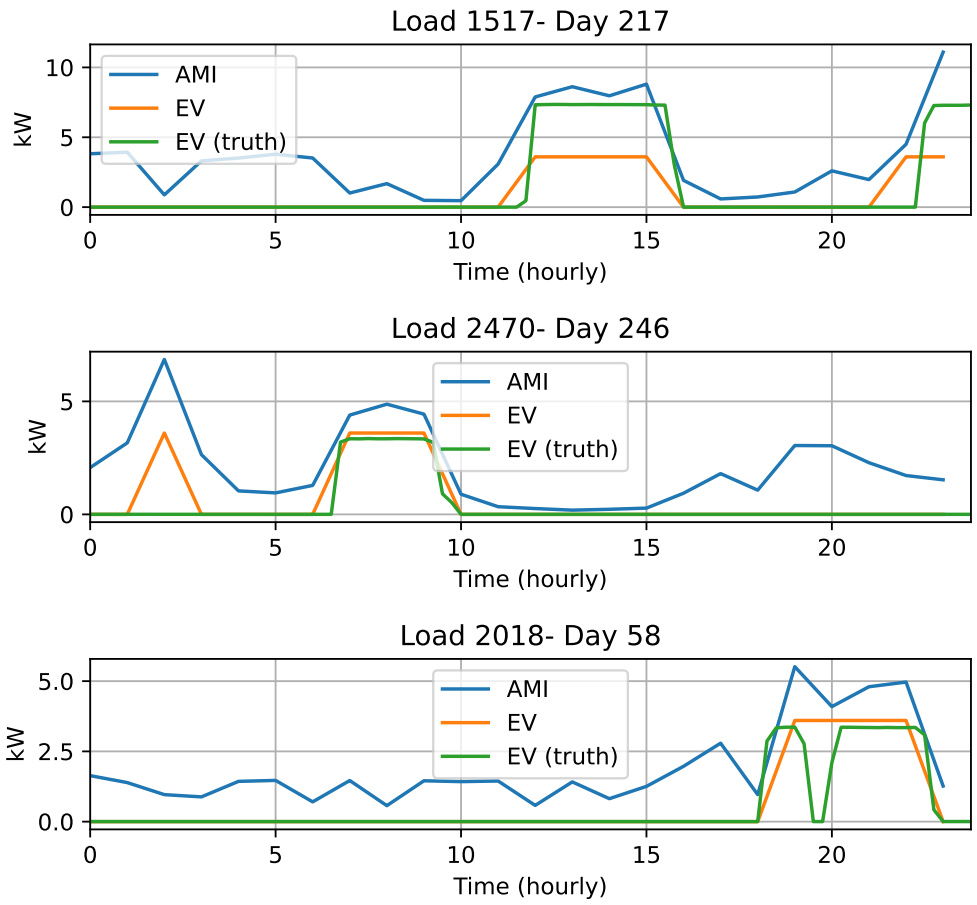

Figure 3.2 EV charging events detected for the same customer/day as in Figure 3.1 but from smart meter data measured at every hour

To benchmark the performance of our proposed approach to detect the EV charging events, we compare it with two other algorithms: one based on signal decomposition [50] and the other using a trained CNN model [44]. We adopt the two metrics used in [50] to evaluate the detection performance on customer i's data:

- *F1 Score* F1 that measures the accuracy of detection results. The score is defined in terms of sample counts in True Positive (TP), False Positive (FP), and False Negative (FN) conditions:

$$\mathrm{F1}_i = \frac{2TP_i}{2TP_i + FP_i + FN_i}.$$

- *Explained Variance Score* $\mathrm{E}_{\mathrm{var}}$ that measures the dispersion or discrepancy between the detected and true EV consumption data. The $\mathrm{E}_{\mathrm{var}}$ score is defined as:

$$\mathrm{E}_{\mathrm{var},i} = 1 - \frac{\mathrm{Var}(\mathrm{P}_i^{\mathrm{EV}} - \mathrm{P}_{i,\mathrm{true}}^{\mathrm{EV}})}{\mathrm{Var}(\mathrm{P}_{i,\mathrm{true}}^{\mathrm{EV}})},$$

  where $\mathrm{P}_i^{\mathrm{EV}}, \mathrm{P}_{i,\mathrm{true}}^{\mathrm{EV}} \in \mathbb{R}^{N_{\mathrm{D}}T}$ are the detected and true EV charging consumption for all days, respectively.

We remark that the closer the two metric values are to 1, the better the performance of the algorithm is.

Although the benchmark algorithms also use Pecan Street datasets to test the performance, it is not clear what customers and time periods are included in the datasets. Therefore, it is not possible to directly compare the metric values of a specific customer. Instead, we report the minimum, mean, median, and maximum of F1 and $\mathrm{E}_{\mathrm{var}}$ values obtained for all customers in the dataset used in this work, and compare them with those reported in [44, 50] using their datasets. The values are shown in Table 3.1. We note that the performance of our approach is comparable to that of the benchmark algorithms. Although the minimum, mean, and median values from our approach are slightly lower, we should emphasize that the meter data used in both benchmark algorithms have 1-minute intervals, while data with 15-minute intervals are used in our work. As pointed out in [50], as the data measurement interval increases, the accuracy of the algorithm decreases (e.g., the mean $\mathrm{E}_{\mathrm{var}}$ drops to 0.69 if data with 15-minute intervals are used in [50]). Further, to obtain high accuracy, the CNN approach [44], being a supervised-learning method, needs a large number of labelled training samples which are difficult to obtain in practice. While the method in [50] does not require training, tuning of the hyperparamters in both stages of the decomposition is required to differentiate EV charging from the use of air conditioners. In our approach, by leveraging the readily available contextual information of EV charging events, we do not require high-resolution data, and we achieve comparable accuracy with that of the literature without any model training or hyperparameter tuning.

	Proposed approach		**Decomposition** [50]		**CNN** [44]	
	F1	E_{var}	F1	E_{var}	F1	E_{var}
Min	0.696	0.512	0.771	0.611	0.765	0.857
Mean	0.876	0.805	0.906	0.831	0.892	0.890
Median	0.889	0.819	0.909	0.852	0.911	0.891
Max	0.967	0.972	0.982	0.974	0.925	0.924

Table 3.1 Performance comparison with other algorithms

Next, we compute the empirical distributions for customers' charging habits as in (3.18) based on charging events detected for all customers during a full year. We use the meter data with 15-minute intervals due to the better accuracy of the detection results. We compare the estimated PMFs and the cumulative distribution functions (CDFs, except for the charger power levels) computed from the detection results with those from the ground truth in Figure 3.3.

We remark that in the distributions of the charging start time, high probabilities of starting the charging at midnight are observed. This is because some charging events start during the evening and continue until the next day. In this case, as we only detect events during one day's time window, the event is broken into two parts with the second part starting at midnight the next day. Also, as we only detect events lasting more than 1 hour, we obtain a zero probability for charging events starting on and after 11PM and for charging duration less than 1 hour, which are observable differences when comparing the distributions in Figure 3.3.

The following can be inferred from the results for the customers in this Pecan Street dataset:

- Customers tend to charge EVs during evenings until early mornings, with slightly higher probabilities starting in the evenings;
- Each charging event usually does not last more than 9 hours;
- Daily energy consumption for charging EVs rarely exceed 60 kWh, and;
- More than half of the EVs are charged at 3.6 kW.

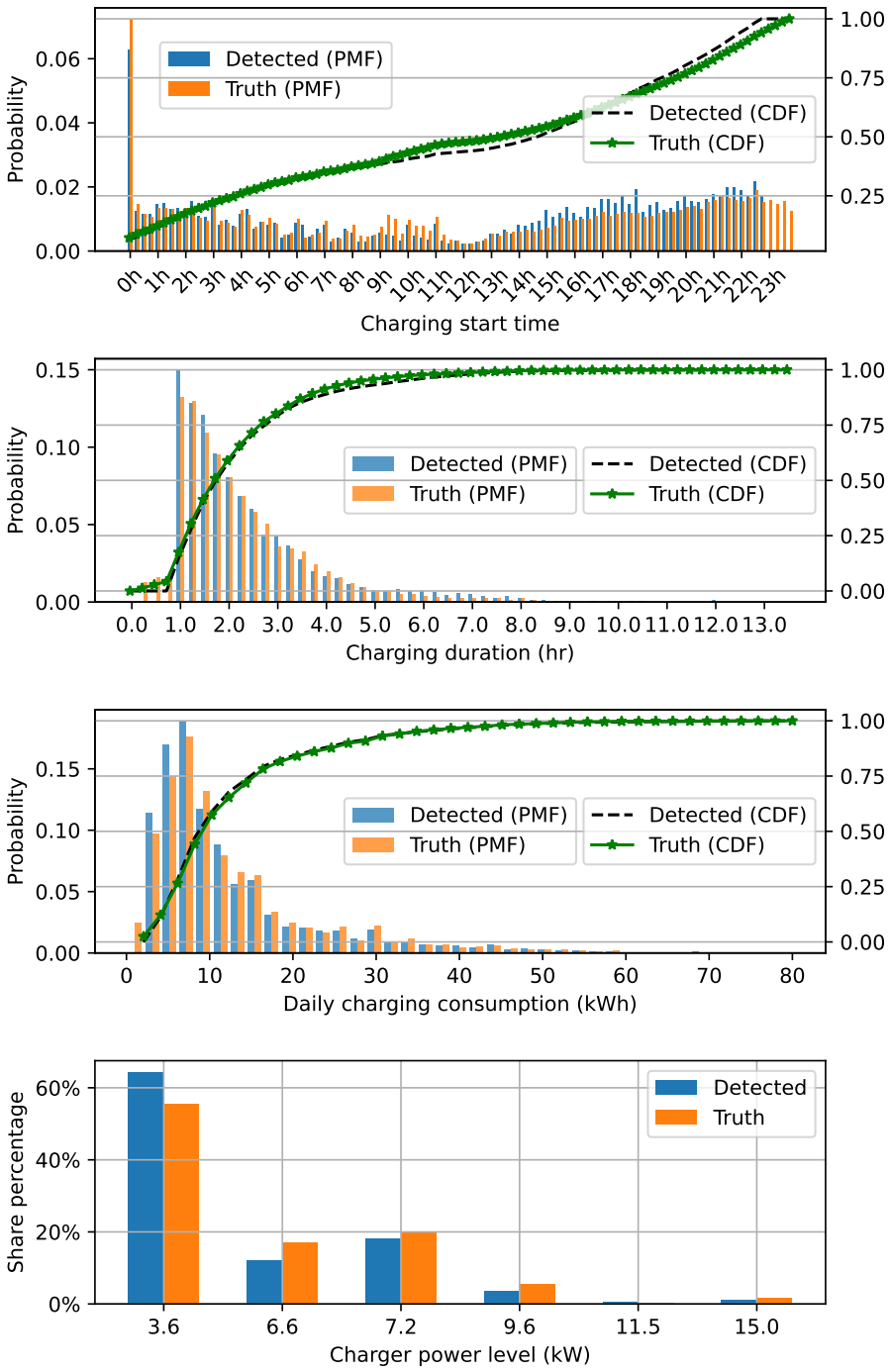

Figure 3.3 Distributions of start time, duration, daily energy, and charger power levels based on detected charging events

3.4.2 Impact analysis of EV charging

In this part of the case study, we use the inferred charging patterns to study the impact of EV charging to the distribution network using the stochastic method presented in Chapter 2 (Refer to Section 4.3.1 of Chapter 4 for details on how the method is extended to time-series analyses). We use the same IEEE-8500 test feeder as in Chapter 2 to demonstrate the results. We construct the set of all possible per-unit charging profiles based on the detected results using (3.19) and (3.20). The resulting set contains a total of 4224 profiles. We then use (3.21) to calculate the probability that each per-unit profile will be adopted by the customers on the network. We illustrate the probabilities of all profiles as a heat map in Figure 3.4, where each profile is represented by the tuple $(\textit{start time}, \textit{duration})$. For example, $(8\text{PM}, 2\text{h}30\text{m})$ represents the profile for which charging starts at 8PM and lasts for 2 hours and 30 minutes. To get the EV charging profiles in kW, i.e., the set $\mathcal{L}_{\text{EV}}$, we multiply the per-unit profiles with the 6 power levels in $\mathcal{P}$. To apply the REM method of Chapter 2, we need to know the probabilities of adopting profiles in $\mathcal{L}_{\text{EV}}$. For simplicity, we assume that the distribution of power levels and the probabilities that per-unit charging profiles are adopted by the customers are independent. Hence, the probabilities $\Pr[\mathcal{L}_{\text{EV}}]$ are obtained by multiplying the per-unit profile probabilities in (3.21) with the distribution of the power levels, which is shown in the bottom right plot of Figure 3.3.

In Figure 3.5, we show the impacts of EV charging on the loading level of the substation transformer at penetration rates of 10%, 30%, 50%, and 80%. The penetration rate follows the Definition 2.1 which is the ratio of the number of EVs connected to the network over the total number of customers. We use both the inferred probabilities and the true probabilities as in Figure 3.4 to perform the impact analyses. At each penetration rate, we show the loading curve over one day without any EV connected and compare the loading curves obtained from the two sets of probabilities. We observe that as the penetration grows, impacts to the transformer loading level increase, and the transformer becomes overloaded during the evening hours at 80% EV penetration. Due to differences in the profile distributions, errors between the two loading curves are more observable at higher penetration rates. We extract the per-unit errors at all penetrations and show them in Figure 3.6. Errors are mostly higher during the 9h-11h and evening hours, which are the periods where differences in the profile distributions are more observable in Figure 3.4. At 80% penetration rate, the worst error is around 0.06 p.u. or 6%.

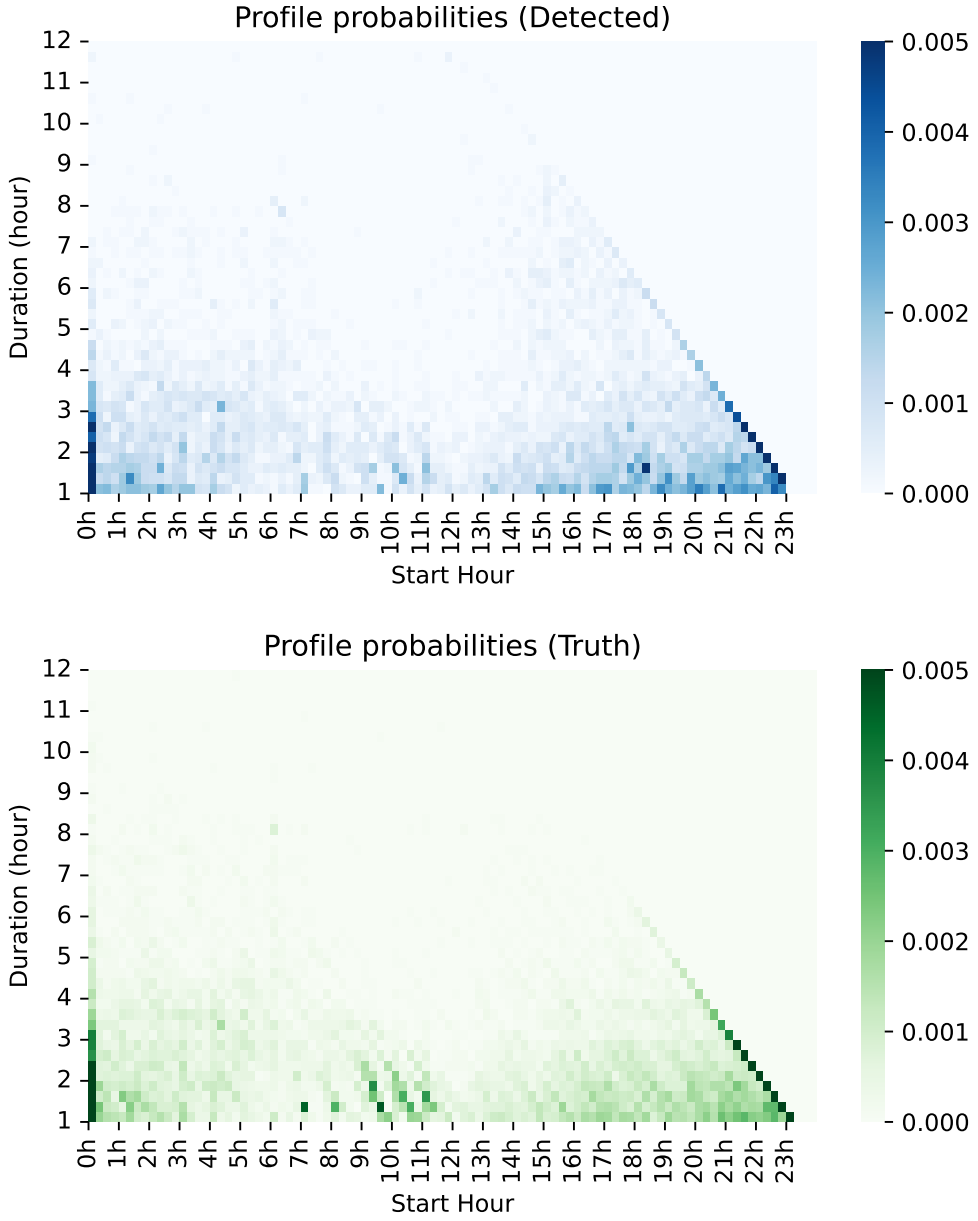

Figure 3.4 Probabilities of profiles used in the stochastic EV impact analysis

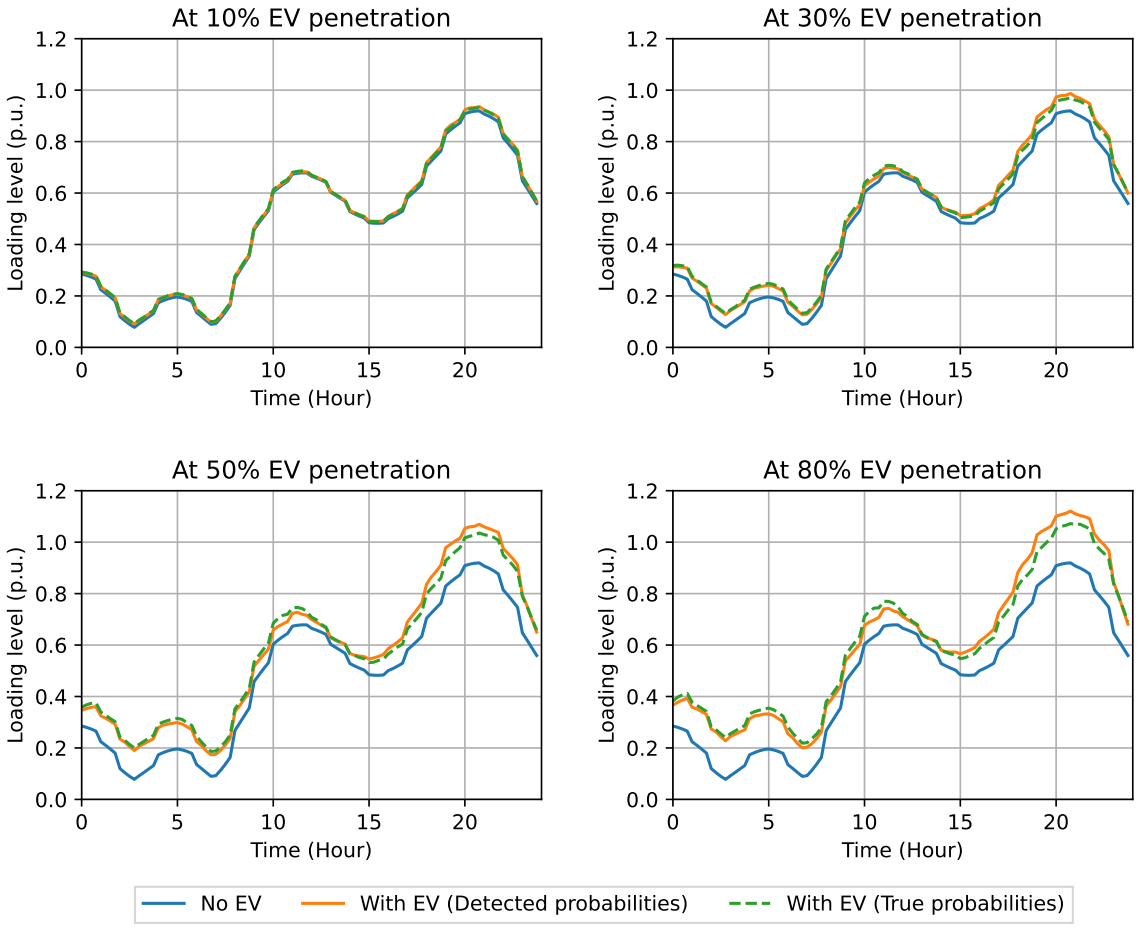

Figure 3.5 Comparison of the substation transformer loading levels using detected and true profile probabilities at various EV penetration rates

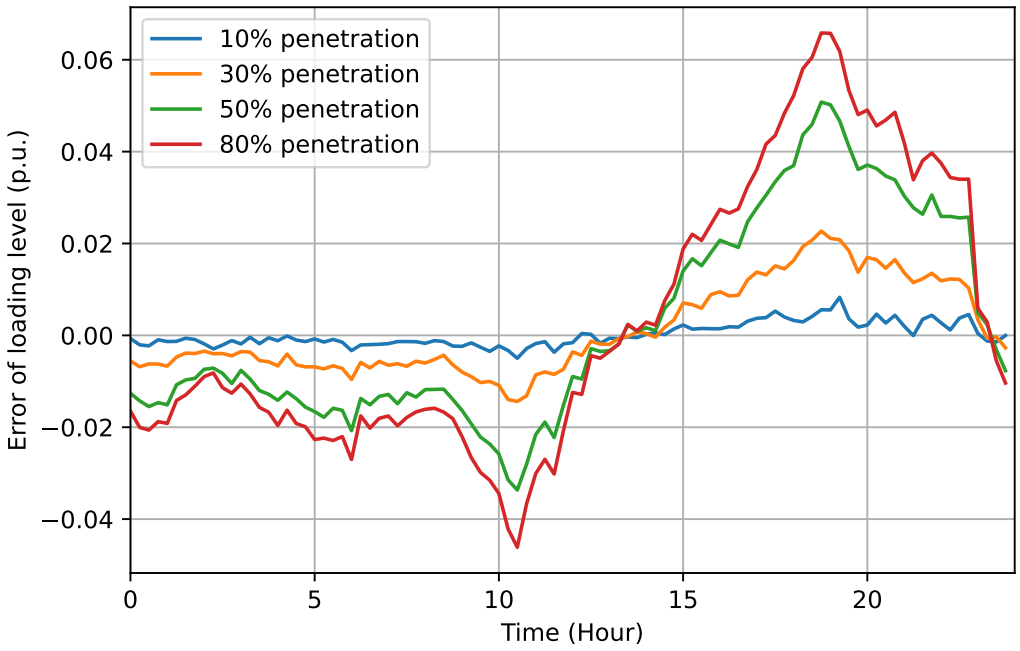

Figure 3.6 Result errors of the substation transformer loading levels using detected and true profile probabilities at various EV penetration rates

3.5 Conclusion

In this chapter, a non-intrusive and training-free method is proposed to detect BTM EV charging events based on customers' smart meter data. Our approach does not require labelled training data nor hyperparameter tuning, and achieves a similar level of accuracy in extracting information of charging events as that of the literature by using meter data measured at every 15 minutes. Through a data-driven approach, we infer customers' charging patterns in terms of probability distributions of charging profiles from the detection results during an entire year. We compare the inferred probability distributions with those from the ground truth, and illustrate that even if there exist some minor differences between the two sets of distributions, no significant error occurs in the results of EV charging impact analyses. Using the inferred probability distributions from our approach allows utilities to better understand customers' EV charging behaviours and to evaluate impacts that EV charging may bring to their power distribution networks. In practice, as EV owners' charging behaviours may shift over time, the variations can be captured by periodically applying the method on customers' smart meter data to update the inferred probability distributions.

The detection approach presented in this chapter requires that the meter data contain only consumption; in other words, if customers have power-generating devices installed such as

PV or battery systems, the generation must be subtracted from the meter data such that EV charging events are not under-estimated. As this information may not be always available to utilities in practice, in the future we wish to extend our approach by adding an extra step to estimate BTM generation (e.g., [115]) and exclude them from the meter data. Further, our approach can be improved by relaxing the assumption of rectangular waveform during active charging events, i.e., by considering variations of charging power in time.

As illustrated in the case studies, we use the inferred probability data for EV charging and assess the EV impacts during a day. At high EV penetration rates, it is possible that network equipment may be overloaded for continuous periods during the day. If such overloading patterns repeatedly occur on each day during the year, we can expect that the equipment are stressed and premature failure can happen, leading to much more serious events and even faults on the distribution network. As a measure of prevention, mitigation strategies should be prepared for better planning and operation of the networks. In the next chapter, we present an approach to mitigate equipment overload on distribution networks with high EV penetration. If some equipment is assessed as having risks of being overloaded under the extracted charging behaviours of EV owners, we aim to design a strategy to shift customers' EV charging behaviours through incentive programs. Details on how the REM presented in Chapter 2 is extended to perform a stochastic time-series impact analysis using given EV charging probability data are also discussed. The time-series REM (ts-REM) is used to quickly assess the impacts when customers' charging behaviours are shifted under the designed mitigation plans.

CHAPTER 4 A CONVEX REFORMULATION OF BI-LEVEL OPTIMIZATION FOR MITIGATING ELECTRIC VEHICLE CHARGING OVERLOADS ON DISTRIBUTION NETWORKS

4.1 Introduction

As the electrification of the transportation sector promotes the adoption of electric vehicles, the penetration of EVs is rapidly increasing in power distribution networks. While EVs offer the advantage of reducing reliance on fossil fuels and lowering greenhouse gas emissions, charging them can pose significant challenges to power distribution networks, especially in scenarios with high EV penetration. In the previous chapter, we illustrated an example where the substation transformer of a distribution network has a risk of being overloaded due to EV charging. Besides equipment overloading, other abnormal operating conditions may also occur such as voltage fluctuations, phase imbalances, harmonic distortions, etc. [1, 2]. From the perspective of utilities, stochastic analysis methods like the REM developed in Chapter 2 are necessary to study the impact that EV charging may have on the network conditions. These impact analyses consider the uncertainties in EV charging-related variables, e.g., locations, start time, duration, and power levels, and help reveal potential abnormal conditions on power networks [21, 22]. Based on the analysis results, it is important to address the identified network issues through mitigation plans and network optimization to ensure safe grid operations and maintain high-quality service.

In this chapter, we propose strategies to mitigate potential overloading issues to key network equipment, e.g., a substation transformer. We aim to minimize the loss of equipment's lifetime and to avoid premature failures due to the overloading caused by EV charging [116,117]. Customers are invited to participate and contribute to the implementation of the mitigation strategies by receiving incentives from the utilities and changing their charging habits. The idea is to reduce customers' probability of charging their EVs during the period when the equipment is most heavily loaded, i.e., the peak period, and to increase the probability of charging EVs when the equipment is lightly loaded. The main advantage of the approach is that the strategy is implementable without direct or real-time observations of customers' EV charging events, because no control is imposed when an EV is being charged. Hence, customers are not obliged to follow any real-time price or control signals and no communication infrastructure is necessary. Further, the strategy can be uniformized and applied to customers on multiple large networks.

The following contributions are discussed in this chapter:

- Formulating a bi-level optimization problem to design mitigation strategies aiming to shift EV charging from the peak period when equipment is heavily loaded, to the off-peak period when the equipment is lightly loaded. The problem is then reformulated into a computationally tractable single-level convex program.
- Considering two types of incentive programs based on the solution to the convex program: reward for reducing power consumption during the peak period and designing a TOU tariff during different periods of a day.
- Embedding the convex program into a novel search algorithm to efficiently determine optimal incentive levels and the corresponding shift in customer charging probabilities. The proof of convergence is provided and the optimality of the converged value is discussed.

The rest of the chapter is organized as follows: Section 4.2 presents the assumptions and motivations for the problem statement. In Section 4.3, we derive a bi-level optimization problem to design the mitigation strategy. Instead of directly solving the non-linear optimization problem, we reformulate it to a convex problem in Section 4.4, and embed it into a search algorithm to determine the reward level and the TOU tariff. Section 4.6 illustrates the results of the proposed mitigation strategy to an overloaded substation transformer due to EV charging on a modified IEEE-8500 test feeder. Finally, we conclude in Section 4.7 and point out some future work directions.

4.2 Problem statement

When EV owners connect their vehicles to the power network for charging, more power demand is seen by the equipment upstream to the customers, especially for those near the source of the network. Here, we focus on charging impacts from residential EVs, as they account for up to 80% of charging events [109], and have more diversity and variance in charging patterns. As observed in the case studies of Chapter 3 on the Pecan Street dataset, EV chargings are more frequent during the evening, which coincides with the peak time of the network and equipment may be overloaded. To prevent accelerated aging of the equipment leading to premature failure, mitigation strategies are required. To consider uncertainties in customers' behaviours in charging their EVs when designing such mitigation strategies, we characterize their daily charging patterns in terms of probabilities, and we look at the expected daily power demand for EV charging. We remark that our approach can be extended to other customer types than residential without limitations as long as corresponding charging patterns and probabilities are provided.

4.2.1 Assumptions on EV data

We assume that the following EV data is provided, which can be gathered from either statistical analysis of EV charging data [118], estimated from EV usage and travel data [119], or extracted from historical smart meter data of EV owners using the method developed in Chapter 3.

- A set of L charging profiles $\mathcal{L}_{\mathrm{EV}} = \{l^j_{\mathrm{EV}}(t)\}_{j=1,2,\cdots,L}$, where $l^j_{\mathrm{EV}}(t)$ is an EV charging profile in kW during an entire day discretized over the set $\mathcal{T} = \{1, 2, \cdots, T\}$. Here, T is the cardinality of $\mathcal{T}$ and depends on the time step, e.g., $T = 96$ if each time step has a duration of $\Delta t = 15$ minutes. For a profile, if charging is active at t, $l^j_{\mathrm{EV}}(t) > 0$ and $l^j_{\mathrm{EV}}(t) = 0$ otherwise.
- Probabilities $\Pr^i[\mathcal{L}_{\mathrm{EV}}] \in [0, 1]^L$ attached to customer $i \in \{1, 2, \cdots, N_{\mathrm{m}}\}$, where N_{m} is the total number of customers, and $\Pr^i(j)$ is the probability of a charging profile l^j_{EV} in $\mathcal{L}_{\mathrm{EV}}$ being adopted. For customers who do not own any EV, $\Pr^i(j) = 0, \forall l^j_{\mathrm{EV}} \in \mathcal{L}_{\mathrm{EV}}$.

Note that we do not presume any type of distribution for $\Pr^i$, hence it can be of any arbitrary probability distribution.

4.2.2 Motivation

The expected charging power $\mathbb{E}[S_{e,\mathrm{EV}}](t) \in \mathbb{R}$ of an EV connected downstream of equipment e at time t on all connected phases is expressed by:

$$\begin{aligned} \mathbb{E}[S_{e,\mathrm{EV}}](t) &= \frac{1}{|\mathcal{K}_e|} \sum\nolimits_{i \in \mathcal{K}_e} \mathbb{E}[S^i_{e,\mathrm{EV}}](t) \\ \mathbb{E}[S^i_{e,\mathrm{EV}}](t) &= \sum\nolimits_j l^j_{\mathrm{EV}}(t) \Pr^i(j), \end{aligned} \tag{4.1}$$

where $\mathcal{K}_e$ is the set of customers who are downstream of e, and $|\mathcal{K}_e|$ is its cardinality. If all customers on the network are downstream of e, then $|\mathcal{K}_e| = N_{\mathrm{m}}$. If EV owning customers tend to charge their vehicles during peak hours (denoted by $\mathcal{T}^{\mathrm{P}} \subset \mathcal{T}$), i.e., these customers possess high probabilities of adopting charging profiles that are active during $\mathcal{T}^{\mathrm{P}}$ (denoted by $\mathcal{L}^{\mathrm{P}}_{\mathrm{EV}} \subset \mathcal{L}_{\mathrm{EV}}$), then it is expected that $\mathbb{E}[S_{e,\mathrm{EV}}](t)$ is large for $t \in \mathcal{T}^{\mathrm{P}}$. Consequently, the extra loading due to EV charging will be significant, and the probability of overloading network equipment is then greatly increased, especially when the EV penetration is high. Conversely, if a control mechanism is in place to limit $\mathbb{E}[S_{e,\mathrm{EV}}](t)$ for $t \in \mathcal{T}^{\mathrm{P}}$, the equipment overloading can be mitigated.

Considering (4.1), $\mathbb{E}[S_{e,\mathrm{EV}}](t)$ during $\mathcal{T}^{\mathrm{P}}$ can be reduced if the probabilities $\Pr^i[\mathcal{L}^{\mathrm{P}}_{\mathrm{EV}}]$ of all customers are decreased while those in $\Pr^i[\mathcal{L}_{\mathrm{EV}} \setminus \mathcal{L}^{\mathrm{P}}_{\mathrm{EV}}]$ are increased. In other words, we are shifting high values of $\mathbb{E}[S_{e,\mathrm{EV}}](t)$ for $t \in \mathcal{T}^{\mathrm{P}}$ to other time periods. Under such a strategy, we can mitigate potential overloading issues to network equipment due to EV charging during $\mathcal{T}^{\mathrm{P}}$ by reducing customers' probabilities of charging their EVs in this period. In the following section, we discuss how modifications to $\Pr^i$ are made when customer i participates in a mitigation strategy.

4.2.3 Modification to charging profile probabilities

We partition the time period $\mathcal{T}$ and the set of profile types $\mathcal{L}_{\mathrm{EV}}$ into the following disjoint sets:

$$\begin{aligned} \mathcal{T} &= \mathcal{T}^{\mathrm{P}} \cup \mathcal{T}^{\mathrm{OP}} \cup \mathcal{T}^{\mathrm{MP}} \\ \mathcal{L}_{\mathrm{EV}} &= \mathcal{L}^{\mathrm{P}}_{\mathrm{EV}} \cup \mathcal{L}^{\mathrm{OP}}_{\mathrm{EV}} \cup \mathcal{L}^{\mathrm{MP}}_{\mathrm{EV}}, \end{aligned} \tag{4.2}$$

where

- $\mathcal{T}^{\mathrm{P}}$ is the peak period and $\mathcal{L}^{\mathrm{P}}_{\mathrm{EV}}$ is the set of profiles where charging is active during $\mathcal{T}^{\mathrm{P}}$. Under a mitigation strategy, customers' probabilities $\Pr^i[\mathcal{L}^{\mathrm{P}}_{\mathrm{EV}}]$ are to be reduced;
- $\mathcal{T}^{\mathrm{OP}}$ is the off-peak period and $\mathcal{L}^{\mathrm{OP}}_{\mathrm{EV}}$ is the set of profiles where charging is active during $\mathcal{T}^{\mathrm{OP}}$, but excluding those in $\mathcal{L}^{\mathrm{P}}_{\mathrm{EV}}$, and customers' probabilities $\Pr^i[\mathcal{L}^{\mathrm{OP}}_{\mathrm{EV}}]$ are to be increased under a mitigation strategy, and;
- $\mathcal{T}^{\mathrm{MP}}$ is the mid-peak period and $\mathcal{L}^{\mathrm{MP}}_{\mathrm{EV}}$ contains the remaining profiles excluding those in $\mathcal{L}^{\mathrm{P}}_{\mathrm{EV}} \cup \mathcal{L}^{\mathrm{OP}}_{\mathrm{EV}}$. Customers' probabilities $\Pr^i[\mathcal{L}^{\mathrm{MP}}_{\mathrm{EV}}]$ remain unchanged under a mitigation strategy.

In general, $\mathcal{T}^{\mathrm{P}}$ should include the hours during which the network is heavily-loaded, hence we can assume that overloading never occurs to equipment during $\mathcal{T}^{\mathrm{OP}}$ and $\mathcal{T}^{\mathrm{MP}}$ periods, even when a mitigation strategy is applied.

Let $\mathbf{y}^{\mathrm{P}} \in \{0,1\}^L = [y^{\mathrm{P}}_j, j = 1, 2, \cdots L]^\top$ be an indicator vector where $y^{\mathrm{P}}_j = 1$ if $j \in \mathcal{L}^{\mathrm{P}}_{\mathrm{EV}}$ and $y^{\mathrm{P}}_j = 0$ otherwise. Similarly, let $\mathbf{y}^{\mathrm{OP}} \in \{0,1\}^L$ be another indicator vector for profiles in $\mathcal{L}^{\mathrm{OP}}_{\mathrm{EV}}$. For given $\Pr^i[\mathcal{L}_{\mathrm{EV}}]$, we have $\Pr^i[\mathcal{L}_{\mathrm{EV}}] = \Pr^{i,\mathrm{P}} + \Pr^{i,\mathrm{OP}} + \Pr^{i,\mathrm{MP}}$, where $\Pr^{i,\mathrm{P}} = \Pr^i[\mathcal{L}_{\mathrm{EV}}] \odot \mathbf{y}^{\mathrm{P}}$, $\Pr^{i,\mathrm{OP}} = \Pr^i[\mathcal{L}_{\mathrm{EV}}] \odot \mathbf{y}^{\mathrm{OP}}$, and $\odot$ is the Hadamard product. It is remarked that $\Pr^{i,\mathrm{P}}, \Pr^{i,\mathrm{OP}}, \Pr^{i,\mathrm{MP}} \in [0,1]^L$.

Denote $\Sigma^{i,\mathrm{P}} = (\Pr^i[\mathcal{L}_{\mathrm{EV}}])^\top \mathbf{y}^{\mathrm{P}} \in [0,1]$ as customer i's total probability of adopting charging profiles in $\mathcal{L}^{\mathrm{P}}_{\mathrm{EV}}$. Suppose that we would like to reduce $\Sigma^{i,\mathrm{P}}$ by an amount $\Delta^i_{\mathrm{prob}} \geq 0$, such

that the customer's probabilities of adopting charging profiles in $\mathcal{L}_{\text{EV}}^{\text{P}}$ are reduced. Let $\widetilde{\text{Pr}}^{i,\text{P}} \in [0,1]^L$ be the resulting probabilities, and we have:

$$\widetilde{\text{Pr}}^{i,\text{P}} = \text{Pr}^{i,\text{P}} - \frac{\Delta^i_{\text{prob}}}{\Sigma^{i,\text{P}}} \text{Pr}^{i,\text{P}}. \tag{4.3}$$

We consider (4.3) as equivalent to scaling down the probabilities in $\text{Pr}^{i,\text{P}}$ such that the sum of reductions adds up to Δ^i_{prob}. To ensure that all elements of $\widetilde{\text{Pr}}^{i,\text{P}}$ are non-negative, we impose $0 \leq \Delta^i_{\text{prob}} \leq \Sigma^{i,\text{P}}$. Conversely, we scale up the probabilities in $\text{Pr}^{i,\text{OP}}$ such that the total probability is increased by Δ^i_{prob}, i.e.,

$$\widetilde{\text{Pr}}^{i,\text{OP}} = \text{Pr}^{i,\text{OP}} + \frac{\Delta^i_{\text{prob}}}{\Sigma^{i,\text{OP}}} \text{Pr}^{i,\text{OP}}, \tag{4.4}$$

where $\Sigma^{i,\text{OP}} = \left(\text{Pr}^i[\mathcal{L}_{\text{EV}}]\right)^\top \mathbf{y}^{\text{OP}} \in [0,1]$. From (4.3) and (4.4), the resulting probability distribution $\widetilde{\text{Pr}}^i[\mathcal{L}_{\text{EV}}] \in [0,1]^L$ obtained by shifting probabilities of charging during $\mathcal{T}^{\text{P}}$ to $\mathcal{T}^{\text{OP}}$ can be expressed by:

$$\widetilde{\text{Pr}}^i[\mathcal{L}_{\text{EV}}] = \widetilde{\text{Pr}}^{i,\text{P}} + \widetilde{\text{Pr}}^{i,\text{OP}} + \text{Pr}^{i,\text{MP}}. \tag{4.5}$$

To acknowledge the fact that not all customers own an EV or are willing to change their charging habits under a mitigation program, we let $\mathcal{K}_p \subseteq \mathcal{K}_e$ be the set of EV owners who participate, and $\lambda_p \in [0,1]$ be the participation factor, which is defined by $\lambda_p = \frac{|\mathcal{K}_p|}{|\mathcal{K}_e|}$. We have:

$$\Delta^i_{\text{prob}} = 0, \ \forall i \in \mathcal{K}_e \setminus \mathcal{K}_p. \tag{4.6}$$

We extend the above process of modifying charging profile probabilities to all customers in a matrix form. By denoting $\mathbf{Pr} \in [0,1]^{|\mathcal{K}_e| \times L}$ as probabilities of all EV charging profiles $\mathcal{L}_{\text{EV}}$ for all customers in $\mathcal{K}_e$, we extract the probabilities of profiles in $\mathcal{L}_{\text{EV}}^{\text{P}}$ of all customers by $\mathbf{Pr}^{\text{P}} = \mathbf{Pr}\mathbf{Y}^{\text{P}}$, where $\mathbf{Y}^{\text{P}} = \text{diag}(\mathbf{y}^{\text{P}}) \in \{0,1\}^{L \times L}$. Similarly, the probabilities of profiles in $\mathcal{L}_{\text{EV}}^{\text{OP}}$ are $\mathbf{Pr}^{\text{OP}} = \mathbf{Pr}\mathbf{Y}^{\text{OP}}$, where $\mathbf{Y}^{\text{OP}} = \text{diag}(\mathbf{y}^{\text{OP}}) \in \{0,1\}^{L \times L}$. We then extend (4.3) to the following matrix form for all customers:

$$\widetilde{\mathbf{Pr}}^{\text{P}} = \mathbf{Pr}^{\text{P}} - (\mathbf{\Sigma}^{\text{P}})^{-1} \mathbf{\Delta}_{\text{prob}} \mathbf{Pr}^{\text{P}}, \tag{4.7}$$

where $\mathbf{\Sigma}^{\text{P}} = \text{diag}\Big(\{\Sigma^{\text{i,P}}, i \in \mathcal{K}_e\}\Big)$ and $\mathbf{\Delta}_{\text{prob}} = \text{diag}\Big(\{\Delta^i_{\text{prob}}, i \in \mathcal{K}_e\}\Big)$ which are both $|\mathcal{K}_e| \times |\mathcal{K}_e|$ square matrices. Similarly, the adjusted probabilities for profiles in $\mathcal{L}_{\text{EV}}^{\text{OP}}$ after adding

$\boldsymbol{\Delta}_{\text{prob}}$ are:

$$\widetilde{\mathbf{Pr}}^{\text{OP}} = \mathbf{Pr}^{\text{OP}} + (\boldsymbol{\Sigma}^{\text{OP}})^{-1}\boldsymbol{\Delta}_{\text{prob}}\mathbf{Pr}^{\text{OP}}, \tag{4.8}$$

where $\boldsymbol{\Sigma}^{\text{OP}} = \text{diag}\Big(\{\Sigma^{\text{i,OP}}, i \in \mathcal{K}_e\}\Big) \in [0,1]^{|\mathcal{K}_e|\times|\mathcal{K}_e|}$. From (4.7) and (4.8), we obtain the modified probabilities of charging profiles for all customers as,

$$\begin{aligned}\widetilde{\mathbf{Pr}} &= \widetilde{\mathbf{Pr}}^{\text{P}} + \widetilde{\mathbf{Pr}}^{\text{OP}} + \mathbf{Pr}^{\text{MP}} \\ &= \mathbf{Pr}^{\text{P}} - (\boldsymbol{\Sigma}^{\text{P}})^{-1}\boldsymbol{\Delta}_{\text{prob}}\mathbf{Pr}^{\text{P}} + \mathbf{Pr}^{\text{OP}} + (\boldsymbol{\Sigma}^{\text{OP}})^{-1}\boldsymbol{\Delta}_{\text{prob}}\mathbf{Pr}^{\text{OP}} + \mathbf{Pr}^{\text{MP}} \\ &= \mathbf{Pr} - \boldsymbol{\Sigma}_{\text{inv}}\begin{bmatrix}\boldsymbol{\Delta}_{\text{prob}}\mathbf{Pr} & \mathbf{0}_{|\mathcal{K}_e|,L} \\ \mathbf{0}_{|\mathcal{K}_e|,L} & \boldsymbol{\Delta}_{\text{prob}}\mathbf{Pr}\end{bmatrix}\mathbf{Y},\end{aligned} \tag{4.9}$$

where $\boldsymbol{\Sigma}_{\text{inv}} = \begin{bmatrix}(\boldsymbol{\Sigma}^{\text{P}})^{-1} & -(\boldsymbol{\Sigma}^{\text{OP}})^{-1}\end{bmatrix} \in \mathbb{R}^{|\mathcal{K}_e|\times 2|\mathcal{K}_e|}$, $\mathbf{0}_{|\mathcal{K}_e|,L}$ is a zero-matrix, and $\mathbf{Y} = \begin{bmatrix}\mathbf{Y}^{\text{P}} & \mathbf{Y}^{\text{OP}}\end{bmatrix}^{\top} \in \{0,1\}^{2L\times L}$.

It is remarked that (4.9) formulates how the probabilities are modified assuming $\boldsymbol{\Delta}_{\text{prob}}$ is given. Recall that for a non-EV owner or non-participating customer $i \notin \mathcal{K}_p$, $\Delta^i_{\text{prob}} = 0$. For each participating customer, we discuss in the next section how Δ^i_{prob} can be determined from an optimization problem, which forms the basis for the mitigation strategy. Without loss of generality, for the rest of the paper we assume that $\lambda_p = 1$, i.e., all customers are participating into the mitigation program.

4.3 Mitigation strategy

Recall that our goal of encouraging EV owners to shift their probabilities of charging periods from $\mathcal{T}^{\text{P}}$ to $\mathcal{T}^{\text{OP}}$ is to avoid overloading the key network equipment and to maintain equipment lifetime. Mitigation strategies should be designed based on optimal values of $\boldsymbol{\Delta}_{\text{prob}}$ which should meet the following conditions: (a) no extensive overloading occurs to the equipment and its nominal lifetime is maintained and; (b) customers are driven by incentives to adopt charging behaviours according to the adjusted $\widetilde{\mathbf{Pr}}$ which does not result in unmotivated costs to utilities.

4.3.1 Stochastic EV impact analysis

First of all, for given $\mathbf{Pr}$ or modified probability data $\widetilde{\mathbf{Pr}}$, a computational efficient stochastic method is needed to evaluate impacts of EV charging to equipment loading level on distribution networks. For this purpose, Monte Carlo simulation-based approaches are not appli-

cable as generating samples and performing power flow analyses on them require important computational resources. Here, we adopt the rapid estimation method (REM) developed in Chapter 2, which analyzes the impact of grid-edge technologies, including EVs to distribution networks under various penetration rates. We extend the method to perform a time-series impact analysis to distribution networks given probability data on EV charging.

Denote $x(p)$ as the network states, e.g., loading levels of an equipment (in per-unit or percentage) of the power distribution network at an EV penetration rate p. The penetration rate is defined as the ratio of the total number of EVs n_{EV} over the total number of customers on the network N_{m}, i.e., $p = n_{\text{EV}}/N_{\text{m}}$. Due to the stochasticity of EV charging events, $x(p)$ is no longer deterministic; rather, it should be characterized by its probability density function (PDF) at p, which is denoted by $m(x, p)$. Recall that the evolution of $m(x, p)$ with respect to p can be described by the following Fokker-Planck equation (FPE):

$$\frac{\partial m(x,p)}{\partial p} + \frac{\partial}{\partial x}\Big\{m(x,p)u(x,p)\Big\} = d\frac{\partial^2 m(x,p)}{\partial x^2}, \tag{4.10}$$

subject to $m_0 = m(x, p^0)$. Without loss of generality, let us assume $p^0 = 0$ hereinafter, i.e., the baseline network does not have any EV. In (4.10), the diffusion velocity term d is a small positive constant, and the drift velocity term $u(x, p)$ specifies the rate of change to the network state x at a given p.

As we focus on equipment loading, let $x_{t,e}(p)$ be the loading level of equipment e at time t given EV penetration p, and $g_{t,e}(p)$ be the extra loading due to EV charging. The latter can be approximated by the following:

$$g_{t,e}(p) \approx \frac{n_{\text{EV}}\,\text{Pr}_e(p)\mathbb{E}[S_{e,\text{EV}}](t)}{S_e}, \tag{4.11}$$

where $\text{Pr}_e(p)$ is the time-invariant probability that EVs are connected downstream of e, $\mathbb{E}[S_{e,\text{EV}}](t)$ can be computed by (4.1) which is the expected power of an EV being charged at time t, and $S_e \in \mathbb{R}$ is the rated power of e which is assumed to be known. Refer to Section 2.2.3.1 of Chapter 2 for more details on the calculation of $\text{Pr}_e(p)$.

The drift velocity $u(x_{t,e}, p)$ at time t can then be computed by taking the derivative of $g_{t,e}(p)$ with respect to p. It is remarked that for distribution networks, the drift velocity is usually computed by-phase because the equipment loading level is calculated on each phase separately. However, for the purpose of this chapter we compute it on all connected phases. We then can numerically solve (4.10) by the finite-volume method (FVM) using an implicit scheme (refer to Appendix A or [105]). Thus, we obtain a sequence of PDFs indexed

by p, from which $x_{t,e}(p)$ can take the mean or any percentile value computed from the PDF at p. Refer to Sections 2.2.4 and 2.3 of Chapter 2 for more details on the calculation of the derivative of $g_{t,e}(p)$ with respect to p and the numerical method to solve FPE, respectively.

To evaluate loading levels of e for the period $\mathcal{T}$, denoted by $\mathbf{x}_e = [x_{t,e}]_{t\in\mathcal{T}}^\top \in \mathbb{R}^T$, the analysis must be repeated to calculate $x_{t,e}$ at each $t \in \mathcal{T}$. As the result obtained at time t does not depend on that evaluated at any other t, the process can be parallelized for improved efficiency. The application of REM for such a time-series analysis is denoted as ts-REM hereinafter, and it can be used to evaluate equipment's loading levels at various EV penetration levels with and without mitigation strategies applied. If the ts-REM results indicate that the equipment is frequently overloaded or the overload lasts long at certain EV penetration rate, a higher risk of premature equipment failure is expected which in turn increases the operating and maintenance costs for utilities.

4.3.2 Impact of overloading on equipment lifetime and cost

As overloading often results in higher operating temperature of the equipment, its expected lifetime is reduced if the equipment is periodically overheated due to the loading levels [120]. To assess the reduced lifetime, thermal-aging models are used. For example, IEEE standard C57.91 [121] describes the thermal-aging model for transformers and IEEE standard 1283-2013 [122] describes the model for lines and conductors. Given that the thermal-aging model is already well documented in the IEEE standard, their details are omitted here for conciseness. Let us denote TAM : $\mathbb{R}^T \mapsto \mathbb{R}$ as the thermal-aging model. Recall that $\mathbf{x}_e$ is the equipment loading levels over the period $\mathcal{T}$ which is evaluated by ts-REM, and let $F_{\text{life}} = \text{TAM}(\mathbf{x}_e)$ be an annualized stress factor indicating the ratio of the expected over the nominal lifetime of the equipment. If $F_{\text{life}} = 1$, the equipment's expected lifetime is maintained at its nominal value, whereas the equipment is stressed by the loading levels and the lifetime is reduced when $F_{\text{life}} > 1$.

Let $c(F_{\text{life}})$ denote the additional annual cost of the equipment (depreciation, operating & maintenance, etc.) due to the shortened lifetime, i.e.,

$$c(F_{\text{life}}) = c_{\text{annual}}(\max\{1, F_{\text{life}}\} - 1), \tag{4.12}$$

where $c_{\text{annual}} > 0$ is the total annual cost at the nominal lifetime. We remark that it is possible to have $F_{\text{life}} < 1$. This indicates that the equipment is still in service after its nominal lifetime is reached. However, here we assume that no equipment operates beyond its nominal lifetime for economical and safety reasons. Hence, when $F_{\text{life}} \leq 1$, there is no saving in cost and we

have $c(F_{\text{life}} \leq 1) = 0$.

We remark that there's no limitation to the type of equipment for which the overload cost can be calculated. However, the information of equipment's annual cost c_{annual} and loading pattern of key equipment with large ratings (e.g., substation transformer) are more practically accessible to utilities than those of others (e.g., distribution transformers with small ratings), although the latter can be overloaded under high EV impacts. Hence, in this work we primarily consider key equipment with large ratings as our target for overload mitigation.

4.3.3 Incentives to customers

Recall that incentives are given to customers in exchange for changes in their charging habits, i.e., adjusting $\mathbf{Pr}$ to $\widetilde{\mathbf{Pr}}$ by reducing $\mathbf{\Delta}_{\text{prob}}$ from their total probabilities of charging EVs during $\mathcal{T}^{\text{P}}$. Let $R^i(\Delta^i_{\text{prob}})$ denote the annualized incentive given to customer i, and $\widetilde{F}_{\text{life}}$ the resulting lifetime factor when all customers are adopting $\widetilde{\mathbf{Pr}}$. The total annual incentives given to all customers should not exceed $c(F_{\text{life}}) - c(\widetilde{F}_{\text{life}})$; otherwise, the best option for the utility is to keep operating the equipment at a reduced lifetime F_{life}, because paying incentives to customers becomes a more expensive option. Hence, $c(F_{\text{life}}) - c(\widetilde{F}_{\text{life}})$ is considered as a "budget" for the total incentives, and we have the following constraint on the total incentives:

$$\sum_{i=1}^{N_{\text{m}}} R^i \leq c(F_{\text{life}}) - c(\widetilde{F}_{\text{life}}). \tag{4.13}$$

Even though not all EV owners may contribute to the extra loading of e, i.e., not all customers are downstream of e, they are still entitled to participate in the mitigation strategy and benefit the announced incentives. Hence, the total incentive in (4.13) is summed over all N_{m} customers. We also assume that the incentive applies only to EV consumption, i.e., a separate meter is installed for the EV charger [123]. In this case, $R^i = 0$ if customer i does not own an EV. Further, we remark that if $c(F_{\text{life}}) = 0$, it is not necessary to adjust customers' charging habits hence no incentive is given to customers and $\mathbf{\Delta}_{\text{prob}} = 0$. On the other hand, if $c(F_{\text{life}})$ is too small, e.g., an overloaded distribution transformer on a lateral circuit, there is also no gain to design a mitigation plan than an early replacement of the equipment. To continue the following derivations, we assume that $F_{\text{life}} > 1$ initially with EVs connected to the network before any mitigation strategy is adopted and the cost of loss of lifetime is significant, e.g., a substation transformer whose $c(F_{\text{life}} > 1) \gg 0$.

We then consider two types of incentives: (1) reward for reduced consumption of EV charging during $\mathcal{T}^{\text{P}}$, and (2) time-of-use (TOU) pricing during the entire day. The formulation as well as the objective function of each type of incentive is detailed in the following sections.

4.3.3.1 Reward for reduced consumption for charging during $\mathcal{T}^{\mathrm{P}}$

As each customer contributes to reducing equipment loading during $\mathcal{T}^{\mathrm{P}}$, a reward is given based on the expected reduction of consumption for EV charging. Customer i's expected daily reward is given by:

$$R_{\mathrm{day}}^{i,\mathrm{reward}} = r \sum_{t \in \mathcal{T}^{\mathrm{P}}} \Delta E_t^i \tag{4.14}$$

$$\Delta E_t^i = \Delta t \sum_j l_{\mathrm{EV}}^j(t) \Big(\mathrm{Pr}^i(j) - \widetilde{\mathrm{Pr}}^i(j) \Big), \tag{4.15}$$

where Δt is the time step, ΔE_t^i is the change of EV consumption at time t, and $r \geq 0$ (\$/kWh) is the unit reward applicable to all customers and its value is to be determined. The expected reward for customer i in a year is therefore:

$$R^i = 365 R_{\mathrm{day}}^{i,\mathrm{reward}}. \tag{4.16}$$

In addition, the following constraint is imposed to ensure that each customer's total expected energy consumed for EV charging remains unchanged with and without the reward.

$$\sum_{t \in \mathcal{T}} \Delta E_t^i = 0, \quad \forall i = 1, 2, \cdots, |\mathcal{K}_e|. \tag{4.17}$$

4.3.3.2 TOU pricing

Given that we have partitioned each day into three periods, the electricity rate needs to be determined for each period. Let $p_{\mathrm{rate}}^{\mathrm{nom}} > 0$ (\$/kWh) be the nominal rate. Because customers' charging probabilities in the mid-peak period $\mathcal{T}^{\mathrm{MP}}$ remain unchanged, the rate remains at $p_{\mathrm{rate}}^{\mathrm{nom}}$, i.e., $p_{\mathrm{rate}}^{\mathrm{MP}} = p_{\mathrm{rate}}^{\mathrm{nom}}$. For the off-peak period, the rate is decreased by $\xi \geq 0$, i.e., $p_{\mathrm{rate}}^{\mathrm{OP}} = p_{\mathrm{rate}}^{\mathrm{nom}} - \xi$. For the peak period, a surcharge $\eta \geq 0$ is added to the nominal rate, i.e., $p_{\mathrm{rate}}^{\mathrm{P}} = p_{\mathrm{rate}}^{\mathrm{nom}} + \eta$. Both ξ and η are variables whose values are to be determined. Under such a TOU pricing, customer i's daily savings in electricity price is:

$$\begin{aligned} R_{\mathrm{day}}^{i,\mathrm{TOU}} = {} & (p_{\mathrm{rate}}^{\mathrm{nom}} + \eta) \sum_{t \in \mathcal{T}^{\mathrm{P}}} \Delta E_t^i + (p_{\mathrm{rate}}^{\mathrm{nom}} - \xi) \sum_{t \in \mathcal{T}^{\mathrm{OP}}} \Delta E_t^i \\ & - \eta \sum_{t \in \mathcal{T}^{\mathrm{P}}} E^i + \xi \sum_{t \in \mathcal{T}^{\mathrm{OP}}} E^i + p_{\mathrm{rate}}^{\mathrm{nom}} \sum_{t \in \mathcal{T}^{\mathrm{MP}}} \Delta E_t^i, \end{aligned} \tag{4.18}$$

where

$$E_t^i = \Delta t \sum_j l_{\mathrm{EV}}^j(t)\,\mathrm{Pr}^i(j), \tag{4.19}$$

and ΔE_t^i is defined in (4.15). The annualized reward for customer i is:

$$R^i = 365 R_{\mathrm{day}}^{i,\mathrm{TOU}}. \tag{4.20}$$

The EV charging energy conservation constraint (4.17) also applies. Further, because neither the electricity price during the off-peak period nor each customer's reward can be negative, the following constraints are added:

$$\begin{aligned} p_{\mathrm{rate}}^{\mathrm{OP}} &\geq 0 \\ R_{\mathrm{day}}^{i,\mathrm{TOU}} &\geq 0. \end{aligned} \tag{4.21}$$

4.3.4 Optimization problem formulation

An optimization problem is formulated to identify optimal levels of $\mathbf{\Delta}_{\mathrm{prob}}$ and incentives such that utilities' costs are minimized while the equipment is maintained at its nominal lifetime or as close as possible. This is expressed as:

$$\begin{aligned} \min_{\mathbf{\Delta}_{\mathrm{prob}},r,(\xi,\eta)} \quad & \sum_{i=1}^{N_{\mathrm{m}}} R^i \\ \text{subject to} \quad & \mathbf{\Delta}_{\mathrm{prob}} \in \arg\min_{\mathbf{\Delta}_{\mathrm{prob}}} |\widetilde{F}_{\mathrm{life}} - 1| \\ & \qquad \text{subject to} \quad \mathbf{0} \leq \mathbf{\Delta}_{\mathrm{prob}} \leq \mathbf{\Sigma}^{\mathrm{P}} \\ & \qquad\qquad \mathbf{x}_e = \text{ts-REM}(\widetilde{\mathbf{Pr}}) \\ & \qquad\qquad \widetilde{F}_{\mathrm{life}} = \mathrm{TAM}(\mathbf{x}_e) \\ & \qquad\qquad (4.6), (4.9), (4.12), (4.13), (4.17), \text{and} \\ & \qquad\qquad (4.14) \text{ or } (4.18), (4.21). \end{aligned} \tag{4.22}$$

Recall that ts-REM refers to the time-series REM method presented in Section 4.3.1 which evaluates impacts of EV charging to the equipment loading levels $\mathbf{x}_e$ under $\widetilde{\mathbf{Pr}}$, and TAM refers to the thermal-aging model which computes the lifetime factor under the resulting $\mathbf{x}_e$. Each customer's incentive can either be a reward-based as in (4.16) or a TOU pricing-based as in (4.20). If the latter is adopted, the variable r is replaced by ξ and η in (4.22).

4.4 Convex reformulation

We remark that the form of the total rewards to customers is non-linear and non-convex (i.e., which is the product of incentive levels and changes to consumptions where both are to be determined as variables), and ts-REM and TAM are not linear processes either. Hence, the optimization problem formulated in (4.22) is a bi-level, non-linear, and non-convex problem, which is difficult to solve and global optimality is not guaranteed. In this section, we aim to reformulate (4.22) into a single-level convex optimization problem, which can be efficiently solved.

4.4.1 Approximation of total incentives

The total annualized reward R^i used in (4.13) and then (4.22) is non-convex due to the bilinear form of $R^{i,\text{reward}}_{\text{day}}$ and $R^{i,\text{TOU}}_{\text{day}}$ in (4.14) and (4.18), respectively. To approximate the incentives, we use the price elasticity model [124, 125] to measure a customer's response to the incentive offered, where

$$-\Delta E^i_t = \varepsilon^i \Delta p_{\text{rate}}(t) = \overline{\varepsilon} \frac{E^i_t}{p^{\text{nom}}_{\text{rate}}} \Delta p_{\text{rate}}(t). \tag{4.23}$$

In (4.23), to be consistent with the definition of ΔE^i_t in (4.15), a negative sign is necessary to model the expected change in energy consumption for EV charging at time t when an incentive $\Delta p_{\text{rate}}(t)$ is offered under the mitigation program. For the reward program,

$$\Delta p_{\text{rate}}(t) = \begin{cases} r, & \text{for } t \in \mathcal{T}^{\text{P}} \\ 0, & \text{otherwise.} \end{cases} \tag{4.24}$$

For the TOU pricing,

$$\Delta p_{\text{rate}}(t) = \begin{cases} -\eta, & \text{for } t \in \mathcal{T}^{\text{P}}, \\ \xi, & \text{for } t \in \mathcal{T}^{\text{OP}}, \\ 0, & \text{otherwise.} \end{cases} \tag{4.25}$$

The individual price elasticity ε^i of customer i is related to the energy consumed E^i_t, the nominal electricity price $p^{\text{nom}}_{\text{rate}}$, and an averaged price elasticity factor $\overline{\varepsilon} < 0$ which applies to all participating customers independent of the time period. For non-participating customers or non-EV owners, $\Delta E^i_t = 0,\ \forall t$. It is remarked that we ignore the changes of energy consumed in one period due to the price change in another period, hence cross elasticity factors are not considered [124]. In addition, for given $\overline{\varepsilon}$, $p^{\text{nom}}_{\text{rate}}$, and Δp_{rate}, customers with

higher consumption should contribute more in reducing the consumption under the mitigation strategy.

We apply (4.23) to the two type of incentives, and obtain:

$$\hat{R}^{i,\text{reward}}_{\text{day}} = -\varepsilon^{i,\text{P}} r^2, \tag{4.26}$$

$$\hat{R}^{i,\text{TOU}}_{\text{day}} = -\varepsilon^{i,\text{P}}(\eta^2 + \eta p^{\text{nom}}_{\text{rate}}) - \varepsilon^{i,\text{OP}}(\xi^2 - \xi p^{\text{nom}}_{\text{rate}}) - \eta E^{i,\text{P}} + \xi E^{i,\text{OP}} + p^{\text{nom}}_{\text{rate}} \sum_{t \in \mathcal{T}^{\text{MP}}} \Delta E^i_t, \tag{4.27}$$

where $E^{i,\text{P}} = \sum_{t \in \mathcal{T}^{\text{P}}} E^i_t$, $E^{i,\text{OP}} = \sum_{t \in \mathcal{T}^{\text{OP}}} E^i_t$, $E^{i,\text{MP}} = \sum_{t \in \mathcal{T}^{\text{MP}}} E^i_t$, $\varepsilon^{i,\text{P}} = \overline{\varepsilon} \frac{E^{i,\text{P}}}{p^{\text{nom}}_{\text{rate}}}$, $\varepsilon^{i,\text{OP}} = \overline{\varepsilon} \frac{E^{i,\text{OP}}}{p^{\text{nom}}_{\text{rate}}}$, and E^i_t is defined in (4.19). The total incentives are now expressed as:

$$\hat{R}^i = \begin{cases} 365 \hat{R}^{i,\text{reward}}_{\text{day}}, & \text{if reward} \\ 365 \hat{R}^{i,\text{TOU}}_{\text{day}}, & \text{if TOU.} \end{cases} \tag{4.28}$$

We note that for the TOU type of incentives, constraint (4.21) should apply to $\hat{R}^{i,\text{TOU}}_{\text{day}}$.

4.4.2 Constraint to loading levels

In the second level of (4.22), we aim to maintain the equipment at its nominal lifetime by adjusting equipment's loading level $\mathbf{x}_e$. The lifetime is likely to be shortened (i.e., $\widetilde{F}_{\text{life}} > 1$) when $\mathbf{x}_e$ shows severe or prolonged overloading, mainly due to simultaneous EV charging during the peak hours. While it is natural to add a constraint to limit the loading levels at all time, it is difficult to find an optimal constraint as $\mathbf{x}_e$ is numerically computed by the ts-REM model. Alternatively, as discussed in Section 4.3 and by (4.11), the extra loading to the equipment due to EV charging depends on $\mathbb{E}[S_{e,\text{EV}}](t)$. Hence, constraining $\mathbb{E}[S_{e,\text{EV}}](t)$ would have an equivalent effect to limiting $\mathbf{x}_e$.

We denote $\mathbb{E}[\widetilde{S}_{e,\text{EV}}]$ the resulting loading levels of e evaluated using ts-REM when a mitigation strategy is applied. Let us assume that there exists some time-varying limit $\overline{S}_t$ for $\mathbb{E}[\widetilde{S}_{e,\text{EV}}]$ such that $|\widetilde{F}_{\text{life}} - 1|$ is minimized. Under this assumption, not only can we move the ts-REM and TAM models out of (4.22), we can also remove the second level of (4.22). The

optimization problem (4.22) becomes:

$$\begin{aligned} \min_{\boldsymbol{\Delta}_{\text{prob}},r,(\xi,\eta)} \quad & \sum_{i=1}^{N_{\text{m}}} \hat{R}^i \\ \text{subject to} \quad & \mathbf{0} \leq \boldsymbol{\Delta}_{\text{prob}} \leq \boldsymbol{\Sigma}^{\text{P}} \\ & \mathbb{E}[\widetilde{S}_{e,\text{EV}}](t) \leq \overline{S}_t, \ \forall t \in \mathcal{T} \\ & \sum_{i=1}^{N_{\text{m}}} \hat{R}^i \leq c(F_{\text{life}}) \\ & (4.6), (4.9), (4.17), \text{ and} \\ & (4.26) \text{ or } (4.27), (4.21) \end{aligned} \tag{4.29}$$

Note that as the TAM model is no longer embedded in the optimization problem, the $c(\widetilde{F}_{\text{life}})$ term appearing in (4.13) cannot be evaluated. Hence we have relaxed it by taking the initial cost of $c(F_{\text{life}})$ as the budget. Such a relaxation is exact if $\widetilde{F}_{\text{life}} = 1$, i.e., the nominal lifetime is achievable under a mitigation strategy.

The reformulated optimization problem (4.29) is equivalent to (4.22) if $\widetilde{F}_{\text{life}} = 1$, is convex, and is readily solvable to optimality but depends on $\overline{S}_t$. Next, we discuss how to determine $\overline{S}_t$.

4.4.3 Determination of $\overline{S}_t$

In this subsection, we discuss the calculation of $\overline{S}_t$ which is essential for (4.29).

4.4.3.1 Limit for $\mathcal{T}^{\text{OP}}$ and $\mathcal{T}^{\text{MP}}$

Recall that for a given EV penetration p, $x_{t,e}(p)$ is the loading level at time t which can be expressed by:

$$x_{t,e}(p) = x_{t,e}(p^0) + g_{t,e}(p),$$

where $x_{t,e}(p^0)$ is the loading level of e at p^0 which can be deterministically determined from a power flow analysis. As we assumed that the equipment should never be overloaded during $\mathcal{T}^{\text{OP}}$ and $\mathcal{T}^{\text{MP}}$, we have the following inequality:

$$\begin{aligned} x_{t,e}(p^0) + g_{t,e}(p) \leq 1, \\ g_{t,e}(p) \leq 1 - x_{t,e}(p^0), \ t \in \mathcal{T}^{\text{OP}} \cup \mathcal{T}^{\text{MP}}. \end{aligned} \tag{4.30}$$

As $g_{t,e}(p)$ can be approximated by (4.11), by substituting it into (4.30) we get,

$$\begin{aligned} \frac{n_{\text{EV}} \Pr_e(p) \mathbb{E}[S_{e,\text{EV}}](t)}{S_e} &\leq 1 - x_{t,e}(p^0), \\ \mathbb{E}[S_{e,\text{EV}}](t) &\leq \frac{S_e \left(1 - x_{t,e}(p^0)\right)}{n_{\text{EV}} \Pr_e(p)}, \ t \in \mathcal{T}^{\text{OP}} \cup \mathcal{T}^{\text{MP}}. \end{aligned} \tag{4.31}$$

The right-hand side of (4.31) is the limit for $\mathbb{E}[S_{e,\text{EV}}](t)$ during the off-peak and mid-peak periods which is a sufficient condition to guarantee that the equipment is not overloaded, i.e.,

$$\overline{S}_t = \frac{S_e \left(1 - x_{t,e}(p^0)\right)}{n_{\text{EV}} \Pr_e(p)}, \ t \in \mathcal{T}^{\text{OP}} \cup \mathcal{T}^{\text{MP}}. \tag{4.32}$$

Note that the limit expressed in (4.32) is time-variant and independent of customers' charging probabilities.

4.4.3.2 Search for limit during $\mathcal{T}^{\text{P}}$

While we can analytically compute the limit for the peak period by also imposing that the equipment is not overloaded, the resulting limit may be too restricting to minimize $|\widetilde{F}_{\text{life}} - 1|$, i.e., $\widetilde{F}_{\text{life}} < 1$, or (4.29) may be infeasible hence no solution is possible. Instead, we let $\overline{S}_t = \overline{S}^{\text{P}} > 0$ be constant $\forall t \in \mathcal{T}^{\text{P}}$, and we propose Algorithm 1 to search for an optimal value of $\overline{S}^{\text{P}}$, such that (a) the optimization problem (4.29) is feasible, and (b) $|\widetilde{F}_{\text{life}} - 1|$ is minimized. In general, the search algorithm constructs sequences of upper bounds $\{u_n\}$ and lower bounds $\{l_n\}$. Candidate values of $\overline{S}^{\text{P}}_n$ are evaluated between $\{u_n\}$ and $\{l_n\}$, and the search direction depends on the solution to (4.29) and the resulting $F_{\text{life},n}$ by applying the $\overline{S}^{\text{P}}_n$ limit at iteration n.

Algorithm 1 Search algorithm for optimal $\overline{S}^{\mathrm{P}}$

Initialize

$n \leftarrow 0$

$u_n \leftarrow \max_t\{x_{t,e}(p^0)\}$

$l_n \leftarrow 0$

$\overline{S}^{\mathrm{P}}_n \leftarrow \delta \ll u_n$

while $u_n - l_n > \delta$ **do**

Construct $\overline{S}_t$ using $\overline{S}^{\mathrm{P}}_n$ and (4.32)

Solve the optimization problem (4.29)

$n \leftarrow n + 1$

if a feasible solution is obtained **then**

Compute the resulting $\mathbf{x}_e$ and $F_{\mathrm{life},n}$ from
ts-REM and TAM models, respectively

if $F_{\mathrm{life},n} > 1$ **then**

$\overline{S}^{\mathrm{P}}_n \leftarrow \max\{l_{n-1}, \overline{S}^{\mathrm{P}}_{n-1} \exp(-1/n)\}$

if $\overline{S}^{\mathrm{P}}_n$ has already been tried **then**

$\overline{S}^{\mathrm{P}}_n \leftarrow \frac{(l_{n-1}+\overline{S}^{\mathrm{P}}_{n-1})}{2}$

end if

$u_n \leftarrow \overline{S}^{\mathrm{P}}_{n-1}$

$l_n \leftarrow l_{n-1}$

else if $F_{\mathrm{life},n} \leq 1$ **then**

$\overline{S}^{\mathrm{P}}_n \leftarrow \min\{u_{n-1}, \overline{S}^{\mathrm{P}}_{n-1} \exp(1/n)\}$

if $\overline{S}^{\mathrm{P}}_n$ has already been tried **then**

$\overline{S}^{\mathrm{P}}_n \leftarrow \frac{(u_{n-1}+\overline{S}^{\mathrm{P}}_{n-1})}{2}$

end if

$l_n \leftarrow \overline{S}^{\mathrm{P}}_{n-1}$

$u_n \leftarrow u_{n-1}$

end if

else if no feasible solution is obtained **then**

$\overline{S}^{\mathrm{P}}_n \leftarrow \min\{u_{n-1}, \overline{S}^{\mathrm{P}}_{n-1} \exp(1/n)\}$

if $\overline{S}^{\mathrm{P}}_n$ has already been tried **then**

$\overline{S}^{\mathrm{P}}_n \leftarrow \frac{1}{2}(u_{n-1} + \overline{S}^{\mathrm{P}}_{n-1})$

end if

$l_n \leftarrow \overline{S}^{\mathrm{P}}_{n-1}$

$u_n \leftarrow u_{n-1}$

end if

end while

To show that the sequence of $\overline{S}_n^{\mathrm{P}}$ converges to a limit $\overline{S}_*^{\mathrm{P}}$, i.e., $\lim_{n\to\infty} \overline{S}_n^{\mathrm{P}} = \overline{S}_*^{\mathrm{P}}$, we first discuss monotonic properties of the sequences $\{u_n\}$ and $\{l_n\}$ constructed by the algorithm.

Lemma 1. *Consider Algorithm 1, the following statements hold for $n > 0$:*

(A) The sequence of upper bounds $\{u_n\}$ is monotonically non-increasing, and the sequence of lower bounds $\{l_n\}$ is monotonically non-decreasing.

(B) At any $n > 0$, $u_n \geq l_n$.

(C) $\lim_{n\to\infty} u_n = \inf\{u_n\}$, and $\lim_{n\to\infty} l_n = \sup\{l_n\}$.

Proof. For $n > 0$, we have the following two cases:

(1) If a solution to (4.29) has been found at iteration $n-1$, we can calculate the resulting $F_{\mathrm{life},n}$ and:

(a) if $F_{\mathrm{life},n} > 1$, then $\overline{S}_n^{\mathrm{P}} \leq \overline{S}_{n-1}^{\mathrm{P}}$, $u_n = \overline{S}_{n-1}^{\mathrm{P}}$, and $l_n = l_{n-1}$. Further, as $\overline{S}_n^{\mathrm{P}}$ is bounded below by l_{n-1}, we also have $u_n = \overline{S}_{n-1}^{\mathrm{P}} \geq \overline{S}_n^{\mathrm{P}} \geq l_{n-1} = l_n$.

Applying $\overline{S}_n^{\mathrm{P}}$ at iteration n, we have the following three cases:

(i) if a solution to (4.29) is found and $F_{\mathrm{life},n+1} > 1$, then $u_{n+1} = \overline{S}_n^{\mathrm{P}} \leq \overline{S}_{n-1}^{\mathrm{P}} = u_n$, and $l_{n+1} = l_n$.

(ii) if a solution to (4.29) is found but $F_{\mathrm{life},n+1} \leq 1$, then $u_{n+1} = u_n$, and $l_{n+1} = \overline{S}_n^{\mathrm{P}} \geq l_{n-1} = l_n$.

(iii) if no solution to (4.29) is found, then $u_{n+1} = u_n$, and $l_{n+1} = \overline{S}_n^{\mathrm{P}} \geq l_{n-1} = l_n$.

Hence in cases (a).(i)-(iii), we have $u_{n+1} \leq u_n$ and $l_{n+1} \geq l_n$.

(b) if $F_{\mathrm{life},n} \leq 1$, then $\overline{S}_n^{\mathrm{P}} \geq \overline{S}_{n-1}^{\mathrm{P}}$, $u_n = u_{n-1}$, and $l_n = \overline{S}_{n-1}^{\mathrm{P}}$. Further, as $\overline{S}_n^{\mathrm{P}}$ is bounded above by u_{n-1}, we have $u_n = u_{n-1} \geq \overline{S}_n^{\mathrm{P}} \geq \overline{S}_{n-1}^{\mathrm{P}} = l_n$.

At the next iteration, we have the following three cases:

i. if a solution to (4.29) is found and $F_{\mathrm{life},n+1} > 1$, then $u_{n+1} = \overline{S}_n^{\mathrm{P}} \leq u_{n-1} = u_n$ and $l_{n+1} = l_n$.

ii. if a solution to (4.29) is found but $F_{\mathrm{life},n+1} \leq 1$, then $u_{n+1} = u_n$ and $l_{n+1} = \overline{S}_n^{\mathrm{P}} \geq \overline{S}_{n-1}^{\mathrm{P}} = l_n$.

iii. if no solution to (4.29) is found, then $u_{n+1} = u_n$, and $l_{n+1} = \overline{S}_n^{\mathrm{P}} \geq \overline{S}_{n-1}^{\mathrm{P}} = l_n$.

Hence in cases (b).(i)-(iii), we have $u_{n+1} \leq u_n$ and $l_{n+1} \geq l_n$.

(2) If there exists no solution to (4.29) at iteration $n-1$, then $\overline{S}_n^{\mathrm{P}} \geq \overline{S}_{n-1}^{\mathrm{P}}$, $u_n = u_{n-1}$, and $l_n = \overline{S}_{n-1}^{\mathrm{P}}$. The same argument as in (1).(b) lead to $u_n \geq l_n$.

At the next iteration, by the same argument as in (1).(b), we have $u_{n+1} \leq u_n$ and $l_{n+1} \geq l_n$.

In cases (1) and (2) we show that $u_{n+1} \leq u_n$ and $l_{n+1} \geq l_n$ hold, hence Lemma 1-(A) is proved. In addition, we also show that $u_n \geq l_n$ holds in these cases, hence Lemma 1-(B) is proved.

As $\{u_n\}$ is monotonically non-increasing and is bounded below by $\{l_n\}$, by the monotone convergence theorem, $\{u_n\}$ converges to its infimum. Similarly, $\{l_n\}$ converges to its supremum. Hence Lemma 1-(C) also holds. □

Next, we argue that the candidate value $\overline{S}_n^{\mathrm{P}}$ at iteration n must differ from that at the previous iteration, except in the following special cases.

Lemma 2. *For $n > 0$, the following statements hold for the $\overline{S}_n^P$ computed by Algorithm 1:*

(A) If there exists a solution to (4.29) *at iteration $n-1$ and $F_{life,n} > 1$, then $\overline{S}_n^P = \overline{S}_{n-1}^P$ if and only if $\overline{S}_{n-1}^P = l_{n-1}$.*

(B) If there exists a solution to (4.29) *at iteration $n-1$ and $F_{life,n} \leq 1$ or* (4.29) *is infeasible at iteration $n-1$, then $\overline{S}_n^P = \overline{S}_{n-1}^P$ if and only if $\overline{S}_{n-1}^P = u_{n-1}$.*

Proof. We start with Lemma 2-(A) and prove the statement in both directions.

($\Rightarrow$) If $\overline{S}_{n-1}^{\mathrm{P}} = l_{n-1}$, by the construction of Algorithm 1 we have $\overline{S}_n^{\mathrm{P}} \geq l_{n-1}$ and $\overline{S}_n^{\mathrm{P}} \leq \overline{S}_{n-1}^{\mathrm{P}} = l_{n-1}$ at the same time. Therefore, $\overline{S}_n^{\mathrm{P}} = l_{n-1} = \overline{S}_{n-1}^{\mathrm{P}}$ must hold.

($\Leftarrow$) If $\overline{S}_n^{\mathrm{P}} = \overline{S}_{n-1}^{\mathrm{P}}$, then $\overline{S}_n^{\mathrm{P}}$ can only take the following possible values by Algorithm 1:

(a) $\overline{S}_n^{\mathrm{P}} = l_{n-1}$, then $\overline{S}_n^{\mathrm{P}} = \overline{S}_{n-1}^{\mathrm{P}} = l_{n-1}$.

(b) $\overline{S}_n^{\mathrm{P}} = \frac{(l_{n-1} + \overline{S}_{n-1}^{\mathrm{P}})}{2}$, i.e., $\overline{S}_n^{\mathrm{P}} = l_{n-1}$ has already been tried in previous iterations, then

$$\begin{aligned} 2\overline{S}_{n-1}^{\mathrm{P}} &= l_{n-1} + \overline{S}_{n-1}^{\mathrm{P}} \\ \Leftrightarrow \overline{S}_{n-1}^{\mathrm{P}} &= l_{n-1}. \end{aligned}$$

Hence $\overline{S}_{n-1}^{\mathrm{P}} = l_{n-1}$ always holds if $\overline{S}_n^{\mathrm{P}} = \overline{S}_{n-1}^{\mathrm{P}}$.

Therefore, it is shown that $\overline{S}_n^{\mathrm{P}} = \overline{S}_{n-1}^{\mathrm{P}}$ if and only if $\overline{S}_{n-1}^{\mathrm{P}} = l_{n-1}$ when (4.29) is feasible and $F_{\mathrm{life},n} > 1$.

The proof of Lemma 2-(B) follows the same argument as in Lemma 2-(A), and hence it is omitted. □

By Lemma 1 we established that the sequences $\{u_n\}$ and $\{l_n\}$ are monotonic and convergent. We now show that they converge to the same limit.

Lemma 3. *The sequences $\{u_n\}$ and $\{l_n\}$ constructed by Algorithm 1 converge to the same limit, i.e.,* $\lim_{n\to\infty} u_n = \lim_{n\to\infty} l_n$.

Proof. Suppose that at $n = N$, we have $u_N = u_*, l_N = l_*$. Let $\delta_N \triangleq u_N - l_N \geq 0$. If $\delta_N = 0$, then $u_* = l_*$. By Lemma 1 $\{u_n\}$ and $\{l_n\}$ are monotonic and $u_n \geq l_n,\ \forall n > 0$, then we must have $u_n = l_n = u_* = l_*,\ \forall n > N$. In this case, $\{u_n\}$ and $\{l_n\}$ converge to the same limit and the proof is done.

Now we consider $\delta_N > 0$. At the next iteration $n = N + 1$, the following cases may occur:

(1) If there exists a solution to (4.29) at iteration N and $F_{\mathrm{life},N+1} > 1$, then we have shown in Lemma 1 that $\overline{S}_{N+1}^{\mathrm{P}} \leq \overline{S}_N^{\mathrm{P}}$, $u_{N+1} = \overline{S}_N^{\mathrm{P}}$, and $l_{N+1} = l_N = l_*$. We thus have:

$$\begin{aligned} u_{N+1} - l_{N+1} &= \overline{S}_N^{\mathrm{P}} - l_*, \\ &= (u_* - l_*) + \left(\overline{S}_N^{\mathrm{P}} - u_*\right), \\ &= \delta_N + \left(\overline{S}_N^{\mathrm{P}} - u_*\right). \end{aligned}$$

In what follows, we argue $u_{N+1} - l_{N+1} < \delta_N$ for any value of $\overline{S}_{N+1}^{\mathrm{P}}$ and $\overline{S}_N^{\mathrm{P}}$:

(a) When $\overline{S}_{N+1}^{\mathrm{P}} = \overline{S}_N^{\mathrm{P}}$, by Lemma 2-(A) we have $\overline{S}_N^{\mathrm{P}} = l_N = l_*$. Hence,

$$\begin{aligned} u_{N+1} - l_{N+1} &= \delta_N + \left(\overline{S}_N^{\mathrm{P}} - u_*\right), \\ &= \delta_N + (l_* - u_*), \\ &= \delta_N - \delta_N, \\ &= 0. \end{aligned}$$

(b) When $\overline{S}_{N+1}^{\mathrm{P}} < \overline{S}_N^{\mathrm{P}}$, $u_{N+1} \leq u_N = u_*$ always holds by the monotonicity of $\{u_n\}$. As $F_{\mathrm{life},N+1} > 1$ is assumed, we have $u_{N+1} = \overline{S}_N^{\mathrm{P}}$ which leads to $\overline{S}_N^{\mathrm{P}} \leq u_*$. If $\overline{S}_N^{\mathrm{P}} < u_*$, then $u_{N+1} - l_{N+1} < \delta_N$ must hold.

We now argue that $\overline{S}^{\mathrm{P}}_N = u_*$ cannot happen. By the construction of Algorithm 1, u_N is updated to u_* as $\overline{S}^{\mathrm{P}}_{n_u}$ reaches this value at some iteration $n_u < N$. When $\overline{S}^{\mathrm{P}}_N$ reaches u_* again at iteration N, it would need to be adjusted to $\overline{S}^{\mathrm{P}}_N = \frac{(l_* + \overline{S}^{\mathrm{P}}_{N-1})}{2}$ according to the algorithm. We show by contradiction that the adjusted $\overline{S}^{\mathrm{P}}_N \neq u_*$. Let us assume for now that the adjusted $\overline{S}^{\mathrm{P}}_N = u_*$, we have:

$$\begin{aligned} 2\overline{S}^{\mathrm{P}}_N &= l_* + \overline{S}^{\mathrm{P}}_{N-1} \\ \Leftrightarrow 2u_* &= l_* + \overline{S}^{\mathrm{P}}_{N-1} \\ \Leftrightarrow u_* + (u_* - l_*) &= \overline{S}^{\mathrm{P}}_{N-1} \\ \Leftrightarrow u_* + \delta_N &= \overline{S}^{\mathrm{P}}_{N-1}. \end{aligned} \tag{4.33}$$

As $\overline{S}^{\mathrm{P}}_{N-1}$ is bounded above by u_* and $\delta_N > 0$, (4.33) must not hold. Hence, by contradiction, $\overline{S}^{\mathrm{P}}_N \neq u_*$ and we must have $\overline{S}^{\mathrm{P}}_N < u_*$. In such a case,

$$u_{N+1} - l_{N+1} = \delta_{N+1} < \delta_N.$$

From cases (a) and (b), we establish that the sequence $\{u_n - l_n\}$ is monotonically decreasing and bounded below by 0. Hence by the monotone convergence theorem,

$$\lim_{n\to\infty}(u_n - l_n) = 0 \Leftrightarrow \lim_{n\to\infty} u_n = \lim_{n\to\infty} l_n.$$

(2) By similar argument, we arrive at $\lim_{n\to\infty} u_n = \lim_{n\to\infty} l_n$ when there exists a solution to (4.29) at iteration N with $F_{\text{life},N+1} \leq 1$, or when no solution is found for (4.29) at iteration N.

In cases (1) and (2) we show that $\lim_{n\to\infty} u_n = \lim_{n\to\infty} l_n$, hence this completes the proof. □

Now we state the main result for the convergence of the sequence $\left\{\overline{S}^{\mathrm{P}}_n\right\}$ constructed by the search algorithm.

Theorem 1. *The sequences* $\left\{\overline{S}^{P}_n\right\}, \{u_n\}$, *and* $\{l_n\}$ *generated by Algorithm 1 for* $n > 0$ *converge to* $\overline{S}^{P}_*$.

Proof. The sequence $\left\{\overline{S}^{\mathrm{P}}_n\right\}$ is bounded by $\{u_n\}$ and $\{l_n\}$ for all n. By Lemma 3, we have $\lim_{n\to\infty} u_n = \lim_{n\to\infty} l_n$. Finally, it follows that $\lim_{n\to\infty} \overline{S}^{\mathrm{P}}_n = \overline{S}^{\mathrm{P}}_* = \lim_{n\to\infty} u_n = \lim_{n\to\infty} l_n$ by the squeeze theorem. □

Let $\overline{S}_{t,*}$ be the $\overline{S}_t$ computed in (4.32) for $t \in \mathcal{T}^{\mathrm{OP}} \cup \mathcal{T}^{\mathrm{MP}}$ and the searched $\overline{S}^{\mathrm{P}}_*$ for $t \in \mathcal{T}^{\mathrm{P}}$. The following corollary can be consequently claimed.

Corollary 1. *If $\widetilde{F}_{\mathrm{life}} = 1$ can be achieved, then $\overline{S}_{t,*}$ is an optimal time-varying limit for $\mathbb{E}[\widetilde{S}_{e,EV}]$ to achieve $\widetilde{F}_{\mathrm{life}} = 1$. Further, (4.29) is a convex restriction of (4.22).*

Proof. When applying $\overline{S}_{t,*}$, the resulting adjustment $\mathbf{\Delta}_{\mathrm{prob}}$ and incentives are (i) feasible with respect to the original problem (4.22), and (ii) globally optimal with respect to the reformulated convex problem (4.29) by applying $\overline{S}^{\mathrm{P}}_*$ during $\mathcal{T}^{\mathrm{P}}$. Given that $\widetilde{F}_{\mathrm{life}} = 1$, the relaxation of (4.13) is exact. It therefore follows that (4.29) is a convex restriction of (4.22). □

If there exists no $\overline{S}^{\mathrm{P}}$ to achieve $\widetilde{F}_{\mathrm{life}} = 1$, Theorem 1 still holds and yields some $\overline{S}_{t,*}$ that minimizes $|\widetilde{F}_{\mathrm{life}} - 1|$. In this case, (4.29) is a convex approximation to (4.22). We can still solve for $\mathbf{\Delta}_{\mathrm{prob}}$ and incentives from (4.29), but the relaxation of (4.13) is not exact. In either case, a mitigation strategy is proposed based on the solution of (4.29) when $\overline{S}_{t,*}$ is applied.

4.5 Implementation guidelines

In this section, we discuss about practical details and necessary data to derive the TOU rate based on Algorithm 1.

4.5.1 Extension to multiple equipment and networks

We remark that until now the incentive is computed to mitigate the extra loading due to EV charging on a single equipment, and all EV owners on the network can participate in the mitigation plan. In practice, simultaneous overloads on a set of equipment (denoted as $\mathcal{E}$) may occur, and they may belong to different networks. If we mitigate the overload on one equipment at a time, we obtain heterogeneous strategies and incentive levels which are not realistic to implement, e.g., customers in neighbouring areas but on different networks may have different incentive plans. To design a single incentive policy applicable to all customers on these networks, we make the following modifications to our approach:

- The budget constraint in (4.29) is replaced by:

$$\sum_{i=1}^{N_{\mathrm{M}}} \hat{R}^i \leq \sum\nolimits_{e \in \mathcal{E}} c(F^e_{\mathrm{life}}), \tag{4.34}$$

where N_{M} is the total number of customers on all networks considered, and F^{e}_{life} is the initial lifetime stress factor for each e in $\mathcal{E}$.

- Under the applied strategy, we aim to have the worst $|\widetilde{F}_{\mathrm{life}}|$ value for all equipment in $\mathcal{E}$ as close as possible to 1. Hence, in Algorithm 1, at each iteration n, $\mathbf{x}_e$ for each e is evaluated to compute the corresponding factor $F^{e}_{\mathrm{life},n}$, and the maximum value is used for $F_{\mathrm{life},n}$, i.e., $F_{\mathrm{life},n} = \max_{e\in\mathcal{E}}\{F^{e}_{\mathrm{life},n}\}$.

We want to highlight that this extension also enables to design a strategy to mitigate multiple overloaded distribution transformers, as long as their overload costs can be properly determined.

4.5.2 Implementation and review of the strategy

We first need to determine the baseline network states over the time horizon $\mathcal{T}$ without any EV load. To do so, we perform power flow analyses to the distribution network model $\mathcal{N}$ using customers' time-varying load data. We use ts-REM to assess EV charging impact to the network at a given penetration level, and customers' uncertainties in charging behaviours are characterized by EV owners' charging profiles and probability data. If a separate meter is installed to the EV charger, it is straightforward to obtain EV charging data. Otherwise, it is also possible to extract such information from customers' net meter data using approaches in [50, 126]. Finally, the nominal electricity price and the elasticity factor are used to model customers' sensitivity of consumption to the change of electricity price. If customers' elasticity factor is not available through local statistical studies, an average value can be used from studies such as in [125]. The process using the identified input data and Algorithm 1 is depicted in Figure 4.1 to derive the optimal incentive levels under the mitigation strategy.

After putting the incentives into practice, periodic reviews (e.g., yearly) should be performed to measure the effectiveness of the mitigation strategy by collecting in-field data, e.g., transformer loading, customers EV charging consumption, etc. The main goals are: 1) to confirm equipment overloads are indeed mitigated and 2) to compare customers' shifted charging behaviours with the computed $\mathbf{\Delta}_{\mathrm{prob}}$ values. The latter can be used as a condition for participation, and is also useful in fine-tuning the elasticity factor.

4.6 Numerical study

We use the modified IEEE-8500 test network as in Chapter 2 to illustrate the proposed strategies. We specifically aim to mitigate overloads on the substation transformer. The

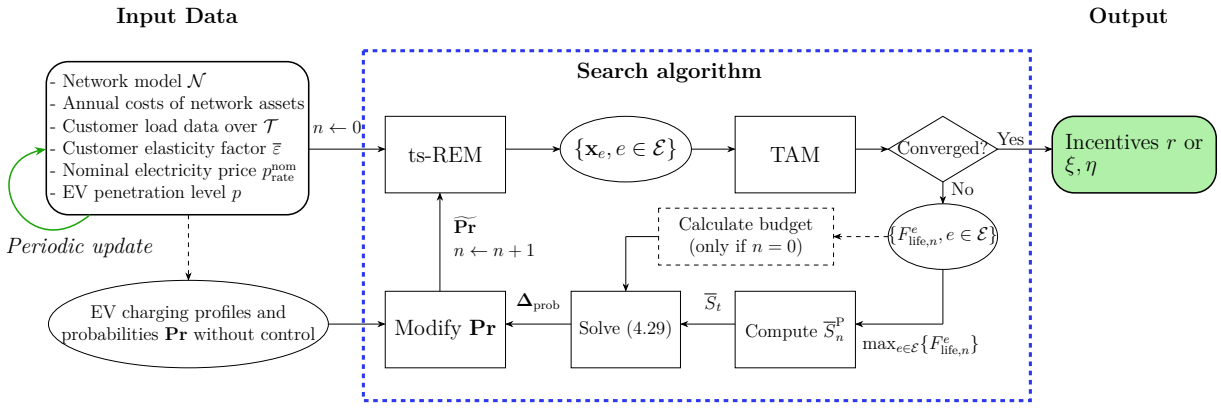

Figure 4.1 Necessary input data and process to derive the incentive levels for the mitigation strategy

following information are assumed:

- $\mathcal{L}_{\text{EV}}$: we follow the approach presented in Chapter 3 to extract EV charging profiles from the Pecan Street database [111] at selected Level-2 power levels, namely 3.6 kW, 6.6 kW, 7.2 kW, and 9.6 kW, with unity power factor. Also, we consider only profiles with charging duration up to 6 hours, as they account for over 90% of all profiles in the dataset (refer to the assumptions on contextual information of EV charging in Chapter 3).

- $\text{Pr}[\mathcal{L}_{\text{EV}}]^i$: we extract multiple sets of probabilities of adopting profiles in $\mathcal{L}_{\text{EV}}$, and each customer i in the test network is attached with a randomly selected set of probabilities. It is observed that most customers have higher probabilities of starting charging between noon and midnight.

- The nominal electricity price is $p^{\text{nom}}_{\text{rate}} = 0.35$ \$/kWh. According to [125], the averaged elasticity factor $\bar{\varepsilon}$ ranges from -0.21 to -0.61 for residential customers. Hence we assume $\bar{\varepsilon} = -0.4$. We want to highlight that different nominal electricity prices can be used depending on the geographic locations, and the optimal incentive levels are determined accordingly, i.e., for high (low) $p^{\text{nom}}_{\text{rate}}$, incentive rates are high (low) to motivate customers to cooperate.

We look at the impact to the substation transformer loading levels at 80% EV penetration for $\mathcal{T} = 24$ hours with a time step of $\Delta t = 1$ hour. Figure 4.2 shows the mean and maxi-

mum/minimum (±2× standard deviation) loading levels which are computed by the ts-REM model.

Looking at the mean loading curve (in orange color), the transformer is overloaded from 3PM until 10PM with the worst loading at over 120%. If such a loading pattern repeats during the entire year, it is determined by TAM that the lifetime factor is $F_{\text{life}} = 1.08$. Suppose that the annual cost associated with the transformer if it is maintained at the nominal lifetime is $c_{\text{annual}} = \$500{,}000$, then from (4.12) an extra cost of \$40,000 per year is incurred to utilities due to the shortened lifetime, which serves as the budget for customer incentives.

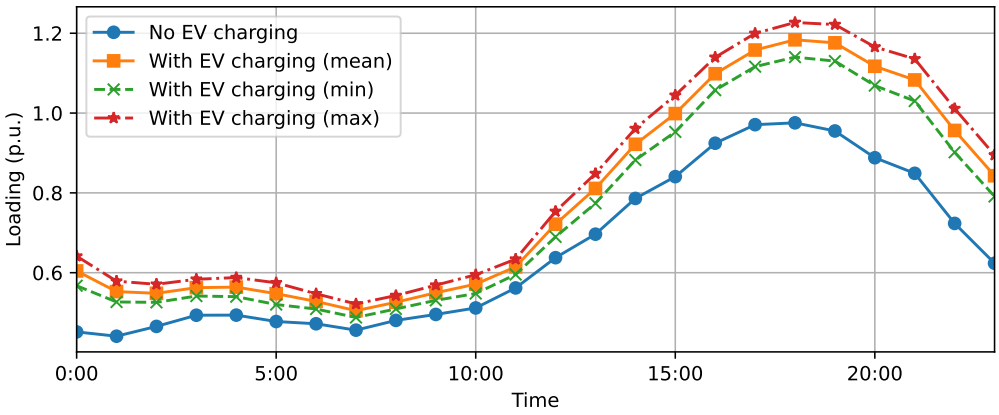

Figure 4.2 Multiple levels of loading curves of the substation transformer with 80% EV penetration

Based on the loading curves in Figure 4.2, we set $\mathcal{T}^{\text{P}}$ and $\mathcal{T}^{\text{OP}}$ to [14:00, 21:00) and [0:00, 8:00), respectively, and the remaining hours to $\mathcal{T}^{\text{MP}}$. Figure 4.3 shows the $\overline{S}_n^{\text{P}}$ value searched at each iteration of Algorithm 1 for the reward type of incentives (top left) and for TOU pricing (top right). Figure 4.3 also shows the corresponding total yearly costs (bottom left) and the incentives levels determined (bottom right) at each iteration. For the reward incentives, $\overline{S}_n^{\text{P}}$ converges to $\overline{S}_*^{\text{P}} = 0.52$, the unit reward is $r = 12.32$ ¢/kWh, and the total extra cost to utilities reduces from an initial \$40,000 to \$23,201 per year (a 42.0% saving). For the TOU pricing, $\overline{S}_n^{\text{P}}$ converges to $\overline{S}_*^{\text{P}} = 0.53$, a discount of $\xi = 15.36$ ¢/kWh is offered during the off-peak time, and a surcharge of $\eta = 12.92$ ¢/kWh is added during the peak time. Under such pricing, the total extra cost to utilities reduces from \$40,000 to \$22,961 per year (a 42.6% saving). It is noted that the TOU program is slightly more efficient and the total cost to implementing the mitigation strategy is less, given the added degree of freedom. We remark that the obtained incentive levels correspond to the nominal price $p_{\text{rate}}^{\text{nom}}$ used. Incentives levels are expected to be higher for higher $p_{\text{rate}}^{\text{nom}}$ used, such that the enough

incentives are offered to customers to participate.

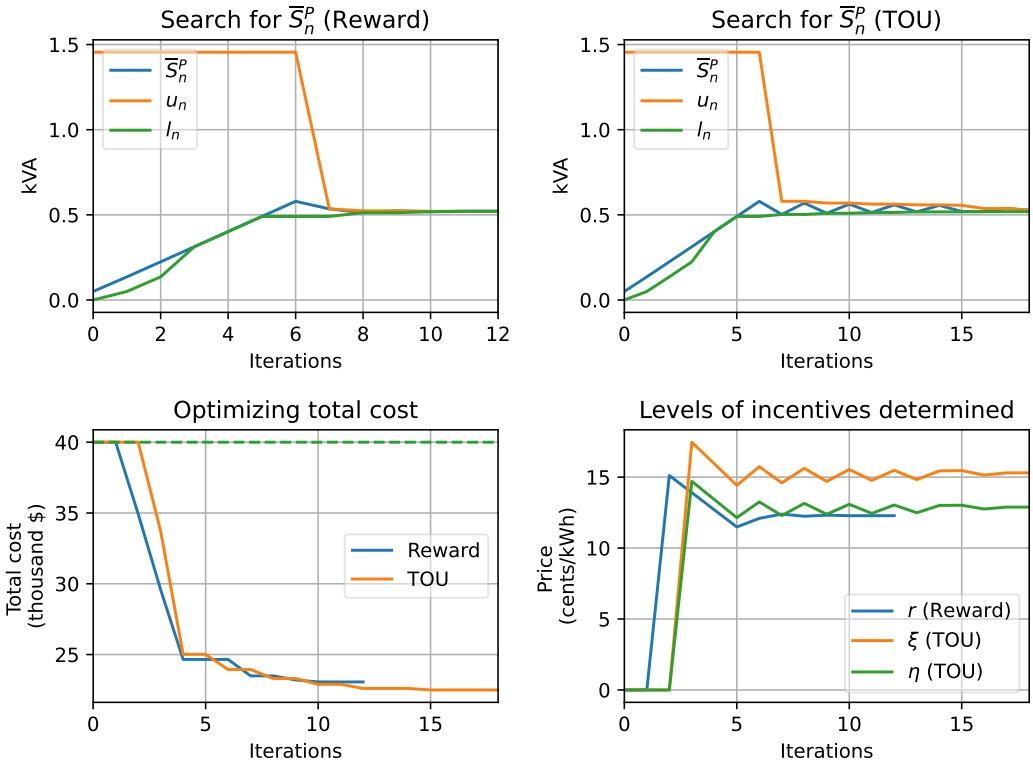

Figure 4.3 The sequences of peak period limits searched (**top**), total costs (**bottom left**), and incentive levels (**bottom right**) during iterations of Algorithm 1

Figure 4.4 shows the results when the mitigation strategies based on the converged solutions for the two types of incentive programs are applied, where the transformer's overload during the peak period has been reduced to an acceptable level while the load is shifted to the off-peak period. Although the transformer is still slightly overloaded for a brief period, its lifetime of service is restored to the nominal value under either type of incentive programs, i.e., $\widetilde{F}_{\text{life}} = 1$.

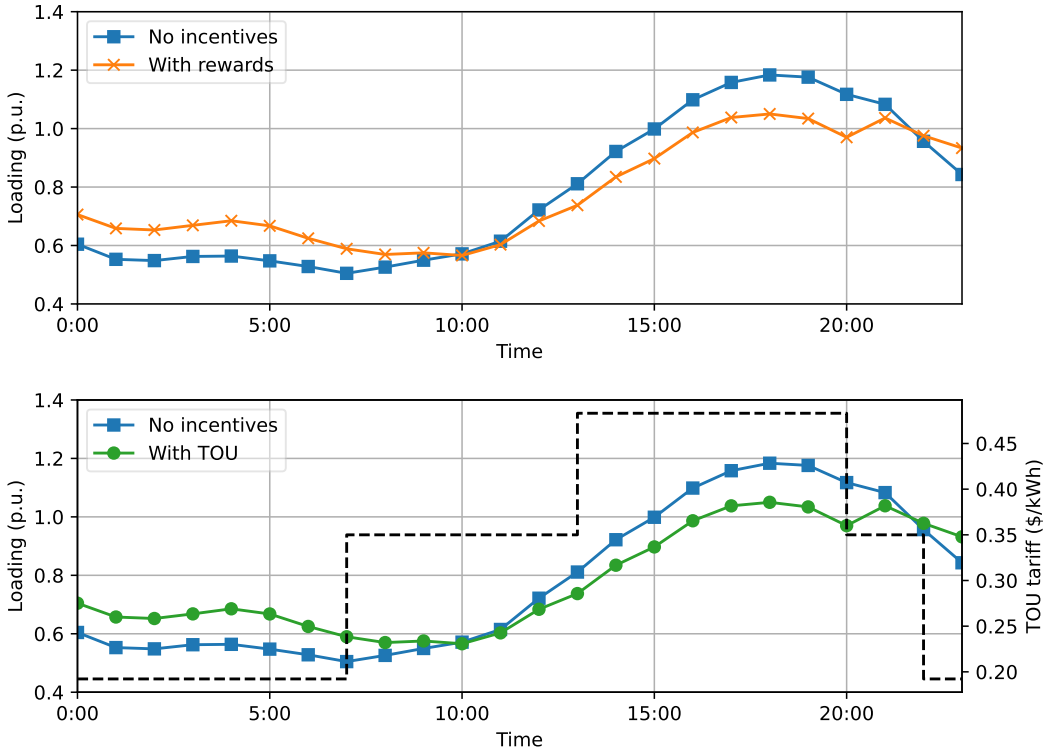

Figure 4.4 Mitigation of the substation transformer overload by offering rewards (**top**) or by applying TOU (**bottom**)

In Figure 4.5, we compare the averaged probabilities of all customers charging their EVs before and after mitigation strategies are applied. It is observed that under the mitigation strategies, customers decrease their probabilities of charging EVs during the peak period and increase those during the off-peak period, while the probabilities of the mid-peak period remain unchanged.

While all customers' averaged probabilities of charging profiles are compared in Figure 4.5, Figure 4.6 shows the change in charging habits in terms of probabilities for three selected customers under the designed mitigation strategies, if they participate in such strategies. It is observed in the top row that these customers initially have different charging behaviours. Customer-1 has the most common habit among all customers who mostly charge their EVs during the peak period, hence they should significantly increase the probabilities of charging during the off-peak period to benefit from the incentives offered under the mitigation strategies. Customer-2 already charges the EV mostly during the off-peak period, hence the change of probabilities is minimal. Customer-3's initial probabilities of all charging profiles are almost uniform. Although the change of probabilities does not need to be not as much as

that of Customer-1, probabilities of charging during the off-peak period should still become higher.

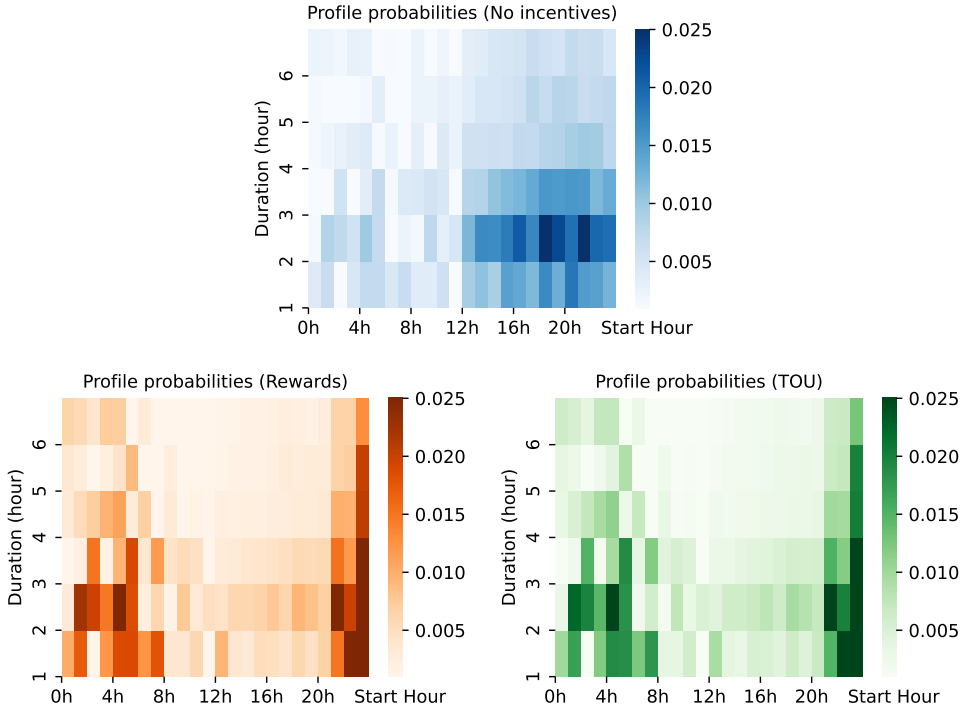

Figure 4.5 Resulting changes to customers' EV charging habits (joint probabilities of charging hours and duration) under mitigation strategies

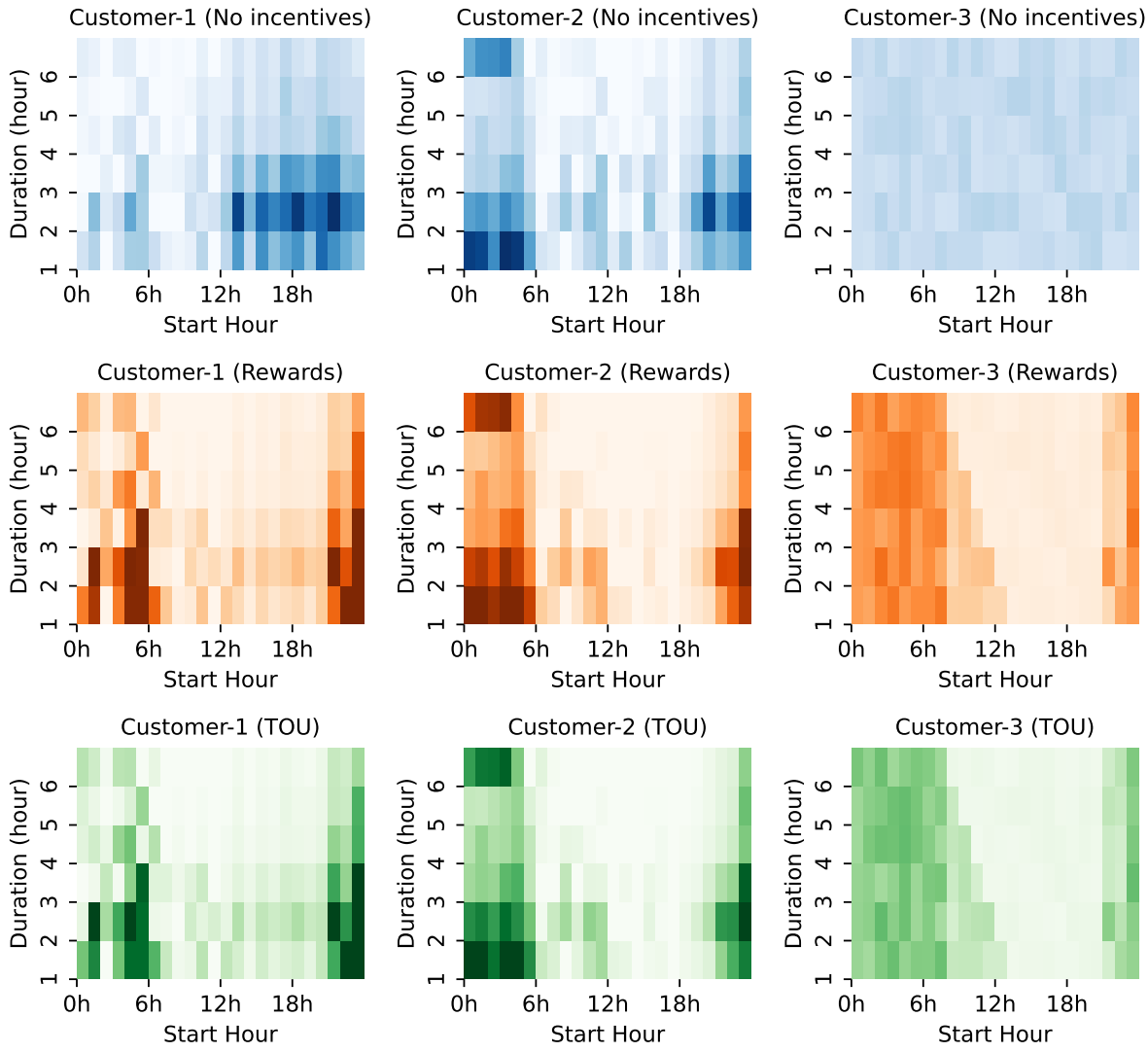

Figure 4.6 Comparison of 3 selected customers' probabilities of charging during the day before adopting a mitigation strategy (**top**) versus those by offering rewards (**middle**) or by applying TOU (**bottom**)

4.7 Conclusion

In this chapter, we propose a mitigation strategy to avoid overloading issues to key network equipment with a high penetration of EVs by shifting customers' probabilities of charging their EVs from the peak hours to the off-peak hours. A bi-level optimization problem is formulated to design the mitigation strategy aiming to maintain equipment's nominal lifetime and minimize associated costs. The bi-level problem is then re-expressed as a convex program, which is embedded into a dedicated search algorithm to determine optimal levels of incentives

offered under the mitigation strategy. We emphasize that with the proposed mitigation strategy, we do not enforce a specific charging schedule to each customer on a daily basis. Rather, customers still have the freedom to charge their EVs during the peak hours when necessary. However, the probabilities of doing so in the long term should be consistent with those determined from the mitigation plan.

Our formulation also accounts for the uncertainty in customers' participation through the λ_p factor, although the numerical example presented considers the full participation of customers, i.e., $\lambda_p = 1$. This offers the opportunity to perform various case studies with different participation rates and sensitivity analyses including validation studies with real customer data for utilities as a next step. Further, we sketch a process in Section 4.5.1 to design a uniformized strategy and incentive plan to all customers on different networks in a region where multiple equipment may be overloaded. Additional case studies can be carried out by following the proposed approach to verify the effectiveness of the single incentive plan to all customers on these networks.

The mitigation plan designed in this chapter aims to reduce the likelihood of equipment being overloaded due to high penetration of EV charging on the network. Although REM can assess voltage levels on the network, we do not consider voltage levels in our formulation for two reasons: (1) the costs associated with abnormal voltage levels are difficult to quantify, and (2) there are other more effective ways to regulate voltage levels, e.g., using voltage regulators. However, the implementation of the overload mitigation plan should also help to reduce the probability of under-voltage conditions on the network during the peak period, i.e., when EV charging loads are shifted outside of peak hours, the through currents are reduced leading to less voltage drops on the network. When PVs are installed to the network as the GET type, it is seen in the numerical example in Section 2.4.4 that we do not have risks of overloading network equipment. However, at high PV penetration levels, certain network sections may have increased probabilities of over-voltage conditions, especially near the substation and voltage regulators where voltages are initially regulated to higher levels. The principle of the mitigation plan discussed in this chapter is not applicable to mitigate the over-voltage issues, because PVs are considered as non-dispatchable DERs and we cannot shift their generation from one period to another. Therefore, another type of control strategies needs to be developed to address the voltage abnormal conditions on PV-rich networks. For this purpose, we present a control strategy under the volt-var optimization framework in the next chapter to minimize the occurrence of abnormal voltage levels and the total network energy losses with uncertainty in PV generation.

CHAPTER 5 VOLT-VAR OPTIMIZATION AND OPTIMAL SETTINGS FOR SMART INVERTERS USING BLACKBOX OPTIMIZATION

5.1 Introduction

Electric power distribution systems face multifaceted challenges, such as maintaining reliable services and operational efficiency, while subject to demand fluctuations and an increasing integration of distributed energy resources (DERs) like photovoltaic systems (PVs). Volt-var optimization (VVO) is a critical technique in modern power distribution systems. It aims to enhance grid efficiency, reduce energy losses, and improve overall system performance by dynamically adjusting voltage levels and reactive power flows. Voltage regulators (VRs), on-load tap changers (OLTCs), and capacitor banks (CBs) are legacy devices that are conventionally used to perform VVO. It is becoming more important to manage and optimize voltage levels in the distribution network with the increasing penetration rate of DERs. As stated in the IEEE-1547 standard [127], DERs should have the capability of injecting or absorbing reactive power for voltage regulation. Hence, they naturally become devices that can be controlled to participate in VVO, in addition to the legacy devices.

In this chapter, we consider PVs as the primary DER type because not only can they be of utility-scale, but they are also installed at residential and commercial areas as GETs. We assume that locations of PVs on the distribution network and their nominal ratings are known; in other words, the network containing these PVs (also known as the "as-planned" network model) is available. However, uncertainty still exists in their actual generation profiles. We propose an efficient and scalable approach to perform VVO, with the following main contributions:

1. We formulate a stochastic program for optimal reactive power dispatch (ORPD) problem which considers variations in loading and DER generation. We include controls for conventional devices in VVO and volt-var control of DERs conforming to the IEEE-1547 standard.

2. RL approaches have shown promise in VVO; however, their interpretability and trustworthiness can be questionable, i.e., RL penalizes policies leading to voltage violations but it is not guaranteed that these policies are not proposed under scenarios with uncertainty. This can pose risks to safety of the power system and it can become difficult to interpret why such policies are given. For better interpretability, we use a multiphase unbalanced power flow solver as the blackbox simulator, and convert the ORPD

problem to a blackbox optimization instance. We also do not need any hyperparameter tuning process as needed in RL for better performance. To the best of our knowledge, no prior work uses blackbox optimization for VVO in the literature.

3. We compare our approach with an RL method on a small-size test feeder in various case studies and illustrate our approach's performance and then scalability on a large-size distribution system.

The rest of the chapter is organized as follows: In Section 5.2, we present the mathematical models for the power flow solver as well as device models considered in VVO. We formulate ORPD stochastic program in Section 5.3 and propose the blackbox optimization approach to solve it. In Section 5.4, we illustrate the performance of our proposed method with numerical studies. We conclude in Section 5.5 by pointing out directions for some future work.

5.2 Mathematical models

To optimize volt-var on the power distribution networks, we need a solver for power flow analyses incorporating the VVO devices and their control schemes. We suppose that the distribution network $\mathcal{N}$ contains buses $\mathcal{B} \subset \mathbb{N}$ and branches/lines $\mathcal{L} \subset \mathcal{B} \times \mathcal{B}$. The branch from nodes m to n is denoted by $l_{mn} \in \mathcal{L}$. A node $m \in \mathcal{B}$ and a branch $l_{mn} \in \mathcal{L}$ can also be indexed by the phase $\phi \in \{a, b, c\}$, e.g., m^a and l^a_{mn} refers to node m and branch l_{mn} on phase a, respectively.

5.2.1 Power flow model

For power distribution networks, multi-phase power flow analyses are required. The Backward-Forward Sweep (BFS) method, also known as the Ladder Iterative or Voltage Drop (VD) method, is often used. While it is computationally efficient for radial and passive distribution networks, other methods are required in VD to handle networks with loops [128] and controlled devices (e.g., OLTC, voltage-controlled generators, etc.) [129]. Many more iterations may be required for convergence, and in some cases, divergence may even occur for certain voltage-sensitivity load models and levels [130]. As VVO involves the optimization of control modes of these devices, we use the Modified Augmented Nodal Analysis (MANA) formulation [131] to perform power flow analyses to better handle the modelling of such devices.

5.2.1.1 MANA formulation

The MANA system of equations for distribution networks has the following general form:

$$\begin{bmatrix} \mathbf{Y} & \mathbf{V}_\mathrm{c} & \mathbf{D}_\mathrm{c} & \mathbf{S}_\mathrm{c} \\ \mathbf{V}_\mathrm{c}^\top & \mathbf{0} & \mathbf{0} & \mathbf{0} \\ \mathbf{D}_\mathrm{c}^\top & \mathbf{0} & \mathbf{0} & \mathbf{0} \\ \mathbf{S}_\mathrm{c}^\top & \mathbf{0} & \mathbf{0} & \mathbf{S}_\mathrm{z} \end{bmatrix} \begin{bmatrix} \mathbf{v} \\ \mathbf{i}_\mathrm{v} \\ \mathbf{i}_\mathrm{d} \\ \mathbf{i}_\mathrm{s} \end{bmatrix} = \begin{bmatrix} \mathbf{i}_\mathrm{inj} \\ \mathbf{v}_\mathrm{v} \\ \mathbf{0} \\ \mathbf{0} \end{bmatrix}, \tag{5.1}$$

where $\mathbf{Y} \in \mathbb{C}^{N_\mathrm{b} \times N_\mathrm{b}}$ is the admittance matrix for N_b by-phase nodes of the network, $\mathbf{V}_\mathrm{c}$ represents the contribution of voltage sources, $\mathbf{D}_\mathrm{c}$ models the branch-dependent relations of devices, and $\mathbf{S}_\mathrm{c}$ and $\mathbf{S}_\mathrm{z}$ are used for closed and open switches, respectively. The column vectors $\mathbf{v}, \mathbf{i}_\mathrm{v}, \mathbf{i}_\mathrm{d}$, and $\mathbf{i}_\mathrm{s}$ contain the unknown values for node voltages, currents of voltage sources, currents in the branch-dependent devices (e.g., currents in the secondary windings of transformers), and switches, respectively. Finally, $\mathbf{i}_\mathrm{inj}$ is the vector of known nodal current injections and $\mathbf{v}_\mathrm{v}$ contains known voltages. Let $\mathbf{x} = [\mathbf{v}^\top, \mathbf{i}_\mathrm{v}^\top, \mathbf{i}_\mathrm{d}^\top, \mathbf{i}_\mathrm{s}^\top]^\top$ denote the unknowns and $\mathbf{b} = [\mathbf{i}_\mathrm{inj}^\top, \mathbf{v}_\mathrm{v}^\top, \mathbf{0}^\top, \mathbf{0}^\top]^\top$ the known values, we can write (5.1) in the simplified form:

$$\mathbf{A}\mathbf{x} = \mathbf{b}. \tag{5.2}$$

The matrix $\mathbf{A}$ is sparse for a typical distribution system due to the admittance matrix $\mathbf{Y}$. Readers are referred to [131] for more details on the MANA formulation.

5.2.1.2 Newton-Raphson power flow solver

To perform a power flow analysis while considering the non-linearity in the distribution networks, a fixed-point method can be used by solving (5.2) iteratively. However, similar to the BFS or VD approach, it suffers from the poor convergence issues, either requiring much more iterations or not converging for networks with multiple voltage-controlled device. Alternatively, the Newton-Raphson (NR) method is used.

Consider a general nonlinear function $\mathbf{f}(\mathbf{x}) = \mathbf{0}$, one can expand $\mathbf{f}(\mathbf{x})$ by a first order Taylor series for given $\mathbf{x}_0$:

$$\begin{aligned} \mathbf{f}(\mathbf{x}) &\approx \mathbf{f}(\mathbf{x}_0) + \mathbf{J}(\mathbf{x}_0)(\mathbf{x} - \mathbf{x}_0) = \mathbf{0}, \\ \mathbf{f}(\mathbf{x}_0) &\approx -\mathbf{J}(\mathbf{x}_0)(\mathbf{x} - \mathbf{x}_0), \end{aligned} \tag{5.3}$$

where $\mathbf{J}$ is the Jacobian matrix. The Newton-Raphson approach is an iterative process by

using (5.3) as the update equation, i.e.,

$$\begin{aligned} \Delta\mathbf{x}^{(k+1)} &= \mathbf{x}^{(k+1)} - \mathbf{x}^{(k)}, \\ \mathbf{f}(\mathbf{x}^{(k)}) &= -\mathbf{J}(\mathbf{x}^{(k)})\Delta\mathbf{x}^{(k+1)}, \end{aligned} \tag{5.4}$$

where k indicates the iteration and $\Delta\mathbf{x}^{(k)}$ is the correction vector. The iterative process stops when a given convergence criterion is reached, e.g., $\Delta\mathbf{x}^{(k)} \to \mathbf{0}$.

When applying the Newton-Raphson method to solve a MANA-formulated power flow, at each iteration we evaluate $\mathbf{f}(\mathbf{x}^{(k)})$ by augmenting (5.2) with power flow constraints from various device models into the following:

$$\mathbf{f}(\mathbf{x}^{(k)}) = \begin{bmatrix} \mathbf{A} & \mathbf{C}_\mathrm{c} \end{bmatrix} \begin{bmatrix} \mathbf{x}^{(k)} \\ \mathbf{x}_\mathrm{c}^{(k)} \end{bmatrix} - \mathbf{b}^{(k)}, \tag{5.5}$$

where $\mathbf{x}_\mathrm{c}$ is the vector of additional state variables augmented (e.g., voltage ratio based on tap position of regulators), and $\mathbf{C}_\mathrm{c}$ is the submatrix for network constraints. We derive the Jacobian matrix $\mathbf{J}(\mathbf{x}^{(k)})$ by taking the first-order partial derivative of $\mathbf{f}(\mathbf{x}^{(k)})$ with respect to $[\mathbf{x}^{(k)^\top}, \mathbf{x}_\mathrm{c}^{(k)^\top}]^\top$, which has the following form:

$$\mathbf{J}(\mathbf{x}^{(k)}) = \begin{bmatrix} \mathbf{A} & \mathbf{C}_\mathrm{c} \\ \mathbf{J}_{21}^{(k)} & \mathbf{J}_{22}^{(k)} \end{bmatrix}, \tag{5.6}$$

where $\mathbf{J}_{21}^{(k)}$ and $\mathbf{J}_{22}^{(k)}$ are submatrices of $\mathbf{J}(\mathbf{x}^{(k)})$ when taking partial derivatives of $\mathbf{f}(\mathbf{x}^{(k)})$ with respect to $\mathbf{x}_\mathrm{c}$. For more details on detailed formulation of $\mathbf{J}(\mathbf{x}^{(k)})$, refer to [131]. From hereinafter, the MANA-formulated power flow using Newton-Raphson is referred as MANA-NR.

5.2.2 Device models for VVO

In this section, we integrate device models of capacitor banks, voltage regulators, transformers with OLTC, and distributed energy resources (DERs) with smart inverters into the power flow.

5.2.2.1 Capacitor bank

In distribution systems, capacitor banks may be installed on one, two, or three phases. For one unit on a single phase $\phi \in \{a, b, c\}$, the capacitor impedance is given by:

$$Z_{\text{cb}}^{\phi} = \frac{V_{\text{LN}}^2}{P_{\text{cb}}^{\text{loss}} - jQ_{\text{cb}}}, \tag{5.7}$$

where $V_{\text{LN}} \in \mathbb{R}$ is a line-neutral voltage magnitude on the phase where the capacitor is connected to, $P_{\text{cb}}^{\text{loss}}$ models the active power losses, and Q_{cb} is the reactive power rating of the capacitor bank. If the unit is installed at node m on phase ϕ, i.e., m^{ϕ}, then its model is integrated into $\mathbf{A}$ from (5.2) through $\mathbf{Y}[i_{m^{\phi}}, i_{m^{\phi}}] = [\gamma_{\text{cb}} Y_{\text{cb}}]$, where $Y_{\text{cb}} = Z_{\text{cb}}^{-1}$, $\gamma_{\text{cb}} \in \{0, 1\}$ indicates whether the capacitor bank is switched On/Off, and $i_{m^{\phi}}$ is the index corresponding to m^{ϕ}. Similarly, for a three-phase capacitor bank installed to m in Wye-Grounded, it is modelled by:

$$\mathbf{Y}_{\text{cb}}^{m} = \gamma_{\text{cb}} \begin{bmatrix} Y_{\text{cb}}^{a} & 0 & 0 \\ 0 & Y_{\text{cb}}^{b} & 0 \\ 0 & 0 & Y_{\text{cb}}^{c} \end{bmatrix}.$$

Note that here we assume that the capacitor unit on each phase cannot be switched On/Off individually (i.e., if $\gamma_{\text{cb}} = 0$ then all units are switched Off) but $Y_{\text{cb}}^{a}, Y_{\text{cb}}^{b}$, and Y_{cb}^{c} do not necessarily have identical values, i.e., capacitors of different sizes can be installed.

5.2.2.2 Voltage regulator

A voltage regulator is an autotransformer whose turn ratio can be varied to either "step up" (boost) or "step down" (buck) the voltage level through the "tap positions". Similar to the capacitor bank, a regulator can be installed on one, two, or three phases. As the series impedance and shunt admittance of an autotransformer are negligible, a regulator installed between nodes m and n in Wye-Grounded is modelled into $\mathbf{A}$ through $\mathbf{Y}_{\text{vr}}^{mn} = \mathbf{0}_{2p \times 2p}$ which is zero-matrix of dimension $2p \times 2p$, where p is the number of connected phases of the regulator. In addition, for each connected phase ϕ, a vector $\mathbf{d}_{\text{vr}}^{mn,\phi} = [-a_{\text{vr}}^{\phi}, 1]^{\top}$ is added to $\mathbf{D}_{\text{c}}$ at corresponding indices to model the dependency between the primary and secondary currents on phase ϕ. Here, a_{vr}^{ϕ} is the voltage-ratio on phase ϕ, which is given by $a_{\text{vr}}^{\phi} = 1 \pm 0.00625 T_{\text{vr}}^{\phi}$ assuming $\pm 10\%$ regulation range with a total of 32 tap steps, where $T_{\text{vr}}^{\phi} \in \mathbb{N}$ is the tap number.

Let $V_m^{\phi} = V_{m,\text{R}}^{\phi} + jV_{m,\text{I}}^{\phi}$ be the phasor voltage at node m on phase ϕ whose magnitude

$|V_m^\phi| = \sqrt{(V_{m,\mathrm{R}}^\phi)^2 + (V_{m,\mathrm{I}}^\phi)^2}$ is to be regulated to a desired level $V_{m\mathrm{D,vr}}^\phi \in \mathbb{R}$. Hence, the voltage constraint $f_{\mathrm{c,vr}}^{(k)} = |V_m^\phi|^{(k)} - V_{m\mathrm{D,vr}}^\phi$ is included in $\mathbf{f}(\mathbf{x}^{(k)})$ by augmenting a_{vr}^ϕ as an additional state variable to $\mathbf{x}^{(k)}$ in the MANA formulation. We then calculate specific terms in $\mathbf{J}(\mathbf{x}^{(k)})$ related to the voltage constraint of the regulator, where more details can be found in [132] .

5.2.2.3 Transformer with OLTC

Transformers with OLTC regulate the voltages in a similar way as that for voltage regulators; however, transformers have multiple windings hence their impedance must be modelled. Generally a simplified model is used for transformers in MANA representation where only the series impedance (reference to the secondary side) is modelled and the magnetizing branch and no-load losses are neglected (however, they can be modelled as constant-impedance loads in MANA and readers can refer to [133] for load models). For example, for a single-unit transformer installed between nodes m and n on phase ϕ in Wye-Grounded with zero grounding impedance, it is represented by:

$$\mathbf{Y}_{\mathrm{xfo}}^{mn,\phi} = \begin{bmatrix} 0 & 0 & 0 \\ 0 & Y_{\mathrm{s}} & -Y_{\mathrm{s}} \\ 0 & -Y_{\mathrm{s}} & Y_{\mathrm{s}} \end{bmatrix},$$

where Y_{s} is the series admittance of the transformer. Note that $\mathbf{Y}_{\mathrm{xfo}}^{mn,x}$ is a 3×3 matrix where the middle column corresponds to the internal node on the secondary side before the series impedance. In addition, to model the dependency between currents in primary and secondary windings, a vector $\mathbf{d}_{\mathrm{xfo}}^{mn,\phi} = [-g_{\mathrm{xfo}}^\phi, 1]^\top$ is added to $\mathbf{D}_{\mathrm{c}}$ corresponding to indices of m^ϕ and n^ϕ, where g_{xfo}^ϕ is the turn ratio of the transformer according to the selected tap position. For models on three-phase transformers and in other configurations, readers are referred to [134].

For a transformer with OLTC, its turn ratio g_{xfo}^ϕ is no longer fixed but depends on the tap number. To model the OLTC, a similar model as that of the voltage regulator is used, where the voltage V_n^ϕ on the secondary side (node n^ϕ) is regulated to a desired level $V_{n\mathrm{D,xfo}}^\phi$, i.e., the voltage constraint $f_{\mathrm{c,xfo}}^{(k)} = |V_n^\phi|^{(k)} - V_{n\mathrm{D,xfo}}^\phi$ is included in $\mathbf{f}(\mathbf{x}^{(k)})$ by augmenting the turn ratio g_{xfo}^ϕ as an additional state variable to $\mathbf{x}^{(k)}$.

5.2.2.4 Inverter volt-var curve

Inverter-based DERs such as photovoltaic (PV) systems, wind turbines, and battery storages have the capability of regulating voltages by adjusting their reactive power output. The amount of reactive power to absorb or to inject to the grid depends on the volt-var curve (or droop) settings in the DERs, which serves as a "policy" allowing DERs to act in a decentralized way to regulate the voltage. The volt-var curves should follow the guidelines provided in the IEEE-1547 standard [127]. An example is shown in Figure 5.1. The amount of reactive power absorbed/injected is determined by the DER's voltage magnitude v at the point of connection such that:

$$Q_{\text{der}}(v) = \begin{cases} Q_1, & \text{if } v < V_1, \\ Q_1(V_2 - v)/(V_2 - V_1), & \text{if } V_1 \le v < V_2, \\ 0, & \text{if } V_2 \le v \le V_3, \\ Q_2(V_4 - v)/(V_4 - V_3), & \text{if } V_3 < v < V_4, \\ Q_2, & \text{otherwise}, \end{cases} \tag{5.8}$$

where the two reactive power limits Q_1 and Q_2 and the five per-unit voltage magnitudes $V_{\text{Ref}}, V_1, V_2, V_3$, and V_4 are to be specified by the DER operator, which collectively define a volt-var curve C_{der}.

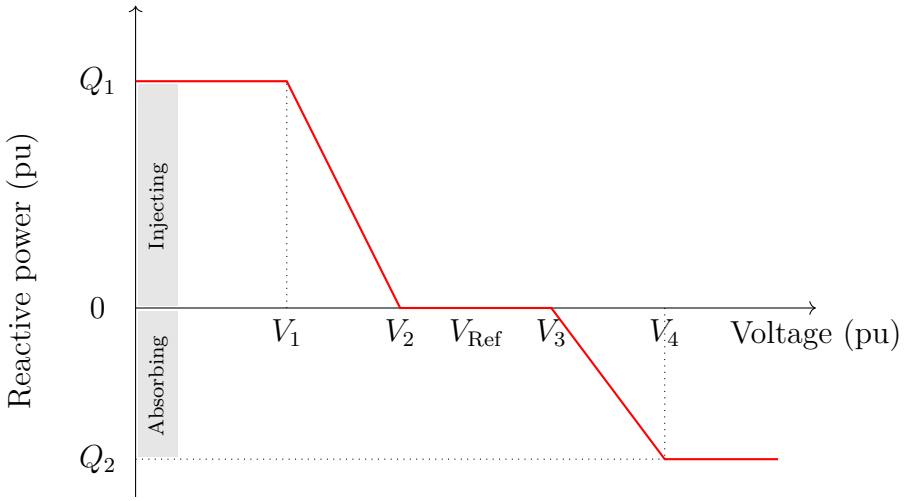

Figure 5.1 Example of the volt-var curve as specified by IEEE 1547 standard

It is remarked that the inverter has a nominal rating S_{nom} in kVA, and in any case, the apparent power of the DER should not exceed this rating, i.e., $\sqrt{P_{\text{der}}^2 + Q_{\text{der}}^2} \le S_{\text{nom}}$, where P_{der} is the active power which may be fixed generation or follow a volt-watt control. If S_{nom}

is exceeded, either P_{der} or Q_{der} needs to be reduced depending on the precedence mode of watt/var. Once P_{der} and Q_{der} are determined, we can model a DER as a PQ device with constant impedance in MANA. We also add PQ constraints in $\mathbf{f}(\mathbf{x}^{(k)})$ and corresponding terms in $\mathbf{J}^{(\mathbf{k})}$. The process to derive specific terms in $\mathbf{J}^{(\mathbf{k})}$ related to the PQ constraints follows the same as that in [131].

5.3 Optimization problem for VVO

We now formulate the VVO problem by first introducing the control variables.

5.3.1 Decision variables

Suppose that the network contains N_{cb} capacitor banks, N_{vr} voltage regulators, N_{xfo} transformers with OLTC, and N_{der} DERs. The following control variables are available for voltage-regulating devices described in Section 5.2.2:

- Each capacitor bank has an On/Off state $\gamma_{\text{cb}} \in \{0, 1\}$, hence we have $\mathbf{\Gamma}_{\text{cb}} = [\gamma_{\text{cb}_i}, i = 1, \cdots, N_{\text{cb}}]^\top$ for all capacitor banks.
- Desired voltage levels for all voltage regulators $\mathbf{V}_{\text{D,vr}} = [V_{\text{D,vr}_i}, i = 1, \cdots, N_{\text{vr}}]^\top$ where $V_{\text{D,vr}} \in [\underline{V}_{\text{D,vr}}, \overline{V}_{\text{D,vr}}]$, and $\underline{V}_{\text{D,vr}}$ and $\overline{V}_{\text{D,vr}}$ are the lower and upper bounds of admissible voltage levels, respectively. For simplicity we assume that the same $V_{\text{D,vr}_i}$ value is set to all connected phases of a regulator, but it is possible to use different values by phase which increases the dimension of $\mathbf{V}_{\text{D,vr}}$ accordingly.
- Desired voltage levels for transformers with OLTCs $\mathbf{V}_{\text{D,xfo}} = [V_{\text{D,xfo}_i}, i = 1, \cdots, N_{\text{xfo}}]^\top$, where $V_{\text{D,xfo}} \in [\underline{V}_{\text{D,xfo}}, \overline{V}_{\text{D,xfo}}]$ is applied to all phases, and $\underline{V}_{\text{D,xfo}}$ and $\overline{V}_{\text{D,xfo}}$ are the lower and upper bounds of admissible voltage levels, respectively. It is also possible to have desired values by phase.
- Each DER needs to have a volt-var curve C_{der} specified. Hence a set of curves $\mathbf{C}_{\text{der}} = [C_{\text{der}_i}, i = 1, \cdots, N_{\text{der}}]^\top$ needs to be determined. Recall that each C_{der_i} consists of seven variables to be specified. For the allowable range of each variable, refer to the IEEE-1547 standard [127]. In practice, multiple DERs can use an identical curve hence $\mathbf{C}_{\text{der}}$ does not necessarily contain N_{der} elements in this case.

We denote all control variables on the network by $\mathbf{X} = [\mathbf{\Gamma}_{\text{c}}^\top, \mathbf{V}_{\text{D,vr}}^\top, \mathbf{V}_{\text{D,xfo}}^\top, \mathbf{C}_{\text{der}}^\top]^\top$, and their constraints collectively by $g(\mathbf{X}) \leq 0$.

5.3.2 Stochastic program

In VVO, several objectives can be considered such as minimizing network losses, maintaining system voltage levels, correcting power factors, etc. To account for the uncertainty in demand and generation profiles over a period of time $\mathcal{T} = [0, \Delta t, 2\Delta t, \cdots, (T-1)\Delta t]$ with T time steps, let $\mathbf{D} = \{\mathbf{d}_i^{\mathcal{T}}, i = 1, \cdots, N_{\mathrm{m}}\} \in \mathbb{C}^{N_{\mathrm{m}} \times T}$ be demand profiles of the N_{m} loads and $\mathbf{G} = \{\mathbf{g}_i^{\mathcal{T}}, i = 1, \cdots, N_{\mathrm{der}}\} \in \mathbb{C}^{N_{\mathrm{der}} \times T}$ be generation profiles of the N_{der} DERs on the network. Each load's demand and DER's generation at time t are random on sample spaces $\mathcal{D}$ and $\mathcal{G}$ with arbitrary probability distributions, respectively.

It is desired that the optimal settings for the control variables on the network should be maintained over $\mathcal{T}$ for random $\mathbf{D}, \mathbf{G}$. This makes it easy for utilities and network operators to adopt the strategy without constantly changing the settings under various network loading and generation conditions during $\mathcal{T}$. Hence, we formulate the VVO problem as a stochastic program to minimize the expected total energy losses E_{loss} (in kWh) on the network during $\mathcal{T}$:

$$\begin{aligned} \min_{\mathbf{X}} \quad & \mathbb{E}_{\mathbf{D},\mathbf{G}}[E_{\mathrm{loss}}] \\ \text{subject to} \quad & g(\mathbf{X}) \leq 0 \\ & \mathbf{V}, \mathbf{I} = \text{MANA-NR}(\mathcal{N}, \mathbf{X}, \mathbf{D}, \mathbf{G}), \\ & \underline{v} \leq \frac{|v_n|}{v_n^{\mathrm{base}}} \leq \overline{v}, \ \forall v_n \in \mathbf{V}. \end{aligned} \tag{5.9}$$

Recall that MANA-NR is the MANA-formulated power flow using Newton-Raphson. For N_{b} by-phase nodes on the network, $\mathbf{V}, \mathbf{I} \in \mathbb{C}^{N_{\mathrm{b}} \times T}$ are nodal voltages and currents for all $t \in \mathcal{T}$, respectively, $\underline{v}, \overline{v}$ are the per-unit lower and upper limits of voltage levels, respectively, e.g., $\underline{v} = 0.95$ p.u., and $\overline{v} = 1.05$ p.u., $|v_n|$ is the voltage magnitude of node n, and v_n^{base} is the base voltage of node n. We solve (5.9) using a scenario-based approach. Suppose that we construct a set of scenarios $\mathcal{S}$ where demand and generation in each scenario $s \in \mathcal{S}$ are denoted by $\mathbf{D}^s$ and $\mathbf{G}^s$, respectively. Then, the expected total energy losses is approximated by:

$$\mathbb{E}_{\mathbf{D},\mathbf{G}}[E_{\mathrm{loss}}] \approx \frac{1}{|\mathcal{S}|} \sum_{s \in \mathcal{S}} E_{\mathrm{loss}}^s, \tag{5.10}$$

where $|\mathcal{S}|$ is the cardinality of $\mathcal{S}$, and E_{loss}^s is computed by the following equation for given $\mathbf{D}^s$ and $\mathbf{G}^s$.

$$E_{\mathrm{loss}}^s = \Delta t \sum_{t \in \mathcal{T}} P_{\mathrm{loss}}^t(\mathbf{D}^s, \mathbf{G}^s), \tag{5.11}$$

and P^t_{loss} at time t is computed by:

$$P^t_{\text{loss}} = \sum_{l_{mn} \in \mathcal{B}} (P^t_m - P^t_n),$$

where the active loss on the branch l_{mn} is the difference of P^t_m denoting the active power flowing out of m on l_{mn} and P^t_n which is the active power flowing into n on l_{mn} at t. Both P^t_m and P^t_n can be computed from the nodal voltages and currents obtained from the power flow solution as outlined in Section 5.2.1 for given $\mathbf{D}^s$ and $\mathbf{G}^s$ at time t. The scenario-based stochastic optimization problem is therefore:

$$\begin{aligned} \min_{\mathbf{X}} \quad & \frac{1}{|\mathcal{S}|} \sum_{s \in \mathcal{S}} E^s_{\text{loss}} \\ \text{subject to} \quad & g(\mathbf{X}) \leq 0 \\ & \mathbf{V}^s, \mathbf{I}^s = \text{MANA-NR}(\mathcal{N}, \mathbf{X}, \mathbf{D}^s, \mathbf{G}^s), \ \forall s \\ & \underline{v} \leq \frac{|v_n|}{v^{\text{base}}_n} \leq \overline{v}, \ \forall v_n \in \mathbf{V}^s, \ \forall s \\ & (5.11) \ \forall s, \end{aligned} \tag{5.12}$$

where $\mathbf{V}^s, \mathbf{I}^s \in \mathbb{C}^{N_\text{b} \times T}$ contain the scenario-dependent nodal voltages and currents for all $t \in \mathcal{T}$, respectively. A voltage magnitude constraint applies to each element v_n in $\mathbf{V}^s$ such that the magnitudes of all nodal voltages should be maintained within the range $[\underline{v}, \overline{v}]$. The constraint should hold for each $s \in \mathcal{S}$. Generally, (5.12) is nonlinear and nonconvex due to MANA-NR. It is thus an NP-hard problem which is difficult to solve [93]. While it is possible to linearize (5.12) or to relax it to a convex problem to solve it efficiently as done in the literature, we lose the advantage of MANA-NR and the power flow solution may be inaccurate or infeasible. Consequently, control setpoints obtained from the optimization may not be effective and can fail to address the objective of VVO.

5.3.3 Blackbox approach

Although we have the detailed mathematical formulation of MANA-NR from Section 5.2, it is not always guaranteed that a feasible solution to (5.12) satisfying the voltage magnitude constraint could be found with MANA-NR itself being an iterative process. To simplify the solution process, we try to decouple MANA-NR from the optimization problem where the power flow to $\mathcal{N}$ can be performed assuming that $\mathbf{X}$ is given. Using this concept, we move the MANA-NR out of (5.12) and treat it as a blackbox function with $\mathbf{X}$ as input and $\mathbf{V}^s, \mathbf{I}^s$ as output for each scenario $s \in \mathcal{S}$. We then attempt to solve the problem using

blackbox optimization technique such as the Mesh Adaptive Direct Search (MADS) method implemented in the NOMAD solver [135] to search for an optimal (or near-optimal) local solution of $\mathbf{X}$, through blackbox evaluations in a centralized manner. Once the solution is implemented on the network, the volt-var control is done in a decentralized way, e.g., the amount of reactive power injected or absorbed depends on the local voltage level measured at the DER and its volt-var curve settings.

We remark that the voltage magnitude constraint in (5.12) is hard, i.e., any solution must satisfy this constraint, otherwise the solution is rejected. This not only increases the computational efforts for a feasible solution, but can also lead to the case where no feasible solution is returned. To deal with this, we consider the voltage magnitude constraint as relaxable, i.e., it is not necessarily satisfied during the blackbox evaluation of a possible solution. We then include it in the objective function f_{obj} such that any violation will incur a significant penalty to f_{obj}, i.e.,

$$f_{\text{obj}} = \mathbb{E}_{\mathbf{D},\mathbf{G}}[E_{\text{loss}}] + \rho \mathbb{E}_{\mathbf{D},\mathbf{G}}[T_{\text{uv,ov}}] \tag{5.13}$$

$$\mathbb{E}_{\mathbf{D},\mathbf{G}}[T_{\text{uv,ov}}] \approx \frac{1}{|\mathcal{S}|} \sum_{s \in \mathcal{S}} \sum_{v_n \in \mathbf{V}^s} \mathbb{1}_{\text{uv,ov}}(v_n), \tag{5.14}$$

where $\rho > 0$ is a large number as the penalty weight and $\mathbb{1}_{\text{uv,ov}}$ is an indicator function for under and over-voltage conditions, i.e., $\mathbb{1}_{\text{uv,ov}}(v_n) = 1$ if $\frac{|v_n|}{v_n^{\text{base}}} \notin [\underline{v}, \overline{v}]$. This allows NOMAD to quickly generate a mesh of variables in the search space which does not lead to abnormal voltage conditions. In addition, if a solution leads to non-converging power flows on the network, the solution is infeasible and the corresponding search space is avoided in the following evaluations.

The process is depicted in Figure 5.2 subject to a computation budget which is the maximum number of blackbox evaluations N_j. The objective is thus to find a solution by BBO which does not lead to any violation of the voltage magnitude constraint, i.e., where the second term in (5.13) vanishes. If such a solution is found, then it is also feasible for (5.12). In the case where we are unable to find a feasible solution, i.e., some violation of voltage levels still exists, the formulation aims to find a policy that minimizes the severity of the violation subject to a high penalty of ρ. Comparing to RL approaches in the literature [86–89], we enhance the trustworthiness where the solution space leading to abnormal voltage levels and/or non-converging power flows on the network is avoided. Finally, the first-order convergence to local optimality of NOMAD has been proven under mild assumptions [136]. Further, we also use the Variable Neighbourhood Search (VNS) technique [137] to try to approach the globally optimal solution within the evaluation budget N_j. Although we do not perform a convergence

analysis in this work, we demonstrate that our approach has a faster (local) convergence rate in the numerical studies in the next section.

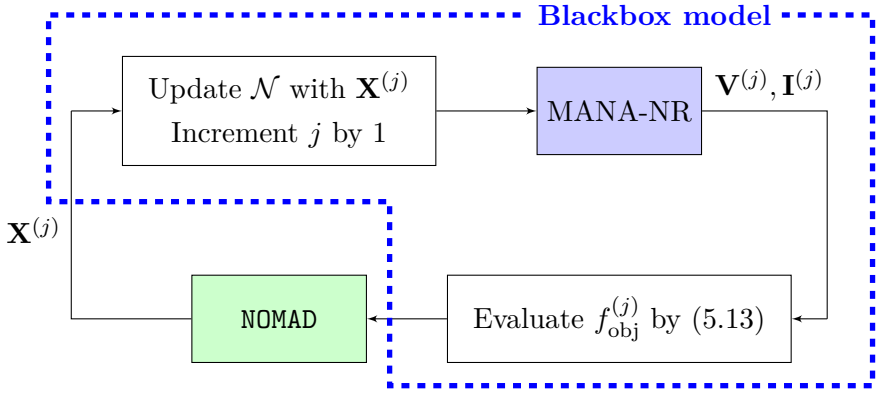

Figure 5.2 Illustration of the proposed blackbox optimization approach

5.4 Numerical examples

In the following case studies, we use the IEEE-123 and the IEEE-8500 test feeders and add some DERs to them to demonstrate the effectiveness and the scalability of our proposed approach. In each scenario, each load is attached with a daily demand where the active power is obtained through multiplying the kW data of the load in the original test feeder by a consumption profile in percentage from the Pecan Street Dataport [111]. The power factor of the load in the original test feeder is retained such that reactive power can be calculated based on the active power profile attached to each load. DERs are assumed to be PVs in our studies, and there are two types: utility-owned and user-owned PVs. Nominal capacities for utility-owned PVs are assumed given and detailed in each case, and we randomly choose a nominal capacity in the range of $[5, 10]$ kVA for each user-owned PV. We randomize the daily solar radiance profiles under different weather types [107] to generate daily generation profiles for each PV. In all cases, we consider 30 days' profiles hence 30 scenarios, and profiles of selected loads and PV generation for one week (168 hours), i.e., 7 scenarios, are illustrated in Figure 5.3. To perform the MANA-NR power flow, we use the CYME Distribution Analysis software (CYMDIST) [138] as the blackbox simulator. To benchmark results of our proposed approach, we compare with a reinforcement learning-based approach (RL) utilizing multi-agent deep Q-network (DQN) [86] for VVO on the IEEE-123 network. We remark that we use the specified parameters as set out in [86] without any tuning.

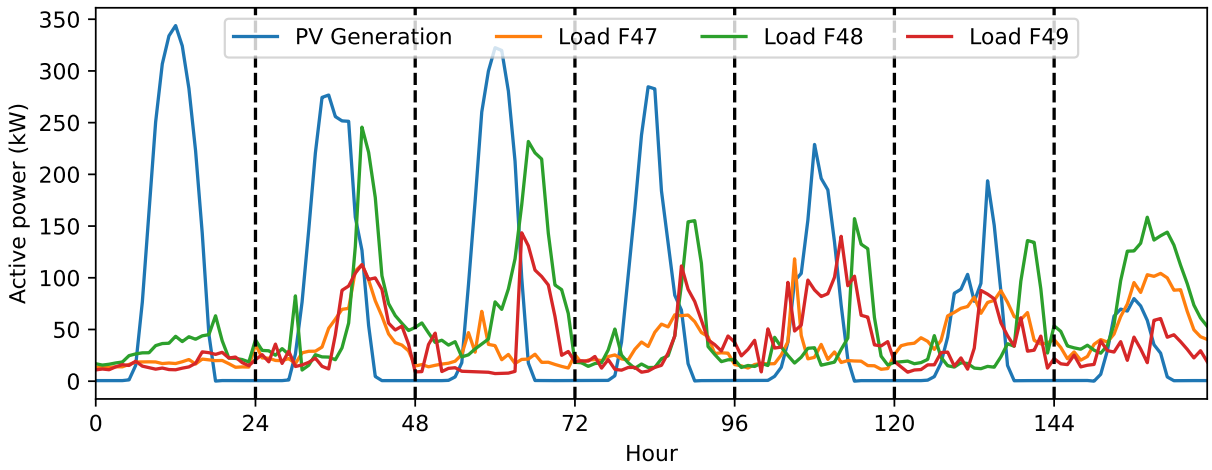

Figure 5.3 Active power profiles of one week for 3 loads and 1 PV (7 scenarios)

5.4.1 Utility-owned PVs on IEEE-123 test feeder

In the first case, we add three utility-owned PVs on the IEEE-123 test feeder. Their locations and nominal capacities are shown in Table 5.1. There are also four capacitor banks and four voltage regulators whose locations are shown in Figure 5.4, and their controls are included in the VVO strategy. Although we have no limitation to setting different desired voltages on voltage regulator's phases, for simplicity, it is assumed that the same desired voltage (on a 120 V base) is used on all connected phases, hence we have a total of 8 control variables for capacitor banks and voltage regulators.

Table 5.1 Utility-owned PVs on IEEE-123 test feeder

ID	Node	Capacity (kVA)
PV1	35	345
PV2	52	345
PV3	97	690

5.4.1.1 Single volt-var curve for all PVs

We first consider the case where the same volt-var curve is adopted for all PVs, hence we have a total of 15 control variables in VVO. We perform $N_j = 600$ blackbox evaluations and present the optimal settings for capacitor banks and voltage regulators in Table 5.2 along with those in the baseline case before VVO and the benchmark RL approach. We also compare the expected energy losses $\mathbb{E}[E_{\text{loss}}]$ and the expected abnormal voltage duration $\mathbb{E}[T_{\text{uv,ov}}]$,

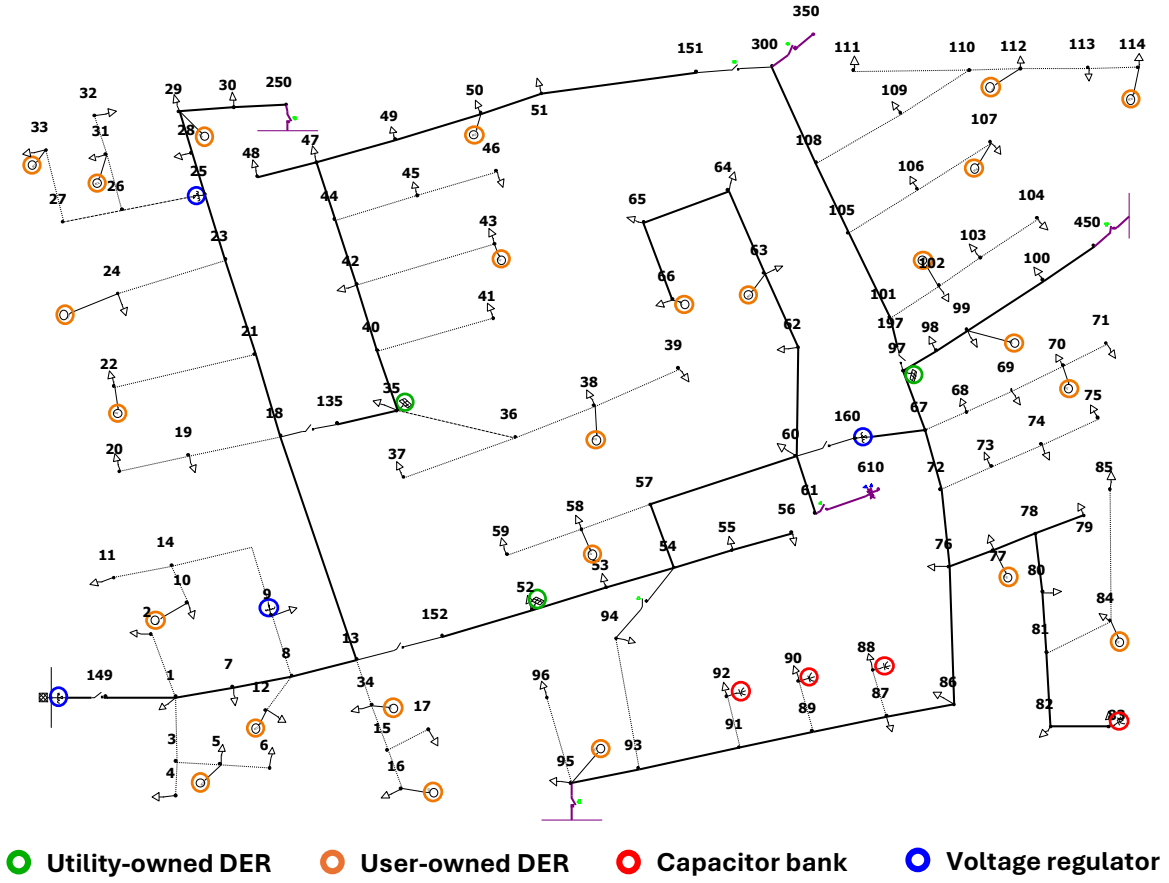

Figure 5.4 One-line diagram of the modified IEEE-123 test feeder

which are computed by (5.10) and (5.14), respectively. We remark that for simplicity of notations, the subscript of $\mathbf{D}, \mathbf{G}$ is dropped in the expected values in the numerical examples hereinafter. It is observed that the expected daily losses are reduced from 263.36 kWh to 150.59 kWh (42.8% reduction) while the best from the RL approach (after 1,000 training episodes) gives 165.43 kWh (37.2% reduction). In both approaches, we are able to remove the abnormal voltage conditions in all scenarios. On the left side of Figure 5.5, settings for the volt-var curve applied to all PVs are shown. The cumulative average values of the objective function are compared on the right side of Figure 5.5 as the number of blackbox evaluations or training samples in RL increases. We observe that our proposed approach quickly finds a feasible region of solutions in less than 100 evaluations, while most solutions in the RL approach suffer violations of voltage constraints in the beginning and it takes much more training iterations before a Q-function is properly learned.

We test the performance of the obtained optimal VVO settings by evaluating the daily

Table 5.2 Optimal settings for capacitor banks and regulators after VVO on IEEE-123 test feeder (single volt-var curve for PVs)

	Location	Base	BBO	RL
Capacitor bank (Connection state)	90	On	Off	Off
	92	On	Off	On
	88	On	On	On
	83	On	Off	Off
Regulator (Desired voltage, V)	160-67	124	119.3	116.9
	9-14	120	116.9	117.5
	150-149	120	122.1	124.1
	25-26	120	116.1	121.1
$\mathbb{E}[E_{\text{loss}}]$ (kWh)		263.36	150.59	165.43
$\mathbb{E}[T_{\text{uv,ov}}]$ (hour)		12.3	0	0

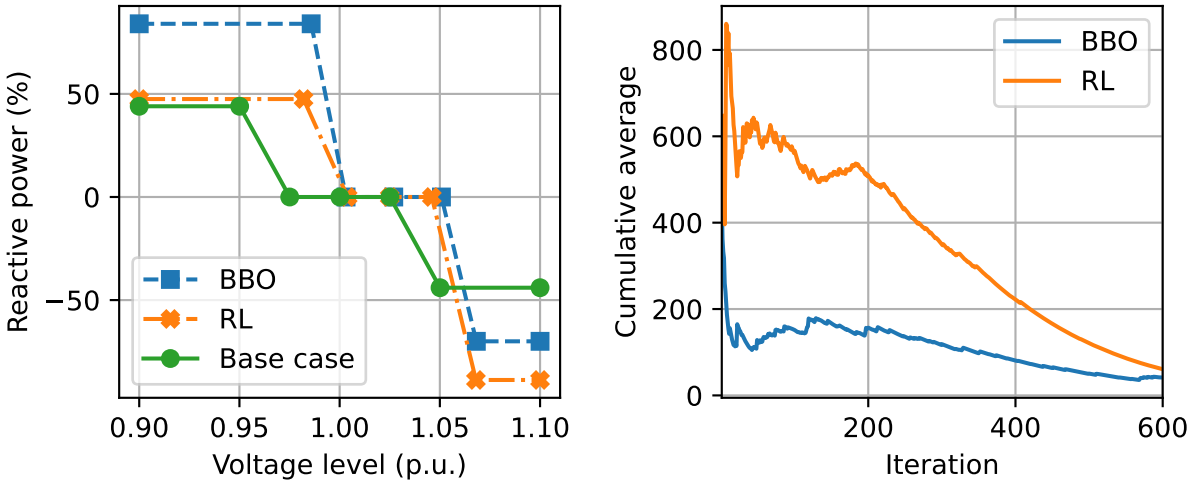

Figure 5.5 Comparison of volt-var curves (**right**) and cumulative averages of f_{obj} values (**left**) using the proposed blackbox approach vs. the RL approach

energy losses for another 30 days' profiles (out-of-sample) which are not used in any blackbox evaluation. The minimum, maximum, and average losses are compared and summarized in Table 5.3. In Figure 5.6, daily energy losses for 15 selected days are illustrated, where the load and generation profiles of the first 7 days are included in the scenarios (in-sample) for BBO and RL training while those of the latter 8 days are not (out-of-sample). We notice that both approaches can greatly reduce the losses observed in the base case, and losses using the BBO strategy are less than those using the RL solution in all days. Although not shown in the table or the figure, neither of the VVO solutions cause abnormal voltages on the network in all these scenarios.

Table 5.3 Comparison of performance on 30 out-of-sample scenarios (single volt-var curve for PVs)

		Base	BBO	RL
E_{loss} (kWh)	Minimum	165.35	61.56	70.74
	Maximum	298.88	166.32	176.77
	Average	245.14	112.51	124.09

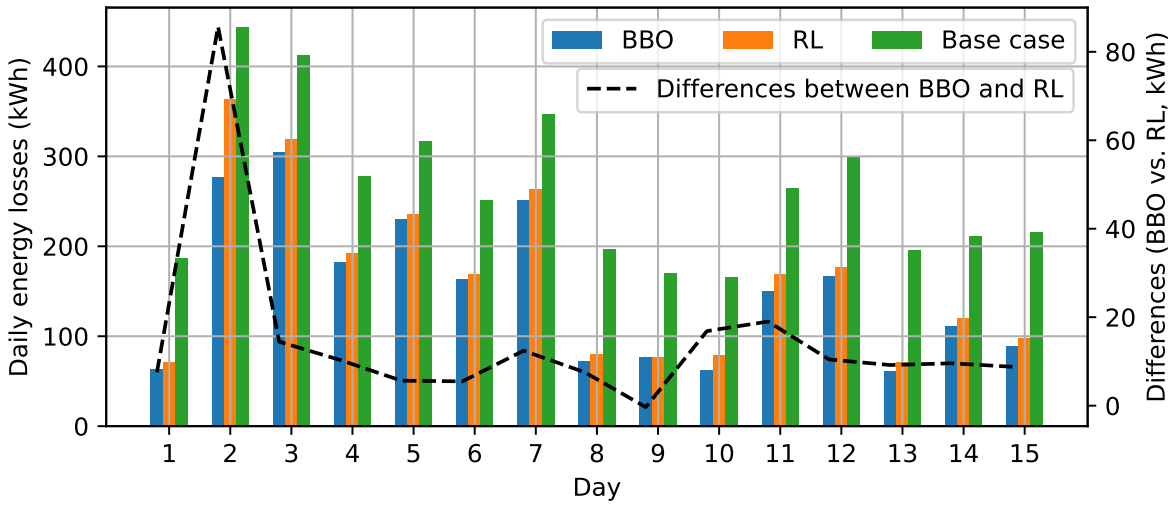

Figure 5.6 Comparison of daily energy losses for 15 days using VVO settings from the proposed BBO approach vs. the RL approach (single volt-var curve)

5.4.1.2 Individual volt-var curve for all PVs

Given that the utility owns the PVs, it is not difficult for them to customize the volt-var curve for each PV to better adapt to network conditions. In this case, we optimize the volt-var curve settings for each PV individually as well as those for capacitor banks and regulators. The number of control variables to optimize increases to 25 accordingly, hence $N_j = 1{,}500$ blackbox evaluations and 4,000 RL training episodes are executed. In Table 5.4, optimal settings for capacitors and regulators are listed and volt-var curve settings for each PV are shown in Figure 5.7. The expected daily energy losses are reduced to 146.93 kWh (44.2% reduction) and 151.53 kWh (42.5% reduction) for the BBO and RL approaches during training, respectively, which are both improved from the results in the same volt-var curve case in Section 5.4.1.1.

Table 5.5 shows the performance of the obtained optimal settings using the same set of out-of-sample scenarios as in the previous case. The daily energy losses 7 in-sample and 8 out-of-sample scenarios are presented in Figure 5.8, where the BBO approach outperforms

Table 5.4 Optimal settings for capacitor banks and regulators after VVO on IEEE-123 network (individual volt-var curve for PVs)

	Location	**Base**	**BBO**	**RL**
Capacitor bank (Connection state)	90	On	Off	Off
	92	On	Off	Off
	88	On	Off	Off
	83	On	Off	Off
Regulator (Desired voltage, V)	160-67	124	120.4	119.3
	9-14	120	118.5	121.1
	150-149	120	124.1	124.7
	25-26	120	118.1	121.1
$\mathbb{E}[E_{\text{loss}}]$ (kWh)		263.36	146.93	151.53
$\mathbb{E}[T_{\text{uv,ov}}]$ (hour)		12.3	0	0

the RL approach in 13 out of the 15 scenarios and incurs only slightly more losses in 2 days.

Table 5.5 Comparison of performance on 30 out-of-samples scenarios (individual volt-var curve for PVs)

		Base	**BBO**	**RL**
E_{loss} (kWh)	Minimum	165.35	55.09	55.98
	Maximum	298.88	149.15	155.09
	Average	245.14	104.04	108.98

5.4.2 Utility-owned and user-owned PVs on IEEE-123 feeder

In the last case on the IEEE-123 test feeder, we add single-phase PVs to 25 loads, which is equivalent to a 30% penetration level, and their locations are identified in Figure 5.4. Given that these PVs are customer-owned, utilities cannot customize the volt-var settings individually; however, it is still possible to optimize a "factory default" curve and apply it to all PVs before installation. Hence in this case, each utility-owned PV still has its own curve and all user-owned PVs are assigned with the same curve, which comes to a total of 30 variables to optimize. After running N_j = 2,000 blackbox evaluations and 6,000 training episodes for RL, we list regulators and capacitor banks' settings using the BBO and RL approaches in Table 5.6, as well as the comparison of expected losses and expected duration of abnormal voltages.

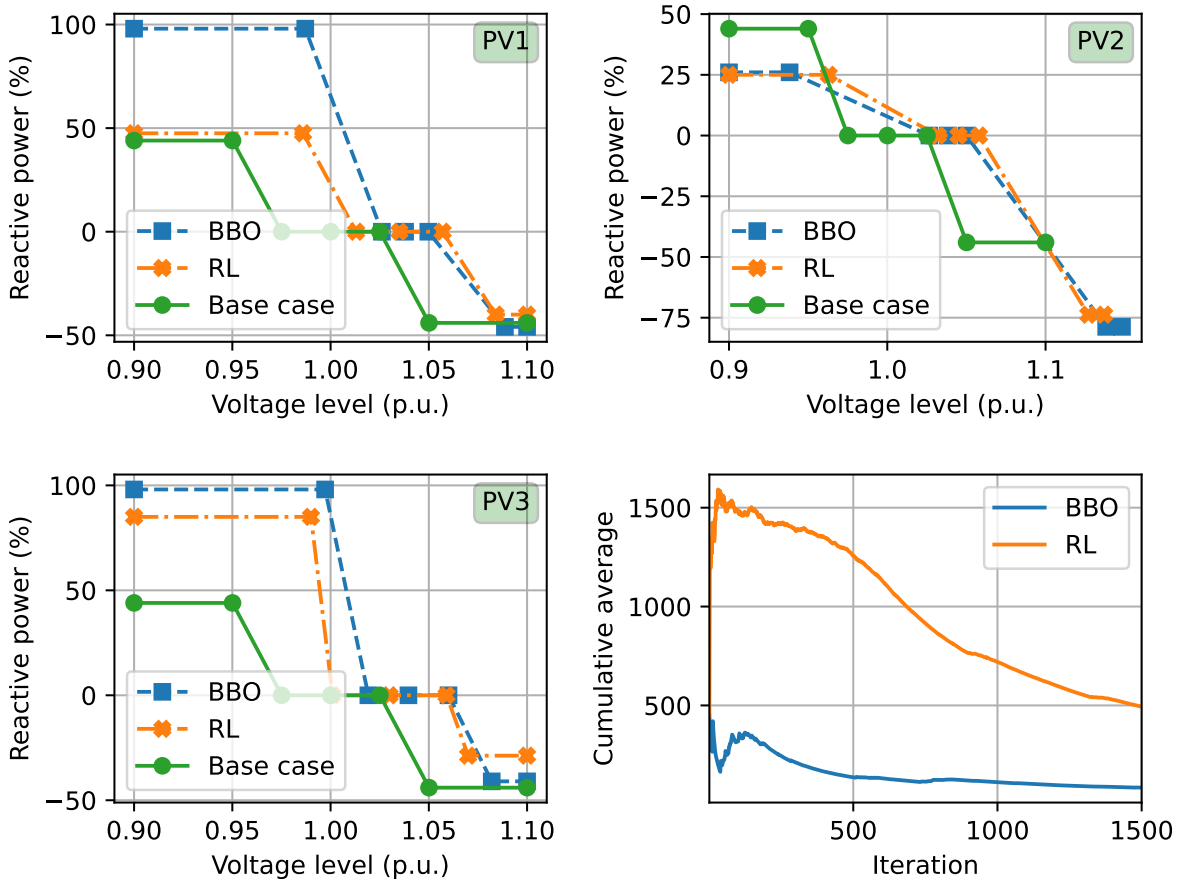

Figure 5.7 Comparison of individual volt-var curve for each PV and cumulative averages of f_{obj} values using the proposed BBO approach vs. the RL approach

Table 5.6 Optimal settings for capacitor banks and regulators after VVO on IEEE-123 network (utility-owned and user-owned PVs)

	Location	**Base**	**BBO**	**RL**
Capacitor bank (Connection state)	90	On	On	Off
	92	On	On	On
	88	On	On	On
	83	On	Off	Off
Regulator (Desired voltage, V)	160-67	124	118.1	116.6
	9-14	120	116.9	121.2
	150-149	120	122.9	122.8
	25-26	120	116.3	120.5
$\mathbb{E}[E_{\text{loss}}]$ (kWh)		257.84	154.31	156.27
$\mathbb{E}[T_{\text{uv,ov}}]$ (hour)		7.6	0	0

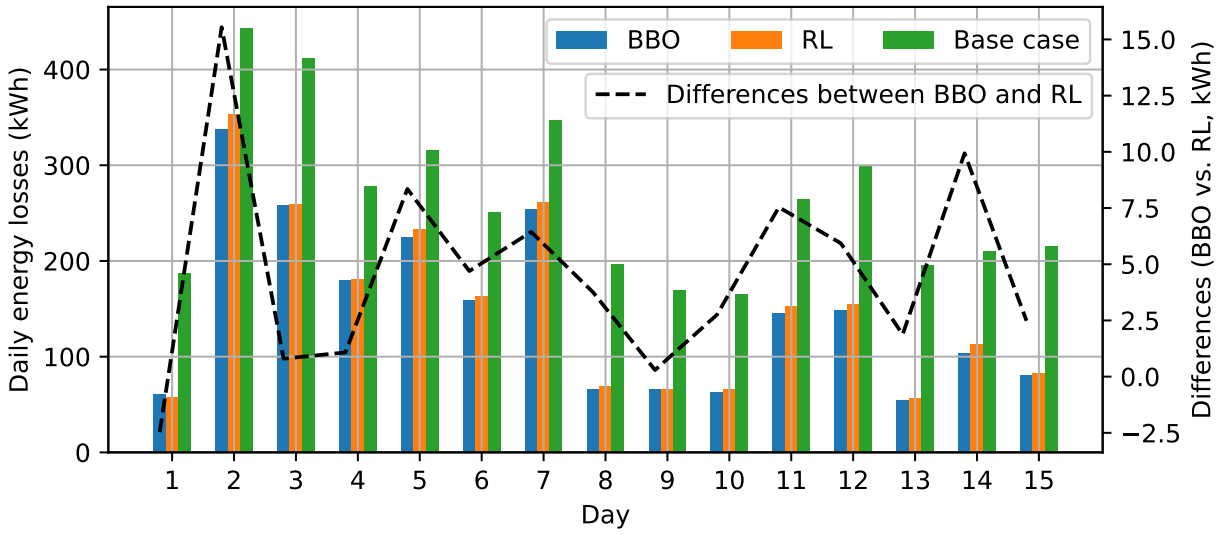

Figure 5.8 Comparison of daily losses for 15 days using VVO settings from the proposed BBO approach vs. the RL approach (individual volt-var curve)

The resulting volt-var curve settings for the 3 utility-owned PVs and the single curve for all customer-owned PVs are shown in Figure 5.9. The expected energy losses are reduced to 154.31 kWh (40.15% reduction) by the BBO approach and to 156.27 kWh (39.39% reduction) by the RL approach during training. In all scenarios after VVO, we do not observe any violation of voltage constraints, i.e., $\mathbb{E}[T_{\text{uv,ov}}] = 0$.

The performance when applying the optimal settings to out-of-sample scenarios is illustrated in Table 5.7 and Figure 5.10. Among the 15 scenarios in Figure 5.10, losses using the RL approach are slightly lower in 4 scenarios, but the blackbox approach outperforms in all other scenarios and has better performance when looking at $\mathbb{E}[E_{\text{loss}}]$.

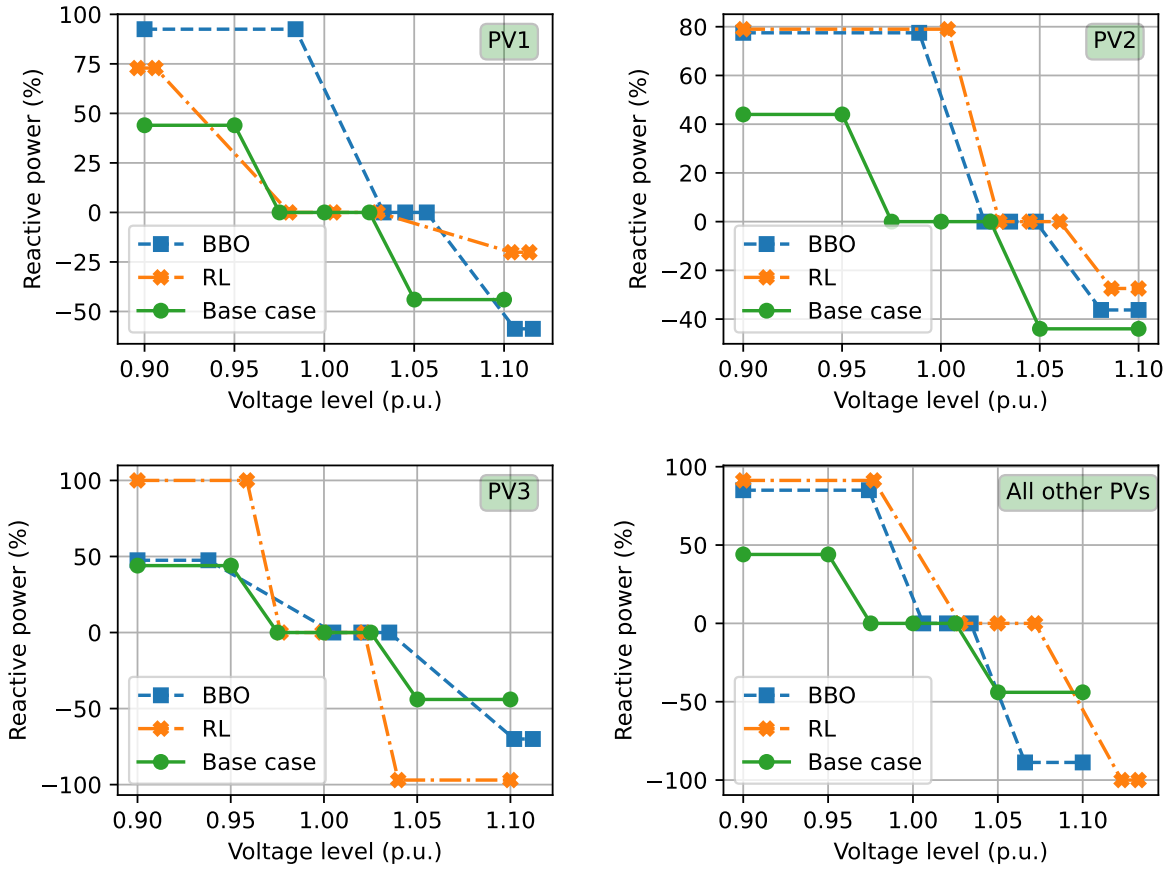

Figure 5.9 Comparison of volt-var curves for utility-owned and customer-owned PVs using the proposed BBO approach vs. the RL approach

Table 5.7 Comparison of performance on 30 out-of-samples scenarios (utility-owned and user-owned PVs)

		Base	**BBO**	**RL**
E_{loss} (kWh)	Minimum	157.46	62.24	58.75
	Maximum	299.12	180.49	191.84
	Average	239.68	115.78	119.92

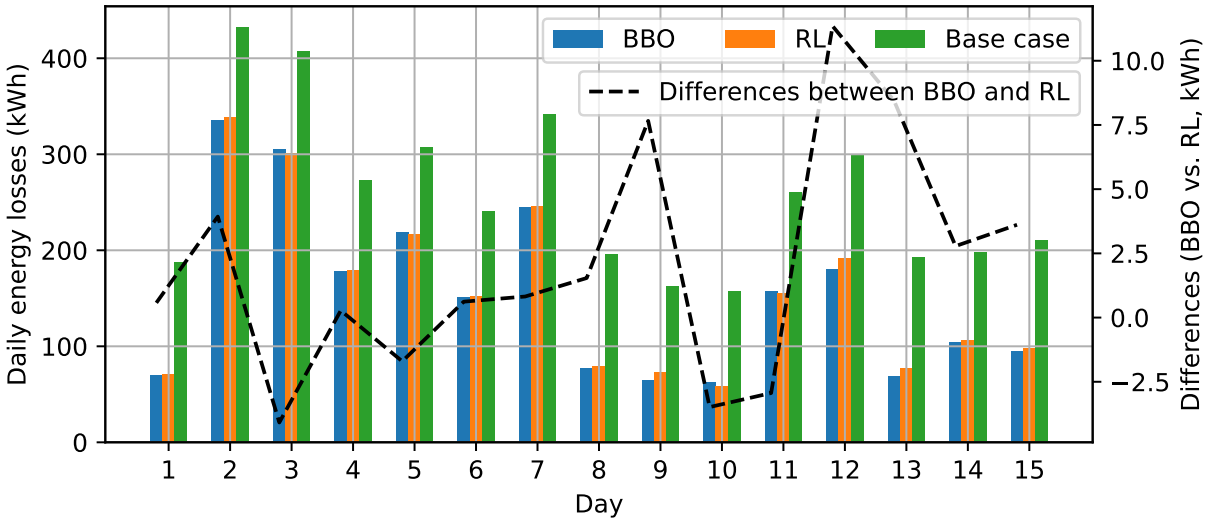

Figure 5.10 Comparison of daily losses for 15 days using VVO settings from the proposed BBO vs. the RL approach (utility-owned and user-owned PVs)

5.4.3 Utility-owned and user-owned PVs on IEEE-8500 feeder

In this study case, we aim to demonstrate the scalability of our proposed BBO approach by testing it on the modified IEEE-8500 feeder. A large-scale PV farm with a 1.5 MVA rating is added to Section LN5562932-1 which is assumed to be owned and operated by the utility. A total of 178 user-owned single-phase PVs (representing 15% penetration rate) with capacity in the range of $[5, 10]$ kVA are randomly added to the network. Locations of the utility-owned and user-owned PVs as well as conventional devices for VVO (4 capacitor banks and 4 voltage regulators) on the network are shown in Figure 5.11. The sizes of nominal capacities of user-owned PVs are indicated by the colour depths.

It is remarked that in this case study we do not run the RL approach as benchmark for two reasons: (1) based on the results of the IEEE-123 network, RL would require a large number of training episodes and the training will take much longer time on a large network; and (2) the main purpose is to demonstrate the scalability of our approach for an effective VVO strategy on a large-scale network, rather than comparing the performance with other approaches.

After executing $N_j = 2000$ blackbox evaluations, the optimal settings for the 4 capacitor banks and 4 voltage regulators on the network are listed in Table 5.8. Meanwhile, we optimize two sets of volt-var curves: one for the PV farm and the other one for all customer-owned PVs, and the curves are shown in Figure 5.12. We observe that the expected energy losses

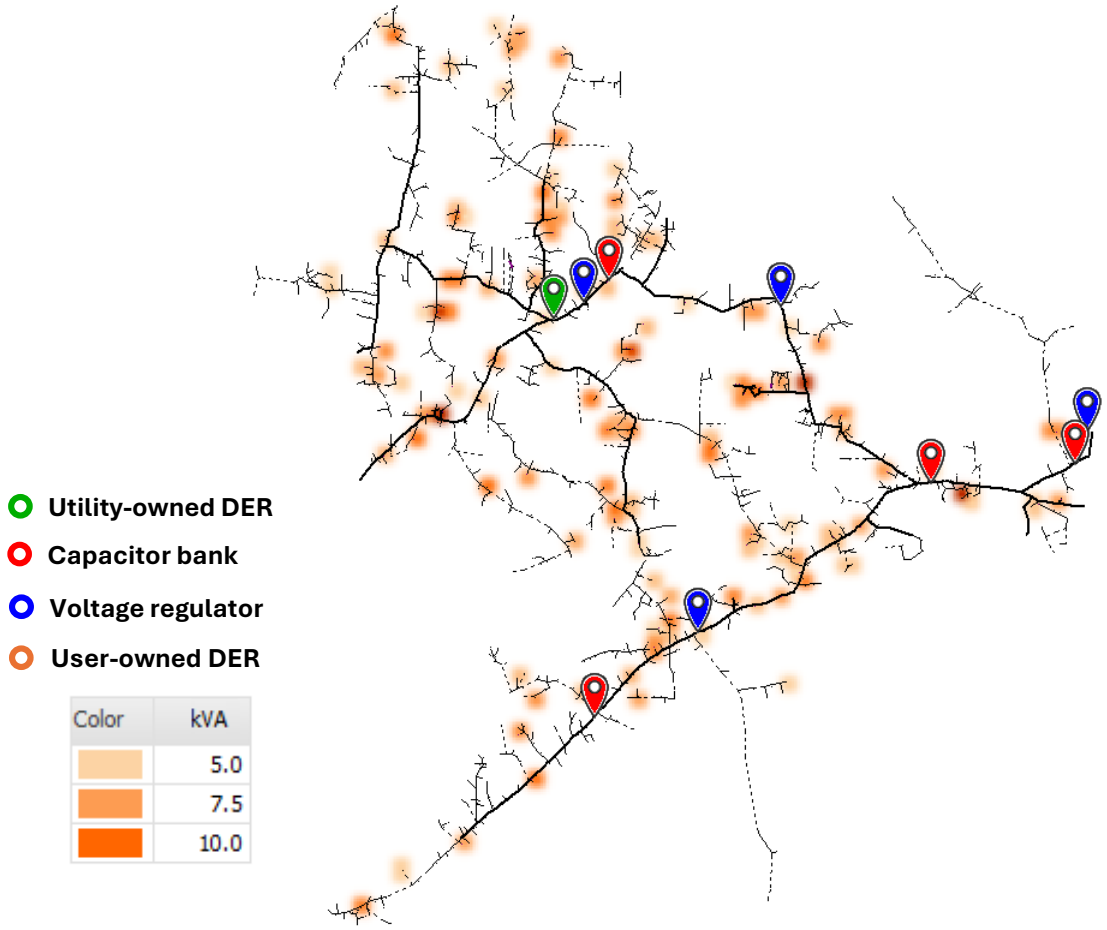

Figure 5.11 One-line diagram of the modified IEEE-8500 test feeder with utility-owned and user-owned PVs added

are reduced from 4774.74 kWh to 4555.46 kWh (4.6% reduction). Given the size the network and limited number of voltage regulating devices, these settings do not completely remove the abnormal voltage conditions on the network; however, we are still able to significantly reduce the severity in terms of the number of affected nodes and the expected duration of under or over-voltage, i.e., from 12,864 hours for 1,195 nodes down to 202.3 hours for 228 nodes (98.4% reduction).

Table 5.8 Optimal settings for capacitor banks and regulators after VVO on IEEE-8500 network

	Location	Base	BBO
Capacitor bank (Connection state)	CAPBANK0	On	On
	CAPBANK1	On	On
	CAPBANK2	On	Off
	CAPBANK3	On	On
Regulator (Desired voltage, V)	FEEDER_REG	125.85	123.43
	VREG_2	125.78	124.04
	VREG_3	124.53	122.03
	VREG_4	124.50	124.38
$\mathbb{E}[E_{\text{loss}}]$ (kWh)		4774.74	4555.46
$\mathbb{E}[T_{\text{uv,ov}}]$ (hour)		12864.0[1]	202.3[2]

[1] Expected duration for a total of 1195 nodes which have experienced abnormal voltage conditions in 30 scenarios.

[2] The number of nodes with abnormal voltage conditions is reduced to 228 in 30 scenarios.

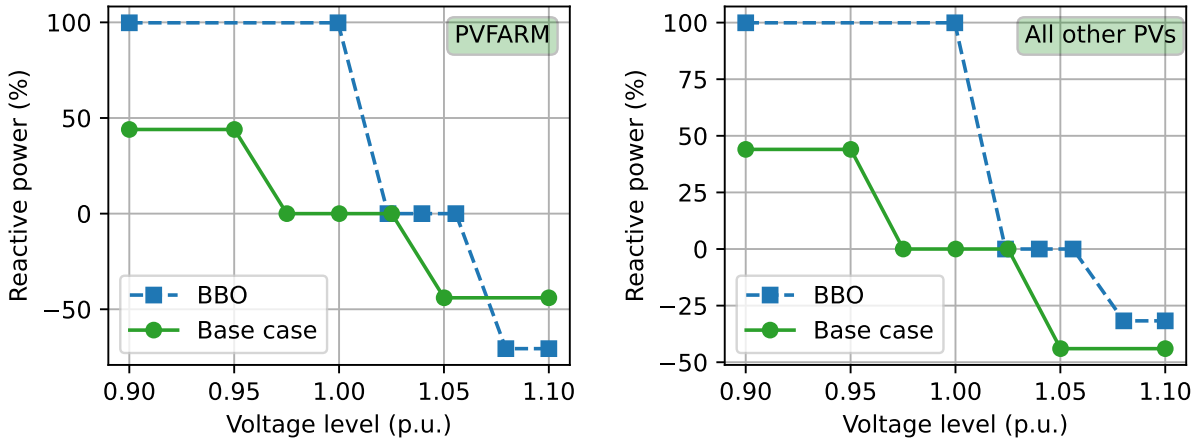

Figure 5.12 Comparison of volt-var curves for utility-owned and customer-owned PVs for IEEE-8500 network

Finally, we evaluate the performance of the obtained settings on 30 out-of-sample scenarios by showing the minimum, maximum and average values of losses and total duration of abnormal

voltage conditions in Table 5.9. We also show the losses and duration of abnormal voltages for 15 scenarios in Figures 5.13 and 5.14, where the first 7 are in-sample and the latter 8 are out-of-sample scenarios.

Table 5.9 Comparison of performance on 30 out-of-samples scenarios on IEEE-8500 network

		Base	**BBO**
E_{loss} (kWh)	Minimum	3274.4	2944.7
	Maximum	6172.7	5923.2
	Average	4722.2	4399.8
$T_{\text{uv,ov}}$ (hour)	Minimum	19375	142
	Maximum	27747	668
	Average	23226.3	374

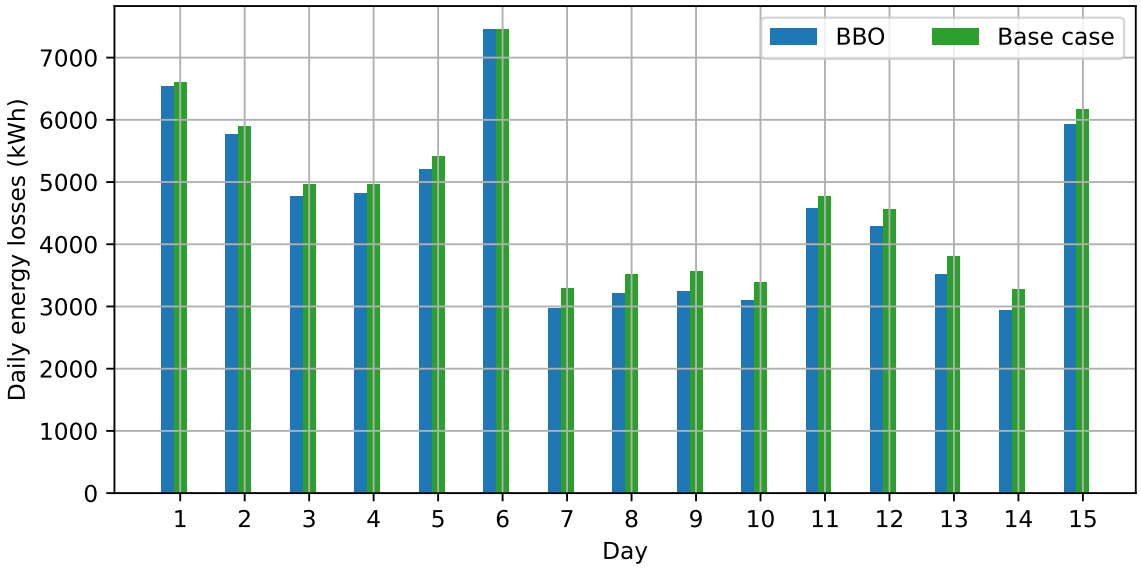

Figure 5.13 Comparison of daily energy losses for 15 days using the obtained VVO settings on IEEE-8500 network

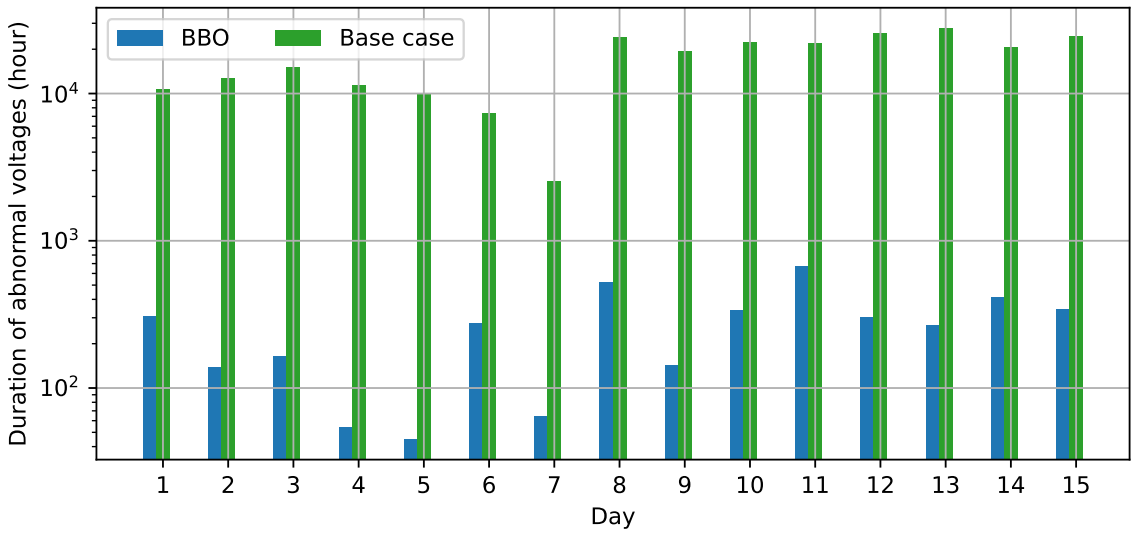

Figure 5.14 Comparison of duration of abnormal voltage conditions for 15 days using the obtained VVO settings on IEEE-8500 network

5.5 Conclusion

In this chapter, we propose to use blackbox optimization to develop control strategies for VVO to minimize network losses and violations of voltage levels. Settings for conventional devices of VVO are considered as well as volt-var curves for DERs. It has been demonstrated that the derived solutions are effective under different network loading conditions and DER generation scenarios. The approach is scalable to large distribution networks and near-optimal solutions can be found in much less iterations than those in state-of-art RL methods. Although the performance of RL methods can be improved through tuning of hyperparameters [139], the tuning itself is an optimization problem in the hyperparameter space, and solving the problem adds further burden to already heavy computational efforts of RL. Our approach is practical and can allow utilities to design long-term or seasonal VVO strategies using historical or forecast data on their network without frequently adjusting settings for controllable devices. We also want to emphasize that our approach is not limited to using CYME as the blackbox simulator, but other solvers (open-source, commercial, or even non-MANA-based) can also be used, as long as the discrete tap positions and nonlinear network constraints are properly modelled such that effects of the VVO policy can be simulated.

We assume that the "as-planned" network model is available such that it can be treated as a blackbox in our proposed approach. In other words, the locations of DERs and their nominal ratings are known, despite uncertainty in generation profiles. In practice, if the DERs are of

GET type, i.e., customer-owned and installed at customers' sites, utilities have no visibility of nor information about these DERs. Hence, it will be challenging to find an optimal policy in this case and the policy may not be effective to regulate voltage levels on the network. A potential solution is to detect the presence of DERs and estimate the system capacity from the smart meter data [115], which are readily available to utilities. The inferred information can then be used to build the network model and apply our approach to design a VVO policy.

We also implicitly assume that all customers participate in the VVO policy such that they agree to let utilities update the volt-var curve settings on the DERs they own when necessary. In practice, not all customers are willing to let utilities tap into their systems even if utilities are aware of the presence of all customer-owned DERs. In such a case, a participation factor can be included in our approach and we add some additional uncertainty in the locations of the participating customers. Similar to our proposed approach in Chapter 4 to invite EV owners to join the mitigation strategy to shift their charging habits, incentive programs can be designed and embedded into the search for an optimal VVO strategy. Numerical case studies should be carried out to evaluate the performance and effectiveness of the VVO strategy obtained.

Finally, we aim to extend the scope of our approach by considering the following: (1) including active power control (e.g., volt-watt curve) for DERs in the control strategy so to be compliant with the IEEE-1547 standard, and (2) using by-phase settings for voltage regulators in the VVO policy.

CHAPTER 6 CONCLUSION

In this dissertation, we consider grid-edge technologies (GETs) like electric vehicles and photovoltaic systems which are connected to the distribution systems at customers' locations at increasing penetration rates. Utilities have limited observability of the presence of these technologies and stochasticity is induced by how customers are using them. The use of these technologies may cause abnormal conditions to the distribution networks, such as equipment being overloaded and non-acceptable voltage levels. Hence, their impacts must be studied for planning and safe operations of the networks; however, due to the randomness involved, it is challenging to properly model them on the distribution networks. Assessment method needs to be developed to evaluate the impacts at various levels of penetration of the technologies and uncertainties must be considered. If abnormal conditions are likely to occur according to the impact analysis results, optimization strategies and mitigation plans should be designed to minimize the likelihood of such abnormal conditions.

6.1 Summary of work

In Chapter 2, we develop a rapid estimation method (REM) to perform a stochastic analysis on the impact of EVs and PVs to power distribution networks without performing repetitive power flow analyses to multiple scenarios, i.e., Monte Carlo simulations. To deal with the uncertainty in locations of EVs/PVs and their consumption/generation profiles, we compute the probability density functions of the network states of interests (equipment loading level and node/bus voltage) at given penetration rates by solving the Fokker-Planck equation. For any specific penetration level, probabilities of equipment overloading and node/bus voltage exceeding specific limits can then be calculated, which indicates susceptible equipment or network sections to EV/PV impacts. To improve the accuracy of our method, an optional calibration step is also proposed. We illustrate the performance our our approach on a large-scale realistic distribution network, and the results are benchmarked with Monte Carlo simulations. It is illustrated that the REM results well follow those from Monte Carlo simulations with minimal errors, hence we greatly improve the computational efficiency when conducting stochastic impact analyses for EVs and PVs on the distribution networks. While minor errors can be observed when comparing with results from Monte Carlo simulations (e.g., mainly at tail regions of the PDFs or outside of $2\times$ quantiles), we want to emphasize that the computational speed is significantly improved, allowing utilities to do quick screening on their distribution networks to identify locations sensitive to impacts of GETs. Utilities

can still perform power flow analyses on these identified locations for more accurate results. We also obtain a sequence of PDFs indexed by the penetration rates, hence the results can indicate GET impacts to the networks for changing penetration levels with time.

To apply the REM to study impacts of EV charging, probability data characterizing customers' EV charging profiles are required. However, these information are not always available, because utilities do not have direct access to the charging events as EV chargers are normally installed behind-the-meter. In Chapter 3, a non-intrusive and training-free method is proposed to detect BTM EV charging events based on customers' smart meter data, which are readily available to utilities. The approach does not require labelled training data nor hyperparameter tuning, and achieves a similar level of accuracy in extracting information of charging events as that of the literature. Through a data-driven approach, we infer customers' charging patterns in terms of probability distributions of charging profiles from the detection results during an entire year. We compare the inferred probability distributions with those from the ground truth, and illustrate that even if there exist some minor differences between the two sets of distributions, no significant error occurs in the results of EV charging impact analyses.

In the numerical examples of Chapters 2 and 3 for impacts of EV charging to distribution networks, we observe that key network equipment like substation transformers may be identified as being overloaded especially at high penetration of EVs. To avoid premature failure of these equipment and to maintain their usable lifetime, utilities need to develop strategies to mitigate the overloads. In Chapter 4, we propose a mitigation strategy to avoid overloading issues to key network equipment by shifting customers' probabilities of charging their EVs from the peak hours to the off-peak hours. We first formulate a bi-level optimization problem to design the mitigation strategy aiming to maintain equipment's nominal lifetime and minimize associated costs. We then re-express the bi-level problem as a convex program, and embed it into a dedicated search algorithm to determine optimal levels of incentives offered under the mitigation strategy. The proposed mitigation strategy is not an EV charging schedule that customers must follow; rather, customers still have the freedom to charge their EVs during the peak hours when necessary. However, the probabilities of doing so in the long term should be consistent with those used in the mitigation plan to receive the corresponding incentives.

In Chapter 5, we shift our focus to PVs. Unlike EVs which consume power, PVs inject power to the distribution networks. Hence, overloading or under-voltage issues are less likely to occur. However, a high penetration of PVs can lead to over-voltage problem on the network which needs to be regulated. In this chapter, we propose an optimal reactive power dispatch

(ORPD) stochastic program for volt-var optimization (VVO) of power distribution networks, while uncertainties in demand and PV generation are considered. In the proposed stochastic program, we consider not only control settings for voltage regulators, capacitor banks, and on-load tap changers which are conventional devices for VVO, but also the capability of inverter-based PVs to absorb and inject reactive power to regulate the voltage levels. Instead of directly solving this NP-hard problem, we use a power flow solver as a blackbox simulator and solve the problem by a scenario-based stochastic blackbox optimization (BBO). The derived solution has been demonstrated to be effective under various demand and DER generation scenarios. Comparing to reinforcement learning-based methods, our approach is more sample efficient, and provide trustworthy and interpretable solutions. Our approach is practical and can allow utilities to design long-term or seasonal VVO strategies using historical or forecast data on their network without frequently adjusting settings for controllable devices.

Finally, to validate the performance and the scalability of all the methods and approaches developed in this dissertation, they have been tested on the IEEE-8500 test feeder which is a realistic large-scale distribution system.

6.2 Future work

In this dissertation, we consider EVs and PVs as the main GET types because of their increasing presence on today's distribution networks. GET also includes demand response (DR) programs, which are attracting on-going attention due to their effectiveness and efficiency in balancing demand with supply and optimizing the use of existing network infrastructure against challenges in grid operations. With the set of offset profiles of DR characterized, i.e., how customers' demands are varied under the DR program, we can use the proposed REM approach to assess impacts of DR programs, and the combined impacts with other GET types can also be analyzed. Thanks to the computational efficiency of REM, we can use it to evaluate performance of different kinds of DR programs while uncertainties like participation factors are taken accounted for. Further work can also done in optimizing the structure of the DR program to coordinate with other GET types for optimal grid performance.

As pointed out in Chapter 3, to accurately detect EV charging events from the smart meter data, there is a need to first estimate customers' BTM generation such as from PV or battery systems. This allows to use only the consumption data in the EV detection methodology. The detection of PV generation from the smart meter data also informs utilities on the location and nominal capacities of existing PVs on the network. These are useful information to model PVs in the "as-planned" network model, which is essential to design optimal VVO strategies to regulate voltage levels on the network.

Last but not least, in some numerical examples, we made certain assumptions to simplify the simulations although our proposed approaches do not have these limitations. For example, in Chapter 3, we consider constant power throughout the entire EV charging event. In Chapter 4, our formulation for the design of mitigation strategies accounts for the uncertainty in customers' participation through the λ_p factor; however, the numerical example presented considers the full participation of customers, i.e., $\lambda_p = 1$. Our approach can also be applied to design a uniformized strategy and incentive plan to all customers on different networks, while only the substation transformer is assumed to be overloaded in the numerical example. In Chapter 5, we implicitly assume that all customers participate in the VVO policy such that they allow utilities to update the volt-var curve settings on the PVs they own when necessary. In practice, these assumptions may not hold, e.g., EV charging power may be lowered at the start and towards the end of charging to protect battery cells, not all EV owners are interested in changing their routine schedule of charging their EVs even though incentives are offered, or not all customers are willing to let utilities tap into their PV systems. These open up opportunities to further develop our methodologies when these assumptions are relaxed, and to validate and improve the performance of our proposed approaches through additional case studies.

REFERENCES

[1] S. Habib, M. M. Khan, F. Abbas, L. Sang, M. U. Shahid, and H. Tang, "A comprehensive study of implemented international standards, technical challenges, impacts and prospects for electric vehicles," *IEEE Access*, vol. 6, pp. 13 866–13 890, 2018.

[2] M. Ashfaq, O. Butt, J. Selvaraj, and N. Rahim, "Assessment of electric vehicle charging infrastructure and its impact on the electric grid: A review," *International Journal of Green Energy*, vol. 18, no. 7, pp. 657–686, 2021.

[3] R. A. Jabr, R. Singh, and B. C. Pal, "Minimum loss network reconfiguration using mixed-integer convex programming," *IEEE Transactions on Power Systems*, vol. 27, no. 2, pp. 1106–1115, 2012.

[4] F. Gomes, S. Carneiro, J. Pereira, M. Vinagre, P. Garcia, and L. De Araujo, "A new distribution system reconfiguration approach using optimum power flow and sensitivity analysis for loss reduction," *IEEE Transactions on Power Systems*, vol. 21, no. 4, pp. 1616–1623, 2006.

[5] S. Shao, T. Zhang, M. Pipattanasomporn, and S. Rahman, "Impact of TOU rates on distribution load shapes in a smart grid with PHEV penetration," in *IEEE PES T&D 2010*, 2010, pp. 1–6.

[6] Y. Cao, S. Tang, C. Li, P. Zhang, Y. Tan, Z. Zhang, and J. Li, "An optimized EV charging model considering TOU price and SOC curve," *IEEE Transactions on Smart Grid*, vol. 3, no. 1, pp. 388–393, 2012.

[7] K. Clement-Nyns, E. Haesen, and J. Driesen, "The impact of charging plug-in hybrid electric vehicles on a residential distribution grid," *IEEE Transactions on Power Systems*, vol. 25, no. 1, pp. 371–380, 2010.

[8] E. Sortomme, M. M. Hindi, S. D. J. MacPherson, and S. S. Venkata, "Coordinated charging of plug-in hybrid electric vehicles to minimize distribution system losses," *IEEE Transactions on Smart Grid*, vol. 2, no. 1, pp. 198–205, 2011.

[9] M. J. E. Alam, K. M. Muttaqi, and D. Sutanto, "Mitigation of rooftop solar PV impacts and evening peak support by managing available capacity of distributed energy storage systems," *IEEE Transactions on Power Systems*, vol. 28, no. 4, pp. 3874–3884, 2013.

[10] X. Liu, A. Aichhorn, L. Liu, and H. Li, "Coordinated control of distributed energy storage system with tap changer transformers for voltage rise mitigation under high photovoltaic penetration," *IEEE Transactions on Smart Grid*, vol. 3, no. 2, pp. 897–906, 2012.

[11] A. Lesage-Landry and D. S. Callaway, "Batch reinforcement learning for network-safe demand response in unknown electric grids," *Electric Power Systems Research*, vol. 212, p. 108375, 2022.

[12] H. Ahmadi, J. R. Martí, and H. W. Dommel, "A framework for volt-VAR optimization in distribution systems," *IEEE Transactions on Smart Grid*, vol. 6, no. 3, pp. 1473–1483, 2015.

[13] A. Dubey and S. Santoso, "Electric vehicle charging on residential distribution systems: Impacts and mitigations," *IEEE Access*, vol. 3, pp. 1871–1893, 2015.

[14] A. Dubey, S. Santoso, and M. P. Cloud, "Understanding the effects of electric vehicle charging on the distribution voltages," in *2013 IEEE Power Energy Society General Meeting*, 2013, pp. 1–5.

[15] A. Dubey, S. Santoso, and M. Cloud, "Comparative analysis of effects of electric vehicle loads on distribution system voltages," in *2014 IEEE PES T&D Conference and Exposition*, 2014, pp. 1–5.

[16] J. Gomez and M. Morcos, "Impact of EV battery chargers on the power quality of distribution systems," *IEEE Transactions on Power Delivery*, vol. 18, no. 3, pp. 975–981, 2003.

[17] M. Cohen and D. Callaway, "Effects of distributed PV generation on California's distribution system, part 1: Engineering simulations," *Solar Energy*, vol. 128, pp. 126–138, 2016.

[18] M. A. Cohen, P. A. Kauzmann, and D. S. Callaway, "Effects of distributed PV generation on California's distribution system, part 2: Economic analysis," *Solar Energy*, vol. 128, pp. 139–152, 2016.

[19] A. Y. Elrayyah, M. Z. C. Wanik, and A. Bouselham, "Simplified approach to analyze voltage rise in LV systems with PV installations using equivalent power systems diagrams," *IEEE Transactions on Power Delivery*, vol. 32, no. 4, pp. 2140–2149, 2017.

[20] A. Rodriguez-Calvo, R. Cossent, and P. Frías, "Integration of PV and EVs in unbalanced residential LV networks and implications for the smart grid and advanced metering infrastructure deployment," *International Journal of Electrical Power & Energy Systems*, vol. 91, pp. 121–134, 2017.

[21] R.-C. Leou, C.-L. Su, and C.-N. Lu, "Stochastic analyses of electric vehicle charging impacts on distribution network," *IEEE Transactions on Power Systems*, vol. 29, no. 3, pp. 1055–1063, 2014.

[22] S. Habib, M. M. Khan, F. Abbas, M. Numan, Y. Ali, H. Tang, and X. Yan, "A framework for stochastic estimation of electric vehicle charging behavior for risk assessment of distribution networks," *Frontiers in Energy*, vol. 14, no. 2, pp. 298–317, 2020.

[23] D. Salles, C. Jiang, W. Xu, W. Freitas, and H. E. Mazin, "Assessing the collective harmonic impact of modern residential loads—part i: Methodology," *IEEE Transactions on Power Delivery*, vol. 27, no. 4, pp. 1937–1946, 2012.

[24] C. Jiang, R. Torquato, D. Salles, and W. Xu, "Method to assess the power-quality impact of plug-in electric vehicles," *IEEE Transactions on Power Delivery*, vol. 29, no. 2, pp. 958–965, 2014.

[25] A. Navarro-Espinosa and L. F. Ochoa, "Probabilistic impact assessment of low carbon technologies in LV distribution systems," *IEEE Transactions on Power Systems*, vol. 31, no. 3, pp. 2192–2203, 2016.

[26] R. Y. Rubinstein and D. P. Kroese, *Simulation and the Monte Carlo method*. John Wiley & Sons, 2016.

[27] T. Hou, D. Nuyens, S. Roels, and H. Janssen, "Quasi-monte carlo based uncertainty analysis: Sampling efficiency and error estimation in engineering applications," *Reliability Engineering & System Safety*, vol. 191, p. 106549, 2019.

[28] D. Krupenev, D. Boyarkin, and D. Iakubovskii, "Improvement in the computational efficiency of a technique for assessing the reliability of electric power systems based on the monte carlo method," *Reliability Engineering & System Safety*, vol. 204, p. 107171, 2020.

[29] N. Mehboob, M. Restrepo, C. A. Canizares, C. Rosenberg, and M. Kazerani, "Smart operation of electric vehicles with four-quadrant chargers considering uncertainties," *IEEE Transactions on Smart Grid*, vol. 10, no. 3, pp. 2999–3009, 2018.

[30] R. Allan, A. L. Da Silva, and R. Burchett, "Evaluation methods and accuracy in probabilistic load flow solutions," *IEEE Transactions on Power Apparatus and Systems*, vol. PAS-100, no. 5, 1981.

[31] P. Zhang and S. Lee, "Probabilistic load flow computation using the method of combined cumulants and gram-charlier expansion," *IEEE Transactions on Power Systems*, vol. 19, no. 1, pp. 676–682, 2004.

[32] C.-L. Su, "Probabilistic load-flow computation using point estimate method," *IEEE Transactions on Power Systems*, vol. 20, no. 4, pp. 1843–1851, 2005.

[33] Y. Xu, L. Mili, and J. Zhao, "Probabilistic power flow calculation and variance analysis based on hierarchical adaptive polynomial chaos-anova method," *IEEE Transactions on Power Systems*, vol. 34, no. 5, pp. 3316–3325, 2019.

[34] D. Métivier, M. Vuffray, and S. Misra, "Efficient polynomial chaos expansion for uncertainty quantification in power systems," *Electric Power Systems Research*, vol. 189, p. 106791, 2020.

[35] K. Ye, J. Zhao, Y. Zhang, X. Liu, and H. Zhang, "A generalized computationally efficient copula-polynomial chaos framework for probabilistic power flow considering nonlinear correlations of pv injections," *International Journal of Electrical Power & Energy Systems*, vol. 136, p. 107727, 2022.

[36] E. M. S. Duque, P. P. Vergara, P. H. Nguyen, A. Van Der Molen, and J. G. Slootweg, "Conditional multivariate elliptical copulas to model residential load profiles from smart meter data," *IEEE Transactions on Smart Grid*, vol. 12, no. 5, pp. 4280–4294, 2021.

[37] H. Sheng and X. Wang, "Probabilistic power flow calculation using non-intrusive low-rank approximation method," *IEEE Transactions on Power Systems*, vol. 34, no. 4, pp. 3014–3025, 2019.

[38] J. Saarenpää, M. Kolehmainen, and H. Niska, "Geodemographic analysis and estimation of early plug-in hybrid electric vehicle adoption," *Applied Energy*, vol. 107, pp. 456–464, 2013.

[39] M. A. Tamor, C. Gearhart, and C. Soto, "A statistical approach to estimating acceptance of electric vehicles and electrification of personal transportation," *Transportation Research Part C: Emerging Technologies*, vol. 26, pp. 125–134, 2013.

[40] S. Carley, R. M. Krause, B. W. Lane, and J. D. Graham, "Intent to purchase a plug-in electric vehicle: A survey of early impressions in large us cites," *Transportation Research Part D: Transport and Environment*, vol. 18, pp. 39–45, 2013.

[41] S. Wang, L. Du, J. Ye, and D. Zhao, "Robust identification of EV charging profiles," in *2018 IEEE Transportation Electrification Conference and Expo (ITEC)*, 2018, pp. 1–6.

[42] B. I. Fesche, V. Hoffmann, K. Ingebrigtsen, I. N. Christie, and M. Punnerud, "Signal discovery in the smart grid-finding: Electric vehicle charging patterns in power consumption data," *CIRED 2019 Conference*, no. 1531, 2019.

[43] V. Hoffmann, B. I. Fesche, K. Ingebrigtsen, I. N. Christie, and M. Punnerud, "Automated detection of electric vehicles in hourly smart meter data," *CIRED 2019 Conference*, no. 1531, 2019.

[44] D. Yang, X. Gao, L. Kong, Y. Pang, and B. Zhou, "An event-driven convolutional neural architecture for non-intrusive load monitoring of residential appliance," *IEEE Transactions on Consumer Electronics*, vol. 66, no. 2, pp. 173–182, 2020.

[45] A. Verma, A. Asadi, K. Yang, and S. Tyagi, "A data-driven approach to identify households with plug-in electrical vehicles (PEVs)," *Applied Energy*, vol. 160, pp. 71–79, 2015.

[46] A. Verma, A. Asadi, and K. Yang, "Analyzing household charging patterns of plug-in electric vehicles (PEVs): A data mining approach," *Computers & Industrial Engineering*, vol. 128, pp. 964–973, 2019.

[47] P. Zhang, C. Zhou, B. G. Stewart, D. M. Hepburn, W. Zhou, and J. Yu, "An improved non-intrusive load monitoring method for recognition of electric vehicle battery charging load," *Energy Procedia*, vol. 12, pp. 104–112, 2011, the Proceedings of International Conference on Smart Grid and Clean Energy Technologies (ICSGCE 2011).

[48] A. Shaw and B. P. Nayak, "Electric vehicle charging load filtering by power signature analysis," in *2017 International Conference on Data Management, Analytics and Innovation (ICDMAI)*, 2017, pp. 71–75.

[49] Z. Zhang, J. H. Son, Y. Li, M. Trayer, Z. Pi, D. Y. Hwang, and J. K. Moon, "Training-free non-intrusive load monitoring of electric vehicle charging with low sampling rate," in *IECON 2014 - 40th Annual Conference of the IEEE Industrial Electronics Society*, 2014, pp. 5419–5425.

[50] Y. Xiang, Y. Wang, S. Xia, and F. Teng, "Charging load pattern extraction for residential electric vehicles: A training-free nonintrusive method," *IEEE Transactions on Industrial Informatics*, vol. 17, no. 10, pp. 7028–7039, 2021.

[51] A. A. Munshi and Y. A.-R. I. Mohamed, "Unsupervised nonintrusive extraction of electrical vehicle charging load patterns," *IEEE Transactions on Industrial Informatics*, vol. 15, no. 1, pp. 266–279, 2019.

[52] A. A. Munshi and Y. A.-R. Mohamed, "Extracting and defining flexibility of residential electrical vehicle charging loads," *IEEE Transactions on Industrial Informatics*, vol. 14, no. 2, pp. 448–461, 2018.

[53] O. Parson, S. Ghosh, M. Weal, and A. Rogers, "Non-intrusive load monitoring using prior models of general appliance types," *Proceedings of the AAAI Conference on Artificial Intelligence*, vol. 26, no. 1, pp. 356–362, Sep. 2021.

[54] S. Wang, L. Du, J. Ye, and D. Zhao, "A deep generative model for non-intrusive identification of EV charging profiles," *IEEE Transactions on Smart Grid*, vol. 11, no. 6, pp. 4916–4927, 2020.

[55] P. A. Schirmer and I. Mporas, "Non-intrusive load monitoring: A review," *IEEE Transactions on Smart Grid*, vol. 14, no. 1, pp. 769–784, 2023.

[56] A. Sahoo, K. H. Mistry, and T. E. Baker, "The costs of revving up the grid for electric vehicles," Boston Consulting Group, https://www.bcg.com/publications/2019/costs-revving-up-the-grid-for-electric-vehicles (last accessed on 2024-10-06).

[57] R. Karandeh, V. Cecchi, J. Enslin, T. Moss, C. Stowe, E. Stuckey, and S. Whisenant, "Placement evaluation of distributed energy storage for integrating EV charging and pv solar infrastructure," in *2021 IEEE 12th International Symposium on Power Electronics for Distributed Generation Systems (PEDG)*, 2021, pp. 1–7.

[58] N. Gupta, "Probabilistic optimal reactive power planning with onshore and offshore wind generation, EV, and PV uncertainties," *IEEE Transactions on Industry Applications*, vol. 56, no. 4, pp. 4200–4213, 2020.

[59] S. Rafique, M. S. H. Nizami, U. B. Irshad, M. J. Hossain, and S. C. Mukhopadhyay, "EV scheduling framework for peak demand management in LV residential networks," *IEEE Systems Journal*, vol. 16, no. 1, pp. 1520–1528, 2021.

[60] M. Liu, P. K. Phanivong, Y. Shi, and D. S. Callaway, "Decentralized charging control of electric vehicles in residential distribution networks," *IEEE Transactions on Control Systems Technology*, vol. 27, no. 1, pp. 266–281, 2017.

[61] S. Li, W. Hu, D. Cao, Z. Zhang, Q. Huang, Z. Chen, and F. Blaabjerg, "A multi-agent deep reinforcement learning based approach for the optimization of transformer life using coordinated electric vehicles," *IEEE Transactions on Industrial Informatics*, vol. 18, no. 11, pp. 7639–7652, 2022.

[62] M. Botkin-Levy, A. Engelmann, T. Mühlpfordt, T. Faulwasser, and M. R. Almassalkhi, "Distributed control of charging for electric vehicle fleets under dynamic transformer ratings," *IEEE Transactions on Control Systems Technology*, vol. 30, no. 4, pp. 1578–1594, 2022.

[63] J. Martinez-Piazuelo, N. Quijano, and C. Ocampo-Martinez, "Decentralized charging coordination of electric vehicles under feeder capacity constraints," *IEEE Transactions on Control of Network Systems*, vol. 9, no. 4, pp. 1600–1610, 2021.

[64] Z. Ma, D. S. Callaway, and I. A. Hiskens, "Decentralized charging control of large populations of plug-in electric vehicles," *IEEE Transactions on Control Systems Technology*, vol. 21, no. 1, pp. 67–78, 2013.

[65] M. A. Tajeddini and H. Kebriaei, "A mean-field game method for decentralized charging coordination of a large population of plug-in electric vehicles," *IEEE Systems Journal*, vol. 13, no. 1, pp. 854–863, 2019.

[66] S. Shao, M. Pipattanasomporn, and S. Rahman, "Grid integration of electric vehicles and demand response with customer choice," *IEEE Transactions on Smart Grid*, vol. 3, no. 1, pp. 543–550, 2012.

[67] C. Hodge, K. Hauck, S. Gupta, and J. C. Bennett, "Vehicle cybersecurity threats and mitigation approaches," National Renewable Energy Lab. (NREL), Golden, CO (United States), Tech. Rep., 2019.

[68] Z. Yang, A. Bose, H. Zhong, N. Zhang, Q. Xia, and C. Kang, "Optimal reactive power dispatch with accurately modeled discrete control devices: A successive linear approximation approach," *IEEE Transactions on Power Systems*, vol. 32, no. 3, pp. 2435–2444, 2017.

[69] A. Inaolaji, A. Savasci, and S. Paudyal, "Distribution grid optimal power flow in unbalanced multiphase networks with volt-var and volt-watt droop settings of smart inverters," *IEEE Transactions on Industry Applications*, vol. 58, no. 5, pp. 5832–5843, 2022.

[70] E. Davoodi, E. Babaei, B. Mohammadi-Ivatloo, and M. Rasouli, "A novel fast semidefinite programming-based approach for optimal reactive power dispatch," *IEEE Transactions on Industrial Informatics*, vol. 16, no. 1, pp. 288–298, 2020.

[71] S. G. Constante F., J. C. López, and M. J. Rider, "Optimal reactive power dispatch with discrete controllers using a branch-and-bound algorithm: A semidefinite relaxation approach," *IEEE Transactions on Power Systems*, vol. 36, no. 5, pp. 4539–4550, 2021.

[72] M. He, Z. Soltani, M. Ghaljehei, M. Esmaili, S. Ma, M. Chen, M. Khorsand, R. Ayyanar, and V. Vittal, "A SOCP-Based ACOPF for operational scheduling of three-phase unbalanced distribution systems and coordination of PV smart inverters," *IEEE Transactions on Power Systems*, vol. 39, no. 1, pp. 229–244, 2024.

[73] Y. Xu, Z. Y. Dong, R. Zhang, and D. J. Hill, "Multi-timescale coordinated voltage/var control of high renewable-penetrated distribution systems," *IEEE Transactions on Power Systems*, vol. 32, no. 6, pp. 4398–4408, 2017.

[74] T. M. Aljohani, A. Saad, and O. A. Mohammed, "Two-stage optimization strategy for solving the VVO problem considering high penetration of plug-in electric vehicles to unbalanced distribution networks," *IEEE Transactions on Industry Applications*, vol. 57, no. 4, pp. 3425–3440, 2021.

[75] T. Ding, S. Liu, W. Yuan, Z. Bie, and B. Zeng, "A two-stage robust reactive power optimization considering uncertain wind power integration in active distribution networks," *IEEE Transactions on Sustainable Energy*, vol. 7, no. 1, pp. 301–311, 2016.

[76] C. Zhang, Y. Xu, Z. Dong, and J. Ravishankar, "Three-stage robust inverter-based voltage/var control for distribution networks with high-level PV," *IEEE Transactions on Smart Grid*, vol. 10, no. 1, pp. 782–793, 2019.

[77] P. Li, C. Zhang, Z. Wu, Y. Xu, M. Hu, and Z. Dong, "Distributed adaptive robust voltage/var control with network partition in active distribution networks," *IEEE Transactions on Smart Grid*, vol. 11, no. 3, pp. 2245–2256, 2020.

[78] J. A. Taylor, *Convex Optimization of Power Systems*. Cambridge University Press, 2015.

[79] R. A. Jabr, "Power flow based volt/var optimization under uncertainty," *Journal of Modern Power Systems and Clean Energy*, vol. 9, no. 5, pp. 1000–1006, 2021.

[80] S. Li, W. Wu, and Y. Lin, "Robust data-driven and fully distributed volt/var control for active distribution networks with multiple virtual power plants," *IEEE Transactions on Smart Grid*, vol. 13, no. 4, pp. 2627–2638, 2022.

[81] T. Xu, W. Wu, Y. Hong, J. Yu, and F. Zhang, "Data-driven inverter-based volt/var control for partially observable distribution networks," *CSEE Journal of Power and Energy Systems*, vol. 9, no. 2, pp. 548–560, 2023.

[82] E. Pourjafari and M. Reformat, "A support vector regression based model predictive control for volt-var optimization of distribution systems," *IEEE Access*, vol. 7, pp. 93 352–93 363, 2019.

[83] S. Li, Y. Sun, M. Ramezani, and Y. Xiao, "Artificial neural networks for volt/var control of der inverters at the grid edge," *IEEE Transactions on Smart Grid*, vol. 10, no. 5, pp. 5564–5573, 2019.

[84] L. Miao, Y. Peng, Z. Li, W. Xi, and T. Cai, "Data-driven volt/var control based on constrained temporal convolutional networks with a corrective mechanism," *Electric Power Systems Research*, vol. 224, p. 109738, 2023.

[85] X. Sun, J. Qiu, Y. Tao, Y. Ma, and J. Zhao, "A multi-mode data-driven volt/var control strategy with conservation voltage reduction in active distribution networks," *IEEE Transactions on Sustainable Energy*, vol. 13, no. 2, pp. 1073–1085, 2022.

[86] Y. Zhang, X. Wang, J. Wang, and Y. Zhang, "Deep reinforcement learning based volt-var optimization in smart distribution systems," *IEEE Transactions on Smart Grid*, vol. 12, no. 1, pp. 361–371, 2021.

[87] S. Wang, J. Duan, D. Shi, C. Xu, H. Li, R. Diao, and Z. Wang, "A data-driven multi-agent autonomous voltage control framework using deep reinforcement learning," *IEEE Transactions on Power Systems*, vol. 35, no. 6, pp. 4644–4654, 2020.

[88] Y. Pei, Y. Yao, J. Zhao, F. Ding, and K. Ye, "Data-driven distribution system coordinated PV inverter control using deep reinforcement learning," in *2021 IEEE Sustainable Power and Energy Conference (iSPEC)*, 2021, pp. 781–786.

[89] W. Wang, N. Yu, J. Shi, and Y. Gao, "Volt-var control in power distribution systems with deep reinforcement learning," in *2019 IEEE International Conference on Communications, Control, and Computing Technologies for Smart Grids (SmartGridComm)*, 2019, pp. 1–7.

[90] D. Cao, J. Zhao, W. Hu, F. Ding, Q. Huang, Z. Chen, and F. Blaabjerg, "Data-driven multi-agent deep reinforcement learning for distribution system decentralized voltage control with high penetration of PVs," *IEEE Transactions on Smart Grid*, vol. 12, no. 5, pp. 4137–4150, 2021.

[91] H. Liu and W. Wu, "Online multi-agent reinforcement learning for decentralized inverter-based volt-var control," *IEEE Transactions on Smart Grid*, vol. 12, no. 4, pp. 2980–2990, 2021.

[92] X. Yang, H. Liu, and W. Wu, "Attention-enhanced multi-agent reinforcement learning against observation perturbations for distributed volt-var control," *IEEE Transactions on Smart Grid*, pp. 1–1, 2024.

[93] S. Burer and A. N. Letchford, "Non-convex mixed-integer nonlinear programming: A survey," *Surveys in Operations Research and Management Science*, vol. 17, no. 2, pp. 97–106, 2012.

[94] C. Audet and W. Hare, *Derivative-Free and Blackbox Optimization*. Springer Series in Operations Research and Financial Engineering, Springer International Publishing, 2017.

[95] F. Li, R. P. Malhamé, and J. Le Ny, "Mean field game based control of dispersed energy storage devices with constrained inputs," in *2016 IEEE 55th Conference on Decision and Control (CDC)*, 2016.

[96] K. Wang and M. L. Crow, "The Fokker-Planck Equation for power system stability probability density function evolution," *IEEE Transactions on Power Systems*, vol. 28, no. 3, pp. 2994–3001, 2013.

[97] S. Chen, T. Zhang, H. B. Gooi, R. D. Masiello, and W. Katzenstein, "Penetration rate and effectiveness studies of aggregated bess for frequency regulation," *IEEE Transactions on Smart Grid*, vol. 7, no. 1, pp. 167–177, 2015.

[98] S. Akagi, R. Takahashi, A. Kaneko, M. Ito, J. Yoshinaga, Y. Hayashi, H. Asano, and H. Konda, "Upgrading voltage control method based on photovoltaic penetration rate," *IEEE Transactions on Smart Grid*, vol. 9, no. 5, pp. 3994–4003, 2016.

[99] S. Chen, T. Zhang, H. B. Gooi, R. D. Masiello, and W. Katzenstein, "Penetration rate and effectiveness studies of aggregated bess for frequency regulation," *IEEE Transactions on Smart Grid*, vol. 7, no. 1, pp. 167–177, 2016.

[100] P. E. Kloeden and E. Platen, "Stochastic differential equations," in *Numerical Solution of Stochastic Differential Equations*. Springer, 1992.

[101] H. Risken, *The Fokker-Planck Equation Methods of Solution and Applications*, 2nd ed., ser. Springer Series in Synergetics, 18. Berlin, Heidelberg: Springer Berlin Heidelberg, 1996.

[102] J.-S. Lacroix, I. Kocar, and M. Belletête, "Accelerated computation of multiphase short circuit summary for unbalanced distribution systems using the concept of selected inversion," *IEEE Transactions on Power Systems*, vol. 28, no. 2, pp. 1515–1522, 2013.

[103] I. Kocar, J. Mahseredjian, U. Karaagac, G. Soykan, and O. Saad, "Multiphase load-flow solution for large-scale distribution systems using MANA," *IEEE Transactions on Power Delivery*, vol. 29, no. 2, pp. 908–915, 2014.

[104] R. J. LeVeque and R. J. Leveque, *Numerical methods for conservation laws*. Springer, 1992, vol. 214.

[105] R. J. LeVeque *et al.*, *Finite volume methods for hyperbolic problems*. Cambridge university press, 2002, vol. 31.

[106] R. F. Arritt and R. C. Dugan, "The IEEE 8500-node test feeder," in *IEEE PES T&D 2010*, 2010, pp. 1–6.

[107] High-resolution solar radiation datasets. https://www.nrcan.gc.ca/energy/renewable-electricity/solar-photovoltaic/18409 (last accessed on 2022-04-25).

[108] J. M. Chambers, *Graphical methods for data analysis*. Chapman and Hall/CRC, 2018.

[109] G. Tal, D. Chakraborty, A. Jenn, J. H. Lee, and D. Bunch, "Factors affecting demand for plug-in charging infrastructure: An analysis of plug-in electric vehicle commuters," *UC Office of the President: University of California Institute of Transportation Studies*, 2020.

[110] S. Habib, M. M. Khan, F. Abbas, and H. Tang, "Assessment of electric vehicles concerning impacts, charging infrastructure with unidirectional and bidirectional chargers, and power flow comparisons," *International Journal of Energy Research*, vol. 42, no. 11, pp. 3416–3441, 2018.

[111] Pecan Street Dataport, http://dataport.pecanstreet.org (last accessed on 2022-04-25).

[112] K. S. Cetin and A. Novoselac, "Single and multi-family residential central all-air HVAC system operational characteristics in cooling-dominated climate," *Energy and Buildings*, vol. 96, pp. 210–220, 2015.

[113] E. Proedrou, "A comprehensive review of residential electricity load profile models," *IEEE Access*, vol. 9, pp. 12 114–12 133, 2021.

[114] L. W. Davis, "Electric vehicles in multi-vehicle households," *Applied Economics Letters*, vol. 30, no. 14, pp. 1909–1912, 2023.

[115] S. Lin and H. Zhu, "Enhancing the spatio-temporal observability of grid-edge resources in distribution grids," *IEEE Transactions on Smart Grid*, vol. 12, no. 6, pp. 5434–5443, 2021.

[116] M. Soleimani and M. Kezunovic, "Mitigating transformer loss of life and reducing the hazard of failure by the smart EV charging," *IEEE Transactions on Industry Applications*, vol. 56, no. 5, pp. 5974–5983, 2020.

[117] I. Diahovchenko, R. Petrichenko, L. Petrichenko, A. Mahnitko, P. Korzh, M. Kolcun, and Z. Čonka, "Mitigation of transformers' loss of life in power distribution networks with high penetration of electric vehicles," *Results in Engineering*, vol. 15, p. 100592, 2022.

[118] T. Jonas, N. Daniels, and G. Macht, "Electric vehicle user behavior: An analysis of charging station utilization in canada," *Energies*, vol. 16, no. 4, 2023.

[119] S. Habib, M. M. Khan, F. Abbas, M. Numan, Y. Ali, H. Tang, and X. Yan, "A framework for stochastic estimation of electric vehicle charging behavior for risk assessment of distribution networks," *Frontiers in Energy*, vol. 14, no. 2, pp. 298–317, 2020.

[120] W. Fu, J. D. McCalley, and V. Vittal, "Risk assessment for transformer loading," *IEEE Transactions on Power Systems*, vol. 16, no. 3, pp. 346–353, 2001.

[121] "IEEE guide for loading mineral-oil-immersed transformers and step-voltage regulators," *IEEE Std C57.91-2011 (Revision of IEEE Std C57.91-1995)*, pp. 1–123, 2012.

[122] *IEEE Std 1283-2013 (Revision of IEEE Std 1283-2004): IEEE Guide for Determining the Effects of High-Temperature Operation on Conductors, Connectors, and Accessories*. IEEE.

[123] "Electric Vehicle (EV) rate plans – (EV-B) rate by PG&E," https://www.pge.com/en/account/rate-plans/find-your-best-rate-plan/electric-vehicles.html (last accessed on 2024-10-08).

[124] D. Kirschen, G. Strbac, P. Cumperayot, and D. de Paiva Mendes, "Factoring the elasticity of demand in electricity prices," *IEEE Transactions on Power Systems*, vol. 15, no. 2, pp. 612–617, 2000.

[125] X. Labandeira, J. M. Labeaga, and X. López-Otero, "A meta-analysis on the price elasticity of energy demand," *Energy Policy*, vol. 102, pp. 549–568, 2017.

[126] F. Li, É. Campeau, I. Kocar, and A. Lesage-Landry, "Inferring electric vehicle charging patterns from smart meter data for impact studies," in *XXIII Power Systems Computation Conference*, 2024, To be published.

[127] "IEEE standard for interconnection and interoperability of distributed energy resources with associated electric power systems interfaces," *IEEE Std 1547-2018 (Revision of IEEE Std 1547-2003)*, 2018.

[128] D. Shirmohammadi, H. W. Hong, A. Semlyen, and G. Luo, "A compensation-based power flow method for weakly meshed distribution and transmission networks," *IEEE Transactions on Power Systems*, vol. 3, no. 2, pp. 753–762, 1988.

[129] C. S. Cheng and D. Shirmohammadi, "A three-phase power flow method for real-time distribution system analysis," *IEEE Transactions on Power Systems*, vol. 10, no. 2, pp. 671–679, 1995.

[130] E. Bompard, E. Carpaneto, G. Chicco, and R. Napoli, "Convergence of the backward/forward sweep method for the load-flow analysis of radial distribution systems," *International Journal of Electrical Power & Energy Systems*, vol. 22, no. 7, pp. 521–530, 2000.

[131] I. Kocar, J. Mahseredjian, U. Karaagac, G. Soykan, and O. Saad, "Multiphase load-flow solution for large-scale distribution systems using MANA," *IEEE Transactions on Power Delivery*, vol. 29, no. 2, pp. 908–915, 2014.

[132] B. Cetindag, I. Kocar, A. Gueye, and U. Karaagac, "Modeling of step voltage regulators in multiphase load flow solution of distribution systems using newton's method and augmented nodal analysis," *Electric Power Components and Systems*, vol. 45, no. 15, pp. 1667–1677, 2017.

[133] W. H. Kersting, "Distribution system modeling and analysis," in *Electric Power Generation, Transmission, and Distribution.* CRC press, 2018.

[134] J.-S. Lacroix, "Multiphase short-circuit analysis solver in phase domain using a modified-augmented-nodal analysis approach," Master's thesis, École Polytechnique de Montréal, April 2012.

[135] C. Audet, S. Le Digabel, V. R. Montplaisir, and C. Tribes, "Algorithm 1027: NOMAD version 4: Nonlinear optimization with the MADS algorithm," *ACM Trans. Math. Softw.*, vol. 48, no. 3, September 2022.

[136] S. Le Digabel, "Algorithm 909: Nomad: Nonlinear optimization with the mads algorithm," *ACM Trans. Math. Softw.*, vol. 37, no. 4, Feb. 2011. [Online]. Available: https://doi.org/10.1145/1916461.1916468

[137] C. Audet, V. Béchard, and S. L. Digabel, "Nonsmooth optimization through mesh adaptive direct search and variable neighborhood search," *Journal of Global Optimization*, vol. 41, pp. 299–318, 2008.

[138] CYME Power Engineering Software, https://www.cyme.com/software/, version 9.4.

[139] T. Eimer, M. Lindauer, and R. Raileanu, "Hyperparameters in reinforcement learning and how to tune them," in *Proceedings of the 40th International Conference on Machine Learning.* ICML'23, 2023.

APPENDIX A NUMERICAL SOLUTION OF THE FPE

We discuss the numerical methods that can be used to solve the FPE for $m(x,p)$.

Explicit method

One can solve for $m(x,p)$ by conservation laws using finite element methods. Given $m_0 = m(x,p^0)$ is a probability density, we should have the total mass $M(p^0) = \int_{-\infty}^{+\infty} m(x,p^0)\mathrm{d}x = 1$. As $m(x,p)$ propagates with the penetration rate p, its total mass should be conserved at any $p \geq p^0$, i.e.

$$M(p) = \int_{-\infty}^{+\infty} m(x,p)\mathrm{d}x = 1. \tag{A.1}$$

To describe the propagation, we first define a mesh by discretizing the $x-p$ plane. The $(N_x+1)\times(K+1)$ discrete mesh points for the penetration rate p and the state x can be defined for $N_x, K \in \mathbb{Z}^+$,

$$\begin{aligned} p_i &= i\Delta p, \quad i = 0,1,2,\ldots,K-1,K, \\ x_j &= x_{\min} + j\Delta x, \quad j = 0,1,2,\ldots,N_x-1,N_x. \end{aligned} \tag{A.2}$$

Here, $x_{\min}$ some minimum value for x-axis which is dependent on the network state we are estimating.

Let $m(x_j,p)$ be the mass density at $x = x_j$ at penetration rate p for any $0 < j < N_x$. We can approximate $m(x_j,p)$ by the mass within the grid cell $[x_{j-\frac{1}{2}}, x_{j+\frac{1}{2}}]$ averaged over Δx, i.e.,

$$m(x_j,p) \approx \frac{M_j(p)}{\Delta x} \triangleq \frac{1}{\Delta x}\int_{x_{j-\frac{1}{2}}}^{x_{j+\frac{1}{2}}} m(x,p)\mathrm{d}x. \tag{A.3}$$

Denote $f(x,p) \triangleq m(x,p)u(x,p)$ the flux of mass at point x. Integrating (2.4) on both sides

over cell $\left[x_{j-\frac{1}{2}}, x_{j+\frac{1}{2}}\right]$ and dividing by Δx, we get

$$\begin{aligned}
&\frac{1}{\Delta x}\int_{x_{j-\frac{1}{2}}}^{x_{j+\frac{1}{2}}}\frac{\partial m(x,p)}{\partial p}\mathrm{d}x+\frac{1}{\Delta x}\int_{x_{j-\frac{1}{2}}}^{x_{j+\frac{1}{2}}}\frac{\partial f(x,p)}{\partial x}\mathrm{d}x=\frac{d}{\Delta x}\int_{x_{j-\frac{1}{2}}}^{x_{j+\frac{1}{2}}}\frac{\partial^2 m(x,p)}{\partial x^2}\mathrm{d}x,\\
&\frac{1}{\Delta x}\int_{x_{j-\frac{1}{2}}}^{x_{j+\frac{1}{2}}}\frac{\partial m(x,p)}{\partial p}\mathrm{d}x+\frac{1}{\Delta x}\left(f(x_{j+\frac{1}{2}},p)-f(x_{j-\frac{1}{2}},p)\right)\\
&\qquad\qquad=\frac{d}{\Delta x}\left(\frac{\partial m(x_{j+\frac{1}{2}},p)}{\partial x}-\frac{\partial m(x_{j-\frac{1}{2}},p)}{\partial x}\right).
\end{aligned}\tag{A.4}$$

Suppose that $m(x,p)$ is differentiable with respect to p at point (x,p), one can approximate $m(x,p+\Delta p)$ by expanding a Taylor series, where

$$m(x,p+\Delta p)=m(x,p)+\frac{\partial m(x,p)}{\partial p}\Delta p+\frac{\partial^2 m(x,p)}{\partial p^2}\frac{\Delta p^2}{2}+\ldots.\tag{A.5}$$

Solving (A.5) for $\frac{\partial m(x,p)}{\partial p}$, one gets,

$$\frac{\partial m(x,p)}{\partial p}=\frac{m(x,p+\Delta p)-m(x,p)}{\Delta p}-\frac{\partial^2 m(x,p)}{\partial p^2}\frac{\Delta p^2}{2}+\mathcal{O}(\Delta p^3).\tag{A.6}$$

If truncating all terms with partial derivatives of order 2 and higher in (A.6), one gets,

$$\frac{\partial m(x,p)}{\partial p}=\frac{m(x,p+\Delta p)-m(x,p)}{\Delta p}.\tag{A.7}$$

The derivative expressed in (A.7) is also referred as derivatives by Forward Euler Method, which has a local truncation error of $\mathcal{O}(\Delta p^2)$.

Integrating (A.7) on both sides over cell $\left[x_{j-\frac{1}{2}}, x_{j+\frac{1}{2}}\right]$ and dividing by Δx, we get

$$\begin{aligned}
\frac{1}{\Delta x}\int_{x_{j-\frac{1}{2}}}^{x_{j+\frac{1}{2}}}\frac{\partial m(x,p)}{\partial p}\mathrm{d}x&=\frac{1}{\Delta p\Delta x}\int_{x_{j-\frac{1}{2}}}^{x_{j+\frac{1}{2}}}\left(m(x,p+\Delta p)-m(x,p)\right)\mathrm{d}x\\
&=\frac{1}{\Delta p}\left(\frac{1}{\Delta x}\int_{x_{j-\frac{1}{2}}}^{x_{j+\frac{1}{2}}}m(x,p+\Delta p)\mathrm{d}x-\frac{1}{\Delta x}\int_{x_{j-\frac{1}{2}}}^{x_{j+\frac{1}{2}}}m(x,p)\mathrm{d}x\right)\\
&=\frac{1}{\Delta p}\left(\frac{M_j(p+\Delta p)}{\Delta x}-\frac{M_j(p)}{\Delta x}\right)\\
&\approx\frac{1}{\Delta p}\left(m(x_j,p+\Delta p)-m(x_j,p)\right).
\end{aligned}\tag{A.8}$$

Note that in (A.8), we used the definition of average mass in (A.3).

Now for the second and third terms in (A.4), evaluations of function values at points $x_{j+\frac{1}{2}}$ and $x_{j-\frac{1}{2}}$ are not possible, as these "half" points in fact do not exist in the mesh we discretized; therefore, it is necessary to approximate the function values at these points.

By definition of $f(x,p)$, the term $\frac{1}{\Delta x}\left(f(x_{j+\frac{1}{2}},p)-f(x_{j-\frac{1}{2}},p)\right)$ can be interpreted as the *average* change of flux over the cell $\left[x_{j-\frac{1}{2}},x_{j+\frac{1}{2}}\right]$. If we assume that this average change of flux remains constant over the cell $[x_{j-1},x_{j+1}]$, the second term in (A.4) can be expressed by,

$$\frac{1}{\Delta x}\left(f(x_{j+\frac{1}{2}},p)-f(x_{j-\frac{1}{2}},p)\right)=\frac{1}{2\Delta x}\left(f(x_{j+1},p)-f(x_{j-1},p)\right). \tag{A.9}$$

For the spatial first derivative terms $\frac{\partial m(x_{j+\frac{1}{2}},p)}{\partial x}$ and $\frac{\partial m(x_{j-\frac{1}{2}},p)}{\partial x}$, we can approximate their values by evaluating at the closest points x_j and x_{j-1} respectively,

$$\begin{aligned}\frac{\partial m(x_{j+\frac{1}{2}},p)}{\partial x}&\approx\frac{\partial m(x_j,p)}{\partial x},\\ \frac{\partial m(x_{j-\frac{1}{2}},p)}{\partial x}&\approx\frac{\partial m(x_{j-1},p)}{\partial x}.\end{aligned} \tag{A.10}$$

Hence, by Forward Euler method again, we have approximate right-hand side term of (A.4) by,

$$\begin{aligned}\frac{\partial m(x_j,p)}{\partial x}&=\frac{m(x_{j+1},p)-m(x_j,p)}{\Delta x},\\ \frac{\partial m(x_{j-1},p)}{\partial x}&=\frac{m(x_j,p)-m(x_{j-1},p)}{\Delta x},\\ \frac{d}{\Delta x}\left(\frac{\partial m(x_{j+\frac{1}{2}},p)}{\partial x}-\frac{\partial m(x_{j-\frac{1}{2}},p)}{\partial x}\right)&\approx\frac{d}{\Delta x}\left(\frac{\partial m(x_j,p)}{\partial x}-\frac{\partial m(x_{j-1},p)}{\partial x}\right)\\ &=\frac{d\left(m(x_{j+1},p)+m(x_{j-1},p)-2m(x_j,p)\right)}{(\Delta x)^2}.\end{aligned} \tag{A.11}$$

Substituting the results in (A.8), (A.9) and (A.11) into (A.4), we get

$$\begin{aligned}&\frac{1}{\Delta p}\left(m(x_j,p+\Delta p)-m(x_j,p)\right)+\frac{1}{2\Delta x}\left(f(x_{j+1},p)-f(x_{j-1},p)\right)\\ &\qquad=\frac{d\left(m(x_{j+1},p)+m(x_{j-1},p)-2m(x_j,p)\right)}{(\Delta x)^2},\\ &m(x_j,p+\Delta p)=m(x_j,p)-\frac{\Delta p}{2\Delta x}\left(f(x_{j+1},p)-f(x_{j-1},p)\right)\\ &\qquad+\frac{d\Delta p\left(m(x_{j+1},p)+m(x_{j-1},p)-2m(x_j,p)\right)}{(\Delta x)^2}.\end{aligned} \tag{A.12}$$

In (A.12) we describe how the mass $m(x_j, p)$ can be computed (or updated) given an initial value $m_0(x)$ on the discretized mesh. This is known as an explicit scheme. For more details about explicit schemes, the reader is referred to [104]. In order to obtain a convergent and stable solution of $m(x, p)$ from (A.12), the so-called Courant-Friedrichs-Lewy (or *CFL*) condition must be satisfied, which is

$$|u|\frac{\Delta p}{\Delta x} \leq 1. \tag{A.13}$$

To make sure that the CFL condition is always satisfied at all times, in practice we usually use $|u|_{\max}$ in (A.13). Refer to [104] for more details of the CFL condition and its relation to convergence and stability of (A.12), as well as other explicit schemes.

Implicit Method

When solving for $m(x, p)$, if we work with a small range of x, we would have to choose a small Δx step to have a sufficiently refined grid. Given that the CFL condition in (A.13) must be satisfied if explicit numerical methods are used, this indicates that Δp may be even smaller, hence making the computation slow and expensive.

Alternatively, we can consider an implicit scheme. In the explicit scheme, we evaluate all spatial derivative terms at p. For the implicit scheme, we are going to evaluate them at $(p + \Delta p)$. Hence we rewrite (A.12) to the following,

$$\begin{aligned} m(x_j, p+\Delta p) = m(x_j, p) &- \frac{\Delta p}{2\Delta x}\left(f(x_{j+1}, p+\Delta p) - f(x_{j-1}, p+\Delta p)\right) \\ &+ \frac{d\Delta p\left(m(x_{j+1}, p+\Delta p) + m(x_{j-1}, p+\Delta p) - 2m(x_j, p+\Delta p)\right)}{(\Delta x)^2}. \end{aligned} \tag{A.14}$$

We cannot directly solve $m(x_j, p + \Delta p)$ in terms of values at p by the resulting implicit scheme. However, we can express $m(x_j, p)$ in terms of values of the next step at $(p + \Delta p)$, hence this implicit scheme can also be referred as a *backward* scheme.

Substituting $f(x_{j+1}, p + \Delta p) = m(x_{j+1}, p + \Delta p)u(x_{j+1}, p + \Delta p)$ and $f(x_{j-1}, p + \Delta p) =$

$m(x_{j-1}, p+\Delta p)u(x_{j-1}, p+\Delta p)$ into (A.14), we get,

$$\begin{aligned} m(x_j, p) &= s_j m(x_j, p+\Delta p) + s_{j+1} m(x_{j+1}, p+\Delta p) + s_{j-1} m(x_{j-1}, p+\Delta p), \text{ where } s \in \mathbb{R}, \\ s_j &= 1 + \frac{2d\Delta p}{(\Delta x)^2}, \\ s_{j+1} &= \frac{\Delta p}{2\Delta x} u(x_{j+1}, p+\Delta p) - \frac{d\Delta p}{(\Delta x)^2}, \\ s_{j-1} &= -\frac{\Delta p}{2\Delta x} u(x_{j-1}, p+\Delta p) - \frac{d\Delta p}{(\Delta x)^2}. \end{aligned} \tag{A.15}$$

Let $m(x,p)$ and $m(x,p+\Delta p)$ denote the mass density at p and $(p+\Delta p)$ respectively, and write them into the following $(N_x+1)\times 1$ column vectors

$$m(x,p) = \begin{bmatrix} m(x_0,p) \\ m(x_1,p) \\ \vdots \\ m(x_{N_x-1},p) \\ m(x_N,p) \end{bmatrix}, \quad m(x,p+\Delta p) = \begin{bmatrix} m(x_0,p+\Delta p) \\ m(x_1,p+\Delta p) \\ \vdots \\ m(x_{N_x-1},p+\Delta p) \\ m(x_N,p+\Delta p) \end{bmatrix}. \tag{A.16}$$

Then for matrix $\boldsymbol{S}_u \in \mathbb{R}^{(N_x+1)\times(N_x+1)}$, we have,

$$\begin{aligned} m(x,p) &= \boldsymbol{S}_u m(x, p+\Delta p), \\ S_{j,j} &= 1 + \frac{2d\Delta p}{(\Delta x)^2}, j = 0, 1, \ldots, N_x \\ S_{j,j-1} &= -\frac{\Delta p}{2\Delta x} u(x_{j-1}, p+\Delta p) - \frac{d\Delta p}{(\Delta x)^2}, j = 1, 2, \ldots, N_x \\ S_{j,j+1} &= \frac{\Delta p}{2\Delta x} u(x_{j+1}, p+\Delta p) - \frac{d\Delta p}{(\Delta x)^2}, j = 0, 1, \ldots, N_x - 1. \end{aligned} \tag{A.17}$$

Hence, given any $m(x,p)$, one can compute $m(x,p+\Delta p)$ by,

$$m(x, p+\Delta p) = \boldsymbol{S}_u^{-1} m(x,p). \tag{A.18}$$

Note that $\boldsymbol{S}_u$ is a tridiagonal matrix with identical non-zero diagonal elements, and each row contains at least 1 non-zero off-diagonal element. Hence for any given row of $\boldsymbol{S}_u$, it must be linearly independent of any other row in $\boldsymbol{S}_u$. Therefore, $\boldsymbol{S}_u$ has a rank of (N_x+1), and, therefore, is non-singular.

In general, the stability condition for implicit schemes does not depend on Δx or Δp. It is also possible that this scheme is unconditionally stable (independent of n and also $u(x, p)$).